UNIVERSITY OF CALIFORNIA

Los Angeles

The physiology and pathology of iron in pregnancy

A dissertation submitted in partial satisfaction of the

requirements for the degree Doctor of Philosophy

in Molecular, Cellular, and Integrative Physiology

by

Allison Lynn Fisher

2020

ABSTRACT OF THE DISSERTATION

The physiology and pathology of iron in pregnancy

by

Allison Lynn Fisher

Doctor of Philosophy in Molecular, Cellular, and Integrative Physiology

University of California, Los Angeles, 2020

Professor Elizabeta Nemeth, Committee Chair

Iron is an essential nutrient required for vital metabolic and cellular processes. Despite its importance, it is poorly understood how maternal and fetal iron homeostasis is regulated during pregnancy, including the contribution of the maternal, placental, and fetal signals during healthy pregnancy or in conditions of iron deficiency and excess. Maternal iron insufficiency causes anemia, which is a global health problem linked to adverse outcomes. Iron availability in maternal circulation is ensured by the physiological suppression of the hormone hepcidin. We showed that suppression of maternal hepcidin during pregnancy is essential for embryo health, as high maternal hepcidin activity induced by administering a hepcidin mimetic to pregnant mice caused severe iron restriction and anemia in dams and embryos, low birthweight, and embryo mortality. Using mouse models, we showed that during maternal iron deficiency, maternal hepcidin is further suppressed, but this is not sufficient to maintain plasma iron levels and embryo iron endowment. With severe

iron deficiency, the placenta altered iron transporters to preserve its own iron and metabolic function at the expense of the fetus, ultimately protecting the fetus from the consequences of placental dysfunction.

We further showed that embryo hepcidin does not regulate placental iron transfer under physiological conditions. However, in mouse, rhesus macaques and human pregnancies complicated by inflammation, we found that fetal hepcidin was increased and associated with fetal hypoferremia. The fetus's ability to respond to inflammatory signals represents a conserved mechanism thought to be important in fetal host defense.

We discovered in mouse models an adverse interaction between maternal iron excess and inflammation that led to embryotoxicity which was not observed with either condition alone. Embryotoxicity was observed not only in a mouse model of systemic acute inflammation induced by bacterial lipopolysaccharide, but also with chronic inflammation caused by diet-induced obesity. We found that maternal iron excess increased oxidative stress in the placenta and embryo endothelium, which sensitized the placental and embryo endothelium to inflammation-induced lethal apoptotic damage. The interaction between iron excess and inflammation is dependent on TNFα-signaling and can be reversed by maternal anti-TNFα and antioxidant therapy. These findings raise important questions about the safety of indiscriminate iron supplementation in pregnant women with underlying inflammation.

We analyzed the interaction between iron, inflammation, and the endothelium in cultured endothelial cells. Iron loading induced cholesterol biosynthesis, promoted novel TNFR1 proteolytic processing, and sensitized cells to TNFα-mediated apoptosis. We determined that during iron excess, the contribution of altered cholesterol homeostasis is the driving pathogenic

mediator of apoptosis. Altered cholesterol metabolism by iron excess in endothelial cells may contribute to iron-mediated toxicity in human iron overload disorders.

We further described that iron deficiency in pregnant mice also adversely interacts with inflammation caused by acute and chronic inflammation, triggered respectively by lipopolysaccharide and diet-induced obesity. Only the combination of maternal iron deficiency and inflammation caused embryo malformations and demise. Iron deficiency potentiated placental inflammation in complicated pregnancies, and in normal pregnancies iron deficiency induced TNFα-receptor 1 expression in mouse and human placentas, representing possible mechanisms for how iron deficiency worsens outcomes in inflamed pregnancies.

We defined the pathophysiology of iron regulation in pregnancy and articulated several novel concepts: placental adaptation to limited iron availability, the roles of maternal and fetal hepcidin, and adverse synergy between iron and inflammation. The discovery of the interaction between iron and inflammation highlights the utility of iron status as a modifying factor to ameliorate severity of injury in inflamed pregnancy and in a variety of inflammatory conditions outside of pregnancy. These concepts have translational impact and may eventually inform the clinical management of pregnant women worldwide.

The dissertation of Allison Lynn Fisher is approved.

Kenneth Dorshkind

Elaine Hsiao

Tomas Ganz

Elizabeta Nemeth, Committee Chair

University of California, Los Angeles

2020

PREFACE

This dissertation was supported in part by NIH National Research Service Award Institutional Training Grant (T32) and Individual Predoctoral Fellowship (F31). All the work was performed primarily by me except for co-authored work presented in Chapters 1 and 2, which was primarily done by Dr. Veena Sangkhae. Specific author contributions are indicated in each Chapter. The Chapters listed below are reprints or versions of published or submitted manuscripts, reproduced with permission:

The introduction is a version of:

Fisher AL, Nemeth E. Iron homeostasis during pregnancy. Am J Clin Nutr. 2017;106(Suppl 6):1567S–1574S. doi:10.3945/ajcn.117.155812.

Chapter 1 is a reprint of:

Sangkhae V, **Fisher AL**, Wong S, Koenig MD, Tussing-Humphreys L, Chu A, Lelic M, Ganz T and Nemeth E. Effects of maternal iron status on placental and fetal iron homeostasis. J Clin Invest. 2020;130(2):625-640. https://doi.org/10.1172/JCI127341.

Chapter 2 is a reprint of:

Sangkhae V, **Fisher AL**, Chua KJ, Ruchala P, Ganz T and Nemeth E. Maternal hepcidin determines embryo iron homeostasis. Blood. 2020 Jun 25. doi: 10.1182/blood.2020005745

Chapter 3 is a reprint of:

Fisher AL, Sangkhae V, Presicce P, Chougnet C, Jobe AH, Kallapur SG, Tabbah S, Buhimschi CS, Buhimschi IA, Ganz T and Nemeth E. Fetal and amniotic fluid iron homeostasis in healthy and complicated murine, macaque, and human pregnancy. JCI Insight 2020 Feb 27;5(4):e135321. https://doi.org/10.1172/jci.insight.135321.

Chapter 4 is a version of:

Fisher AL, Sangkhae V, Balušíková K, Palaskas NJ, Ganz T and Nemeth E. Iron-dependent apoptosis causes embryotoxicity in inflamed and obese pregnancy. Submitted manuscript.

Chapter 5 is a version of:

Fisher AL, Srole DN, Palaskas NJ, Meriwether D, Reddy Srinivasa T, Ganz T and Nemeth E. Iron loading induces cholesterol synthesis and sensitizes endothelial cells to TNFα-mediated apoptosis. Submitted manuscript.

TABLE OF CONTENTS

VITA

Education

California Polytechnic University, Pomona 2013-2015
Pomona, CA
Master of Science in Biological Sciences

University of Connecticut 2008-2013
Storrs, CT
Bachelor of Science in Animal Science

Fellowships & Awards

Ruth L. Kirschstein National Research Service Award 2019-2020
Individual Predoctoral Fellowship F31HD097931

UCLA Dissertation Year Fellowship 2019-2020

Center for the Study of Women Travel Grant 2019

Best Poster Presentation Awards
Molecular, Cellular and Integrative Physiology Retreat, Los Angeles, CA 2019
Society for Reproductive Investigation, San Diego, CA 2018

Molecular, Cellular and Integrative Physiology Training Grant 2016-2017
Ruth L. Kirschstein Research Service Award T32GM065823

Publications

Sangkhae V, **Fisher AL**, Chua KJ, Ruchala P, Ganz T and Nemeth E. Maternal hepcidin determines embryo iron homeostasis. Blood. 2020 Jun 25. doi: 10.1182/blood.2020005745

Fisher AL, Sangkhae V, Presicce P, Chougnet C, Jobe AH, Kallapur SG, Tabbah S, Buhimschi CS, Buhimschi IA, Ganz T and Nemeth E. Fetal and amniotic fluid iron homeostasis in healthy and complicated murine, macaque, and human pregnancy. JCI Insight 2020 Feb 27;5(4):e135321.

Sangkhae V, **Fisher AL**, Wong S, Koenig MD, Tussing-Humphreys L, Chu A, Lelic M, Ganz T and Nemeth E. Effects of maternal iron status on placental and fetal iron homeostasis. J Clin Invest 2020 Feb 3;130(2):625-640.

Wang Y, Wehling-Hendricks M, Welc S, **Fisher AL**, Zou Q, Tidball JG. Aging of the immune system causes reductions in muscle stem cell populations, promotes their shift to a fibrogenic phenotype and modulates sarcopenia. FASEB J 2019 Jan;33(1):1415-1427.

Fisher AL and Nemeth E. Iron homeostasis during pregnancy. Am J Clin Nutr 2017. 106 (Suppl 6), 1567-74S.

Fisher AL, Greene HM, Talmadge RJ, Nout-Lomas YS. Lactate-guided conditioning program using variable exercise intensities improves fitness and alters muscle enzyme activity but not inflammatory response in horses. Comparative Exercise Physiology 2016. 12(4): 183-192.

Hauss AA, Stablein CK, **Fisher AL**, Greene HM, Nout-Lomas YS. Validation of the Lactate Plus Lactate Meter in the Horse and Its Use in a Conditioning Program. J Eq Vet Sci 2014. 34: 1064-8.

Select Presentations

Fisher AL. Maternal Iron Excess & Inflammation Synergize to Cause Embryotoxicity through Fetal Endothelial Cell Apoptosis. Molecular, Cellular and Integrative Physiology Department Retreat. Los Angeles, CA, February 2020. Oral presentation.

Fisher AL, Sangkhae V, Palaskas NJ, Ganz T and Nemeth E. Maternal high iron and inflammation during pregnancy synergize to cause embryotoxicity. BioIron, Heidelberg, Germany, May 2019. Oral presentation.

Fisher AL, Sangkhae V, Palaskas NJ, Ganz T and Nemeth E. Mechanism of adverse interaction between iron and inflammation during pregnancy. Society for Reproductive Investigation, Paris, France, March 2019. Oral presentation.

Fisher AL, Sangkhae V, Palaskas NJ, Ganz T and Nemeth E. Maternal Iron Excess and Inflammation Synergize to Impair Fetal Development. Molecular, Cellular and Integrative Physiology Department Retreat. Los Angeles, CA, February 2019. **Best Poster Award.**

Fisher AL, Sangkhae V, Ganz T and Nemeth E. Mechanism of adverse interaction between iron and inflammation during pregnancy. Department of Medicine Annual Research Day, Los Angeles, CA, October 2018. Poster presentation.

Fisher AL, Sangkhae V, Gabayan V, Ganz T and Nemeth E. Maternal Iron Excess and Inflammation Synergize to Impair Fetal Development. Society for Reproductive Investigation, San Diego, CA, March 2018. **Best Poster Award.**

Fisher AL, Sangkhae V, Gabayan V, Nemeth E, Ganz T. Synergistic action of maternal inflammation and iron causes adverse fetal outcomes. Keystone Symposia: Maternal-Fetal Crosstalk: Harmony vs. Conflict. Washington, DC, October 2017. Poster presentation.

Fisher AL, Sangkhae V, Gabayan V, Valore E, Ganz T and Nemeth E. Regulation of iron in normal and complicated pregnancy. Molecular, Cellular and Integrative Physiology Department Retreat. Los Angeles, CA, February 2017. Poster presentation.

OVERVIEW: IRON HOMEOSTASIS DURING PREGNANCY

1. Elemental iron

Iron is the most abundant element on Earth by mass. Iron is distributed in the Earth's crust, mantle, and cores, constituting over 80% of the inner and outer cores (6). While iron is one of the most abundant metals on Earth, its bioavailability to organisms is low due to Earth's oxygen-rich atmosphere, which readily oxidizes ferrous iron (Fe^{2+}) to nearly insoluble ferric iron (Fe^{3+}). Iron is a transition element that can change its oxidation state from -2 to +6.

2. Biological functions of iron

Iron has an essential role in vital cellular and metabolic processes. In biological systems, iron is predominantly found in the ferrous (+2) and ferric (+3) forms, frequently within prosthetic groups such as iron-sulfur clusters or heme. Iron functions as a co-factor in many chemical reactions in the body because of its ability to readily accept and donate electrons. Iron is a component of the electron transport chain in cytochromes that participate in electron shuttling (7,8). Iron is also involved in DNA replication and repair as a cofactor for DNA polymerase (9). Furthermore, iron is a component of proteins that transport or store oxygen (hemoglobin or myoglobin), and proteins that participate in gene expression, cell proliferation and differentiation, hormone synthesis, intermediary metabolism, and host defense (10,11). Within biological systems, iron is transported and stored bound to proteins (transferrin, ferritin), as free iron is highly reactive and can catalyze generation of reactive oxygen species such as hydroxyl radicals via the Fenton reaction.

3. Iron economy

An average adult human has 3-4 g of total body iron, more than half of which is contained in erythrocyte hemoglobin (2-3 g). The liver is the main organ for iron storage, with up to 1 g of iron

stored in ferritin in hepatocytes and macrophages. Iron bound to the iron-carrier protein transferrin is distributed to tissues in blood plasma which contains only 2-4 mg iron. Most of the plasma iron is directed to the bone marrow for hemoglobin synthesis by erythroid precursors, which require 20-25 mg iron per day. This daily iron requirement is provided by the recycling of senescent red blood cells by splenic macrophages. The lifespan of human red blood cells is ~120 days, thus 0.8% of red blood cells are destroyed and replaced daily (12). Only 1-2 mg of iron are lost daily through

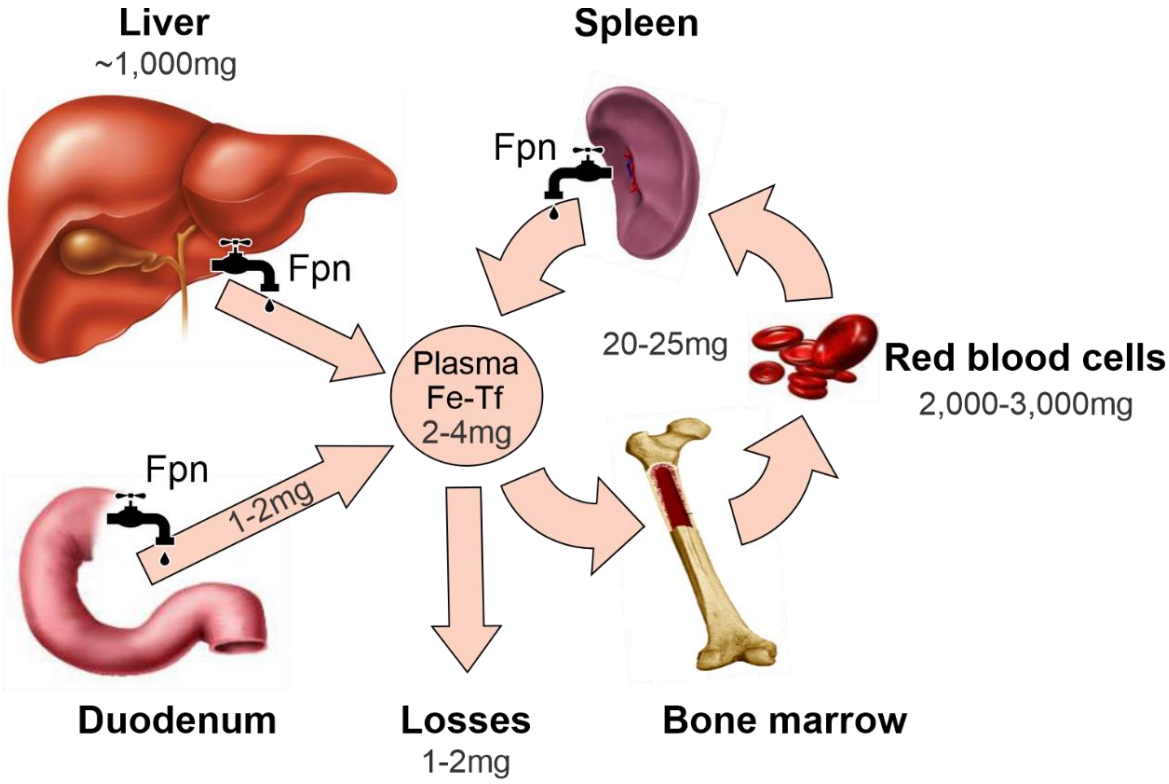

Figure 1. Iron distribution in the body. An adult contains about 3-4g of total body iron, most of which is localized in red blood cells (2,000-3,000mg), erythroid precursors in the bone marrow, or stored in the liver (~1,000mg). Iron recycled from red blood cells by splenic macrophages (20-25mg iron daily) or from dietary absorption (1-2mg daily) is transported into plasma where it is directed towards tissues for utilization (primarily by bone marrow) or storage in the liver. Minimal amounts of iron are lost daily (1-2mg daily) through desquamation and minor blood loss, which is compensated for by dietary absorption. Ferroportin (Fpn), the only known iron exporter, exports iron into the plasma from three main sources: duodenum, liver, and spleen. Dietary iron (1-2 mg/day) is transferred from the duodenum into plasma, and 20-25 mg/day of recycled iron is delivered to plasma by macrophages in the spleen.

desquamation of epithelial surfaces or menstrual blood loss, which are compensated for by dietary absorption (1-2 mg/day). Recently, it was reported that mature red blood cells can also directly export iron (likely released from oxidized hemoglobin) into circulation (13), providing up to 20% of daily iron flows. Despite rapid turnover of plasma iron, plasma iron concentrations are relatively stable **(Figure 1),** implying the existence of a tight regulatory system.

Iron metabolism is generally similar between laboratory rodents and humans, although species differences exist in terms of absorption and turnover rates (described in **Table 1**). These differences are important in laboratory mice which are commonly used for studying iron metabolism. Compared to humans, the average lifespan of a mouse red blood cell is ~40 days (14) and the mouse has ~1 mg of iron in erythrocyte hemoglobin (15). In contrast to humans who depend on iron recycling to meet dietary iron needs, rodents absorb from the diet as much as 50% of their daily iron turnover and depend less on iron recycling. In an adult mouse, ~15-25 µg of iron is recycled daily for utilization by bone marrow for new red blood cells (15). Importantly, dietary iron absorption and losses are proportionally greater than in humans, making it easier to alter body iron content through dietary changes.

Table 1. Comparative iron parameters in adult humans vs. mice, adapted from (15)

Parameter	**Human**	**Mice**
Red blood cell lifespan	120 days	40 days
Total red blood cell iron	2,000-3,000 mg	0.6-1 mg
Daily RBC iron turnover	17-25 mg	15-25 µg
Daily iron absorption	1-2 mg	15-20 µg
Daily dietary iron requirement	8-18 mg	140 µg
Normal dietary iron source	Heme and nonheme omnivore	Nonheme herbivore

4. Iron transport

Cellular iron homeostasis is maintained by transport proteins that direct iron into and out of cells, and distribute iron for utilization, recycling, and storage.

4.1 Systemic iron transport

The major sources of plasma iron include intestinal iron absorption from dietary sources, macrophage recycling of senescent red blood cells, mobilization of liver iron stores, and iron released from mature red blood cells. Iron is transported into plasma from these sources by the sole iron exporter, ferroportin. In plasma, iron is bound to the carrier protein transferrin where it is distributed to tissues for utilization or storage.

4.2 Cellular iron transport

Non-heme and heme iron are absorbed from the diet in the duodenum. Dietary non-heme ferric iron is reduced to ferrous iron by ferrireductase duodenal cytochrome B (DCYTB) on the enterocyte apical membrane (16) and is transported into enterocyte cytoplasm by divalent metal transporter-1 (DMT1) (17,18). Enterocytes of carnivores also take up heme, which is degraded by heme oxygenase-1 to release iron for reutilization (19). In both cases, ferrous iron is transported out of the enterocyte and into portal blood by ferroportin on the basolateral membrane (20), is oxidized to ferric iron by the ferroxidase hephaestin (21), and is loaded onto transferrin in circulation. Iron destined for storage in enterocyte ferritin and not for transport into blood would be eventually lost through enterocyte shedding which occurs every 3 days in humans and mice (22).

Most iron in circulation is bound to transferrin, which binds one or two iron atoms. Transferrin delivers iron to cells through transferrin receptor 1 (TFR1) on the cell membrane. Transferrin-TFR1 complexes are internalized into endosomes, which become acidified, causing

iron to dissociate from transferrin. The endosomal ferrireductase STEAP3 reduces ferric iron to ferrous iron (23), which is transported into the cytosol by DMT1. Once in the cell, iron is trafficked for the synthesis of heme and iron sulfur clusters, used for cytoplasmic ferroprotein synthesis, stored in ferritin, or exported out of the cell by ferroportin. Iron movement within cytoplasm is likely directed by chaperones poly C binding proteins (PCBPs) 1 and 2 (24,25). After ferroportin exports iron, it is oxidized to ferric iron by ferroxidase ceruloplasmin (26).

5. Iron toxicity

In iron overload conditions, the iron-carrying capacity of transferrin is exceeded, and iron appears in plasma complexed with low-molecular weight molecules, and these iron species are collectively referred to as non-transferrin bound iron (NTBI). NTBI is highly reactive and can generate reactive oxygen species, and NTBI accumulation in cells leads to their dysfunction, with specific tissue toxicities dependent on both the rate and extent of NTBI accumulation. Most NTBI in plasma is cleared by the liver, as hepatocytes import NTBI through the essential manganese transporter ZIP14 (27,28), but NTBI can also be taken up by the pancreas, kidney, and heart (29). Iron accumulation in the liver increases the risk of hepatic fibrosis, cirrhosis, and hepatocellular carcinoma (30), as well as cardiomyopathy, diabetes and other endocrinopathies (31,32). Endothelial cells are the most proximal cell type exposed to circulating NTBI. We evaluated the effects of NTBI accumulation on cultured human endothelial cells in Chapter 5 and showed that NTBI causes apoptosis of endothelial cells by altering cellular cholesterol metabolism.

6. Systemic iron regulation

Hepcidin is the master regulator of plasma nonheme iron concentrations and tissue iron distribution (33). Hepcidin is a 25-amino acid peptide hormone that is produced and secreted from hepatocytes in the liver (34). Hepcidin acts by inhibiting the major iron flows into plasma: intestinal iron absorption, release from macrophages that recycle iron from old red blood cells and mobilization of stored iron from the liver. Hepcidin exerts its effects through its receptor, the iron exporter, ferroportin (FPN). FPN is highly expressed in all the tissues that export large amounts of iron into plasma (20). Hepcidin binds to FPN and occludes it, triggering FPN degradation (35,36), and resulting in iron sequestration in target cells and decreased iron flow into plasma. Thus, iron delivery to consuming tissues (e.g. bone marrow and placenta with fetus) is inversely correlated with hepcidin concentrations.

7. Regulation of hepcidin

Hepcidin is transcriptionally regulated by multiple stimuli: intracellular and extracellular iron concentrations, erythropoiesis, inflammation, and pregnancy. Hepcidin regulation during pregnancy is discussed in section 8.2.

7.1 Regulation of hepcidin by iron

Hepcidin regulation by iron is mediated by the bone morphogenetic protein (BMP) pathway **(Figure 2A-B)**. Hepatocytes sense circulating iron-transferrin levels by transferrin receptors 1 and 2, which interact with hemochromatosis protein HFE to modulate BMP signaling and hepcidin transcription (37,38). BMP ligands are produced by sinusoidal endothelial cells in proportion to the iron content of the liver (39,40). BMP6 and 2 stimulate hepcidin transcription by hepatocytes by binding to BMP receptors to phosphorylate SMAD1/5/8, which complex with SMAD4 to enter

the nucleus and bind BMP-responsive elements on the hepcidin promoter (41). The BMP-BMP receptor complex requires coreceptors including membrane-anchored hemojuvelin (42). BMP2, BMP6 and hemojuvelin are essential for normal iron homeostasis (43,44). The transmembrane serine protease 6 (TMPRSS6) cleaves hemojuvelin and functions as a negative regulator of this pathway (45). We evaluated regulation of maternal hepcidin by iron deficiency and iron loading in Chapter 1 using mouse models and showed that although the baseline hepcidin levels are lower than in non-pregnant mice, iron regulatory mechanisms are preserved in pregnancy.

7.2 Regulation of hepcidin by erythropoiesis

Erythropoiesis places a large demand on iron homeostasis. Iron is required for red blood cell synthesis as a component of heme in erythrocyte hemoglobin. Increased red blood cell synthesis occurs with hematopoietic stress such as blood loss, rapid growth, or in anemias. To meet the increased iron demands of erythropoietic stress, hepcidin production is suppressed by the hormone erythroferrone which is produced by erythroblasts in the bone marrow in response to erythropoietin **(Figure 2C)** (46). Erythroferrone acts by interfering with BMP-SMAD signaling (47), acting as a ligand trap for the physiological form of BMP ligand in vivo, BMP2/6 (48). Erythroferrone-mediated hepcidin suppression promotes enhanced iron absorption and mobilization from stores for utilization by the bone marrow. Elevated erythroferrone contributes to inappropriately low hepcidin production and lethal iron overload in anemias with ineffective erythropoiesis including β-thalassemia (49).

7.3 Regulation of hepcidin by inflammation

Inflammation has a potent effect on iron homeostasis. Inflammatory cytokine IL-6 induces hepcidin transcription through the JAK-STAT3 pathway **(Figure 2D)** (50-53). Inflammation-induced hepcidin production decreases iron transport into plasma causing hypoferremia. Hepcidin-

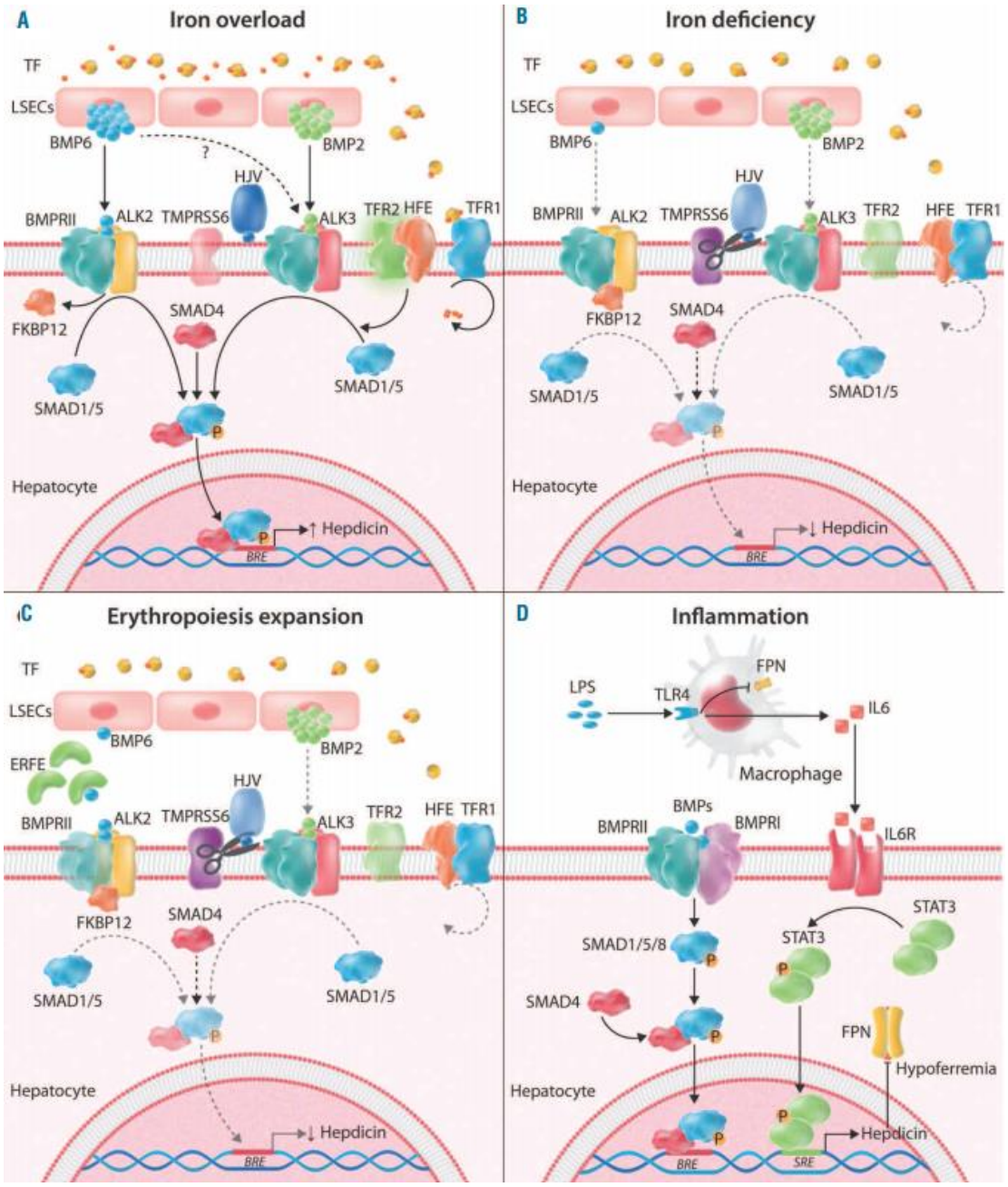

Figure 2. Regulation of hepcidin expression (2). Hepcidin expression is regulated by **(A-B)** iron, **(C)** erythropoiesis, and **(D)** inflammation. **(A)** In proportion to iron content, BMP ligands are produced by liver sinusoidal endothelial cells (LSECs). BMP2 and 6 bind to BMP type II receptors (BMPRII) and phosphorylate and activate BMP type I receptors (BMPRI). BMPRIs phosphorylate SMAD1/5/8, which complexes with SMAD4, translocates to the nucleus, and binds BMP-responsive elements (BRE) on the hepcidin promoter to stimulate hepcidin transcription. **(B)** In iron deficiency TMPRSS6 cleaves HJV and inactivates the BMP2/6 pathways, suppressing hepcidin expression. **(C)** ERFE, produced by erythroid cells, sequesters BMP2/6, suppressing hepcidin expression. **(D)** Inflammation (e.g. LPS via TLR-4 signaling) triggers IL6 production by macrophages, which stimulates JAK2-STAT3 to induce hepcidin.

mediated hypoferremia evolved as a critical host defense mechanism to prevent appearance of non-transferrin bound iron that supports the rapid growth of certain gram-negative pathogens (54). However, inflammation-induced hypoferremia can be maladaptive in chronic inflammatory conditions, where elevated hepcidin contributes to iron-restricted anemia (55). We evaluated the regulation of maternal and fetal hepcidin by inflammation during pregnancy in Chapter 3 in mice, macaques and human pregnancy, and showed that both maternal and fetal hepcidin can be induced by inflammation, causing hypoferremia. Although prolonged iron restriction would have negative consequences on maternal erythropoiesis and fetal development, acute iron restriction likely serves a protective role during infections with siderophilic pathogens.

7.4 Autocrine/paracrine roles of hepcidin

In recent years, generation of floxed-hepcidin mice has enabled conditional deletion of hepcidin in different cell types and has revealed tissue-specific roles of the locally produced hepcidin. Ablation of cardiomyocyte hepcidin led to cardiomyocyte iron deficiency, and contractile and metabolic dysfunction of the heart (56). Ablation of hepcidin in macrophages, on the other hand, improved cardiac repair and regeneration in a model of acute myocardial infarction (57). Ablation of hepcidin in keratinocytes worsened necrotizing fasciitis by impairing the recruitment of neutrophils (58). Ablation of hepcidin in dendritic cells impaired mucosal healing in a mouse model of inflammatory bowel disease (59). In all these models, systemic iron homeostasis was not affected, suggesting that local production of hepcidin can regulate cellular iron homeostasis in an autocrine/paracrine manner. We evaluated the role of local hepcidin production in the placenta and embryo on placental and embryo iron homeostasis using mouse models in Chapters 1 and 2, and showed that neither placental nor embryo hepcidin regulate placental iron transfer under physiological conditions.

8. Iron homeostasis during pregnancy

Sections 8 and 9 are a pre-copyedited, author-produced version of an article accepted for publication in The American Journal of Clinical Nutrition following peer review. The version of record [Fisher AL, Nemeth E, Iron homeostasis during pregnancy, The American Journal of Clinical Nutrition 2017; 106 (suppl_6): 1567S–1574S] is available online at: https://doi.org/10.3945/ajcn.117.155812.

8.1 Iron requirements

Pregnancy presents a major challenge to systemic iron homeostasis. During pregnancy, physiologic iron demands increase substantially to support fetoplacental development and maternal adaptation to pregnancy. Baseline maternal body iron losses during 9 months are estimated at ~230 mg (60), and would be higher were it not for the cessation of menstruation. The development of the placenta and fetus requires ~ 360 mg of iron. An additional 450 mg of iron is needed to expand maternal red blood cell (RBC) mass during pregnancy. Thus, ~1 g of iron must be acquired during pregnancy to preserve the maternal iron balance and support feto-placental development. Some of that iron is recycled after pregnancy when erythrocyte mass contracts to

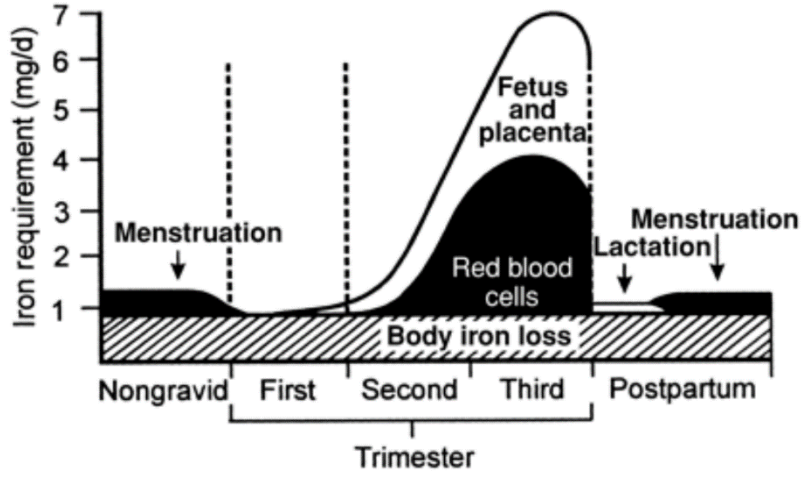

Figure 3. Iron requirements during pregnancy (4). Daily iron requirements in a 55-kg woman. In the first trimester, iron requirements (~0.8 mg/d) are lower because menstruation stops. As pregnancy advances, maternal red blood cell mass expands and placental and fetal growth accelerates, resulting in the rise in physiologic iron requirements to 3.0 - 7.5 mg/d in the third trimester.

pre-pregnancy concentrations except for the iron lost through bleeding at delivery (~150 mg). Therefore, the average net pregnancy-related loss of iron to the mother is estimated to be 740 mg. Iron requirements, however, are not uniform throughout the three trimesters of pregnancy. In the first trimester, the requirements (estimated at ~0.8 mg/d) are lower than before pregnancy because menstruation stops. As pregnancy advances, maternal RBC mass increases and placental and fetal growth accelerates, resulting in the rise in physiologic iron requirements to 3.0 - 7.5 mg/d in the third trimester (4) **(Figure 3)**.

8.2 Regulation of iron availability

As assessed by the uptake of stable or radioactive iron isotopes, nonheme iron absorption during pregnancy increases as gestation progresses (61,62). It is likely that heme absorption increases in a similar manner (63). Moreover, iron stores are efficiently mobilized during pregnancy, as reflected by the decreased liver and spleen iron content in animal models compared to non-pregnancy concentrations (64-66). Both processes increase iron availability for transfer across the placenta and for maternal hematological adaptation.

The regulation of iron availability during pregnancy is, at least in part, dependent on maternal hepcidin concentrations. Relatively few studies have examined hepcidin during pregnancy, but initial reports indicate that in healthy pregnancies maternal hepcidin concentrations are suppressed in the second and third trimester in humans (67,68) or during the second and third week of a three week pregnancy in mice (3,69). The lowering of maternal hepcidin allows for increased supply of iron into the circulation, both from the enhanced absorption of dietary iron and enhanced release of iron from stores (3). One study in 19 pregnant women who ingested stable iron isotopes in their third trimesters confirmed that the net dietary nonheme and heme iron that

was transferred to the fetus was inversely correlated with maternal serum hepcidin (measured at delivery) (70).

The mechanism of maternal hepcidin suppression during pregnancy is completely unknown. Plasma dilution may partially contribute, although the magnitude of hepcidin decrease cannot be explained by only a 30-50% increase in plasma volume. Moreover, plasma dilution would not explain the profound suppression of hepatic hepcidin mRNA observed in animal studies (69). Gradual development of iron deficiency may also be a signal to suppress hepcidin. Hepcidin is lowest in pregnant women with iron-restricted erythropoiesis; however, even mothers with replete iron stores have very low hepcidin concentrations at delivery (71), thus suggesting that maternal hepcidin may be actively suppressed during pregnancy. Using mouse models, we evaluated the importance of maternal hepcidin suppression during pregnancy in Chapter 2 and demonstrated that it is essential for a healthy pregnancy, as administration of a hepcidin mimetic during mouse pregnancy causes maternal and embryo anemia, tissue iron deficiency, and low birth weight in embryos (72).

Major stimuli known to regulate hepcidin production include iron (both circulating and stored iron increase hepcidin), erythropoietic activity (suppresses hepcidin) and inflammation (increases hepcidin) (33). The regulation of hepcidin by all of these pathways appears to be preserved during pregnancy (72,73). In human studies, throughout pregnancy and even at delivery, maternal hepcidin concentrations positively correlate with serum ferritin and transferrin saturation and inversely with soluble transferrin receptor and hemoglobin, indicating the stimulation of hepcidin production by iron and suppression of hepcidin production by iron deficiency and erythropoietic activity (68,70,71,74). Immediately after delivery, serum hepcidin concentrations

increase (67), presumably due to physiological changes associated with labor and delivery, and do not correlate with serum ferritin or iron concentrations.

How iron supplementation affects maternal hepcidin during pregnancy is not known. Ingestion of iron supplements in nonpregnant adults increases hepcidin rapidly (75-77), and consequently decreases iron absorption. If iron supplementation in pregnancy has the same effect on maternal hepcidin, daily iron supplementation may not be optimal to achieve the most efficient iron absorption. Indeed, a 2015 Cochrane review of randomized trials from 15 countries found that maternal and infant outcomes at birth were not better with daily compared to intermittent iron supplementation, but intermittent supplementation was associated with fewer side effects (78). We evaluated how changes in maternal iron status affect hepcidin during pregnancy in mouse models in Chapter 1. We evaluated the effect of iron deficiency as well as dietary iron supplementation or parenteral iron administration. We showed that iron administration induces maternal hepcidin and this protected the fetus from severe iron overload.

Hepcidin concentrations measured in either serum or urine do not correlate with inflammatory markers in healthy pregnancies (67,74), including those with multiple gestations (79), suggesting that the mild inflammation that occurs in healthy pregnancies is not sufficient to increase hepcidin. However, it is possible that hepcidin may be inappropriately increased in complicated pregnancies that are associated with more intense inflammation, and this increase could compromise iron availability during pregnancy. Elevated hepcidin would be expected to impair iron absorption from supplements commonly prescribed to pregnant women and could impair the efficacy of intravenous iron therapy. Mildly elevated serum hepcidin concentrations are reported in obese compared to lean pregnant women (80,81), and in preeclamptic compared with healthy pregnancies (82). These concentrations did not have an obvious negative impact on

hematologic or iron variables in the mother or neonate in these studies, suggesting that hepcidin concentrations were still sufficiently low to allow effective iron utilization during pregnancy.

8.3 Changes in hematologic variables

Like many organ systems during pregnancy, the maternal hematological system undergoes profound physiological changes to accommodate the development of the fetus and placenta. The total blood volume (plasma volume plus RBC volume) increases ~1.5 L to facilitate blood flow in the uterus and placenta for nutrient and oxygen delivery to the fetus, and to blunt the effects of blood loss at delivery (83). The plasma volume starts increasing during the first trimester and expands until 30-34 weeks, reaching a 30-50% greater volume than in nonpregnant women (84,85). A lesser increase in plasma volume is associated with pathologies such as intrauterine growth restriction and/or preeclampsia (86).

Maternal RBC mass starts to increase at 8-10 weeks of gestation and continues to increase until delivery. Compared to pre-pregnancy concentrations, the RBC mass increases by 15-20% in women not taking iron supplements, and 20-30% in women taking iron supplements (87). The RBC life span has been reported to be slightly decreased during normal pregnancies (~9% decrease in rats and assumed to be similar in women) (88,89).

Erythropoietin production increases during pregnancy, driving the increase in RBC mass. Erythropoietin concentrations approximately double by the end of the third trimester (90). As in nonpregnant adults, the kidney is the main source of maternal erythropoietin during pregnancy (91,92). Erythropoietin production can be modulated by iron and anemia during pregnancy. In humans, the erythropoietin increase was greater with iron deficiency (90), and conversely, iron supplementation was associated with lower erythropoietin levels in the third trimester (93).

Fetal RBC production is independent of its maternal counterpart. Maternal erythropoietin does not cross the placenta (94,95). The fetus produces its own erythropoietin but mostly in the liver, which is also its main erythropoietic organ during the second half of pregnancy. After 30 weeks of gestation, the fetus also starts producing erythropoietin in the kidney (96). Fetal erythropoietin production (as measured by cord blood concentration) is higher when the mother is anemic or has other hypoxic complications (e.g. smoking, fetal growth restriction and intrauterine fetal hypoxia) (97-99).

Physiologic anemia of pregnancy occurs during a healthy pregnancy because of a greater increase in plasma volume relative to the increase in RBC mass. In women who are not taking iron supplements, the hemoglobin concentration and hematocrit decrease steadily to reach a nadir at approximately 28-36 weeks (on average, ~2 g/dL lower than the pre-pregnancy hemoglobin concentrations) (100). Mean corpuscular volume mildly decreases between 26 and 38 weeks, which is likely because placental iron transfer is most intense during this period, thereby decreasing iron availability for maternal erythropoiesis. Iron supplementation is reported to result in ~1 g/dL higher hemoglobin concentration at term compared with those in unsupplemented women (101,102).

8.4 Changes in iron variables

Serum ferritin concentration is the most frequently used marker of iron stores. Ferritin is secreted mostly by macrophages and, to a lesser extent, by hepatocytes, in proportion to their intracellular iron contents; thus, serum ferritin is proportional to body iron stores. In pregnancy, serum ferritin concentration gradually decreases to reach the lowest concentrations in the third trimester (101,103,104). In addition to hemodilution, this decrease likely reflects efficient iron mobilization from stores in agreement with the progressive hepcidin decrease during pregnancy.

Similar to other iron parameters, serum iron and transferrin saturation both decrease during pregnancy, but less so in iron-supplemented pregnancies (101,102). The plasma iron compartment is very small compared with iron stores (several milligrams vs several hundred milligrams), is subject to diurnal variation, and can change rapidly, e.g. after iron ingestion. Because of these effects, serum iron and transferrin saturation are inferior to serum ferritin in diagnosing iron deficiency (102,105).

Soluble transferrin receptor is generated by cleavage and by vesicular shedding of transferrin receptor 1 (TfR1) from the plasma membrane during erythroid maturation. The amount of soluble transferrin receptor reflects both the number of young erythrocytes and the degree of their iron deficiency because cellular TfR1 concentrations are regulated by intracellular iron via the iron responsive-element binding proteins (IRPs) IRP 1 and IRP2. In pregnancy, soluble transferrin receptor concentrations do not seem to change compared to non-pregnant concentrations unless maternal erythropoiesis is iron-deficient (106). Thus, soluble transferrin receptor concentration may only mildly increase by the third trimester in the iron-replete population but increase substantially in women with iron deficiency anemia.

9. Placental iron transport

During human pregnancy, the placenta retains ~90 mg of iron for its own function, and transports ~270 mg to the fetus. Most of the iron transfer occurs during the third trimester (107), which coincides with the lowest maternal hepcidin expression, allowing for a maximal rate of iron supply into maternal circulation. Maternal transferrin production steadily increases during pregnancy (87), which may function to increase iron delivery to the placenta.

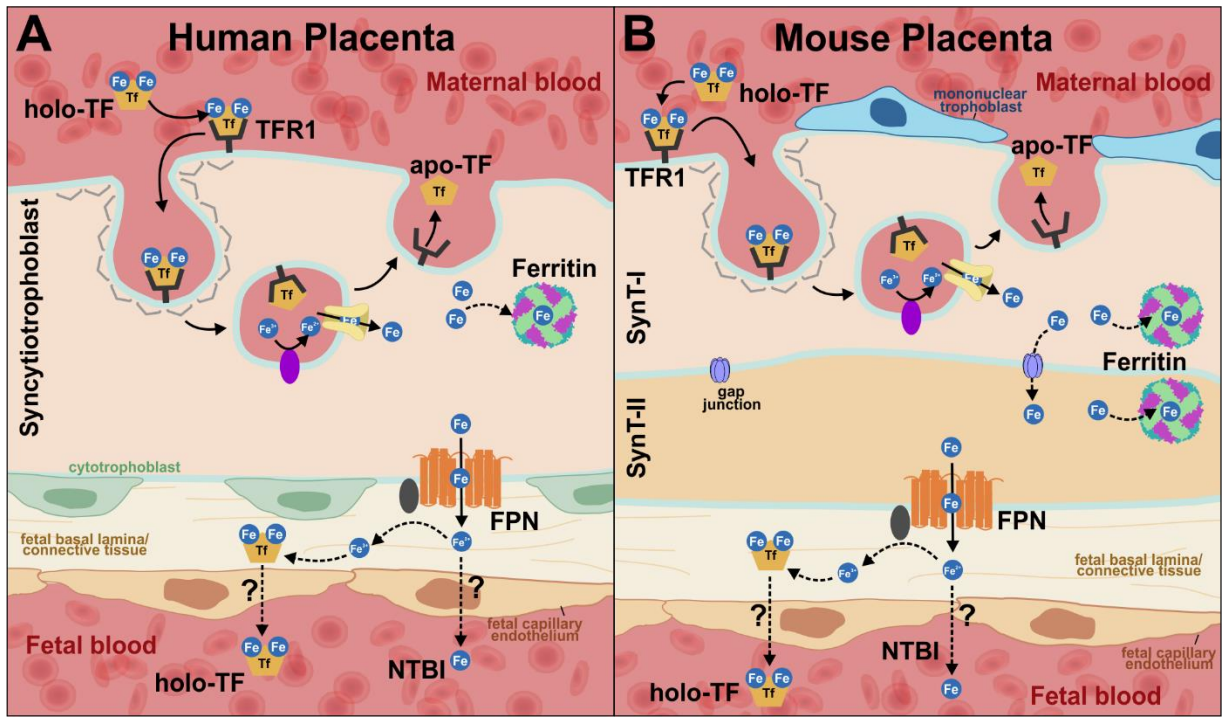

Figure 4. Anatomical features of human and mouse placentas (adapted from (5)). (A) Human placenta has a single layer of syncytiotrophoblast, with iron transporter transferrin receptor 1 (TFR1) on the apical side and ferroportin (FPN) on the basolateral side. **(B)** Mouse placenta with two syncytiotrophoblast layers (SynT-I and -II), with Tfr1on SynT-I and Fpn on SynT-II. In both humans and mice, Tfr1 faces maternal blood and Fpn faces fetal blood.

In the placenta, the primary barrier between maternal and fetal circulation is the syncytiotrophoblast. The syncytiotrophoblast expresses numerous nutrient transporters including those mediating iron transport and is thus the main layer of nutrient exchange. Whether other cell types (mesenchymal cells, Hofbauer cells, endothelial cells) mediate iron transport is unknown.

Although the placental transport mechanisms are similar between humans and rodents, species differences exist in placental architecture. Both human and rodent placentas are hemochorial, meaning that maternal blood directly contacts fetal chorion. In mouse placentas, the labyrinth contains two syncytiotrophoblast layers (SynT-I and -II) whereas human placentas only contain one layer, although the layers are functionally similar (108). In mice, SynT-I faces maternal circulation and SynT-II faces fetal circulation. Furthermore, the distribution of

transporters is similar in human and rodent placentas where TFR1 is facing maternal blood (on SynT-I in mice) and FPN is facing fetal blood (on SynT-II in mice) (5) **(Figure 4)**.

9.1 Placental trafficking of transferrin-bound iron

Iron is delivered to the placenta by maternal circulation, where iron is found complexed with transferrin, ferritin, or heme. The predominant source of iron taken up by the placenta is thought to be transferrin-bound iron. Global deficiency of TFR1 in mice results in embryo lethality before embryonic day 12.5 due to severe anemia, despite evidence of erythropoiesis at E10.5 (109), suggesting that other iron sources contribute to early embryonic development.

The transport of nonheme iron across the placenta to the fetus is unidirectional; iron is not transferred from the fetus to the mother (107). Despite its importance in fetal development, the mechanism of placental iron transport is incompletely understood.

Uptake of transferrin-bound iron from maternal circulation is mediated by iron importer TFR1 present on the apical membrane of placental syncytiotrophoblast (**Figure 5**) (110). TFR1 is located on the apical membrane (111,112), and the TFR1-TF complex is internalized via clathrin-coated vesicles similar to iron-transferrin endocytosis that occurs in other cell types (113). In the acidic environment (pH 5.4) of the vesicle, iron dissociates from transferrin, and ferric iron is reduced to ferrous iron by ferrireductases, possibly six-transmembrane epithelial of prostate (STEAP) 3 and STEAP 4 (114). Following the release of iron, the apotransferrin-TFR1 complex is recycled back to the membrane. The pH of the extracellular space (pH 7.4) facilitates dissociation of apotransferrin from TFR1, which is released into circulation to be reutilized, and the cycle repeats. Maternal iron deficiency has been associated with increased placental TFR1 expression in humans and in animal models (115,116).

How iron is transported from the vesicle into cytoplasm is not fully understood, but iron transporters DMT1, Zrt/Irt-like protein (ZIP)8, and ZIP14 have been identified as potential candidates. DMT1, which plays a critical role for endosomal iron release in erythroid cells (117), strongly localizes to human placental syncytium (112,118). However, the discovery that neonatal DMT1-null mice have normal iron content (118) suggests that DMT1 is not the sole endosomal iron transporter in placenta. ZIP8 is also abundantly expressed in placenta (119). ZIP8 hypomorphic embryos are severely anemic in utero and do not survive more than 48 hours after

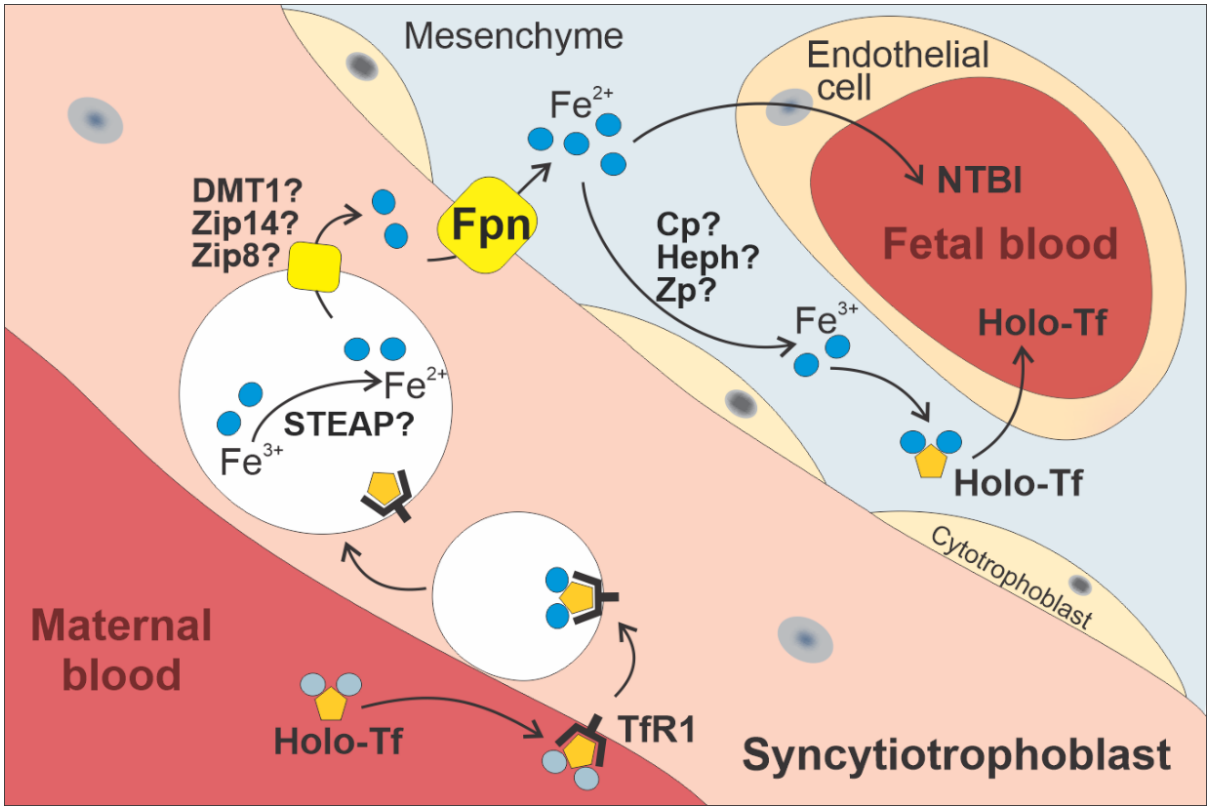

Figure 5. Placental iron transport (1). Maternal iron-Tf binds to TfR1 on the apical side of syncytiotrophoblast and is internalized. In the endosome, iron dissociates from Tf, is reduced, and is exported into cytoplasm. Iron is exported by Fpn on the basal side of syncytiotrophoblast and oxidized to be loaded onto fetal Tf or transported into fetal blood as NTBI through unknown mechanisms. Cp, ceruloplasmin; DMT1, divalent metal transporter 1; Fpn, ferroportin; Heph, hephaestin; NTBI, non–transferrin-bound iron; STEAP, 6-transmembrane epithelial antigen of prostate; Tf, transferrin; TfR1, transferrin receptor 1; Zip, Zrt/Irt-like protein; Zp, zyklopen.

birth (120); however, whether this is related to ZIP8 function in placental iron transport or also in fetal RBC needs to be clarified. ZIP14 is also highly expressed in the mouse placenta. ZIP14 mutant mice have no abnormal birth phenotype other than low birth weight (121), suggesting its non-essential or redundant role in the placenta.

Iron is transported out of the syncytiotrophoblast by ferroportin (111,122) **(Figure 5)**. Complete knockout of ferroportin is embryonic lethal whereas conditional knockout of ferroportin that preserves its expression in the placenta results in normal embryonic development and birth (20), confirming the essential role of ferroportin in placental iron export. Ferroportin likely exports iron into the fetal stroma. Once there, iron still needs to cross the endothelium to reach fetal circulation. With consideration that non-transferrin-bound iron is found in fetal circulation (123), it is possible that some form of non-transferrin-bound iron is transported across fetal endothelial cells. Alternatively, after being exported from the syncytiotrophoblast by ferroportin, iron may be oxidized to the Fe^{+3} form before loading onto fetal transferrin. There are three known mammalian multi-copper ferroxidases: ceruloplasmin, hephaestin, and zyklopen. Although all of them have been detected in the placenta (124-126), knockout mouse models indicate that none of them are individually essential or have redundant roles (127-129). Once iron is loaded onto fetal transferrin, it may be transported to fetal circulation through endothelial cells, although this mechanism is unclear (110).

Whether heme is transported across the placenta is much less understood. Feline leukemia virus subgroup C receptor-related protein (FLVCR1) is a heme exporter that is highly expressed in the placenta (130) and has two isoforms, FLVCR1a is expressed on the cell surface, and FLVCR1b is expressed on mitochondria, but the role of each isoform and their localization and

regulation remain to be determined. Maternal anemia is associated with lower placenta FLVCR1 expression (131), but the biological implication of this observation is not yet understood.

Studies in animal models demonstrate the transport of labelled ferritin from the dam to the fetus (132), although the physiological relevance of this is unclear as circulating ferritin is typically iron-poor. Ferritin uptake by the placenta might involve TFR1 (133) and/or SCARA5 (scavenger receptor class A member 5) (134). Although the transporters for NTBI, ferritin, and heme are expressed in the placenta, it is unknown whether any of these molecules represent an important iron source for placental transport or fetal development.

9.2 Regulation of placental iron transport

Placental ferroportin is localized on syncytiotrophoblast facing fetal circulation and could be subject to regulation by fetal-derived hepcidin. However, compared to already low maternal hepcidin concentrations, fetal hepcidin concentrations are much lower. Moreover, iron endowment of the fetus is unaffected by genetic ablation of fetal and placental hepcidin (3,72), indicating that embryonic or placental hepcidin is too low to regulate iron transfer across the placenta. Thus, under normal conditions, iron availability for placental iron transport is dependent on maternal plasma iron concentrations and therefore on maternal hepcidin. Fetal hepcidin, nevertheless, can regulate placental ferroportin under certain conditions, as fetuses with hepcidin overexpression or mutations in the hepcidin regulator TMPRSS6 are severely anemic (135,136). Systemic and intraamniotic inflammation are also demonstrated to induce fetal hepcidin and cause fetal hypoferremia (137), but whether inflammation-induced fetal hepcidin regulates iron transporters in the placenta remains to be determined.

In mice, expression of TFR1 and FPN in the placenta increase with gestational age (3), presumably to meet the increasing iron requirements of the developing fetus. We evaluated how

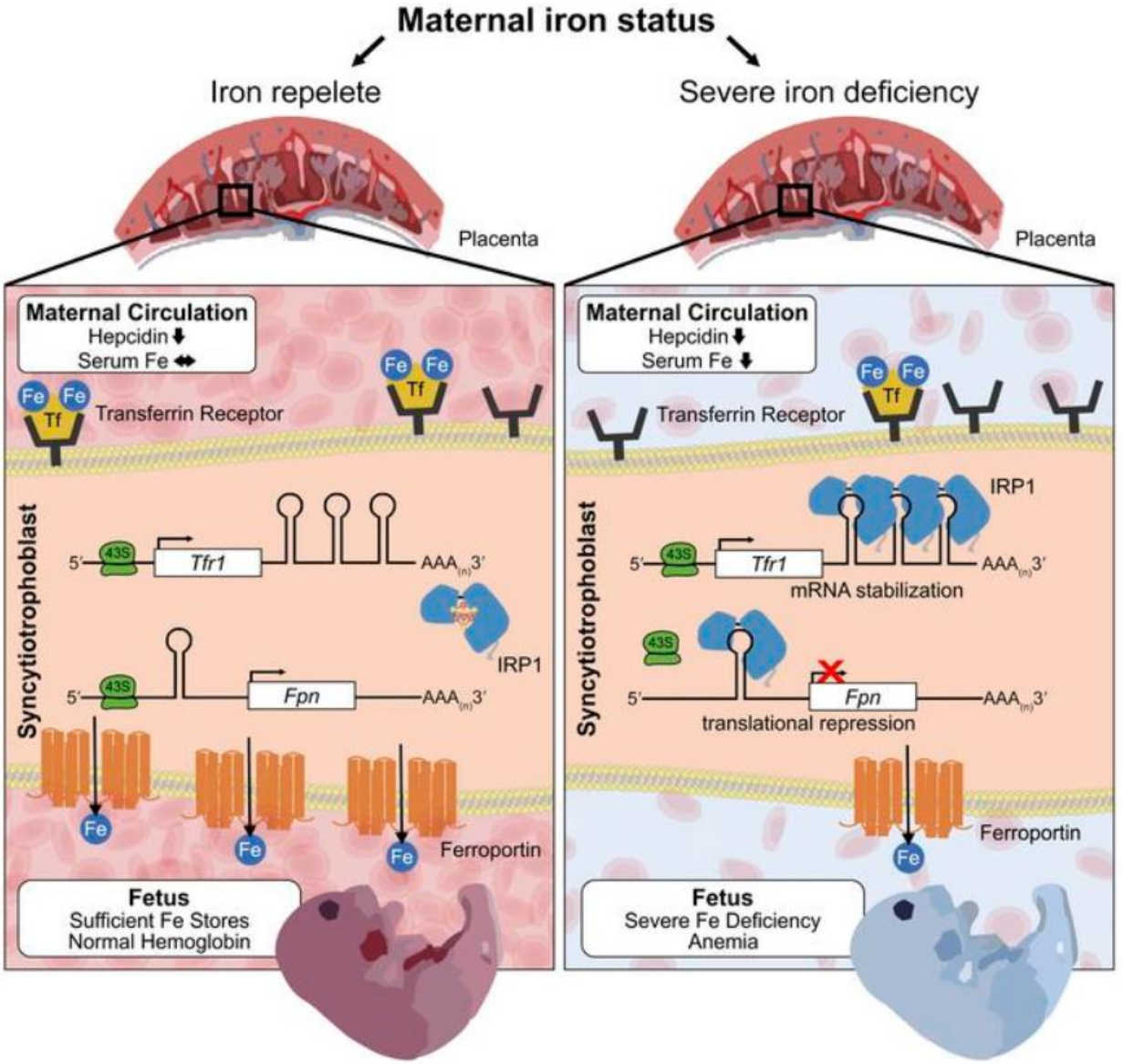

Figure 6. Effect of severe maternal iron deficiency on iron transporters in the placenta (3). (Left panel) Placental iron transporters in iron replete pregnancies. **(Right panel)** With maternal iron deficiency, iron regulatory protein 1 (IRP1) binds to 3' iron-response elements (IRE) within the UTR of *Tfr1* to promote stabilization, whereas binding to the 5' IRE within *Fpn* prevents translation of ferroportin mRNA. Through these mechanisms, during limited iron availability the placenta retains iron for itself, causing severe fetal iron deficiency and anemia.

maternal iron status affects the delivery of iron to the placenta and fetus in Chapter 1. We showed that both TFR1 and FPN are regulated by changes in maternal iron status in mouse and human placentas. Iron deficiency increases and iron loading decreases TFR1 (3,72). FPN is strongly

regulated by maternal iron deficiency (3) **(Figure 6)**. During maternal iron deficiency the placenta decreases FPN, which prioritizes its own iron at the expense of fetal iron deficiency, an adaptation mediated by iron regulatory protein 1 (IRP1) (3). In vitro models show that iron deficiency impairs trophoblast mitochondrial function, and thus the placental adaptation to low iron availability likely evolved to protect the fetus from the consequences of generalized placental dysfunction (3).

10. Iron disorders in pregnancy

Adequate iron supply is essential for a healthy pregnancy. Consequently, both maternal iron deficiency and iron excess are associated with pregnancy complications. We evaluated the effects of maternal iron excess and iron deficiency on the placenta and embryo development in mouse models in Chapters 4 and 6, respectively.

10.1 Iron deficiency and anemia

To meet the accelerating physiologic iron requirements, both dietary iron absorption as well as mobilization of iron from stores need to increase. Even with the most optimal diet containing high amounts of bioavailable iron, absorption of iron is only 3-4 mg/d (138), and is even lower with diets containing low amounts of bioavailable iron (138,139), characteristic of those in developing countries (139). Thus, increased dietary iron absorption is insufficient to meet the demands of pregnancy. Furthermore, many women enter pregnancy with insufficient iron stores, predisposing women to iron deficiency during pregnancy. In the United States, the prevalence of iron deficiency among pregnant women and women of child-bearing age has been reported to be 12%, with a higher rate in Black and Hispanic women (19 and 22%, respectively) (140,141). There is a higher incidence of iron deficiency in developing countries, reaching up to 60% of pregnant women in some African countries (141,142).

10.2 Iron overload

Pregnancies associated with iron excess include patients with hereditary hemochromatosis or β-thalassemia, the latter having well-documented pregnancy complications including prematurity, abortion, and intrauterine fetal death (143,144). However, even normal pregnancies may be exposed to excess iron when iron-supplemented, at least in part due to profoundly decreased maternal hepcidin allowing for highly efficient absorption of medicinal iron. Adverse effects associated with maternal iron excess during pregnancy are discussed in section 13.

11. Iron supplementation

Recognition of the detrimental effects of iron deficiency and anemia on maternal and infant health has led to the policy of iron supplementation during pregnancy, even without screening for preexisting iron deficiency. Iron supplementation is generally recommended in countries where risk for iron deficiency is high in women and children (145), but also in the United States and Canada (146), where more women are iron-replete than iron-deficient. Iron supplementation results in a lesser serum ferritin decrease in the third trimester. However, because ferritin production is also regulated by inflammatory cytokines, serum ferritin may not accurately reflect iron stores in the presence of inflammation. Nevertheless, in the developed world, more women are iron-replete than iron deficient when they become pregnant, prompting considerations of the potential risks of indiscriminate iron supplementation.

12. Inflammation and pregnancy

The maternal immune system plays an essential role in maintaining a healthy pregnancy. The maternal immune system is involved in implantation, angiogenesis and vascular remodeling at the

maternal-fetal interface, and in the development of the fetal immune system. In healthy pregnancy, the immune system regulates systemic levels of various cytokines and chemokines to maintain a non-inflammatory environment and to prevent fetal rejection. In complicated pregnancies, the presence of inflammation disrupts the coordinated regulation of cytokines and chemokines resulting in pregnancy complications. In developing countries, inflammation during pregnancy is common because of the high burden of endemic infections. In high-resource countries, common conditions associated with chronic systemic inflammation include obesity, diabetes, and autoimmune diseases, and for acute inflammation, bacterial and viral infections. We evaluated the effects of maternal acute and chronic inflammation during pregnancy in mouse models in Chapters 4 and 6 and found a dramatic adverse synergy between inflammation and either side of the maternal iron spectrum (iron deficiency and iron excess).

12.1 Acute inflammation with infections

Viral and bacterial infections during pregnancy are associated with adverse pregnancy outcomes including increased risk for preterm birth, neuropsychiatric disorders including schizophrenia and bipolar disorder, stillbirth, and birth defects in offspring (147-151). Rodent models that investigate the underlying mechanisms of maternal immune activation implicate IL-6 (152,153), IL-17 (154), and IL-2 (155) in schizophrenia- and autism-like behaviors. In humans, elevated maternal IL-8 was associated with increased risk of schizophrenia in adult offspring (156).

12.2 Chronic inflammatory conditions

Obesity is a chronic inflammatory condition and both obese humans and animal models are reported to have elevated cytokines including TNFα and IL-6 compared to lean controls (157-159). In humans, maternal obesity during pregnancy is associated with increased risk of antenatal complications, maternal morbidity, and adverse neonatal outcomes (160). Compared to women

with normal BMI, obese pregnant women have an increased risk of gestational diabetes mellitus, pre-eclampsia, induction of labor, delivery by emergency caesarian section, postpartum hemorrhage, infections, macrosomia, and intrauterine fetal death (161,162). Women with autoimmune disorders including systemic lupus erythematosus, rheumatoid arthritis and systemic sclerosis are considered a high-risk population for pregnancy complications, as these disorders are associated with adverse fetal outcomes and drug teratogenic risks (163,164).

13. U-shaped risk curve for iron status and pregnancy outcomes

Iron deficiency and anemia are global concerns among women of reproductive age. Although hemoglobin is physiologically decreased during pregnancy due to expansion of plasma volume that exceeds the increase in maternal RBC mass (dilutional anemia of pregnancy), greater than normal decrease in hemoglobin is associated with adverse outcomes (165). In pregnant women, iron deficiency and anemia are associated with poor mental and physical performance, increased cardiovascular strain, and increased risk of peripartum blood transfusions (166). Severe anemia greatly increases the risk of maternal mortality and accounts for nearly 20% of maternal deaths worldwide (167). Iron deficiency and anemia in the mother also has detrimental effects for the fetus such as increased risk of premature birth (<37 weeks' gestation), intrauterine growth restriction, and fetal death. In a prospective study in 829 pregnant women in China, preterm birth was associated with maternal anemia in early pregnancy (168). Risk of preterm delivery increased 1.6-fold when hemoglobin in the first trimester was between 10.0 and 10.9 g/dL, 2.6-fold when hemoglobin was between 9.0 and 9.9 g/dL, and 3.6-fold when hemoglobin was <9.0 g/dL (168). Despite the anemia-defining cutoffs of 10.5-11 g/d L (88), an analysis of nearly 150,000 pregnancies in the United Kingdom showed that the lowest rate of perinatal mortality was found

when maternal hemoglobin concentration during pregnancy was between 9 and 11 g/dL (169). The highest birth weight was also recorded in mothers whose hemoglobin concentration fell to 9-11 g/dL during pregnancy (170). These favorable outcomes may be related to an optimal plasma volume expansion (incidentally resulting in slightly lower hemoglobin concentrations), rather than any beneficial effect of iron deficiency and anemia.

The absence of a decrease in hemoglobin concentration during pregnancy is also associated with poor outcomes including preeclampsia, intrauterine growth retardation, preterm birth, and stillbirth (171-173). When the lowest recorded maternal hemoglobin concentrations were >11 g/dL, perinatal mortality increased (169). In a study of 44,000 singleton pregnancies in the United Kingdom, both low (<10.4 g/dL) and high (>13.2 g/dL) hemoglobin concentrations were associated with higher rates of preterm birth (174). A higher hemoglobin concentration is thought to relate to the failure to increase plasma volume, and adverse consequences may be caused by increased blood viscosity and decreased placental perfusion (169).

Ferritin also shows a U-shaped associated with birth outcomes. Abnormally low serum ferritin is associated with detrimental outcomes (175,176). High concentrations of serum ferritin are also associated with increased risk of preterm (<37 weeks' gestation) and very preterm (<32 weeks' gestation) birth, particularly when ferritin is elevated in the third trimester (177,178). One prospective study in pregnant women also indicated that failure of ferritin to drop in the second and third trimesters increased the risk of very preterm delivery by more than eightfold (179). High maternal high iron stores has also been linked to gestational diabetes, impaired fetal growth, and neurodevelopmental deficiencies (180-182). However, apart from reflecting higher iron stores in the mother, higher serum ferritin could also be reflecting the presence of inflammation in complicated pregnancies, as ferritin production is increased by inflammation. Thus, the association

of high ferritin with adverse pregnancy outcomes could reflect the effects of iron excess, or inflammation, or the combination of the two. Early evidence in animal models also shows that high iron may be teratogenic only during specific periods of embryonic development (183). In a study in 500 pregnant mice, intraperitoneal injection with ferric gluconate in early pregnancy (embryonic day 6-9) increased resorption on all days of gestation tested, yet malformation rate in pups was greatest when iron was injected on days eight (33%) and nine (17%), with primarily encephalic abnormalities (183). We demonstrated in Chapter 4 in mouse models that iron excess by itself did not have severe detrimental effect on the pregnancy, but when coexisting with acute or chronic inflammation, iron excess caused embryo demise or malformations. These findings suggest that the association of high ferritin with adverse pregnancy outcomes in humans may result from the interaction between iron and inflammation.

14. Summary

In this dissertation, we defined the molecular pathophysiology of iron regulation and transport during pregnancy, an understudied area to which we made several significant contributions. We demonstrated that maternal homeostatic adaptions during pregnancy are essential for fetal health and development and defined a novel phenomenon by which the placenta responds to severe maternal iron deficiency during pregnancy (Chapter 1). We clarified the roles of maternal and fetal hepcidin in normal pregnancy (Chapter 2) and those complicated by inflammation (Chapter 3). We discovered a novel interaction between iron and inflammation whereby maternal iron excess worsens inflammation-induced pregnancy complications causing severe fetal malformations and demise, occurring in a model of acute inflammation with LPS and chronic inflammation with diet-induced obesity (Chapter 4). We provided specific evidence that placental and fetal endothelial

cells are susceptible to injury from changes in iron content, and that iron excess sensitizes them to inflammation-induced apoptosis through oxidative stress, which was prevented by maternal anti-TNFα and antioxidant therapy (Chapter 4). We identified that in endothelial cells, iron modulates cholesterol homeostasis and induces proteolytic processing of a novel TNFα-receptor (Chapter 5). We further demonstrate that iron deficiency similarly interacts with both acute and chronic inflammation to worsen pregnancy complications, possibly occurring through iron-mediated changes in placental TNFα-receptor (Chapter 6). Taken together, our studies help explain the mechanisms underlying commonly observed pregnancy complications. Overall, these innovative concepts have both fundamental and translational impact and may eventually inform the clinical management of pregnant women worldwide.

15. Reference list

1. Fisher, A. L., and Nemeth, E. (2017) Iron homeostasis during pregnancy. *The American journal of clinical nutrition* **106**, 1567S-1574S
2. Camaschella, C., Nai, A., and Silvestri, L. (2020) Iron metabolism and iron disorders revisited in the hepcidin era. *Haematologica*, haematol.2019.232124
3. Sangkhae, V., Fisher, A. L., Wong, S., Koenig, M. D., Tussing-Humphreys, L., Chu, A., Lelić, M., Ganz, T., and Nemeth, E. (2020) Effects of maternal iron status on placental and fetal iron homeostasis. *The Journal of Clinical Investigation* **130**, 625-640
4. Bothwell, T. H. (2000) Iron requirements in pregnancy and strategies to meet them. *Am. J. Clin. Nutr* **72**, 257S-264S
5. Sangkhae, V., and Nemeth, E. (2019) Placental iron transport: The mechanism and regulatory circuits. *Free Radic Biol Med* **133**, 254-261
6. Frey, P. A., and Reed, G. H. (2012) The Ubiquity of Iron. *ACS Chemical Biology* **7**, 1477-1481
7. Johnson, D. C., Dean, D. R., Smith, A. D., and Johnson, M. K. (2005) Structure, function, and formation of biological iron-sulfur clusters. *Annu Rev Biochem* **74**, 247-281
8. Poulos, T. L. (2014) Heme enzyme structure and function. *Chem Rev* **114**, 3919-3962
9. Zhang, C. (2014) Essential functions of iron-requiring proteins in DNA replication, repair and cell cycle control. *Protein Cell* **5**, 750-760
10. Geissler, C., and Singh, M. (2011) Iron, meat and health. *Nutrients* **3**, 283-316
11. Ganz, T., and Nemeth, E. (2015) Iron homeostasis in host defence and inflammation. *Nat Rev Immunol* **15**, 500-510
12. Ganz, T. (2013) Systemic Iron Homeostasis. *Physiological Reviews* **93**, 1721-1741

13. Zhang, D.-L., Wu, J., Shah, B. N., Greutélaers, K. C., Ghosh, M. C., Ollivierre, H., Su, X.-z., Thuma, P. E., Bedu-Addo, G., Mockenhaupt, F. P., Gordeuk, V. R., and Rouault, T. A. (2018) Erythrocytic ferroportin reduces intracellular iron accumulation, hemolysis, and malaria risk. *Science* **359**, 1520-1523

14. VAN PUTTEN, L. M., and Croon, F. (1958) The Life Span of Red Cells in the Rat and the Mouse as Determined by Labeling with DFP32 in Vivo. *Blood* **13**, 789-794

15. Ganz, T., and Nemeth, E. (2012) Hepcidin and iron homeostasis. *Biochimica et Biophysica Acta (BBA) - Molecular Cell Research* **1823**, 1434-1443

16. McKie, A. T., Barrow, D., Latunde-Dada, G. O., Rolfs, A., Sager, G., Mudaly, E., Mudaly, M., Richardson, C., Barlow, D., Bomford, A., Peters, T. J., Raja, K. B., Shirali, S., Hediger, M. A., Farzaneh, F., and Simpson, R. J. (2001) An Iron-Regulated Ferric Reductase Associated with the Absorption of Dietary Iron. *Science* **291**, 1755

17. Gunshin, H., Mackenzie, B., Berger, U. V., Gunshin, Y., Romero, M. F., Boron, W. F., Nussberger, S., Gollan, J. L., and Hediger, M. A. (1997) Cloning and characterization of a mammalian proton-coupled metal-ion transporter. *Nature* **388**, 482-488

18. Fleming, M. D., Trenor, C. C., Su, M. A., Foernzler, D., Beier, D. R., Dietrich, W. F., and Andrews, N. C. (1997) Microcytic anaemia mice have a mutation in Nramp2, a candidate iron transporter gene. *Nature Genetics* **16**, 383-386

19. Poss, K. D., and Tonegawa, S. (1997) Heme oxygenase 1 is required for mammalian iron reutilization. *Proceedings of the National Academy of Sciences* **94**, 10919-10924

20. Donovan, A., Lima, C. A., Pinkus, J. L., Pinkus, G. S., Zon, L. I., Robine, S., and Andrews, N. C. (2005) The iron exporter ferroportin/Slc40a1 is essential for iron homeostasis. *Cell*

Metab **1**, 191-200

21. Vulpe, C. D., Kuo, Y.-M., Murphy, T. L., Cowley, L., Askwith, C., Libina, N., Gitschier, J., and Anderson, G. J. (1999) Hephaestin, a ceruloplasmin homologue implicated in intestinal iron transport, is defective in the sla mouse. *Nature Genetics* **21**, 195-199
22. Darwich, A. S., Aslam, U., Ashcroft, D. M., and Rostami-Hodjegan, A. (2014) Meta-Analysis of the Turnover of Intestinal Epithelia in Preclinical Animal Species and Humans. *Drug Metabolism and Disposition* **42**, 2016
23. Ohgami, R. S., Campagna, D. R., Greer, E. L., Antiochos, B., McDonald, A., Chen, J., Sharp, J. J., Fujiwara, Y., Barker, J. E., and Fleming, M. D. (2005) Identification of a ferrireductase required for efficient transferrin-dependent iron uptake in erythroid cells. *Nature Genetics* **37**, 1264-1269
24. Leidgens, S., Bullough, K. Z., Shi, H., Li, F., Shakoury-Elizeh, M., Yabe, T., Subramanian, P., Hsu, E., Natarajan, N., Nandal, A., Stemmler, T. L., and Philpott, C. C. (2013) Each Member of the Poly-r(C)-binding Protein 1 (PCBP) Family Exhibits Iron Chaperone Activity toward Ferritin. *Journal of Biological Chemistry* **288**, 17791-17802
25. Shi, H., Bencze, K. Z., Stemmler, T. L., and Philpott, C. C. (2008) A Cytosolic Iron Chaperone That Delivers Iron to Ferritin. *Science* **320**, 1207-1210
26. Harris, Z. L., Durley, A. P., Man, T. K., and Gitlin, J. D. (1999) Targeted gene disruption reveals an essential role for ceruloplasmin in cellular iron efflux. *Proceedings of the National Academy of Sciences* **96**, 10812-10817
27. Jenkitkasemwong, S., Wang, C. Y., Coffey, R., Zhang, W., Chan, A., Biel, T., Kim, J. S., Hojyo, S., Fukada, T., and Knutson, M. D. (2015) SLC39A14 is required for the development of hepatocellular iron overload in murine models of hereditary

hemochromatosis. *Cell Metab* **22**, 138-150

28. Coffey, R., and Knutson, M. D. (2017) The plasma membrane metal-ion transporter ZIP14 contributes to nontransferrin-bound iron uptake by human beta-cells. *Am J Physiol Cell Physiol* **312**, C169-c175

29. Wang, C. Y., and Knutson, M. D. (2013) Hepatocyte divalent metal-ion transporter-1 is dispensable for hepatic iron accumulation and non-transferrin-bound iron uptake in mice. *Hepatology* **58**, 788-798

30. Kew, M. C. (2014) Hepatic iron overload and hepatocellular carcinoma. *Liver Cancer* **3**, 31-40

31. Swaminathan, S., Fonseca, V. A., Alam, M. G., and Shah, S. V. (2007) The Role of Iron in Diabetes and Its Complications. *Diabetes Care* **30**, 1926

32. Gujja, P., Rosing, D. R., Tripodi, D. J., and Shizukuda, Y. (2010) Iron overload cardiomyopathy: better understanding of an increasing disorder. *J Am Coll Cardiol* **56**, 1001-1012

33. Ganz, T., and Nemeth, E. (2012) Hepcidin and iron homeostasis. *Biochim. Biophys. Acta* **1823**, 1434-1443

34. Park, C. H., Valore, E. V., Waring, A. J., and Ganz, T. (2001) Hepcidin, a urinary antimicrobial peptide synthesized in the liver. *J Biol Chem* **276**, 7806-7810

35. Nemeth, E., Tuttle, M. S., Powelson, J., Vaughn, M. B., Donovan, A., Ward, D. M., Ganz, T., and Kaplan, J. (2004) Hepcidin Regulates Cellular Iron Efflux by Binding to Ferroportin and Inducing Its Internalization. *Science* **306**, 2090-2093

36. Aschemeyer, S., Qiao, B., Stefanova, D., Valore, E. V., Sek, A. C., Ruwe, T. A., Vieth, K. R., Jung, G., Casu, C., Rivella, S., Jormakka, M., Mackenzie, B., Ganz, T., and Nemeth,

E. (2018) Structure-function analysis of ferroportin defines the binding site and an alternative mechanism of action of hepcidin. *Blood* **131**, 899-910

37. D'Alessio, F., Hentze, M. W., and Muckenthaler, M. U. (2012) The hemochromatosis proteins HFE, TfR2, and HJV form a membrane-associated protein complex for hepcidin regulation. *J Hepatol* **57**, 1052-1060

38. Schmidt, P. J., Toran, P. T., Giannetti, A. M., Bjorkman, P. J., and Andrews, N. C. (2008) The transferrin receptor modulates Hfe-dependent regulation of hepcidin expression. *Cell Metab* **7**, 205-214

39. Canali, S., Zumbrennen-Bullough, K. B., Core, A. B., Wang, C. Y., Nairz, M., Bouley, R., Swirski, F. K., and Babitt, J. L. (2017) Endothelial cells produce bone morphogenetic protein 6 required for iron homeostasis in mice. *Blood* **129**, 405-414

40. Canali, S., Wang, C. Y., Zumbrennen-Bullough, K. B., Bayer, A., and Babitt, J. L. (2017) Bone morphogenetic protein 2 controls iron homeostasis in mice independent of Bmp6. *Am J Hematol* **92**, 1204-1213

41. Casanovas, G., Mleczko-Sanecka, K., Altamura, S., Hentze, M. W., and Muckenthaler, M. U. (2009) Bone morphogenetic protein (BMP)-responsive elements located in the proximal and distal hepcidin promoter are critical for its response to HJV/BMP/SMAD. *Journal of Molecular Medicine* **87**, 471-480

42. Babitt, J. L., Huang, F. W., Wrighting, D. M., Xia, Y., Sidis, Y., Samad, T. A., Campagna, J. A., Chung, R. T., Schneyer, A. L., Woolf, C. J., Andrews, N. C., and Lin, H. Y. (2006) Bone morphogenetic protein signaling by hemojuvelin regulates hepcidin expression. *Nature Genetics* **38**, 531-539

43. Niederkofler, V., Salie, R., and Arber, S. (2005) Hemojuvelin is essential for dietary iron

sensing, and its mutation leads to severe iron overload. *The Journal of Clinical Investigation* **115**, 2180-2186

44. Meynard, D., Kautz, L., Darnaud, V., Canonne-Hergaux, F., Coppin, H., and Roth, M.-P. (2009) Lack of the bone morphogenetic protein BMP6 induces massive iron overload. *Nature Genetics* **41**, 478-481

45. Silvestri, L., Pagani, A., Nai, A., De Domenico, I., Kaplan, J., and Camaschella, C. (2008) The serine protease matriptase-2 (TMPRSS6) inhibits hepcidin activation by cleaving membrane hemojuvelin. *Cell Metab* **8**, 502-511

46. Kautz, L., Jung, G., Valore, E. V., Rivella, S., Nemeth, E., and Ganz, T. (2014) Identification of erythroferrone as an erythroid regulator of iron metabolism. *Nat Genet* **46**, 678-684

47. Arezes, J., Foy, N., McHugh, K., Sawant, A., Quinkert, D., Terraube, V., Brinth, A., Tam, M., LaVallie, E. R., Taylor, S., Armitage, A. E., Pasricha, S. R., Cunningham, O., Lambert, M., Draper, S. J., Jasuja, R., and Drakesmith, H. (2018) Erythroferrone inhibits the induction of hepcidin by BMP6. *Blood* **132**, 1473-1477

48. Wang, C.-Y., Xu, Y., Traeger, L., Dogan, D. Y., Xiao, X., Steinbicker, A. U., and Babitt, J. L. (2020) Erythroferrone lowers hepcidin by sequestering BMP2/6 heterodimer from binding to the BMP type I receptor ALK3. *Blood* **135**, 453-456

49. Kautz, L., Jung, G., Du, X., Gabayan, V., Chapman, J., Nasoff, M., Nemeth, E., and Ganz, T. (2015) Erythroferrone contributes to hepcidin suppression and iron overload in a mouse model of beta-thalassemia. *Blood* **126**, 2031-2037

50. Nemeth, E., Rivera, S., Gabayan, V., Keller, C., Taudorf, S., Pedersen, B. K., and Ganz, T. (2004) IL-6 mediates hypoferremia of inflammation by inducing the synthesis of the iron

regulatory hormone hepcidin. *The Journal of Clinical Investigation* **113**, 1271-1276

51. Pietrangelo, A., Dierssen, U., Valli, L., Garuti, C., Rump, A., Corradini, E., Ernst, M., Klein, C., and Trautwein, C. (2007) STAT3 Is Required for IL-6-gp130–Dependent Activation of Hepcidin In Vivo. *Gastroenterology* **132**, 294-300
52. Wrighting, D. M., and Andrews, N. C. (2006) Interleukin-6 induces hepcidin expression through STAT3. *Blood* **108**, 3204-3209
53. Rodriguez, R., Jung, C. L., Gabayan, V., Deng, J. C., Ganz, T., Nemeth, E., and Bulut, Y. (2014) Hepcidin induction by pathogens and pathogen-derived molecules is strongly dependent on interleukin-6. *Infection and immunity* **82**, 745-752
54. Stefanova, D., Raychev, A., Arezes, J., Ruchala, P., Gabayan, V., Skurnik, M., Dillon, B. J., Horwitz, M. A., Ganz, T., Bulut, Y., and Nemeth, E. (2017) Endogenous hepcidin and its agonist mediate resistance to selected infections by clearing non-transferrin-bound iron. *Blood* **130**, 245-257
55. Nemeth, E., and Ganz, T. (2014) Anemia of inflammation. *Hematol Oncol Clin North Am* **28**, 671-vi
56. Lakhal-Littleton, S., Wolna, M., Chung, Y. J., Christian, H. C., Heather, L. C., Brescia, M., Ball, V., Diaz, R., Santos, A., Biggs, D., Clarke, K., Davies, B., and Robbins, P. A. (2016) An essential cell-autonomous role for hepcidin in cardiac iron homeostasis. *Elife* **5**
57. Zlatanova, I., Pinto, C., Bonnin, P., Mathieu, J. R. R., Bakker, W., Vilar, J., Lemitre, M., Voehringer, D., Vaulont, S., Peyssonnaux, C., and Silvestre, J. S. (2019) Iron Regulator Hepcidin Impairs Macrophage-Dependent Cardiac Repair After Injury. *Circulation* **139**, 1530-1547
58. Malerba, M., Louis, S., Cuvellier, S., Shambat, S. M., Hua, C., Gomart, C., Fouet, A.,

Ortonne, N., Decousser, J. W., Zinkernagel, A. S., Mathieu, J. R., and Peyssonnaux, C. (2020) Epidermal hepcidin is required for neutrophil response to bacterial infection. *J Clin Invest* **130**, 329-334

59. Bessman, N. J., Mathieu, J. R. R., Renassia, C., Zhou, L., Fung, T. C., Fernandez, K. C., Austin, C., Moeller, J. B., Zumerle, S., Louis, S., Vaulont, S., Ajami, N. J., Sokol, H., Putzel, G. G., Arvedson, T., Sockolow, R. E., Lakhal-Littleton, S., Cloonan, S. M., Arora, M., Peyssonnaux, C., and Sonnenberg, G. F. (2020) Dendritic cell-derived hepcidin sequesters iron from the microbiota to promote mucosal healing. *Science* **368**, 186-189

60. Hallberg, L., and Rossander-Hulten, L. (1991) Iron requirements in menstruating women. *Am. J. Clin. Nutr* **54**, 1047-1058

61. Barrett, J. F., Whittaker, P. G., Williams, J. G., and Lind, T. (1994) Absorption of non-haem iron from food during normal pregnancy. *BMJ (Clinical research ed.)* **309**, 79-82

62. Milman, N. (2006) Iron and pregnancy--a delicate balance. *Annals of hematology* **85**, 559-565

63. Young, M. F., Griffin, I., Pressman, E., McIntyre, A. W., Cooper, E., McNanley, T., Harris, Z. L., Westerman, M., and O'Brien, K. O. (2012) Maternal hepcidin is associated with placental transfer of iron derived from dietary heme and nonheme sources. *J Nutr* **142**, 33-39

64. Hubbard, A. C., Bandyopadhyay, S., Wojczyk, B. S., Spitalnik, S. L., Hod, E. A., and Prestia, K. A. (2013) Effect of dietary iron on fetal growth in pregnant mice. *Comp Med* **63**, 127-135

65. Lin, W., and Kirksey, A. (1976) Effects of different levels of dietary iron on pregnancy superimposed upon growth in the rat. *J. Nutr* **106**, 543-554

66. Gao, G., Liu, S. Y., Wang, H. J., Zhang, T. W., Yu, P., Duan, X. L., Zhao, S. E., and Chang, Y. Z. (2015) Effects of Pregnancy and Lactation on Iron Metabolism in Rats. *Biomed. Res. Int* **2015**, 105325

67. van Santen, S., Kroot, J. J., Zijderveld, G., Wiegerinck, E. T., Spaanderman, M. E., and Swinkels, D. W. (2013) The iron regulatory hormone hepcidin is decreased in pregnancy: a prospective longitudinal study. *Clinical chemistry and laboratory medicine* **51**, 1395-1401

68. Bah, A., Pasricha, S. R., Jallow, M. W., Sise, E. A., Wegmuller, R., Armitage, A. E., Drakesmith, H., Moore, S. E., and Prentice, A. M. (2017) Serum Hepcidin Concentrations Decline during Pregnancy and May Identify Iron Deficiency: Analysis of a Longitudinal Pregnancy Cohort in The Gambia. *J Nutr*

69. Millard, K. N., Frazer, D. M., Wilkins, S. J., and Anderson, G. J. (2004) Changes in the expression of intestinal iron transport and hepatic regulatory molecules explain the enhanced iron absorption associated with pregnancy in the rat. *Gut* **53**, 655-660

70. Young, M. F., Griffin, I., Pressman, E., McIntyre, A. W., Cooper, E., McNanley, T., Harris, Z. L., Westerman, M., and O'Brien, K. O. (2012) Maternal hepcidin is associated with placental transfer of iron derived from dietary heme and nonheme sources. *Journal of Nutrition* **142**, 33-39

71. Rehu, M., Punnonen, K., Ostland, V., Heinonen, S., Westerman, M., Pulkki, K., and Sankilampi, U. (2010) Maternal serum hepcidin is low at term and independent of cord blood iron status. *Eur. J Haematol* **85**, 345-352

72. Sangkhae, V., Fisher, A. L., Chua, K. J., Ruchala, P., Ganz, T., and Nemeth, E. (2020) Maternal Hepcidin Determines Embryo Iron Homeostasis. *Blood*

73. Koenig, M. D., Tussing-Humphreys, L., Day, J., Cadwell, B., and Nemeth, E. (2014) Hepcidin and iron homeostasis during pregnancy. *Nutrients* **6**, 3062-3083

74. Schulze, K. J., Christian, P., Ruczinski, I., Ray, A. L., Nath, A., Wu, L. S., and Semba, R. D. (2008) Hepcidin and iron status among pregnant women in Bangladesh. *Asia Pac. J. Clin. Nutr* **17**, 451-456

75. Moretti, D., Goede, J. S., Zeder, C., Jiskra, M., Chatzinakou, V., Tjalsma, H., Melse-Boonstra, A., Brittenham, G., Swinkels, D. W., and Zimmermann, M. B. (2015) Oral iron supplements increase hepcidin and decrease iron absorption from daily or twice-daily doses in iron-depleted young women. *Blood* **126**, 1981-1989

76. Nemeth, E., Rivera, S., Gabayan, V., Keller, C., Taudorf, S., Pedersen, B. K., and Ganz, T. (2004) IL-6 mediates hypoferremia of inflammation by inducing the synthesis of the iron regulatory hormone hepcidin. *J Clin Invest* **113**, 1271-1276

77. Ganz, T., Olbina, G., Girelli, D., Nemeth, E., and Westerman, M. (2008) Immunoassay for human serum hepcidin. *Blood* **112**, 4292-4297

78. Pena-Rosas, J. P., De-Regil, L. M., Gomez, M. H., Flores-Urrutia, M. C., and Dowswell, T. (2015) Intermittent oral iron supplementation during pregnancy. *Cochrane. Database. Syst. Rev*, CD009997

79. Ru, Y., Pressman, E. K., Cooper, E. M., Guillet, R., Katzman, P. J., Kent, T. R., Bacak, S. J., and O'Brien, K. O. (2016) Iron deficiency and anemia are prevalent in women with multiple gestations. *Am J Clin Nutr* **104**, 1052-1060

80. Dao, M. C., Sen, S., Iyer, C., Klebenov, D., and Meydani, S. N. (2013) Obesity during pregnancy and fetal iron status: is Hepcidin the link? *Journal of perinatology : official journal of the California Perinatal Association* **33**, 177-181

81. Cao, C., Pressman, E. K., Cooper, E. M., Guillet, R., Westerman, M., and O'Brien, K. O. (2016) Prepregnancy Body Mass Index and Gestational Weight Gain Have No Negative Impact on Maternal or Neonatal Iron Status. *Reproductive sciences* **23**, 613-622

82. Toldi, G., Stenczer, B., Molvarec, A., Takats, Z., Beko, G., Rigo, J., Jr., and Vasarhelyi, B. (2010) Hepcidin concentrations and iron homeostasis in preeclampsia. *Clin Chem. Lab Med* **48**, 1423-1426

83. Ramsey, M. (2010) Normal hematological changes during pregnancy and the puerperium. in *The obstetric hematology manual* (Pavord, S., and Hunt, B. eds.), Cambridge University Press, Cambridge. pp 1-11

84. PRITCHARD, J. A. (1965) Changes in blood volume during pregnancy and delivery. *Anesthesiology* **26**, 393-399

85. Peck, T. M., and Arias, F. (1979) Hematologic changes associated with pregnancy. *Clin. Obstet. Gynecol* **22**, 785-798

86. Faupel-Badger, J. M., Hsieh, C. C., Troisi, R., Lagiou, P., and Potischman, N. (2007) Plasma volume expansion in pregnancy: implications for biomarkers in population studies. *Cancer Epidemiol. Biomarkers Prev* **16**, 1720-1723

87. Bauer, K. A. (2016) Hematologic changes in pregnancy. in *UpToDate* (Post, T. W. ed.), UpToDate, Waltham, MA. pp

88. Lurie, S., and Danon, D. (1992) Life span of erythrocytes in late pregnancy. *Obstet. Gynecol* **80**, 123-126

89. Lurie, S., and Mamet, Y. (2000) Red blood cell survival and kinetics during pregnancy. *Eur. J. Obstet. Gynecol. Reprod. Biol* **93**, 185-192

90. McMullin, M. F., White, R., Lappin, T., Reeves, J., and MacKenzie, G. (2003)

Haemoglobin during pregnancy: relationship to erythropoietin and haematinic status. *Eur. J. Haematol* **71**, 44-50

91. Zanjani, E. D., Peterson, E. N., Gordon, A. S., and Wasserman, L. R. (1974) Erythropoietin production in the fetus: role of the kidney and maternal anemia. *J. Lab Clin. Med* **83**, 281-287

92. Clapp, J. F., III, Little, K. D., and Widness, J. A. (2003) Effect of maternal exercise and fetoplacental growth rate on serum erythropoietin concentrations. *Am. J. Obstet. Gynecol* **188**, 1021-1025

93. Barton, D. P., Joy, M. T., Lappin, T. R., Afrasiabi, M., Morel, J. G., O'Riordan, J., Murphy, J. F., and O'Herlihy, C. (1994) Maternal erythropoietin in singleton pregnancies: a randomized trial on the effect of oral hematinic supplementation. *Am. J. Obstet. Gynecol* **170**, 896-901

94. Malek, A., Sager, R., Eckardt, K. U., Bauer, C., and Schneider, H. (1994) Lack of transport of erythropoietin across the human placenta as studied by an in vitro perfusion system. *Pflugers Arch* **427**, 157-161

95. Widness, J. A., Schmidt, R. L., and Sawyer, S. T. (1995) Erythropoietin transplacental passage--review of animal studies. *J. Perinat. Med* **23**, 61-70

96. Dame, C., Fahnenstich, H., Freitag, P., Hofmann, D., bdul-Nour, T., Bartmann, P., and Fandrey, J. (1998) Erythropoietin mRNA expression in human fetal and neonatal tissue. *Blood* **92**, 3218-3225

97. Erdem, A., Erdem, M., Arslan, M., Yazici, G., Eskandari, R., and Himmetoglu, O. (2002) The effect of maternal anemia and iron deficiency on fetal erythropoiesis: comparison between serum erythropoietin, hemoglobin and ferritin levels in mothers and newborns. *J.*

Matern. Fetal Neonatal Med **11**, 329-332

98. Jazayeri, A., Tsibris, J. C., and Spellacy, W. N. (1999) Fetal erythropoietin levels in growth-restricted and appropriately grown neonates with and without abnormal fetal heart rate tracings: a comparison with cord blood gases and Apgar scores. *J. Perinatol* **19**, 255-259

99. Teramo, K. A., and Widness, J. A. (2009) Increased fetal plasma and amniotic fluid erythropoietin concentrations: markers of intrauterine hypoxia. *Neonatology* **95**, 105-116

100. Whittaker, P. G., Macphail, S., and Lind, T. (1996) Serial hematologic changes and pregnancy outcome. *Obstet. Gynecol* **88**, 33-39

101. Milman, N., Agger, A. O., and Nielsen, O. J. (1991) Iron supplementation during pregnancy. Effect on iron status markers, serum erythropoietin and human placental lactogen. A placebo controlled study in 207 Danish women. *Danish medical bulletin* **38**, 471-476

102. Romslo, I., Haram, K., Sagen, N., and Augensen, K. (1983) Iron requirement in normal pregnancy as assessed by serum ferritin, serum transferrin saturation and erythrocyte protoporphyrin determinations. *British journal of obstetrics and gynaecology* **90**, 101-107

103. Larsson, A., Palm, M., Hansson, L. O., and Axelsson, O. (2008) Reference values for clinical chemistry tests during normal pregnancy. *BJOG* **115**, 874-881

104. Milman, N., Bergholt, T., Byg, K. E., Eriksen, L., and Hvas, A. M. (2007) Reference intervals for haematological variables during normal pregnancy and postpartum in 434 healthy Danish women. *Eur. J. Haematol* **79**, 39-46

105. van den Broek, N. R., Letsky, E. A., White, S. A., and Shenkin, A. (1998) Iron status in pregnant women: which measurements are valid? *Br J Haematol* **103**, 817-824

106. Carriaga, M. T., Skikne, B. S., Finley, B., Cutler, B., and Cook, J. D. (1991) Serum transferrin receptor for the detection of iron deficiency in pregnancy. *Am. J. Clin. Nutr* **54**, 1077-1081

107. Cao, C., and O'Brien, K. O. (2013) Pregnancy and iron homeostasis: an update. *Nutrition reviews* **71**, 35-51

108. Rossant, J., and Cross, J. C. (2001) Placental development: lessons from mouse mutants. *Nat Rev Genet* **2**, 538-548

109. Levy, J. E., Jin, O., Fujiwara, Y., Kuo, F., and Andrews, N. C. (1999) Transferrin receptor is necessary for development of erythrocytes and the nervous system. *Nat Genet* **21**, 396-399

110. Cao, C., and Fleming, M. D. (2016) The placenta: the forgotten essential organ of iron transport. *Nutr. Rev* **74**, 421-431

111. Bastin, J., Drakesmith, H., Rees, M., Sargent, I., and Townsend, A. (2006) Localisation of proteins of iron metabolism in the human placenta and liver. *Br. J. Haematol* **134**, 532-543

112. Georgieff, M. K., Wobken, J. K., Welle, J., Burdo, J. R., and Connor, J. R. (2000) Identification and localization of divalent metal transporter-1 (DMT-1) in term human placenta. *Placenta* **21**, 799-804

113. Srai, S. K., Bomford, A., and McArdle, H. J. (2002) Iron transport across cell membranes: molecular understanding of duodenal and placental iron uptake. *Best. Pract. Res. Clin. Haematol* **15**, 243-259

114. Ohgami, R. S., Campagna, D. R., McDonald, A., and Fleming, M. D. (2006) The Steap proteins are metalloreductases. *Blood* **108**, 1388-1394

115. Best, C. M., Pressman, E. K., Cao, C., Cooper, E., Guillet, R., Yost, O. L., Galati, J., Kent,

T. R., and O'Brien, K. O. (2016) Maternal iron status during pregnancy compared with neonatal iron status better predicts placental iron transporter expression in humans. *FASEB J*

116. Gambling, L., Czopek, A., Andersen, H. S., Holtrop, G., Srai, S. K., Krejpcio, Z., and McArdle, H. J. (2009) Fetal iron status regulates maternal iron metabolism during pregnancy in the rat. *Am. J. Physiol Regul. Integr. Comp Physiol* **296**, R1063-R1070

117. Fleming, M. D., Romano, M. A., Su, M. A., Garrick, L. M., Garrick, M. D., and Andrews, N. C. (1998) Nramp2 is mutated in the anemic Belgrade (b) rat: evidence of a role for Nramp2 in endosomal iron transport. *Proc. Natl. Acad. Sci. U. S. A* **95**, 1148-1153

118. Gunshin, H., Fujiwara, Y., Custodio, A. O., Direnzo, C., Robine, S., and Andrews, N. C. (2005) Slc11a2 is required for intestinal iron absorption and erythropoiesis but dispensable in placenta and liver. *J. Clin. Invest* **115**, 1258-1266

119. Wang, C. Y., Jenkitkasemwong, S., Duarte, S., Sparkman, B. K., Shawki, A., Mackenzie, B., and Knutson, M. D. (2012) ZIP8 is an iron and zinc transporter whose cell-surface expression is up-regulated by cellular iron loading. *J. Biol. Chem* **287**, 34032-34043

120. Galvez-Peralta, M., He, L., Jorge-Nebert, L. F., Wang, B., Miller, M. L., Eppert, B. L., Afton, S., and Nebert, D. W. (2012) ZIP8 zinc transporter: indispensable role for both multiple-organ organogenesis and hematopoiesis in utero. *PLOS One* **7**, e36055

121. Hojyo, S., Fukada, T., Shimoda, S., Ohashi, W., Bin, B. H., Koseki, H., and Hirano, T. (2011) The zinc transporter SLC39A14/ZIP14 controls G-protein coupled receptor-mediated signaling required for systemic growth. *PLOS One* **6**, e18059

122. Donovan, A., Brownlie, A., Zhou, Y., Shepard, J., Pratt, S. J., Moynihan, J., Paw, B. H., Drejer, A., Barut, B., Zapata, A., Law, T. C., Brugnara, C., Lux, S. E., Pinkus, G. S., Pinkus,

J. L., Kingsley, P. D., Palis, J., Fleming, M. D., Andrews, N. C., and Zon, L. I. (2000) Positional cloning of zebrafish ferroportin1 identifies a conserved vertebrate iron exporter. *Nature* **403**, 776-781

123. Evans, P., Cindrova-Davies, T., Muttukrishna, S., Burton, G. J., Porter, J., and Jauniaux, E. (2011) Hepcidin and iron species distribution inside the first-trimester human gestational sac. *Mol Hum Reprod* **17**, 227-232

124. Guller, S., Buhimschi, C. S., Ma, Y. Y., Huang, S. T., Yang, L., Kuczynski, E., Zambrano, E., Lockwood, C. J., and Buhimschi, I. A. (2008) Placental expression of ceruloplasmin in pregnancies complicated by severe preeclampsia. *Lab Invest* **88**, 1057-1067

125. Li, Y. Q., Bai, B., Cao, X. X., Yan, H., and Zhuang, G. H. (2012) Ferroportin 1 and hephaestin expression in BeWo cell line with different iron treatment. *Cell Biochem. Funct* **30**, 249-255

126. Chen, H., Attieh, Z. K., Syed, B. A., Kuo, Y. M., Stevens, V., Fuqua, B. K., Andersen, H. S., Naylor, C. E., Evans, R. W., Gambling, L., Danzeisen, R., Bacouri-Haidar, M., Usta, J., Vulpe, C. D., and McArdle, H. J. (2010) Identification of zyklopen, a new member of the vertebrate multicopper ferroxidase family, and characterization in rodents and human cells. *J. Nutr* **140**, 1728-1735

127. Harris, Z. L., Durley, A. P., Man, T. K., and Gitlin, J. D. (1999) Targeted gene disruption reveals an essential role for ceruloplasmin in cellular iron efflux. *Proc. Natl. Acad. Sci. U. S. A* **96**, 10812-10817

128. Vulpe, C. D., Kuo, Y. M., Murphy, T. L., Cowley, L., Askwith, C., Libina, N., Gitschier, J., and Anderson, G. J. (1999) Hephaestin, a ceruloplasmin homologue implicated in intestinal iron transport, is defective in the sla mouse. *Nat. Genet* **21**, 195-199

129. Fuqua, B., Lu, Y., Darshan, D., Frazer, D., Wilkins, S., Page, K., Vulpe, C., and Anderson, G. (2014) The role of multicopper ferroxidases in mammalian iron homeostasis (995.2). *The FASEB Journal* **28**

130. Keel, S. B., Doty, R. T., Yang, Z., Quigley, J. G., Chen, J., Knoblaugh, S., Kingsley, P. D., Vaughn, M. B., Kaplan, J., Palis, J., and Abkowitz, J. L. (2008) A heme export protein is required for red blood cell differentiation and iron homeostasis. *Science* **319**, 825-828

131. Jaacks, L. M., Young, M. F., Essley, B. V., McNanley, T. J., Cooper, E. M., Pressman, E. K., McIntyre, A. W., Orlando, M. S., Abkowitz, J. L., Guillet, R., and O'Brien, K. O. (2011) Placental expression of the heme transporter, feline leukemia virus subgroup C receptor, is related to maternal iron status in pregnant adolescents. *J Nutr* **141**, 1267-1272

132. Lamparelli, R. D., Friedman, B. M., MacPhail, A. P., Bothwell, T. H., Phillips, J. I., and Baynes, R. D. (1989) The fate of intravenously injected tissue ferritin in pregnant guinea-pigs. *Br J Haematol* **72**, 100-105

133. Li, L., Fang, C. J., Ryan, J. C., Niemi, E. C., Lebrón, J. A., Björkman, P. J., Arase, H., Torti, F. M., Torti, S. V., Nakamura, M. C., and Seaman, W. E. (2010) Binding and uptake of H-ferritin are mediated by human transferrin receptor-1. *Proc Natl Acad Sci U S A* **107**, 3505-3510

134. Li, J. Y., Paragas, N., Ned, R. M., Qiu, A., Viltard, M., Leete, T., Drexler, I. R., Chen, X., Sanna-Cherchi, S., Mohammed, F., Williams, D., Lin, C. S., Schmidt-Ott, K. M., Andrews, N. C., and Barasch, J. (2009) Scara5 is a ferritin receptor mediating non-transferrin iron delivery. *Dev Cell* **16**, 35-46

135. Nicolas, G., Bennoun, M., Porteu, A., Mativet, S., Beaumont, C., Grandchamp, B., Sirito, M., Sawadogo, M., Kahn, A., and Vaulont, S. (2002) Severe iron deficiency anemia in

transgenic mice expressing liver hepcidin. *Proc Natl Acad Sci U S A* **99**, 4596-4601

136. Willemetz, A., Lenoir, A., Deschemin, J. C., Lopez-Otin, C., Ramsay, A. J., Vaulont, S., and Nicolas, G. (2014) Matriptase-2 is essential for hepcidin repression during fetal life and postnatal development in mice to maintain iron homeostasis. *Blood* **124**, 441-444

137. Fisher, A. L., Sangkhae, V., Presicce, P., Chougnet, C. A., Jobe, A. H., Kallapur, S. G., Tabbah, S., Buhimschi, C. S., Buhimschi, I. A., Ganz, T., and Nemeth, E. (2020) Fetal and amniotic fluid iron homeostasis in healthy and complicated murine, macaque, and human pregnancy. *JCI Insight* **5**

138. Hallberg, L. a. H., L. (1996) Iron requirements, iron balance and iron deficiency in menstruating pregnant women. in *Iron Nutrition in Health and Disease* (Hallberg, L. a. A., N.-G. ed.), John Libbey and Company, London. pp 165-182

139. Zimmermann, M. B., Chaouki, N., and Hurrell, R. F. (2005) Iron deficiency due to consumption of a habitual diet low in bioavailable iron: a longitudinal cohort study in Moroccan children. *Am J Clin Nutr* **81**, 115-121

140. (2002) Iron deficiency--United States, 1999-2000. *MMWR. Morbidity and mortality weekly report* **51**, 897-899

141. McLean, E., Cogswell, M., Egli, I., Wojdyla, D., and de Benoist, B. (2009) Worldwide prevalence of anaemia, WHO Vitamin and Mineral Nutrition Information System, 1993-2005. *Public Health Nutr* **12**, 444-454

142. Organization, U. N. W. H. (2001) *Iron Deficiency Anaemia: Assesment, Prevention and Control: a Guide for Programme Managers*, World Health Organization

143. Tuck, S. M., Jensen, C. E., Wonke, B., and Yardumian, A. (1998) Pregnancy management and outcomes in women with thalassaemia major. *J Pediatr Endocrinol Metab* **11 Suppl**

3, 923-928

144. Fozza, C., Asara, M. A., Vacca, N., Caggiari, S., Monti, A., Zaccheddu, F., Capobianco, G., Dessole, S., Dore, F., and Antonucci, R. (2017) Pregnancy Outcome among Women with Beta-Thalassemia Major in North Sardinia. *Acta Haematol* **138**, 166-167

145. Allen, L. H., De Benoist, B., Dary, O., Hurrell, R. (2006) *Guidelines on food fortification with micronutrients*, World Health Organization, Geneva, Switzerland

146. O'Brien, K. O., and Ru, Y. (2017) Iron status of North American pregnant women: an update on longitudinal data and gaps in knowledge from the United States and Canada. *Am J Clin Nutr*

147. Racicot, K., and Mor, G. (2017) Risks associated with viral infections during pregnancy. *The Journal of Clinical Investigation* **127**, 1591-1599

148. Page, J. M., Bardsley, T., Thorsten, V., Allshouse, A. A., Varner, M. W., Debbink, M. P., Dudley, D. J., Saade, G. R., Goldenberg, R. L., Stoll, B., Hogue, C. J., Bukowski, R., Conway, D., Reddy, U. M., and Silver, R. M. (2019) Stillbirth Associated With Infection in a Diverse U.S. Cohort. *Obstet Gynecol* **134**, 1187-1196

149. Gibbs, R. S. (2001) The relationship between infections and adverse pregnancy outcomes: an overview. *Ann Periodontol* **6**, 153-163

150. Brown, A. S., Begg, M. D., Gravenstein, S., Schaefer, C. A., Wyatt, R. J., Bresnahan, M., Babulas, V. P., and Susser, E. S. (2004) Serologic evidence of prenatal influenza in the etiology of schizophrenia. *Arch Gen Psychiatry* **61**, 774-780

151. Parboosing, R., Bao, Y., Shen, L., Schaefer, C. A., and Brown, A. S. (2013) Gestational influenza and bipolar disorder in adult offspring. *JAMA Psychiatry* **70**, 677-685

152. Smith, S. E., Li, J., Garbett, K., Mirnics, K., and Patterson, P. H. (2007) Maternal immune

activation alters fetal brain development through interleukin-6. *J Neurosci* **27**, 10695-10702

153. Hsiao, E. Y., and Patterson, P. H. (2011) Activation of the maternal immune system induces endocrine changes in the placenta via IL-6. *Brain Behav Immun* **25**, 604-615

154. Choi, G. B., Yim, Y. S., Wong, H., Kim, S., Kim, H., Kim, S. V., Hoeffer, C. A., Littman, D. R., and Huh, J. R. (2016) The maternal interleukin-17a pathway in mice promotes autism-like phenotypes in offspring. *Science* **351**, 933-939

155. Ponzio, N. M., Servatius, R., Beck, K., Marzouk, A., and Kreider, T. (2007) Cytokine levels during pregnancy influence immunological profiles and neurobehavioral patterns of the offspring. *Ann N Y Acad Sci* **1107**, 118-128

156. Brown, A. S., Hooton, J., Schaefer, C. A., Zhang, H., Petkova, E., Babulas, V., Perrin, M., Gorman, J. M., and Susser, E. S. (2004) Elevated maternal interleukin-8 levels and risk of schizophrenia in adult offspring. *Am J Psychiatry* **161**, 889-895

157. Aronson, D., Bartha, P., Zinder, O., Kerner, A., Markiewicz, W., Avizohar, O., Brook, G. J., and Levy, Y. (2004) Obesity is the major determinant of elevated C-reactive protein in subjects with the metabolic syndrome. *Int J Obes Relat Metab Disord* **28**, 674-679

158. Katsuki, A., Sumida, Y., Murashima, S., Murata, K., Takarada, Y., Ito, K., Fujii, M., Tsuchihashi, K., Goto, H., Nakatani, K., and Yano, Y. (1998) Serum Levels of Tumor Necrosis Factor-α Are Increased in Obese Patients with Noninsulin-Dependent Diabetes Mellitus1. *The Journal of Clinical Endocrinology & Metabolism* **83**, 859-862

159. Roytblat, L., Rachinsky, M., Fisher, A., Greemberg, L., Shapira, Y., Douvdevani, A., and Gelman, S. (2000) Raised interleukin-6 levels in obese patients. *Obes Res* **8**, 673-675

160. Harper, A. (2015) Reducing morbidity and mortality among pregnant obese. *Best Pract*

Res Clin Obstet Gynaecol **29**, 427-437

161. Sebire, N. J., Jolly, M., Harris, J. P., Wadsworth, J., Joffe, M., Beard, R. W., Regan, L., and Robinson, S. (2001) Maternal obesity and pregnancy outcome: a study of 287,213 pregnancies in London. *Int J Obes Relat Metab Disord* **25**, 1175-1182

162. Scott-Pillai, R., Spence, D., Cardwell, C. R., Hunter, A., and Holmes, V. A. (2013) The impact of body mass index on maternal and neonatal outcomes: a retrospective study in a UK obstetric population, 2004-2011. *BJOG* **120**, 932-939

163. Mecacci, F., Pieralli, A., Bianchi, B., and Paidas, M. J. (2007) The impact of autoimmune disorders and adverse pregnancy outcome. *Semin Perinatol* **31**, 223-226

164. Chen, J. S., Roberts, C. L., Simpson, J. M., and March, L. M. (2015) Pregnancy Outcomes in Women With Rare Autoimmune Diseases. *Arthritis Rheumatol* **67**, 3314-3323

165. Garn, S. M., Ridella, S. A., Petzold, A. S., and Falkner, F. (1981) Maternal hematologic levels and pregnancy outcomes. *Semin Perinatol* **5**, 155-162

166. Breymann, C. (2015) Iron Deficiency Anemia in Pregnancy. *Semin Hematol* **52**, 339-347

167. Black, R. E., Allen, L. H., Bhutta, Z. A., Caulfield, L. E., de Onis, M., Ezzati, M., Mathers, C., Rivera, J., Maternal, and Child Undernutrition Study, G. (2008) Maternal and child undernutrition: global and regional exposures and health consequences. *Lancet* **371**, 243-260

168. Zhou, L. M., Yang, W. W., Hua, J. Z., Deng, C. Q., Tao, X., and Stoltzfus, R. J. (1998) Relation of hemoglobin measured at different times in pregnancy to preterm birth and low birth weight in Shanghai, China. *Am J Epidemiol* **148**, 998-1006

169. Little, M. P., Brocard, P., Elliott, P., and Steer, P. J. (2005) Hemoglobin concentration in pregnancy and perinatal mortality: a London-based cohort study. *Am. J. Obstet. Gynecol*

193, 220-226

170. Steer, P. J. (2000) Maternal hemoglobin concentration and birth weight. *Am. J. Clin. Nutr* **71**, 1285S-1287S

171. Huisman, A., and Aarnoudse, J. G. (1986) Increased 2nd trimester hemoglobin concentration in pregnancies later complicated by hypertension and growth retardation. Early evidence of a reduced plasma volume. *Acta Obstet. Gynecol. Scand* **65**, 605-608

172. Murphy, J. F., O'Riordan, J., Newcombe, R. G., Coles, E. C., and Pearson, J. F. (1986) Relation of haemoglobin levels in first and second trimesters to outcome of pregnancy. *Lancet* **1**, 992-995

173. Stephansson, O., Dickman, P. W., Johansson, A., and Cnattingius, S. (2000) Maternal hemoglobin concentration during pregnancy and risk of stillbirth. *JAMA* **284**, 2611-2617

174. Murphy, J. F., O'Riordan, J., Newcombe, R. G., Coles, E. C., and Pearson, J. F. (1986) Relation of haemoglobin levels in first and second trimesters to outcome of pregnancy. *Lancet* **1**, 992-995

175. Scholl, T. O., Hediger, M. L., Fischer, R. L., and Shearer, J. W. (1992) Anemia vs iron deficiency: increased risk of preterm delivery in a prospective study. *Am J Clin Nutr* **55**, 985-988

176. Scholl, T. O., and Hediger, M. L. (1994) Anemia and iron-deficiency anemia: compilation of data on pregnancy outcome. *Am J Clin Nutr* **59**, 492S-500S discussion 500S-501S

177. Goldenberg, R. L., Tamura, T., DuBard, M., Johnston, K. E., Copper, R. L., and Neggers, Y. (1996) Plasma ferritin and pregnancy outcome. *Am J Obstet Gynecol* **175**, 1356-1359

178. Tamura, T., Goldenberg, R. L., Johnston, K. E., Cliver, S. P., and Hickey, C. A. (1996) Serum ferritin: a predictor of early spontaneous preterm delivery. *Obstet Gynecol* **87**, 360-

365

179. Scholl, T. O. (1998) High third-trimester ferritin concentration: associations with very preterm delivery, infection, and maternal nutritional status. *Obstet Gynecol* **92**, 161-166

180. Rawal, S., Hinkle, S. N., Bao, W., Zhu, Y., Grewal, J., Albert, P. S., Weir, N. L., Tsai, M. Y., and Zhang, C. (2017) A longitudinal study of iron status during pregnancy and the risk of gestational diabetes: findings from a prospective, multiracial cohort. *Diabetologia* **60**, 249-257

181. Scholl, T. O. (2005) Iron status during pregnancy: setting the stage for mother and infant. *Am J Clin Nutr* **81**, 1218S-1222S

182. Scholl, T. O., and Reilly, T. (2000) Anemia, iron and pregnancy outcome. *J Nutr* **130**, 443S-447S

183. Kuchta, B. (1982) Experiments and Ultrastructural Investigations on the Mouse Embryo during Early Teratogen-Sensitive Stages. *Acta Anat* **113**, 218-225

CHAPTER 1: EFFECTS OF MATERNAL IRON STATUS ON PLACENTAL AND FETAL IRON HOMEOSTASIS

Effects of maternal iron status on placental and fetal iron homeostasis

Veena Sangkhae,[1] Allison L. Fisher,[1,2] Shirley Wong,[1] Mary Dawn Koenig,[3] Lisa Tussing-Humphreys,[4,5] Alison Chu,[6] Melisa Lelić,[7] Tomas Ganz,[1] and Elizabeta Nemeth[1]

[1]Center for Iron Disorders, Department of Medicine, and [2]Molecular, Cellular and Integrative Physiology Graduate Program, David Geffen School of Medicine at UCLA, Los Angeles, California, USA.

[3]Department of Women's, Children's and Family Health Science, College of Nursing, [4]Division of Academic Internal Medicine, Department of Medicine, and [5]Institute for Health Research and Policy, University of Illinois at Chicago (UIC), Chicago, Illinois, USA. [6]Department of Pediatrics, Division of Neonatology and Developmental Biology, David Geffen School of Medicine at UCLA, Los Angeles, California, USA. [7]Medical Faculty, University of Tuzla, Tuzla, Bosnia and Herzegovina.

Iron deficiency is common worldwide and is associated with adverse pregnancy outcomes. The increasing prevalence of indiscriminate iron supplementation during pregnancy also raises concerns about the potential adverse effects of iron excess. We examined how maternal iron status affects the delivery of iron to the placenta and fetus. Using mouse models, we documented maternal homeostatic mechanisms that protect the placenta and fetus from maternal iron excess. We determined that under physiological conditions or in iron deficiency, fetal and placental hepcidin did not regulate fetal iron endowment. With maternal iron deficiency, critical transporters mediating placental iron uptake (transferrin receptor 1 [TFR1]) and export (ferroportin [FPN]) were strongly regulated. In mice, not only was TFR1 increased, but FPN was surprisingly decreased to preserve placental iron in the face of fetal iron deficiency. In human placentas from pregnancies with mild iron deficiency, TFR1 was increased, but there was no change in FPN. However, induction of more severe iron deficiency in human trophoblast in vitro resulted in the regulation of both TFR1 and FPN, similar to what was observed in the mouse model. This placental adaptation that prioritizes placental iron is mediated by iron regulatory protein 1 (IRP1) and is important for the maintenance of mitochondrial respiration, thus ultimately protecting the fetus from the potentially dire consequences of generalized placental dysfunction.

Conflict of interest: TG and EN are shareholders of and scientific advisors for Intrinsic LifeSciences and Silarus Therapeutics and are consultants for Ionis Pharmaceuticals, Protagonist Therapeutics, Keryx Biopharmaceuticals, La Jolla Pharmaceutical Company, and Vifor Pharma. TG is a consultant for Akebia and Gilead.

Submitted: January 10, 2019; **Accepted:** October 22, 2019; **Published:** December 17, 2019.
Reference information: *J Clin Invest*. 2020;130(2):625–640. https://doi.org/10.1172/JCI127341.

Introduction

Iron is essential for a healthy pregnancy, with approximately 1 gram of iron needed for the expansion of maternal red cell mass and placental and fetal development (1). Severe iron deficiency and iron deficiency anemia during pregnancy have been associated with increased maternal mortality, perinatal death, preterm birth, low birth weight, impaired immune function, and long-term cognitive defects in newborns and infants (2–6). To prevent these adverse outcomes, the WHO currently recommends daily iron supplementation for all pregnant adolescent and adult women (7). On the other side of the spectrum, however, the consequences of high maternal iron levels in pregnancy are not well understood (8). Excess iron can result in the generation of harmful ROS that damage proteins, lipids, and nucleic acids (9), or in increased susceptibility to infection (10). Maternal serum ferritin, a marker of iron stores, has a U-shaped association with adverse pregnancy outcomes (11, 12). However, elevated ferritin is not only a marker of increased iron stores but also of inflammation, and the specific contribution of excess iron has not been resolved. Despite its importance, it is poorly understood how maternal and fetal iron homeostasis during pregnancy is regulated, including the relative contribution of the maternal, placental, and/or fetal signals.

On the systemic level, iron homeostasis is regulated by the hepatic hormone hepcidin, which controls iron absorption and recycling. Hepcidin is induced when systemic iron levels are high and downregulates its receptor, ferroportin (FPN), thereby preventing iron export to blood plasma (13). Thus, changes in hepcidin levels can rapidly modulate plasma iron concentrations. In human pregnancy, maternal hepcidin is suppressed during the second and third trimesters, which is thought to increase iron availability for transfer to the placenta (1). The mechanism of maternal hepcidin suppression is unknown, as is the effect of maternal iron status on this regulatory circuitry.

Iron endowment of the fetus is entirely dependent on iron transport through the placenta. Iron-transferrin (Fe-Tf) from the maternal circulation is taken up by transferrin receptor 1 (TFR1), which is located on the apical surface of the syncytiotrophoblast (14). The complex of Fe-Tf and TFR1 is endocytosed, and iron is released in the endosome and eventually exported on the basal side of the placental syncytiotrophoblast through the iron transporter FPN into the fetal circulation (15). Both TFR1 and FPN are thought to be critical for iron transport across the placenta, as global deletion of either transporter results in embryonic death (16, 17). Embryonic lethality in TFR1-KO mice occurs before E12.5 (16) and in FPN-KO mice before E9.5 (17). However, the placenta- specific role was only demonstrated for FPN, in which preservation of FPN expression in the placenta but not the embryo proper rescued embryonic lethality (17). The regulation of iron transporters in normal pregnancy or in pathologic conditions such as iron deficiency, iron restriction, or inflammation has not been extensively explored. It was reported that expression of placental TFR1 increased in response to maternal iron deficiency in humans and animal models (18, 19), and this was interpreted as a compensatory mechanism to ensure iron delivery to the fetus. Our data refine this model and suggest that both TFR1 and FPN are subject to regulation during iron deficiency, particularly in its more severe forms.

On the cellular level, iron homeostasis is regulated by iron- regulatory proteins 1 and 2 (IRP1 and IRP2), which control the stability or translation of mRNAs containing iron-responsive elements (IREs) on their 3′ or 5′ termini, respectively (20). During cellular iron deficiency, IRPs bind to IREs, repressing the translation of mRNAs encoding proteins involved in cellular iron export (FPN) or storage (ferritin) and stabilizing mRNAs encoding proteins involved in iron uptake (TFR1, DMT1), thus maintaining cellular iron levels in the face of iron deficiency. Double IRP1 and IRP2 deficiency is embryonically lethal, whereas mice with the individual IRP KO are viable (21), but the role of these IRPs in regulating materno-fetal iron transfer has not been explored.

We studied mouse models of pregnancy over its time course, as well as human pregnancies and primary human trophoblast cells (PHTs) in vitro, and examined the mechanisms by which maternal iron status (iron-replete, iron-deficient, and iron-loaded) affects the transfer of iron from the mother to the fetus. We found that maternal hepcidin, through regulation of maternal plasma iron concentrations, determines the amount of iron taken up by the placenta and protects the fetus from iron excess even when the mother is iron overloaded. However, we were surprised to discover that during severe maternal iron deficiency, the placenta downregulates FPN to maintain its own iron homeostasis, resulting in decreased iron availability for transfer to the fetus. We devised the placental iron deficiency index (PIDI), a ratio of placental FPN and TFR1, as a sensitive and biologically relevant measure of iron deficiency of the materno- fetal unit. We present evidence that placental iron homeostasis is mediated by the IRE/IRP system to maintain placental function including functional preservation of the placenta's mitochondrial electron transport chain (ETC).

Results

Effect of maternal iron status on hepcidin and iron availability during pregnancy. In humans, the iron regulatory hormone hepcidin is suppressed during the second and third trimesters of pregnancy (22); however, the mechanisms driving hepcidin suppression remain unknown. To determine whether maternal hepcidin suppression is a consequence of changes in maternal iron status, we assessed suppression in iron-deficient, iron-replete, and iron-loaded WT C57BL/6 dams. Female mice between 6 and 8 weeks of age were either fed a standard chow diet (185 ppm iron) or a low-iron diet (4 ppm iron) 2 weeks prior to and throughout pregnancy, or were injected with 20 mg iron dextran at the time of mating (Figure 1A). Pregnant animals were analyzed on E12.5, E15.5, and E18.5 (gestation in C57BL/6 mice is approximately 19 days). Females that were subjected to the same iron regimen but did not get pregnant were used as controls and were euthanized on the same day as the pregnant dams. In nonpregnant females, expression of hepcidin (*Hamp*) mRNA and protein (Figure 1, B and C) changed as expected, depending on the iron status of the mice: iron deficiency lowered hepcidin and iron loading increased hepcidin levels compared with the iron-replete group (serum hepcidin 19, 83, and 346 ng/mL; $P < 0.001$ deficient vs. replete and $P < 0.001$ replete vs. loaded, by 1-way ANOVA and the Holm-Sidak method for multiple comparisons). Compared with nonpregnant females of the same iron status, pregnant females in each group had decreased hepcidin at all time points examined (E12.5–E18.5), replicating the changes observed in human pregnancy (23). Decreased hepcidin was not caused by hemodilution of pregnancy, as equivalent changes were observed for both liver mRNA and

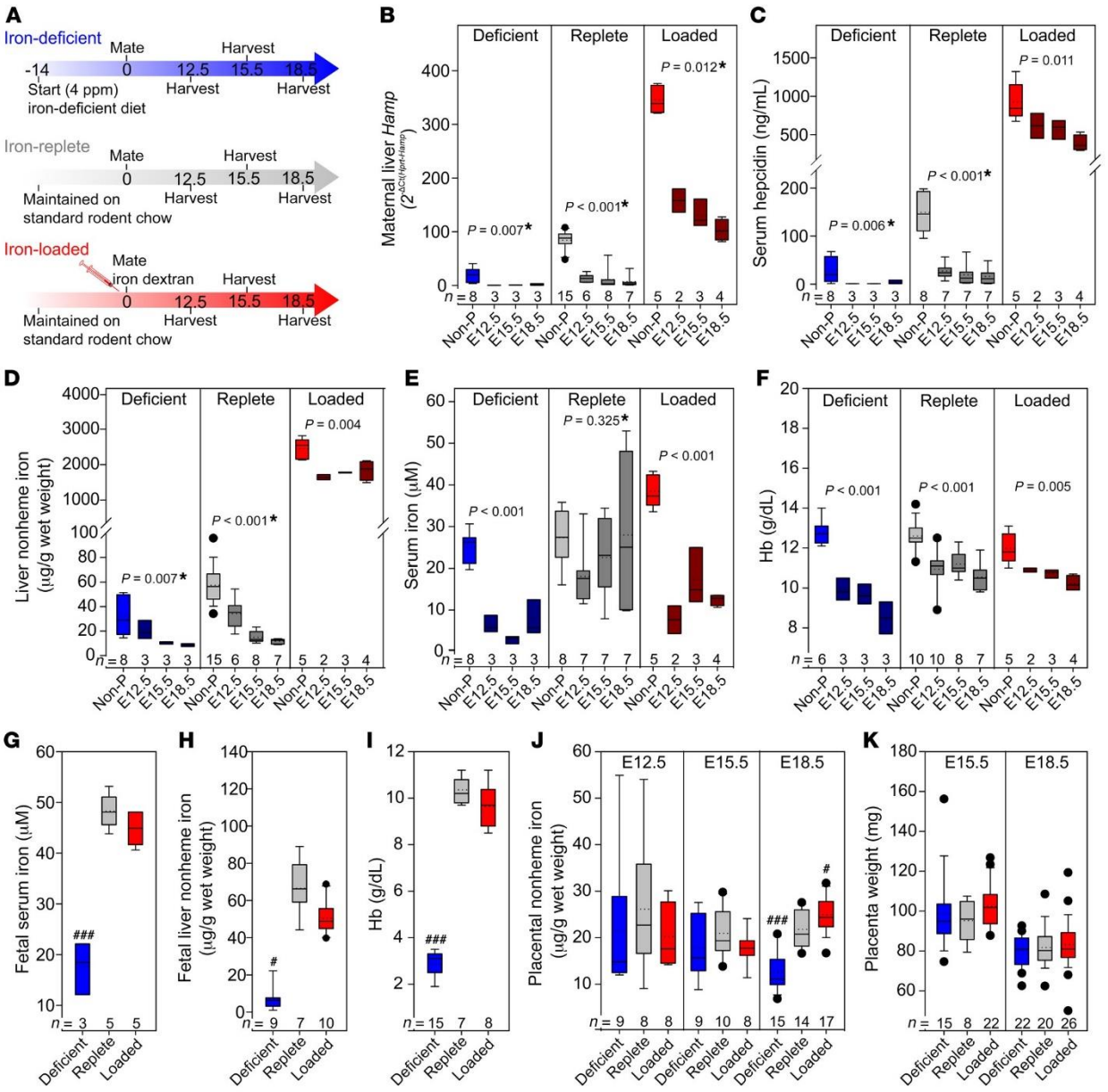

Figure 1. Maternal hepcidin and serum iron levels determine embryo and placental iron status. The iron status of WT C57BL/6 female mice was altered using diet or iron dextran injections. (**A**) Adult females were fed standard chow (185 ppm iron) or a low-iron diet (4 ppm iron) ad libitum 2 weeks prior to and throughout pregnancy or were injected with 20 mg iron dextran at the time of mating. Pregnant females were analyzed at E12.5, E15.5, and E18.5. Nonpregnant (Non-P) females were subjected to an equivalent iron treatment. (**B**–**F**) Maternal measurements of (**B**) hepcidin (*Hamp*) mRNA and (**C**) serum hepcidin. (**D**) Liver nonheme iron. (**E**) Serum iron concentration. (**F**) Hb concentration. Statistical differences between groups was determined by 1-way ANOVA for normally distributed values, or otherwise by 1-way ANOVA on ranks (indicated by a single asterisk after the *P* value). (**G**–**I**) Embryo measurements at E18.5 for (**G**) serum iron and (**H**) liver nonheme iron. (**I**) Hb concentration. (**J**) Placental nonheme iron levels at E12.5, E15.5, and E18.5. (**K**) Placental weight at E15.5 and E18.5 (we did not obtain whole placentas at E12.5). Statistical differences between groups was determined by 1-way ANOVA for normally distributed values followed by the Holm-Sidak method for multiple comparisons versus the iron-replete control group ($^{###}P < 0.001$) or 1-way ANOVA on ranks followed by Dunn's method for multiple comparisons versus the iron-replete control group ($^{#}P < 0.05$). The numbers of animals are indicated in the *x* axes of the box and whisker plots.

serum protein levels (Figure 1, B and C). Importantly, hepcidin suppression was preserved under all maternal iron states: E18.5 serum hepcidin was reduced compared with nonpregnant control levels to 12% in iron-deficient, 11% in iron-replete, and 42% in iron-overloaded conditions (Figure 1C). However, maternal hepcidin was still relatively higher in iron-loaded compared with iron-replete pregnancies, suggesting that iron loading partially counteracts the suppressive pregnancy signal.

Liver nonheme iron concentrations gradually decreased from E12.5 to E18.5 compared with values in nonpregnant control mice, indicating that pregnancy induces iron mobilization from stores (Figure 1D). We surmised that the lowering of hepcidin preceded liver iron mobilization, as at the earliest time point examined, E12.5, hepcidin mRNA and protein levels in iron- replete animals were already nearly maximally suppressed (92% of maximal serum hepcidin suppression), whereas the decrease in levels of liver iron compared with nonpregnant levels was not yet maximally suppressed at E12.5 (51% of maximal liver iron suppression) (Figure 1, B–D, middle panels). More important, as a result of decreased hepcidin and iron mobilization from stores, serum iron concentration was maintained throughout pregnancy in iron-replete dams (Figure 1E, middle panel), despite intense utilization of iron for fetal growth during this period. Maintenance of serum iron levels at E18.5 despite low liver stores may be possible because of the relatively high iron content in standard mouse chow.

Unlike iron-replete mothers, both iron-deficient and iron-overloaded mothers were hypoferremic between E12.5 and E18.5 (Figure 1E). This was expected in the iron-deficient group, as both iron stores and dietary iron content were low and obviously insufficient to maintain serum iron levels, even with profoundly decreased hepcidin. Surprisingly, though, when mothers were iron loaded, serum iron was lower compared with levels in nonpregnant animals ($P < 0.001$, by 1-way ANOVA) and also compared with levels detected in iron-replete pregnant animals ($P = 0.028$ for pregnant iron-replete vs. iron-loaded animals, by 2-way ANOVA) (Figure 1E). This is almost certainly due to the relatively higher level of maternal hepcidin at E12.5–E18.5, limiting the release of excess iron from stores (Figure 1, B and C, right panel). Changes in maternal transferrin saturation (Supplemental Figure 1; supplemental material available online with this article; https://doi.org/10.1172/JCI127341DS1) paralleled the changes in serum iron levels.

In iron-replete and iron-loaded pregnant animals, hemoglobin (Hb) concentrations and RBC counts were lower compared with nonpregnant levels, as expected (Figure 1F and Supplemental Table 1), because of pregnancy-associated plasma volume expansion. In the iron-deficient group, despite a decrease in hepcidin to nearly undetectable levels, mothers developed frank iron deficiency anemia with decreased Hb (diet, $P < 0.001$), RBC counts ($P = 0.002$), mean corpuscular volume (MCV) (diet, $P < 0.001$), and mean corpuscular Hb (MCH) (diet, $P = 0.016$ for iron-deficient vs. iron-replete mice, by 2-way ANOVA) (Figure 1F and Supplemental Table 1).

Maternal regulation of iron bioavailability prevents embryonic iron overload but does not protect the embryo from iron deficiency. To determine the consequences of varied maternal iron status for the embryo and placenta, we measured embryonic hematological and iron parameters for pregnancies at E18.5 (see Figure 1). Embryos from iron-deficient mothers were severely iron deficient, as reflected by the decrease in serum and liver iron concentrations (Figure 1, G and H). Additionally, brain and whole embryo iron concentrations were decreased (Supplemental Figure 2, A and B). Furthermore, embryonic anemia was much more severe than that in their mothers (Hb in Figure 1I; complete CBC in Supplemental Table 2). Thus, maternal adaptations to iron deficiency were not sufficient to protect the embryos from severe iron deficiency anemia. Embryos from iron-loaded pregnancies, however, had serum iron, liver iron, and hematological parameters similar to those of embryos from control iron-replete pregnancies (Figure 1, G–I). These data suggest that maternal iron regulatory mechanisms including that involving hepcidin protect embryos from iron overload even when mothers are iron loaded.

We observed similar results when iron deficiency and iron overload were caused by alternative approaches: feeding the mice an iron-deficient diet starting at mating (short-term) rather than 2 weeks prior to mating (long-term), or feeding females a high-iron diet (10,000 ppm) starting 2 weeks prior to pregnancy instead of injecting the females with iron dextran at mating. A short-term iron-deficient diet resulted in changes in maternal, fetal, and placental parameters similar to those seen with longer-term iron deficiency (Supplemental Figure 3 and Supplemental Tables 3 and 4), with somewhat less impaired maternal hematocrit levels and MCV. Iron loading through a high-iron diet efficiently increased maternal liver iron compared with levels in iron-replete animals at E18.5 ($P = 0.006$; *t* test on ranks for iron-replete vs. 10,000 ppm). Despite maternal iron loading, serum iron concentrations at E18.5 were not higher than those in iron-replete group ($P = 0.709$; 2-tailed *t* test for iron-replete vs. 10,000 ppm), presumably because of the relative increase in maternal hepcidin. In a comparison of the 2 iron-loading models, however, we found that dietary iron loading resulted in higher maternal serum iron levels. This in turn resulted in increased placental iron content and mildly increased fetal liver iron, although fetal liver iron content remained comparable to that in iron-replete fetuses ($P = 0.981$;

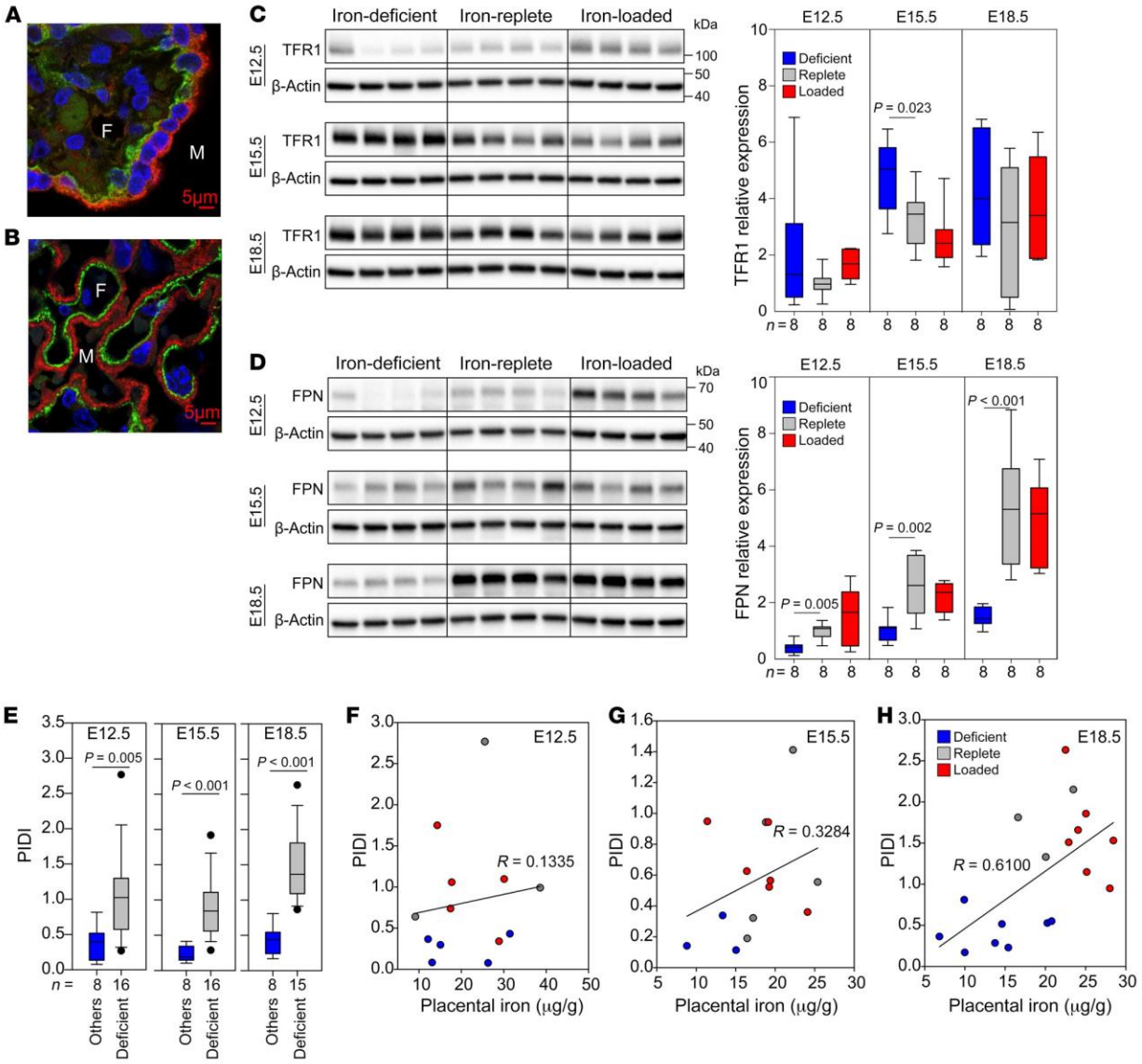

Figure 2. Placental iron transporters respond to changes in maternal iron status. Immunofluorescence staining of human (**A**) and mouse (**B**) placentas for TFR1 (red) and FPN (green). Original magnification, ×100. Nuclei are blue. M, maternal circulation; F, fetal circulation. Mouse placentas from Figure 1 were analyzed by Western blotting to determine the protein concentration of TFR1 (**C**) and FPN (**D**). β-Actin was used as a loading control. Four representative placentas are shown in the Western blots, and a total of 8 placentas (from 3 to 4 different dams per group) were used for quantitation. Data are presented as the mean ± SEM. Statistical differences between groups were determined by 1-way ANOVA for normally distributed values followed by the Holm-Sidak method for multiple comparisons versus the iron-replete control group. (**E**) The PIDI is the ratio of expression of placental FPN protein to placental TFR1 protein and reflects iron export to the fetus relative to iron import into the placenta from the maternal circulation. Statistical differences were determined using a 2-tailed Student's *t* test. (**F**–**H**) Correlation of nonheme iron with the PIDI at E12.5, E15.5, and E18.5. The numbers of animals are indicated in the *x*-axes of the box and whisker plots.

2-tailed *t* test for iron- replete vs. 10,000 ppm) (Supplemental Figure 3, B, F, and H). This suggests that the mode of iron administration during pregnancy could result in subtle differences in iron bioavailability.

When maternal iron availability is low in mice, placental iron homeostasis is prioritized despite fetal iron deficiency. Iron delivery to the fetus is wholly dependent on transfer from the maternal circulation through the placenta, yet factors affecting this transfer

are not fully understood. To evaluate the effect of maternal iron status on placental iron content and transport, we analyzed placentas from the pregnancies depicted in Figure 1 at E12.5, E15.5, and E18.5. Placental nonheme iron in the iron-loaded group was only slightly increased at E18.5 compared with the iron-replete group (Figure 1J). The moderation of fetal overload is likely a consequence of the relatively low serum iron concentrations in the maternal circulation, which are maintained by maternal hepcidin. In iron-deficient pregnancies, placental nonheme iron concentrations were comparable to those for other groups at E12.5 and E15.5 and were mildly decreased at E18.5 compared with placental concentrations in iron-replete or iron-loaded pregnancies (Figure 1J), with no change in placental weight (Figure 1K). The decrease in placental iron concentrations at E18.5 was significantly less than the iron decrease detected in fetal livers or fetal Hb (~2-fold in the placenta compared with a 10-fold decrease in fetal livers and a 3.6-fold decrease in fetal Hb). Furthermore, placental heme iron content measured at E18.5 was not different between iron-deficient and iron-replete pregnancies, whereas fetal liver heme iron at E18.5 was significantly lower in the iron-deficient group (Supplemental Figure 2, C and D). Our data suggest that the placenta prioritizes its own iron homeostasis despite fetal iron deficiency.

The principal transporters mediating cellular iron uptake and efflux, TFR1 and FPN, are abundantly expressed in human and mouse syncytiotrophoblast (Figure 2, A and B). We measured TFR1 and FPN protein levels in placentas at E12.5, E15.5, and E18.5 in iron-deficient, iron-replete, and iron-loaded mouse pregnancies (Figure 2, C and D). Protein levels of both transporters increased with gestational age, presumably to meet the increasing iron needs of the developing embryo. We found that TFR1 expression was maximal by E15.5, whereas FPN expression was maximal at E18.5 (Figure 2, C and D). Interestingly, TFR1 expression was not strongly affected by maternal iron status. During maternal iron deficiency, TFR1 protein levels were moderately increased only at E15.5 compared with levels in the iron-replete group (Figure 2C), but these levels were not significantly higher at the other 2 time points (E12.5 and E18.5). TFR1 expression was not different in the iron-loaded group compared with the iron-replete group at any time point examined. Surprisingly, maternal iron deficiency resulted in significantly decreased FPN protein expression at all time points (Figure 2D), with no difference observed in FPN levels between the iron-replete and iron-loaded groups. Decreased FPN during iron deficiency could compromise iron delivery to the fetus while maintaining placental iron content. This is consistent with our observation that maternal iron deficiency had a more profound impact on fetal iron homeostasis than on the placenta: fetuses had dramatically decreased Hb as well as decreased nonheme and heme iron content in fetal liver, whereas placental nonheme and heme iron levels were much less affected or unaffected (Supplemental Figure 2, C and D). Regulation of placental iron transporters during iron deficiency suggests the existence of placental iron–sensing mechanisms that maintain placental iron homeostasis to the detriment of fetal iron endowment. Interestingly, unlike TFR1 and FPN, we observed that placental ferritin expression did not increase with gestational age (Supplemental Figure 4) and was more responsive to iron loading than was ferroportin (at E18.5). This could be related to ferritin expression in multiple placental cell types (24), unlike FPN, which is primarily expressed in the syncytiotrophoblast.

We devised the PIDI as a ratio of expression of placental FPN to placental TFR1 protein. A decrease in FPN or an increase in TFR1 or changes in both transporters would lead to a lower PIDI, which would be indicative of placental sensing of iron deficiency and a greater risk of fetal iron deficiency. The PIDI was lower in iron-deficient pregnancies compared with that for iron-replete pregnancies at all 3 time points measured (E12.5, E15.5, and E18.5) (Figure 2E), reflecting a consistent placenta response, whereby iron was prioritized to the placenta, resulting in decreased fetal iron endowment. For assessment of placental iron handling, we argue that using the ratio of FPN to TFR1 in the same placental sample is superior to evaluating single transporter levels, as the ratio method minimizes the variability in single transporter expression related to placental sampling inconsistencies, which is of particular concern in human placenta analysis.

The correlation between placental nonheme iron levels and the PIDI was marginal at earlier pregnancy time points (E12.5, $R = 0.1335$; E15.5, $R = 0.3284$) (Figure 2, F and G). This is expected, considering that placental iron levels were maintained in the constant range (Figure 1J) by the alterations in placental iron transporters (Figure 2, C and D). We observed a stronger positive correlation between placental nonheme iron and the PIDI at E18.5 ($R = 0.610$) (Figure 2H), in which greater placental iron deficiency resulted in a lower PIDI, suggesting decreased iron transfer to the embryo.

To formally test the effect of placental TFR1 and FPN changes on placental iron transfer during maternal iron deficiency in mice, we measured iron transport using a stable Fe isotope. At E17.5, iron-replete and iron-deficient WT C57BL/6J dams received a single i.v. injection of 5 μg iron as ^{58}Fe-Tf. Placentas and fetal livers were harvested 6 hours after treatment, and total iron content (nonheme plus heme) in each tissue was measured by inductively coupled plasma–mass spectrometry (ICP-MS) (Figure 3A). We found that injection of ^{58}Fe-Tf did not affect placental TFR1 or FPN expression: in iron-deficient pregnancies, placental FPN remained significantly lower than in iron-replete pregnancies (Figure 3B). We measured both ^{56}Fe and ^{58}Fe in the placenta and fetal liver. The ^{56}Fe isotope has the highest natural abundance and provides information on the long-term iron distribution between the placenta and fetal liver.

The short-term ^{58}Fe transport snapshot demonstrated that ^{58}Fe-Tf was taken up by the placenta and ^{58}Fe was transferred to the fetus, as it was detectable in the fetal liver. ^{58}Fe did not reach the threshold of detectability when we analyzed whole embryos. In placentas, we observed no statistically significant difference in the amount of total ^{58}Fe retained in iron-deficient versus iron-replete pregnancies, although there was a trend toward approximately 10 ng less ^{58}Fe in the iron-deficient placentas (Figure 3C). In fetal livers, we found that total ^{58}Fe content was significantly lower in iron-deficient pregnancies, with an average of approximately 30 ng lower ^{58}Fe than in iron-replete pregnancies (Figure 3D). These data demonstrate that during iron deficiency, decreased placental FPN results in less iron transport to the fetus. Interestingly, our measurements of total ^{56}Fe, which reflects chronic iron transport and handling, showed much greater differences between placental and fetal iron content than did our measurements of ^{58}Fe. We found no statistically significant difference in total ^{56}Fe (heme plus nonheme) between placentas from iron-deficient and iron-replete pregnancies (16.2 ± 13.2 μg and 19.9 ± 16.1 μg, respectively) (Figure 3E). However, fetal liver total ^{56}Fe was 68% lower when mothers were iron deficient (4.9 μg for iron-replete compared with 1.6 μg for iron-deficient dams) (Figure 3F). This substantial decrease in fetal liver total iron content despite the stable placental iron content is consistent with results

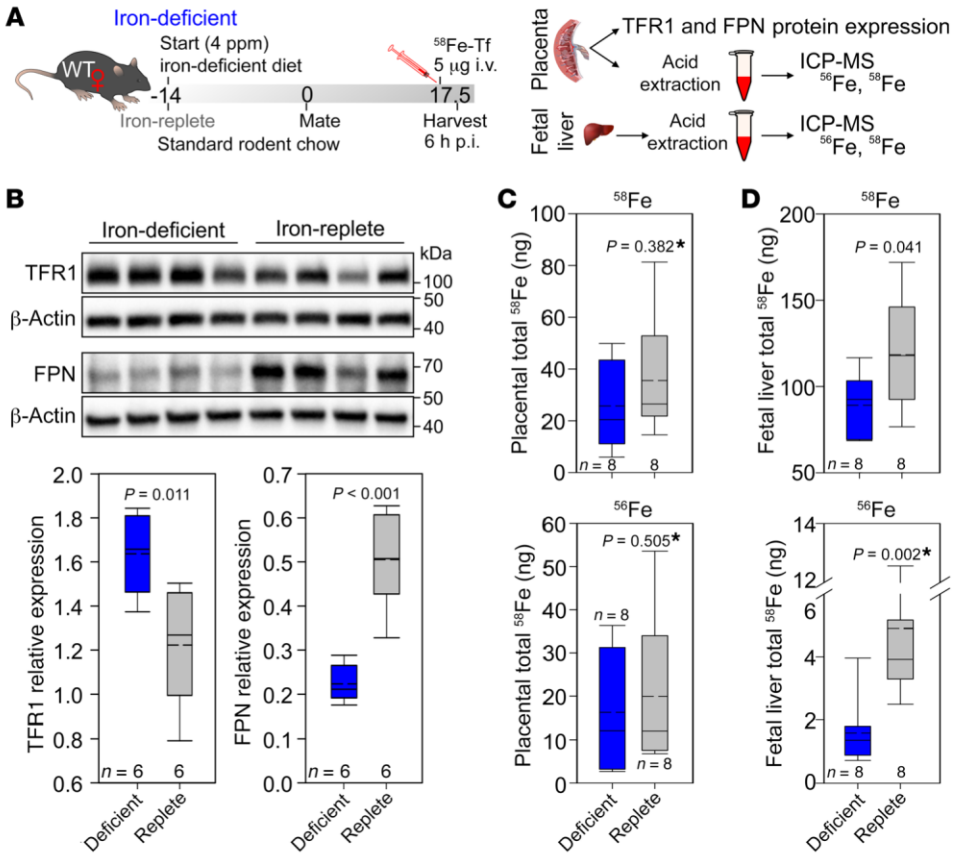

Figure 3. ^{58}Fe transport across the placenta. (**A**) WT C57BL/6 female mice were maintained on a standard chow diet or placed on an iron-deficient diet 2 weeks prior to mating and were maintained on an iron-deficient diet throughout gestation. At E17.5, the dams received a single i.v. injection of ^{58}Fe-Tf. The dams were sacrificed 6 hours post injection (p.i.), and placental and embryonic tissues were collected and analyzed using ICP-MS. (**B**) Placental TFR1 and FPN protein expression was assessed by Western blotting, and quantitation of protein expression relative to β-actin was performed. Total ^{58}Fe content in (**C**) placentas and (**D**) fetal livers. Total ^{56}Fe content in (**E**) placentas and (**F**) fetal livers. (**B**–**F**) Statistical analysis was performed by 2-tailed Student's *t* test for normally distributed values and otherwise by Mann-Whitney *U* rank-sum test (denoted by an asterisk after the *P* value). The numbers of animals are indicated in the *x* axes of the box and whisker plots.

obtained for nonheme iron in our previous experiments. The more profound difference observed in ^{56}Fe content compared with ^{58}Fe could be related to the timing of ^{58}Fe injection, which was near the end of the pregnancy, when the placenta was already fully formed and had acquired most of the iron it needed for its function and was therefore more likely to have sufficient iron for transfer to the fetus.

Regulation of placental iron transporters in human pregnancy. To examine alterations in placental TFR1 and FPN in human pregnancy with varying maternal iron status, we obtained human placental samples at delivery from 39 American women with uncomplicated pregnancies and iron status ranging from normal to moderate iron deficiency. Unlike in our mouse models, iron deficiency in these mothers was not severe enough to cause anemia. TFR1 and FPN levels were quantified by Western blotting and the PIDI calculated for each sample by dividing normalized FPN with TFR1. Data were grouped by maternal serum ferritin levels, with 10 ng/ mL ferritin used as a cutoff for iron deficiency. We assessed serum ferritin levels in the same women at 32–34 weeks' gestation and at delivery. Regardless of the timing of ferritin assessment (32–34 weeks or at delivery), at the protein level, we found that placental TFR1 was mildly but significantly increased in the <10 ng/mL compared with the >10 ng/mL ferritin group, consistent with placental sensing of iron deficiency, although the transferrin receptor (*TFRC*) mRNA differences were not statistically significant (Figure 4, A–D). We also assessed the levels of regnase 1 (*REG1*), a recently described *TFRC* mRNA–targeting ribonuclease (25), and found no difference in *REG1* mRNA expression between the <10 and >10 ng/mL ferritin groups (Supplemental Figure 5, A and B). FPN protein levels remained unchanged between the <10 ng/mL and the >10 ng/mL ferritin groups (Figure 4, E and F). The PIDI, the ratio of placental FPN to TFR1, was significantly lower in the <10 ng/mL ferritin group than in the >10 ng/mL group (Figure 4, G and H). Placental nonheme iron concentrations were not significantly different between the 2 groups of women (Figure 4, I and J), reflecting a maintenance of placental iron homeostasis. The PIDI appeared to be a superior indicator of even mild iron restriction during pregnancy compared with other parameters commonly measured to assess pregnancy iron status including maternal Hb, cord blood Hb, and cord blood ferritin, which did not differ between the <10 ng/mL and >10 ng/mL ferritin groups (Figure 4, K–O).

FPN1 mRNA includes isoforms that contain 5′-IREs or not (26, 27). Only the 5′-IRE–containing isoform is regulated by intracellular iron levels, as its translation is repressed during iron deficiency. In the human placenta, the 5′-IRE–containing isoform is the predominant *FPN* mRNA form (Supplemental Figure 5C) and is over 10,000 times more abundant than the isoform lacking the 5′-IRE. Therefore, FPN translation would be expected to be inhibited by placental iron deficiency. The lack of FPN protein change between the <10 ng/mL and >10 ng/mL ferritin groups is likely attributable to the relatively mild iron deficiency of the placentas in our maternal cohort. To determine whether more severe iron deficiency affects FPN protein levels, we analyzed freshly isolated PHTs grown in DMEM and 10% FBS with addition of the iron chelator desferoxamine (DFO), apo-transferrin (apo-Tf), or holo-transferrin (holo-Tf) for 24 hours. Both DFO and apo-Tf treatment led to a decrease in FPN protein levels compared with the holo-Tf condition (Figure 4P), as well as an increase in TFR1 and a decrease in ferritin levels. We thus surmise that the initial response of the human placenta to mild iron deficiency is to increase TFR1 and that a decrease in FPN only occurs with more severe placental iron deficiency. The mechanism of this differential sensitivity to intracellular iron levels remains to be determined.

Placental IRP1 regulates placental iron transporters in response to changes in maternal iron status. To understand the mechanisms involved in regulating placental iron transporter expression in response to changes in maternal iron status, we used the mouse pregnancy model to analyze the mRNA expression of *Tfrc* and *Fpn*, their known regulators, as well as several other transporters and molecules potentially involved in iron homeostasis. We detected little change in placental *Tfrc* mRNA concentrations (Supplemental Figure 6A). In control iron-replete pregnancies, we detected no difference in *Tfrc* mRNA concentrations between E12.5 and E18.5, suggesting that TFR1 had already reached maximal expression by E12.5. Similar to TFR1 protein results, maternal iron status had small effects on *Tfrc* levels that were significant only at E18.5 (iron- deficient vs. iron-loaded, $P = 0.005$, iron-replete vs. iron- loaded: $P = 0.005$, by 2-way ANOVA comparison at E18.5). We also found no difference in placental *Reg1* mRNA levels related to either gestational age or maternal iron status (Supplemental Figure 6B). To assess *Fpn* mRNA expression levels, we analyzed 2 known transcript variants of FPN, *Fpn1A* and *Fpn1B* (27). As with the human placenta, we found that the iron-regulated, IRE-containing *Fpn1A* transcript was the predominant isoform in the mouse placenta (Supplemental Figure 6, C and D). *Fpn1A* increased with gestational age (Supplemental Figure 6C) but was unaffected by maternal iron status (diet $P = 0.099$, gestation $P < 0.001$, by 2-way ANOVA). *Fpn1B* expression was uniformly low, regardless of the gestational age or maternal iron status. We observed no strong iron-dependent difference in placental mRNA expression of the iron transporter divalent metal transporter 1 (*Dmt1*), homeostatic iron regulator (*Hfe*), ferroxidase zyklopen (*Hephl1*), the heme transporter feline leukemia virus subgroup C receptor–related protein 1 (*Flvcr1*), or the inflammatory markers *Il6* and serum amyloid A1 (*Saa1*) (Supplemental

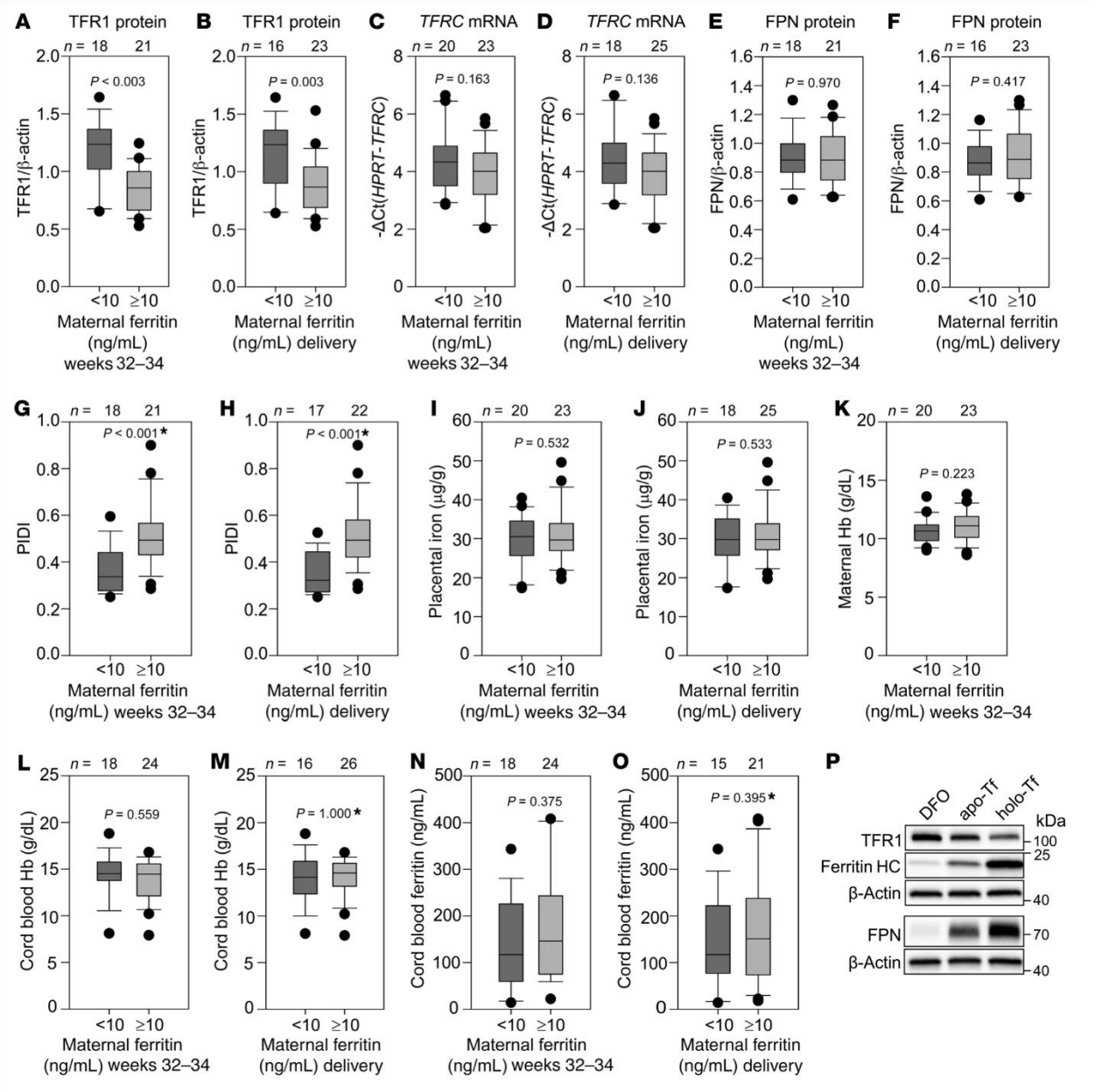

Figure 4. Placental response to maternal iron deficiency in human pregnancy. Placentas from uncomplicated human pregnancies were analyzed by Western blotting to determine protein expression of TFR1 and FPN, normalized to β-actin. qPCR was performed to determine *TFRC* mRNA expression, normalized to *HPRT*. (**A** and **B**) TFR1 protein levels, (**C** and **D**) *TFRC* mRNA levels, and (**E** and **F**) FPN protein levels according to maternal ferritin during weeks 32–34 or at delivery. (**G** and **H**) The PIDI was calculated as the ratio of expression of placental FPN to TFR1 protein, with a lower PIDI reflecting pregnancies at increased risk of fetal iron deficiency. The PIDI was lower in pregnant women with serum ferritin levels below 10 ng/mL than in those with ferritin levels above 10 ng/mL, regardless of whether ferritin was measured at 32–34 weeks of pregnancy or at delivery. No difference between <10 ng/mL and >10 ng/mL ferritin groups was observed for (**I** and **J**) placental nonheme iron concentrations, (**K**) maternal Hb, (**L** and **M**) cord blood Hb, or (**N** and **O**) cord blood ferritin. (**P**) PHTs were treated with 100 μM DFO, apo-Tf or holo-Tf for 24 hours. TFR1, FPN, ferritin heavy chain (HC), and β-actin expression was assessed by Western blotting. Statistical differences between groups was determined by 2-tailed Student's *t* test or Mann-Whitney *U* rank-sum test for non-normally distributed values (denoted by an asterisk after the *P* value). The numbers of animals are indicated above the box and whisker plots.

Figure 6, E–J). The reciprocal change in TFR1 and FPN proteins in response to maternal iron status is consistent with their regulation by the IRE/IRP system, which has been reported to function in human placentas (28, 29). Global single IRP1- or IRP2-KO mice are viable, whereas double-IRP1/IRP2-KO embryos die in utero at E6.5 (30). We measured total IRP activity by EMSA and found significantly increased IRP binding in placentas during iron deficiency (Figure 5A), consistent with decreased FPN protein in the same pregnancies and strongly suggesting that placental iron transporters are regulated by the IRP/IRE system. We were unable to detect any supershift following addition of IRP2 antibody (data not shown), suggesting that IRP1 is the predominant regulator of placental IRE–containing mRNAs. To test the contribution of placental IRP1 to the regulation of placental FPN and TFR1 during maternal iron deficiency, we mated heterozygous IRP1 mice to generate placentas and embryos lacking IRP1 or not. Pregnant dams were placed on a 4-ppm iron diet on E7.5, and placentas were collected on E18.5 (Figure 5B). Loss of IRP1 resulted in loss of placental FPN regulation, and FPN protein was significantly higher during maternal iron deficiency in *Irp1*$^{-/-}$ placentas compared with *Irp1*$^{+/+}$ placentas (Figure 5C). Interestingly, the levels of TFR1 protein or mRNA were not different between *Irp1*$^{+/+}$ and *Irp1*$^{-/-}$ placentas (Figure 5, C and D), indicating that *Tfrc* mRNA is stable even in the absence of IRP1, possibly because of the very low expression of the ribonuclease *Reg1* (Figure 5E). We also evaluated whether in IRP1 deficiency, IRP2 may be increased as a compensatory mechanism and stabilize *Tfrc* mRNA levels. However, we detected no IRP2 activity by EMSA in *Irp1*$^{-/-}$ placentas (Figure 5F). Interestingly, there were no detectable differences between *Irp1*$^{+/+}$ and *Irp1*$^{-/-}$ E18.5 embryos in terms of placental or fetal liver iron concentrations (Figure 5, G and H), probably because of very low iron availability within the entire materno-placental-fetal unit. At the time of harvesting, the *Irp1*$^{+/-}$ dams were severely iron deficient (average maternal liver iron, 9.6 μg/g wet weight, n = 5), anemic (average Hb, 8.58 g/dL), and hypoferremic (average serum iron, 9.7 μM). Additionally, there

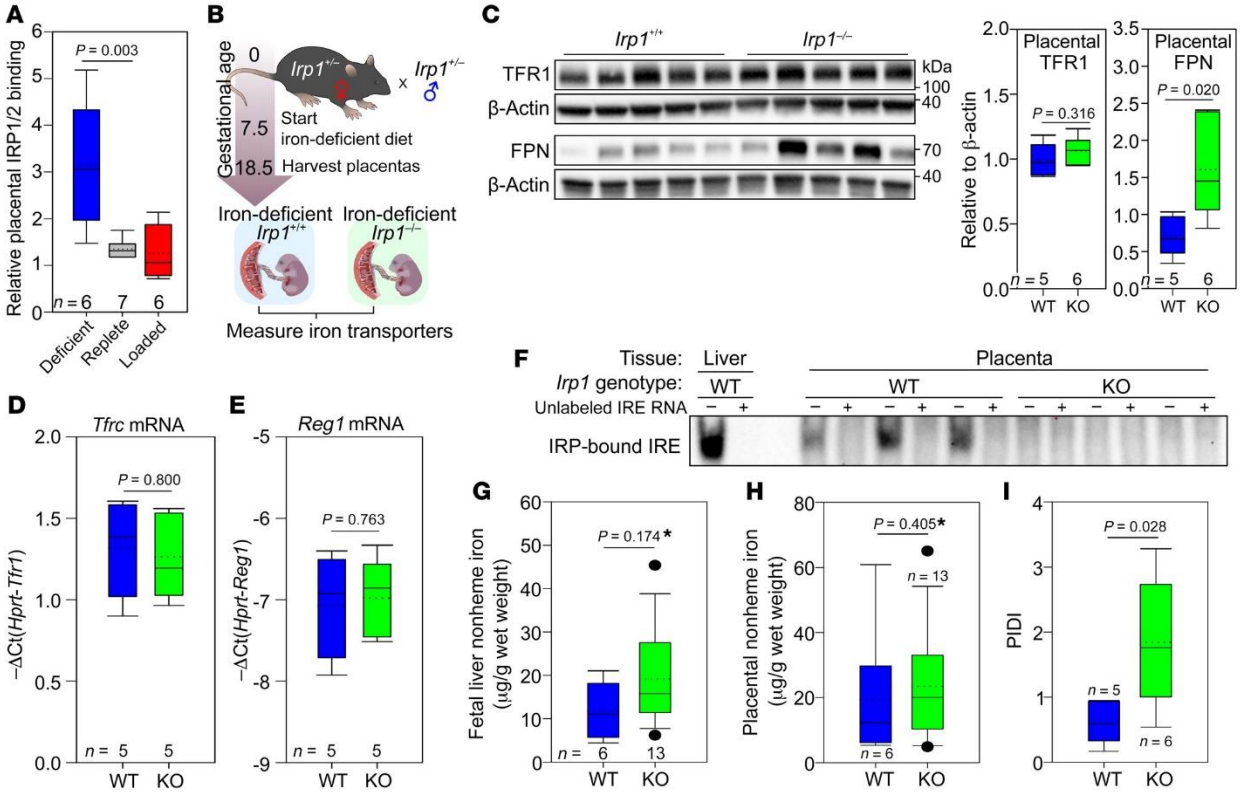

Figure 5. IRP1 mediates placental iron homeostatic responses during maternal iron deficiency. (**A**) Activity of IRP1/2 in placentas from iron-deficient, iron-replete, and iron-loaded pregnancies was analyzed by EMSA. Statistical differences between groups was determined by 1-way ANOVA on ranks followed by Dunn's method for multiple comparisons versus the iron-replete control group ($^{\#}P < 0.05$). (**B**) *Irp1*$^{+/-}$ females were mated with *Irp1*$^{+/-}$ males, and pregnant females were fed an iron-deficient diet from E7.5 until E18.5. Placentas and embryos were harvested on E18.5. (**C**) Placental TFR1 and FPN protein expression was assessed by Western blotting, and quantitation of protein relative to β-actin was performed. (**D**) Placental *Tfrc* mRNA expression. (**E**) Placental *Reg1* mRNA expression. (**F**) IRP-IRE binding as determined by EMSA in *Irp1*$^{+/+}$ and *Irp1*$^{-/-}$ placentas. (**G**) PIDI for *Irp1*$^{+/+}$ and *Irp1*$^{-/-}$ placentas. (**H**) Placental and (**I**) fetal liver nonheme iron concentrations. (**C**–**I**) Statistical analysis was performed by 2-tailed Student's *t* test for normally distributed values and otherwise by Mann-Whitney U rank-sum test (denoted by an asterisk after the *P* value). The numbers of animals are indicated in the *x* axes of the box and whisker plots.

could have been a survival advantage for Irp1–/– compared with Irp1+/+ embryos, as we did not observe the expected Mendelian ratios for embryos from Irp1+/– Irp1+/– matings when the dams were placed on an iron-deficient diet (WT: 16%, heterozygous: 51%, KO: 33%); the differences, however, did not reach statistical significance (P = 0.281; $\chi 2$ test, 2-tailed P value). If IRP1-deficient embryos indeed had a survival advantage, fetal liver iron data for Irp1+/+ embryos may be skewed, as animals with very low iron levels may not survive. Importantly, however, in the absence of IRP1 regulation (*Irp1*$^{-/-}$), placentas had a higher PIDI (ratio of FPN to TFR1 in each placenta) compared with *Irp1*$^{+/+}$ placentas, confirming that IRP1 is the major regulator of placental iron transporters in response to maternal iron deficiency (Figure 5I).

Placental and fetal hepcidin does not regulate fetal iron endowment. During iron deficiency, local hepcidin regulation was reported to be important for cardiac function (31). In the heart, hepcidin protein was paradoxically increased by iron deficiency, even though its mRNA expression was decreased. If hepcidin protein in the placenta or embryo was also unexpectedly stabilized during iron deficiency, this could account for the decreased FPN protein levels in the placenta. Additionally, placental FPN localizes to the basolateral membrane of the syncytiotrophoblast (14) and thus could be subject to regulation by embryonic hepcidin. In fact, in embryos that overexpress hepcidin either because of hepcidin transgene insertion or *Tmprss6* deficiency, placental FPN is downregulated, resulting in severe fetal iron deficiency (32, 33). However, embryonic hepcidin is low in normal mouse pregnancies (32, 33). To test whether the placental response during iron deficiency may be subject to regulation by placental or embryonic hepcidin, we bred heterozygous hepcidin mice and placed the females on either an iron-replete or iron- deficient diet 1 week prior

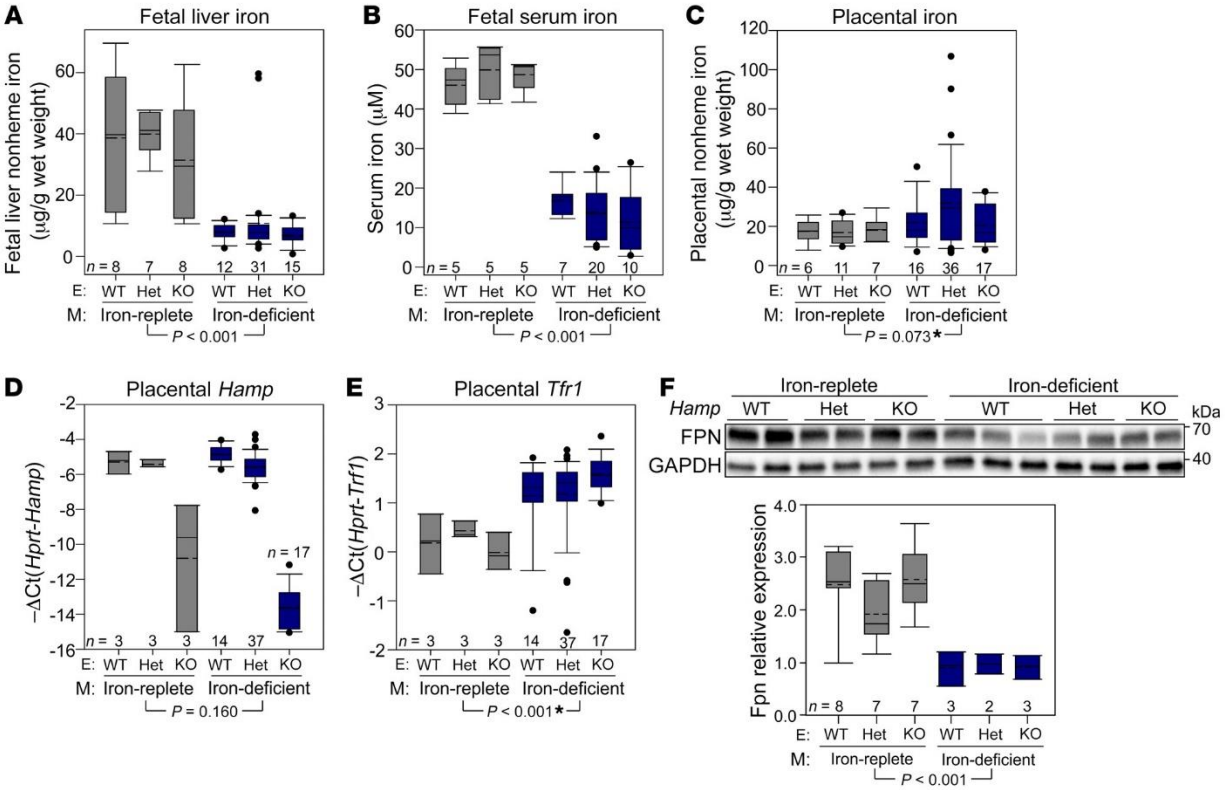

Figure 6. Placental and embryonic hepcidin does not regulate placental iron homeostasis under iron-replete or iron-deficient conditions. *Hamp*$^{+/-}$ female mice were mated with *Hamp*$^{+/-}$ male mice. Females were placed on an iron-replete or iron-deficient diet 1 week prior to mating. Placentas and embryos were analyzed on E18.5. (**A**) Fetal liver iron and (**B**) fetal serum iron concentrations. (**C**) Placental iron concentration, (**D**) *Hamp* expression, (**E**) *Tfrc* expression, and (**F**) FPN protein levels. Statistical differences between groups were determined by 2-way ANOVA (non-normally distributed values are indicated by an asterisk). The *P* value shown is for variation by diet. There were no statistical differences between genotypes for any of the measured parameters. The numbers of animals are indicated in the *x* axes of the box and whisker plots. E, embryos; M, mothers; Het, heterozygous.

to mating, generating iron-replete or iron-deficient *Hamp*$^{+/+}$, *Hamp*$^{+/-}$, or *Hamp*$^{-/-}$ placentas and embryos. As expected, a low-iron diet elicited maternal iron deficiency and anemia (Supplemental Figure 7, A–F), as well as fetal iron deficiency (Figure 6, A and B). However, within the same diet group, we detected no difference in fetal liver iron or serum iron among *Hamp*$^{+/+}$, *Hamp*$^{+/-}$, or

Hamp$^{-/-}$ fetal genotypes. Placental iron concentrations did not differ between iron-replete and iron-deficient groups, or between different *Hamp* genotypes (Figure 6C). Placental *Hamp* mRNA expression was not different between the different diet groups or between WT and heterozygous placentas (Figure 6D). Placental *Tfrc* mRNA was mildly increased and FPN protein significantly decreased in the iron-deficient group, as expected, but again with no difference observed among the different *Hamp* genotypes (Figure 6, E and F). The results indicate that loss of placental and embryonic hepcidin has no effect on placental or fetal liver iron status in iron-replete or iron-deficient pregnancies.

We also measured expression levels of the miRNA miR485-3p (34), which was reported to be induced by cellular iron deficiency and mediate suppression of FPN via a posttranscriptional mechanism. However, we found no difference in mouse miR-485-3p expression between iron-deficient and iron-replete pregnancies (Supplemental Figure 8).

Iron is necessary for trophoblast function. The placenta is a highly metabolically active tissue, consuming approximately 40% of total uterine oxygen uptake (35). This large energy consumption is primarily used for mitochondrial ATP synthesis to support

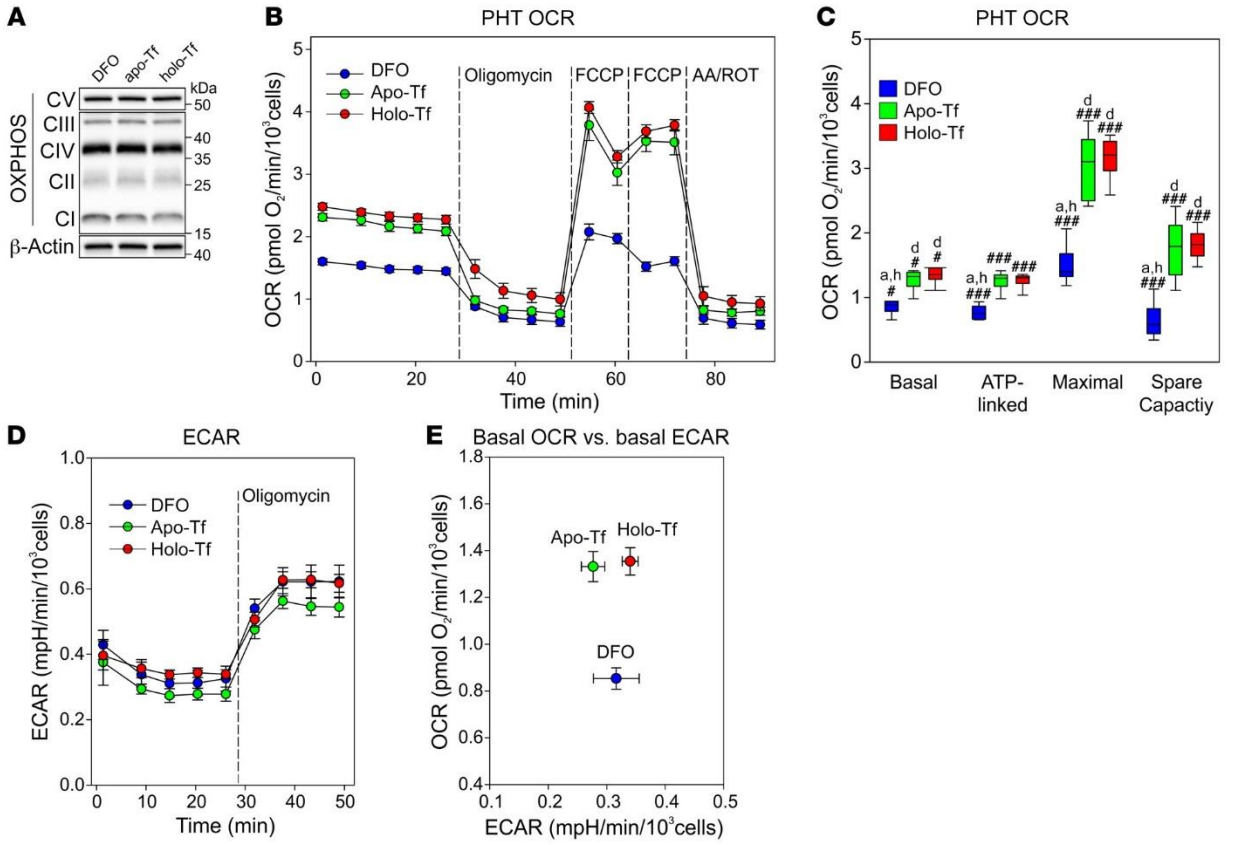

Figure 7. Iron deficiency impairs oxidative phosphorylation in PHTs. PHTs were treated for 24 hours with 100 μM DFO, apo-Tf, or holo-Tf. (**A**) Western blotting for OXPHOS complexes CI–CV. β-Actin was used as a loading control. (**B**) Mitochondrial respiration under basal conditions following injection of oligomycin, the uncoupler FCCP, or the electron transport inhibitors antimycin A and rotenone (AA/ROT). (**C**) Quantitation of basal respiration, ATP-linked respiration, maximal respiratory capacity, and spare respiratory capacity normalized to total cells per well. Statistical differences between groups were determined by 1-way ANOVA for normally distributed values followed by an all-pairwise multiple comparison (Holm-Sidak method) ($^{###}P < 0.001$) or 1-way ANOVA on ranks for non-normally distributed values followed by an all-pairwise multiple comparison (Tukey's test) ($^{#}P < 0.05$). Lowercase letters indicate a statistical difference compared with DFO ("d"), Apo-Tf ("a"), or Holo-Tf ("h") group. *n* = 6 technical replicates. (**D**) ECAR. (**E**) Basal OCR versus basal ECAR.

protein production, nutrient transport, and fetal metabolite waste transport (36). To assess the consequences of iron deficiency for the placenta, we measured the concentrations of ETC complexes CI–CV in E18.5 placentas from iron-replete and iron-deficient pregnancies and found no differences in complex expression (Supplemental Figure 9A). In vivo, however, the placenta is protected from large changes in iron status by its homeostatic response during iron deficiency, i.e., increased iron import through TFR1 and decreased export through FPN. Therefore, we isolated trophoblast cells from term human placentas (PHTs) and cultured them for

24 hours under a range of iron conditions. We used the iron chelator DFO to deplete the cells of iron, holo-Tf to iron load them, and apo-Tf as a baseline control. As shown in Figure 4P, iron deficiency increased the expression of TFR1 and decreased FPN and ferritin. As in mouse placentas, we detected no change in the expression of OXPHOS complexes following iron treatments (Figure 7A), probably because of the protective redistribution of intracellular iron at this time point. We next performed respirometry assays to measure how trophoblast iron levels affect mitochondrial respiration. Iron depletion decreased all the measured bioenergetic parameters of respiration compared with apo-Tf and holo-Tf treatments, with a significantly lower basal, ATP-linked, maximal, and spare respiratory capacity oxygen consumption rate (OCR) in iron-depleted cells (Figure 7, B and C). The reduction in the maximal OCR suggests that iron deficiency may perturb the placenta's ability to generate energy for its synthetic and transport functions. Following inhibition of ATP synthase by oligomycin, PHTs compensated by shifting to glycolysis under all iron conditions (Figure 7D), demonstrating that the cells remained viable. Comparison of the baseline OCR and extracellular acidification rate (ECAR) (Figure 7E) confirmed that iron depletion decreased the OCR but not the ECAR. The uniformly low ECAR indicated that mitochondrial respiration rather than glycolysis is the predominant form of energy production in the trophoblast.

As an alternative trophoblast model, we used BeWo cells, a placental cell line derived from a human choriocarcinoma often used to study placental transport, including that of iron (37). Like PHTs, BeWo cells were treated with DFO, apo-Tf, or holoTf for 24 hours. DFO treatment efficiently depleted cells of iron, with a 70% average reduction in cellular ferritin levels (Supplemental Figure 9, B and C). Additionally, DFO treatment upregulated TFR1 (Supplemental Figure 9, B and D), whereas FPN was undetectable in all groups. Importantly, expression of all ETC complexes decreased in the iron-depleted cells compared with apo-Tf– or holo-Tf–treated cells (Supplemental Figure 9, E and F), suggesting that severe placental iron deficiency could impair the machinery of cellular oxidative phosphorylation.

Taken together, our data support the hypothesis that severe placental iron deficiency could compromise critical determinants of placental function, providing an evolutionary rationale for the prioritization of placental iron retention in iron-deficient pregnancy.

Discussion

Although the importance of iron for a healthy pregnancy is well recognized, how iron transfer from the mother to the fetus is regulated during pregnancy is not well understood. To determine how the maternal-placental-fetal unit responds to changes in maternal iron status, we performed a comprehensive evaluation of mechanisms in mouse models, human pregnancies, and isolated trophoblast. In mouse models, we confirmed that the maternal iron regulatory hormone hepcidin is suppressed during pregnancy, consistent with previous reports in humans (38). However, the mechanism of suppression is not yet known. We show that maternal hepcidin is regulated by maternal iron status during pregnancy, with iron-loaded mothers having higher hepcidin levels than iron-replete or iron- deficient mothers. However, within each group, hepcidin was still suppressed compared with nonpregnant females, revealing a strong effect by a pregnancy-associated factor. Furthermore, reductions of both hepcidin protein and mRNA levels confirmed that maternal hepcidin suppression is not a consequence of hemodilution. Additional studies are required to determine the exact mechanism(s) of maternal hepcidin suppression during pregnancy.

Embryonic hepcidin overexpression in mice, as in transgenic hepcidin embryos or Tmprss6-deficient embryos, was reported to regulate placental FPN expression. However, in normal murine pregnancies, embryonic hepcidin expression is very low (32, 33). In our studies, iron endowment of the fetus was unaffected by genetic ablation of fetal and placental hepcidin in iron-replete or iron-deficient pregnancies, indicating that embryonic or placental hepcidin was too low to regulate iron transfer across the placenta under these conditions.

Importantly, our animal models showed that during iron- replete pregnancy, homeostatic maternal adaptations — hepcidin suppression and iron mobilization from stores — maintained constant maternal serum iron levels throughout the pregnancy despite increased iron utilization in advanced pregnancy. In iron-loaded mothers, maternal hepcidin was relatively increased, preventing the release of excess iron into the maternal circulation and protecting embryos from iron overload, with only a small increase in placental iron.

In contrast to embryonic protection from maternal iron overload, maternal adaptations to iron deficiency, including the profound suppression of hepcidin, were not sufficient to protect the embryos from iron deficiency anemia. We were surprised to uncover a placental response that prioritized placental iron retention despite fetal iron deficiency. In the face of maternal iron deficiency, the murine placenta strongly decreased levels of the iron exporter FPN, resulting in decreased iron transport to the fetus. Although this ensured that the placenta developed only relatively mild iron deficiency, it was to the severe detriment of fetal iron content, with fetuses developing profound iron deficiency anemia as reflected by their low Hb and liver stores. In contrast to our mouse models that were stressed with severe iron deficiency, in human pregnancies that were only modestly iron deficient, expression of TFR1 protein increased but that of FPN did not change. Because human pregnancies with severe maternal iron

deficiency are rare in settings in which fresh placentas can be obtained, we simulated the condition by exposing human trophoblast to a more severe iron deficiency in vitro. In agreement with the mouse model, we observed a decrease in FPN and ferritin.

We propose the PIDI, a ratio of placental iron exporter to importer (FPN/TFR1), as an indicator of fetal exposure to iron deficiency in utero. Using the ratio would minimize the effect of regional differences in human sample collection. TFR1 and FPN expression is restricted to the syncytiotrophoblast; if placental tissue collection includes an area with low or no expression of transporters, this could be erroneously interpreted as a "regulated" low expression of an individual transporter, whereas a ratio of the 2 transporters would account for the sampling variability.

Using mouse models, we also determined the mechanism underlying the altered expression of placental iron transporters following maternal iron deficiency. We demonstrated that placental IRP1 plays a critical role in sensing placental iron levels and consequent modulation of iron transporters and that *Irp1*$^{-/-}$ placentas failed to decrease FPN protein levels in the face of maternal iron deficiency.

The ability of the placenta to retain iron for its needs prior to transport to the fetus is consistent with previous observations that when oxygen supply to the uterus is limited, the majority of the oxygen is consumed by the placenta, and oxygen transfer to the fetus is adversely affected (39). Placental retention of iron during severe iron deficiency would preserve oxidative phosphorylation to supply necessary ATP for placental protein synthesis and transport functions (36). Indeed, we show that severe iron deficiency in primary human placental trophoblast cells impaired mitochondrial respiration, whereas in the BeWo cell line, it even decreased the levels of all 5 ETC complexes. Unlike in BeWo cells, we did not observe an ETC complex decrease in primary trophoblast cells at the 24-hour time point and speculate that the differences in the sensitivity of these 2 cell types to iron deficiency reflect the variability of protective cellular mechanisms against this stress. We argue that prioritization of placental iron retention in response to iron deficiency may have an evolutionary benefit: it would preserve placental iron levels even during iron deficiency so that all iron-dependent placental functions are protected, thus indirectly benefiting the fetus overall despite diminishing fetal iron availability.

Prioritization of placenta iron acquisition over iron transport to the fetus suggests that fetuses are unable to compensate for maternal iron deficiency by increasing placental iron transfer. A common misconception is that the fetus is a "perfect parasite," able to acquire adequate iron irrespective of the mother's iron status (40). However, consistent with our data, several human and macaque studies confirmed that neonatal iron stores are compromised when the mother is iron deficient or anemic (41– 47). Furthermore, in agreement with our model, maternal iron deficiency anemia resulted in a higher placenta/newborn weight ratio (48, 49). Our observation underscores the importance of detecting and treating iron-deficient pregnancies.

One of the current challenges recognized by the US Preventive Services Task Force (50) is the ability to accurately identify iron deficiency in pregnant women to determine whether iron supplementation is necessary. Currently, the most common laboratory measure is maternal Hb, in which low Hb is presumed to be a result of iron deficiency; however, distinguishing actual iron deficiency anemia from Hb changes related to hemodilution remains a challenge (50). The lack of a correlation between maternal Hb and the PIDI in our human study suggests that Hb is not an adequate indicator of maternal iron deficiency or of the risk of fetal iron deficiency. Serum ferritin is another measure used to assess maternal iron status; although often a good indicator, this value can be confounded by infection or inflammation. In our human pregnancies, which did not have inflammation, a maternal serum ferritin level below 10 ng/mL was an accurate indicator of the risk of fetal iron deficiency as determined by the PIDI. Although hepcidin and ferritin are both acute phase reactants that respond to infection and inflammation, some studies have suggested that hepcidin is a better indicator of iron status in pregnant women than ferritin (51, 52). However, we found no correlation between the PIDI and maternal hepcidin levels.

Neonatal iron deficiency has been linked to numerous neurobehavioral effects (4). Most recently, an association was reported between maternal anemia diagnosed earlier in pregnancy (≤30 weeks) and increased offspring risk of autism spectrum disorder, attention-deficit/hyperactivity disorder, and intellectual disability (6). Therefore, it is important that neonatal iron deficiency be accurately quantitated. A commonly used indicator of neonatal iron deficiency is cord blood Hb or cord blood ferritin. However, previous studies indicated that during fetal iron deficiency, iron is preferentially used for Hb synthesis, sacrificing neonatal brain iron endowment (53). Thus, low Hb may only manifest in the most severe forms of iron deficiency. Additionally, in our human study, the lack of a correlation between cord blood Hb or ferritin and the PIDI indicates that cord blood Hb and ferritin may not be sensitive indicators of neonatal iron deficiency. Therefore, we propose that the PIDI may be a superior indicator of iron deficiency in utero. As it can only be measured after birth, the PIDI cannot be used to guide iron supplementation during human pregnancy but may be used for future research studies to identify better markers of neonatal iron deficiency. Our study also shows that in the absence of infection or inflammation, maternal serum ferritin levels below 10 ng/mL may also signal the risk of fetal iron deficiency.

Our study demonstrates how the healthy maternal-placental- fetal unit handles iron. Maternal hepcidin is suppressed, allowing for increased absorption from the diet and release of iron from stores to maintain serum iron concentrations. This allows

for optimal transfer of iron from the maternal circulation through the placenta, via TFR1 and FPN, to the fetus, where iron is then used for erythropoiesis, and any excess is stored in the fetal liver. In states of iron overload, maternal hepcidin is elevated and prevents overloading of the embryo. During iron deficiency, however, the placental homeostatic response retains iron within the placenta and protects the metabolically active placenta from severe iron deficiency and consequently decreased oxidative phosphorylation. Although this occurs at the cost of fetal iron deficiency, it may ultimately protect the fetus from more severe adverse effects of broader placental dysfunction

Methods

Mice. C57BL/6J mice were obtained from The Jackson Laboratory or bred in-house. *Irp1*$^{-/-}$ mice on a C57BL/6 background were provided by Tracey Rouault (54). Hepcidin-KO (*Hamp*$^{-/-}$) mice were originally provided to our laboratory by Sophie Vaulont (55) and backcrossed by us with mice on a C57BL/6 background. Unless otherwise specified, mice received a standard diet (PicoLab Rodent Diet 20, 5053 Irradiated, 185 ppm iron) and were fed ad libitum. The iron-deficient diet (4 ppm) (TD.80396) and the iron-loaded diet (10,000 ppm, TD.08043) were purchased from Envigo Teklad Diets.

To test the effects of maternal iron status, C57BL/6J females were maintained on a standard (iron-replete) diet and then placed on an iron-deficient diet 2 weeks prior to mating and throughout gestation (iron-deficient), or received a single i.p. injection of 20 mg iron dextran (iron loading) (MilliporeSigma, D8517) at mating. For alternative iron deficiency and loading strategies, C57BL/6J females were placed on an iron-deficient diet at mating and throughout gestation (short-term iron-deficient) or on a 10,000-ppm diet 2 weeks prior to mating and throughout gestation. Pregnant females were euthanized at the indicated gestational age, and nonpregnant female controls were euthanized on the same day.

To test the contribution of IRP1 to the maintenance of placental iron homeostasis, *Irp1*$^{+/-}$ female mice were mated with *Irp1*$^{+/-}$ male mice. The pregnant females were placed on an iron-deficient diet at E7.5 until E18.5, at which point they were euthanized and tissues collected for analysis.

To determine the contribution of local placental and embryonic hepcidin, *Hamp*$^{+/-}$ females were maintained on an iron-replete diet or placed on an iron-deficient diet 1 week prior to mating and throughout gestation. *Hamp*$^{+/-}$ females were mated with *Hamp*$^{+/-}$ males, and pregnant females were euthanized when the embryos reached E18.5.

Human subjects. Forty-three pregnant women we recruited in their late second or early third trimester between August 2015 and October 2017 at the UIC Center for Women's Health (UI Health). Women were eligible if the following criteria were met: they had a prepregnancy BMI above 18.5 kg/m^2; they had naturally conceived, had a singleton pregnancy, were at 26–33 gestational weeks, and were obtaining prenatal care and planning to deliver at UI Health; were 17–45 years of age; had a parity of 0–3; were able to read and write English; were gaining the minimum amount of weight compared with their prepregnancy BMI from 23 to 24 gestational weeks onward, based on the recommendations of the Institute of Medicine; and had access to a phone to alert research staff when they were admitted to UI Health for labor and delivery. The following criteria were used to exclude women from this study: live birth or other pregnancy (including ectopic and molar pregnancies) in the previous 12 months; autoimmune disorder; gestational diabetes mellitus or previously diagnosed diabetes; current or previous premature rupture of membranes or chorioamnionitis; previous spontaneous premature birth; current bacterial or viral infection; current steroid or antiinflammatory treatment; previous bariatric surgery; malabsorptive disease; current hyperemesis; hematologic disorder (i.e., sickle cell disease, sickle cell trait, or hemochromatosis); tobacco use in the past 3 months; current alcohol consumption; or current illicit drug use.

One blood sample was collected at 32–34 gestational weeks. Women were asked to fast for 1.5 hours and refrain from all vitamin and mineral supplements for 48 hours prior to the visit. Upon admission to the UI Health Labor and Delivery facility (at 38.9 ± 1.4 weeks), an additional maternal blood sample was obtained. Placentas were processed within 30 minutes of delivery. The placenta was visually divided into quadrants, a was core sampled from each quadrant and sectioned into smaller pieces, and pieces from all 4 cores were combined to provide a representative sample of the tissue. Aliquots were either snap-frozen, or RNAlater (Ambion) was added.

Cell culture. PHTs were prepared from normal-term placentas using a modified trypsin-deoxyribonuclease-dispase/Percoll method (56, 57). PHTs were cultured in DMEM plus 10% FBS. BeWo cells obtained from the American Type Culture Collection (ATCC) (CCL98) were cultured in Ham's F-12K Nutrient Mixture plus 10% FBS. For in vitro iron depletion and iron-loading experiments, PHTs were seeded at 1×10^6/well and BeWo cells at 1×10^5/well in a 6-well, collagen-coated plate (Corning BioCoat), allowed to attach overnight, and treated with 100 μM DFO (MilliporeSigma, D9533), 100 μM apo-Tr (Celliance, 4452-01), or 100 μM holo-Tf (MilliporeSigma, 4455-01) for 24 hours.

Complete blood counts. Mouse complete blood counts (CBCs) were performed on a Hemavet 950FS hematology system (Drew Scientific). Human Hb was determined using an Abbott HemoCue point-of-care monitor.

Iron measurements. Serum, hepatic, and placental nonheme iron concentrations were measured using a previously described method (58) (Sekisui Diagnostics, 157-30). Human maternal and neonatal cord serum iron and serum ferritin were measured at Quest Diagnostics. The unsaturated iron–binding capacity (UIBC) was measured using a Pointe Scientific assay (I7504). The transferrin saturation percentage = (serum iron/total iron-binding capacity [TIBC]) × 100.

^{58}Fe isotope preparation and sample analysis. ^{58}Fe (93% enrichment) was purchased from Trace Sciences International, dissolved in 12N HCl to form H_2 plus $^{58}FeCl_2$, and H_2O_2 was added to oxidize the H_2 plus $^{58}FeCl_2$ to H_2O plus $^{58}FeCl_3$. $^{58}FeCl_3$ was incubated with nitrilotriacetate (NTA) at a molar ratio of 1:5 in 20 mM $NaHCO_3$ for 5 minutes at room temperature to form ^{58}Fe-NTA. Human apo-Tf (Celliance, 4452-01) was dissolved in Tf-loading buffer (0.1 M HEPES, pH 7.5, 0.15 M NaCl) and incubated with ^{58}Fe-NTA at a molar ratio of 1:2 for 2.5 hours at room temperature to form ^{58}Fe-Tf. To remove unbound $^{58}FeCl_3$, the ^{58}Fe-Tf mixture was centrifuged in an Amicon Ultra Filter 30K at 2500 *g* for 15 minutes and washed with Tf-l oading buffer and saline. Each pregnant mouse received a retro-orbital injection of 3.5 mg human ^{58}Fe-Tf (equivalent to 5 μg ^{58}Fe) at E17.5. Tissues were collected 6 hours after injection. Placentas and fetal livers were processed for nonheme iron as previously described (58), and supernatant was submitted for ICP-MS analysis of ^{56}Fe and ^{58}Fe. The remaining iron (mostly heme) was extracted from tissue pellets by digestion in HNO_3 supplemented with H_2O_2, the samples were heated up to 200°C for 15 minutes followed by dilution of samples with 2% HNO_3, and the samples were analyzed by ICP-MS. The sum of nonheme and heme iron was presented as the total iron content. For ^{58}Fe measurements, the natural abundance (0.28% of total Fe) was subtracted from the measured ^{58}Fe values.

Serum hepcidin. Mouse serum hepcidin levels were measured using a sandwich ELISA by Amgen (59).
Quantitative PCR. RNA was prepared using TRIzol (Invitrogen, Thermo Fisher Scientific), and cDNA was synthesized using an iScript cDNA Synthesis Kit (Bio-Rad). Quantitative PCR (qPCR) was performed with SsoAdvanced SYBR Green Supermix (Bio-Rad) (primers are listed in Supplemental Table 5). The samples were run in duplicate on a CFXconnect qPCR instrument (Bio-Rad). miR-485-3p was measured using a QIAGEN miScript Primer Assay (MS00006335).

Immunofluorescence. Formalin-fixed, paraffin-embedded sections (5-μm) of mouse and human placentas were used. Tris- EDTA buffer (10 mM Tris, 1 mM EDTA, pH 9.0) was used for antigen retrieval, and sections were heated to 96°C for 10 minutes. Primary antibodies (Supplemental Table 6) were incubated overnight at room temperature in a humidified chamber and secondary antibodies for 1 hour at room temperature. Images were captured using a Zeiss LSM 700 confocal microscope.

Western blot analysis. Tissues were lysed by homogenization in RIPA buffer and cells by addition of RIPA (Santa Cruz Biotechnology, sc-24948), and lysates were cleared by centrifugation at 17,000 *g* for 15 minutes at 4°C. Protein was quantified using a Pierce BCA Assay (Thermo Fisher Scientific, 23225). Samples for FPN and OXPHOS were prepared in Laemmli sample buffer without a reducing agent, and samples were not boiled. For all other proteins, samples were prepared in Laemmli buffer with DTT and incubated at 100°C for 5 minutes. The samples were resolved on Bio-Rad 4%–20% TGX gels or Any kD TGX gels for OXPHOS, electroblotted onto nitrocellulose (Trans-Blot Turbo System, Bio-Rad), and imaged with a ChemiDoc XRS+ system (Bio-Rad). The primary and secondary antibodies used are listed in Supplemental Table 6. Membranes were stripped using 0.2N NaOH for 10 minutes at room temperature and reprobed for the loading controls. Quantitation was performed using Image Lab Software, version 5.2.1 (Bio-Rad).

PIDI calculation. Since mouse FPN and TFR1 expression was analyzed on separate Western blots, given the need for different handling of the samples, we first normalized each of the proteins to their β-actin loading control and then generated the PIDI as the ratio of normalized FPN to normalized TFR1. In human placenta, because several electrophoresis gels had to be used to analyze the large number of samples, TFR1, FPN, and β-actin values were normalized to the median for each membrane to account for intermembrane variability, and then the values were divided by the normalized β-actin values to account for any loading variation. The normalized FPN values were then divided by the normalized TFR1 values to generate the PIDI.

EMSA. The direct interaction between placental IRP1 and IRP2 and IREs was determined using a LightShift Chemiluminescent RNA EMSA Kit (Thermo Fisher Scientific, 20158). Whole placenta tissue lysate (4 μg) was used for each reaction, and samples were then resolved on a pre-cast 6% DNA retardation gel (Thermo Fisher Scientific, EC6365BOX) and transferred onto a Biodyne B nylon membrane (Thermo Fisher Scientific, 77016) using a Trans-Blot Turbo Transfer System (Bio-Rad) at 200 mA for 30 minutes. Transferred RNA was crosslinked onto the membrane using the "autocrosslink" function on the Stratagene Stratalinker UV Crosslinker 2400. RNA detection was performed using a Chemiluminescent Nucleic Acid Detection Module (Thermo Fisher Scientific, 89880), and membranes were imaged on a ChemiDoc XRS+.

Respirometry assays. The OCR and ECAR were measured using the Seahorse XFe96 flux analyzer (Agilent Technologies). PHTs (40,000/ well or 60,000/well) were plated onto a Seahorse XF96 cell culture plate (Agilent Technologies, 101085-004) coated with collagen (MilliporeSigma, 125-50) and were then cultured for 3 hours to allow attachment, washed 3 times with PBS, and cultured in

DMEM plus 1% FBS supplemented with 100 μM DFO, 100 μM apo-Tf, or 100 μM holo- Tf for 24 hours. At the time of the assay, the treatment medium was removed and replaced with the appropriate prewarmed Seahorse XF Assay Medium (Agilent Technologies) consisting of DMEM containing 10 mM glucose and 4 mM glutamine. Cells were then subjected to a Mitochondria stress test (Agilent Technologies). Oxygen consumption measurements were made approximately every 5 minutes under basal conditions, after the addition of 2.5 μM oligomycin, 1 μM carbonyl cyanide-4-(trifluoromethoxy) phenylhydrazone (FCCP), and 2 μM antimycin A and rotenone. OCR and ECAR measurements were normalized to the number of cells per well following the assay. The contribution from nonmitochondrial respiration as measured following antimycin A and rotenone injection was subtracted from all raw OCR values. Basal OCRs were determined at the last measurement prior to the injection of oligomycin. ATP-linked respiration was determined as the difference between the oligomycin-resistant OCR and basal respiration. Maximal respiration was determined as the highest value after the addition of FCCP. Spare capacity was determined by the difference between maximal FCCP and the basal OCR. ECAR measurements were performed in parallel. Basal ECARs were determined at the last measurement prior to the injection of oligomycin. The post-oligomycin maximum ECAR was the calculated average of 4 measurements taken after oligomycin injection.

Statistics. For box plots, the upper portion of the box plot indicates the 75th percentile and the bottom indicates the 25th percentile, whiskers above the box indicate the 90th percentile, those below the box indicate the tenth percentile, and individual points represent outliers. The solid line within the box indicates the median and the dashed line the mean. Statistical analysis was performed using SigmaPlot scientific graphing and data analysis software (Systat Software). A P value of less than 0.05 was considered statistically significant. Statistical differences between groups were determined using a 1-way ANOVA for normally distributed values followed by the Holm-Sidak method for multiple comparisons; a 1-way ANOVA on ranks followed by Dunn's method for multiple comparisons for non-normally distributed values; a 2-tailed, unpaired Student's t test for normally distributed values; a Mann-Whitney U for non-normally distributed values; or a 2-way ANOVA.

Study approval. All study procedures were approved by the UIC Institutional Review Board (approval no. 2015-0353), and all participants provided written informed consent.

Author contributions

VS designed and performed experiments, analyzed data, and wrote the manuscript. ALF performed experiments and assisted with data interpretation. SW assisted with experiments. MDK and LTH enrolled the study participants and collected human data and samples and edited the manuscript. AC participated in studies using PHTs and edited the manuscript. ML assisted with human placenta studies and method development and edited the manuscript. TG and EN conceived the project, analyzed data, and wrote the manuscript.

Acknowledgments

The authors thank Deliang Zhang and Tracey Rouault for providing *Irp1*-KO mice; the UCLA Translational Pathology Core laboratory for histology processing; the UCLA Broad Stem Cell Center Microscopy Core for providing access to and training on confocal microscopes; Linsey Stiles and Brandon Desousa at the UCLA Mitochondria and Metabolism Core for running the respirometry assays; the UCLA ICP-MS core facility within the UC Center for Environmental Implications of Nanotechnology; Tiffany Coon and Yoel Sadovsky at the Magee-Womens Research Institute for their assistance with primary trophoblast isolation; and Victoria Gabayan and Erika Valore for their assistance with methods development. The study was supported by the Executive Advisory Board of the Iris Cantor–UCLA Women's Health Center and National Center for Advancing Translational Science (NCATS) pilot grants (UCLA CTSI grant UL1TR000124, to EN and VS); an NIH Ruth L. Kirschstein National Research Service Award (T325T32HL072752-13, to VS); a Robert Wood Johnson Foundation, Nurse Faculty Scholars Award (72117, to MDK); a UIC College of Nursing Dean's Fund grant (to MDK and LTH); and a National Institute of Child Health and Human Development (NICHD) NIH grant (R01HD096863, to EN).

Address correspondence to: Elizabeta Nemeth, UCLA David Geffen School of Medicine, 10833 LeConte Ave, CHS 43-229, Los Angeles, California 90095, USA. Phone: 310.825.2841; Email: ENemeth@mednet.ucla.edu

References

1. Fisher AL, Nemeth E. Iron homeostasis during pregnancy. *Am J Clin Nutr*. 2017;106(Suppl 6):1567S–1574S.
2. Ezzati M, Lopez AD, Rodgers A, Vander Hoorn S, Murray CJ, Comparative Risk Assessment Collaborating Group. Selected major risk factors and global and regional burden of disease. *Lancet*. 2002;360(9343):1347–1360.
3. Daru J, et al. Risk of maternal mortality in women with severe anaemia during pregnancy and post partum: a multilevel analysis. *Lancet Glob Health*. 2018;6(5):e548–e554.
4. Georgieff MK. Long-term brain and behavioral consequences of early iron deficiency. *Nutr Rev*. 2011;69(Suppl 1):S43–S48.
5. Scholl TO, Reilly T. Anemia, iron and pregnancy outcome. *J Nutr*. 2000;130(2S Suppl):443S–447S. 6. Wiegersma AM, Dalman C, Lee BK, Karlsson H, Gardner RM. Association of prenatal maternal anemia with neurodevelopmental disorders. *JAMA Psychiatry*. 2019;76(12):1–12.
7. World Health Organization. *Guideline: Daily Iron and Folic Acid Supplementation in Pregnant Women*. Geneva, Switzerland: World Health Organization; 2012.
8. Taylor CL, Brannon PM. Introduction to workshop on iron screening and supplementation in iron-replete pregnant women and young children. *Am J Clin Nutr*. 2017;106(Suppl 6):1547S–1554S.
9. Wardman P, Candeias LP. Fenton chemistry: an introduction. *Radiat Res*. 1996;145(5):523–531.
10. Ganz T. Iron and infection. *Int J Hematol*. 2018;107(1):7–15.
11. Lao TT, Tam KF, Chan LY. Third trimester iron status and pregnancy outcome in non-anaemic women; pregnancy unfavourably affected by maternal iron excess. *Hum Reprod*. 2000;15(8):1843–1848.
12. Dewey KG, Oaks BM. U-shaped curve for risk associated with maternal hemoglobin, iron status, or iron supplementation. *Am J Clin Nutr*. 2017;106(Suppl 6):1694S–1702S.
13. Ganz T. Systemic iron homeostasis. *Physiol Rev*. 2013;93(4):1721–1741.
14. Bastin J, Drakesmith H, Rees M, Sargent I, Townsend A. Localisation of proteins of iron metabolism in the human placenta and liver. *Br J Haematol*. 2006;134(5):532–543.
15. Donovan A, et al. Positional cloning of zebrafish ferroportin1 identifies a conserved vertebrate iron exporter. *Nature*. 2000;403(6771):776–781.
16. Levy JE, Jin O, Fujiwara Y, Kuo F, Andrews NC. Transferrin receptor is necessary for development of erythrocytes and the nervous system. *Nat Genet*. 1999;21(4):396–399.
17. Donovan A, et al. The iron exporter ferroportin/ Slc40a1 is essential for iron homeostasis. *Cell Metab*. 2005;1(3):191 200.
18. Gambling L, et al. Effect of iron deficiency on placental transfer of iron and expression of iron transport proteins in vivo and in vitro. *Biochem J*. 2001;356(Pt 3):883–889.
19. Li YQ, Yan H, Bai B. Change in iron transporter expression in human term placenta with different maternal iron status. *Eur J Obstet Gynecol Reprod Biol*. 2008;140(1):48–54.
20. Muckenthaler MU, Galy B, Hentze MW. Systemic iron homeostasis and the iron-responsive element/iron-regulatory protein (IRE/IRP) regulatory network. *Annu Rev Nutr*. 2008;28:197–213.
21. Ghosh MC, Zhang DL, Rouault TA. Iron misregulation and neurodegenerative disease in mouse models that lack iron regulatory proteins. *Neurobiol Dis*. 2015;81:66–75.
22. van Santen S, Kroot JJ, Zijderveld G, Wiegerinck ET, Spaanderman ME, Swinkels DW. The iron regulatory hormone hepcidin is decreased in pregnancy: a prospective longitudinal study. *Clin Chem Lab Med*. 2013;51(7):1395–1401.
23. van Santen S, Kroot JJ, Zijderveld G, Wiegerinck ET, Spaanderman ME, Swinkels DW. The iron regulatory hormone hepcidin is decreased in pregnancy: a prospective longitudinal study. *Clin Chem Lab Med*. 2013;51(7):1395–1401.
24. Cao C, Fleming MD. The placenta: the forgotten essential organ of iron transport. *Nutr Rev*. 2016;74(7):421–431.
25. Yoshinaga M, et al. Regnase-1 maintains iron homeostasis via the degradation of transferrin receptor 1 and prolyl hydroxylase- domain-containing protein 3 mRNAs. *Cell Rep*. 2017;19(8):1614–1630.
26. Cianetti L, et al. Expression of alternative transcripts of ferroportin-1 during human erythroid differentiation. *Haematologica*. 2005;90(12):1595–1606.
27. Zhang DL, Hughes RM, Ollivierre-Wilson H, Ghosh MC, Rouault TA. A ferroportin transcript that lacks an iron responsive element enables duodenal and erythroid precursor cells to evade translational repression. *Cell Metab*. 2009;9(5):461–473.
28. Georgieff MK, Berry SA, Wobken JD, Leibold EA. Increased placental iron regulatory protein-1 expression in diabetic pregnancies complicated by fetal iron deficiency. *Placenta*. 1999;20(1):87–93.
29. Bradley J, et al. Influence of gestational age and fetal iron status on IRP activity and iron transporter protein expression in third-trimester human placenta. *Am J Physiol Regul Integr Comp Physiol*. 2004;287(4):R894–R901.
30. Smith SR, Ghosh MC, Ollivierre-Wilson H, Hang, Tong W, Rouault TA. Complete loss of iron regulatory proteins 1 and 2 prevents viability of murine zygotes beyond the blastocyst stage of embryonic development. *Blood Cells Mol Dis*. 2006;36(2):283–287.
31. Lakhal-Littleton S, et al. An essential cell-autono-mous role for hepcidin in cardiac iron homeostasis. *Elife*. 2016;5:e19804.
32. Nicolas G, et al. Severe iron deficiency anemia in transgenic mice expressing liver hepcidin. *Proc Natl Acad Sci USA*.

2002;99(7):4596–4601.
33. Willemetz A, et al. Matriptase-2 is essential for hepcidin repression during fetal life and postnatal development in mice to maintain iron homeostasis. *Blood*. 2014;124(3):441–444.
34. Sangokoya C, Doss JF, Chi JT. Iron-responsive miR-485-3p regulates cellular iron homeostasis by targeting ferroportin. *PLoS Genet*. 2013;9(4):e1003408.
35. Bonds DR, Crosby LO, Cheek TG, Hägerdal M, Gutsche BB, Gabbe SG. Estimation of human fetal-placental unit metabolic rate by application of the Bohr principle. *J Dev Physiol*. 1986;8(1):49–54.
36. Rolfe DF, Brown GC. Cellular energy utilization and molecular origin of standard metabolic rate in mammals. *Physiol Rev*. 1997;77(3):731–758.
37. Heaton SJ, et al. The use of BeWo cells as an in vitro model for placental iron transport. *Am J Physiol, Cell Physiol*. 2008;295(5):C1445–C1453.
38. Koenig MD, Tussing-Humphreys L, Day J, Cadwell B, Nemeth E. Hepcidin and iron homeostasis during pregnancy. *Nutrients*. 2014;6(8):3062–3083.
39. Carter AM. Placental oxygen consumption. Part I: in vivo studies--a review. *Placenta*. 2000;21(Suppl A):S31–S37.
40. Allen LH. Anemia and iron deficiency: effects on pregnancy outcome. *Am J Clin Nutr*. 2000; 71(5 Suppl):1280S–1284S.
41. Radlowski EC, Johnson RW. Perinatal iron defi-ciency and neurocognitive development. *Front Hum Neurosci*. 2013;7:585.
42. Scholl TO. Maternal iron status: relation to fetal growth, length of gestation, and iron endowment of the neonate. *Nutr Rev*. 2011;69(Suppl 1):S23–S29. 43. Jaime-Perez JC, Herrera-Garza JL, Gomez- Almaguer D. Sub-optimal fetal iron acquisition under a maternal environment. *Arch Med Res*. 2005;36(5):598–602.
44. Lubach GR, Coe CL. Preconception maternal iron status is a risk factor for iron deficiency in infant rhesus monkeys (Macaca mulatta). *J Nutr*. 2006;136(9):2345–2349.
45. Colomer J, et al. Anaemia during pregnancy as a risk factor for infant iron deficiency: report from the Valencia Infant Anaemia Cohort (VIAC) study. *Paediatr Perinat Epidemiol*. 1990;4(2):196–204.
46. Kilbride J, Baker TG, Parapia LA, Khoury SA, Shuqaidef SW, Jerwood D. Anaemia during pregnancy as a risk factor for iron-deficiency anaemia in infancy: a case-control study in Jordan. *Int J Epidemiol*. 1999;28(3):461–468.
47. De Pee S, Bloem MW, Sari M, Kiess L, Yip R, Kosen S. The high prevalence of low hemoglobin concentration among Indonesian infants aged 3-5 months is related to maternal anemia. *J Nutr*. 2002;132(8):2215–2221.
48. Larsen S, Bjelland EK, Haavaldsen C, Eskild A. Placental weight in pregnancies with high or low hemoglobin concentrations. *Eur J Obstet Gynecol Reprod Biol*. 2016;206:48–52.
49. Lao TT, Tam KF. Placental ratio and anemia in third-trimester pregnancy. *J Reprod Med*. 2000;45(11):923–928.
50. Cantor AG, Bougatsos C, Dana T, Blazina I, McDonagh M. Routine iron supplementation and screening for iron deficiency anemia in pregnancy: a systematic review for the U.S. Preventive Services Task Force. *Ann Intern Med*. 2015;162(8):566–576.
51. Bah A, et al. Serum hepcidin concentrations decline during pregnancy and may identify iron deficiency: analysis of a longitudinal pregnancy cohort in the Gambia. *J Nutr*. 2017;147(6):1131–1137.
52. Schulze KJ, et al. Hepcidin and iron status among pregnant women in Bangladesh. *Asia Pac J Clin Nutr*. 2008;17(3):451–456.
53. Lozoff B, Georgieff MK. Iron deficiency and brain development. *Semin Pediatr Neurol*. 2006;13(3):158–165.
54. Meyron-Holtz EG, et al. Genetic ablations of iron regulatory proteins 1 and 2 reveal why iron regulatory protein 2 dominates iron homeostasis. *EMBO J*. 2004;23(2):386–395.
55. Lesbordes-Brion JC, et al. Targeted disruption of the hepcidin 1 gene results in severe hemochromatosis. *Blood*. 2006;108(4):1402–1405.
56. Nelson DM, Johnson RD, Smith SD, Anteby EY, Sadovsky Y. Hypoxia limits differentiation and up-regulates expression and activity of prostaglandin H synthase 2 in cultured trophoblast from term human placenta. *Am J Obstet Gynecol*. 1999;180(4):896–902.
57. Kliman HJ, Nestler JE, Sermasi E, Sanger JM, Strauss JF. Purification, characterization, and in vitro differentiation of cytotrophoblasts from human term placentae. *Endocrinology*. 1986;118(4):1567–1582.
58. Stefanova D, et al. Endogenous hepcidin and its agonist mediate resistance to selected infections by clearing non-transferrin-bound iron. *Blood*. 2017;130(3):245–257.
59. Kim A, et al. A mouse model of anemia of inflammation: complex pathogenesis with partial dependence on hepcidin. *Blood*. 2014;123(8):1129–1136.

SUPPLEMENTAL MATERIALS

Supplemental Table 1. Maternal Hematologic Parameters

	Iron-deficient				**Iron-replete**				**Iron-loaded**			
	Non-Preg (n=6)	E12.5 (n=3)	E15. (n=3)	E18.5 (n=7)	Non-Preg (n=10)	E12.5 (n=6)	E15.5 (n=3)	E18.5 (n=3)	Non-Preg (n=5)	E12.5 (n=2)	E15.5 (n=3)	E18.5 (n=4)
RBC (10^6/μL)	8.1±0.3	6.9±0.2	7.3±0.2	6.6±0.6	8.6±0.5	7.4±0.5	7.8±0.3	7.4±0.3	7.5±0.5	7.2±0.1	6.4±0.3	6.3±0.1
Hb (g/dL)	12.8±0.6	9.9±0.5	9.7±0.4	8.5±0.7	12.6±0.6	10.9±0.9	11.2±0.6	10.5±0.7	12.0±0.9	10.9±0.1	10.7±0.2	10.2±0.3
HCT (%)	35.3±1.7	28.1±1.2	29.1±0.9	26.6±1.7	45.0±6.8	36.3±4.6	40.5±5.7	38.6±3.6	34.9±3.6	31.2±0.0	29.5±1.1	31.8±3.1
MCV (fL)	43.5±1.1	40.6±1.0	40.0±0.3	40.2±1.0	47.6±5.5	49.2±4.3	52.1±7.4	52.0±3.7	45.4±2.6	43.6±0.7	46.3±0.9	50.2±4.5
MCH (pg)	15.5±0.8	14.3±0.6	13.3±0.2	12.8±0.1	14.7± 0.7	14.9±1.1	14.4±0.7	14.3±1.3	16.0±0.5	15.2±0.1	16.9±0.5	16.2±0.6
Plt (10^3/μL)	924±279	1077±96	1433±17	1115±329	853±223	699±120	916±134	1013±209	942±83	1010±79	973±70	893±137
WBC	4.7±2.4	3.8±1.6	2.5±0.6	3.1±0.5	3.5±1.1	4.1±2.1	3.0±0.6	2.5±0.9	2.8±0.8	2.8±0.8	3.2±1.1	1.6±1.0

Supplemental Table 1: Maternal Hematological Parameters. Hematological parameters of dams with different iron and pregnancy states. Data are presented as mean ± SD. RBC, red blood cell count; Hb, hemoglobin concentration; HCT, hematocrit; MCV, mean corpuscular volume; MCH, mean corpuscular hemoglobin; Plt, platelet count; WBC, white blood cell count.

Supplemental Table 2. Embryo Hematological Parameters			
	Iron-deficient	**Iron-replete**	**Iron-overload**
	E18.5 (n=15)	E18.5 (n=7)	E18.5 (n=8)
RBC (10^6/µL)	1.4±0.2***	2.8±0.2	2.8±0.2
Hb (g/dL)	2.9±0.5***	10.4±0.5	9.7±0.9
HCT (%)	10.6±2.1***	34.6±2.7	32.6±3.3
MCV (fL)	72.9±8.2#	133.7±27.1	116.4±5.6
MCH (pg)	20.2±1.1***	36.7±2.3	34.5±1.4*
Plt (10^3/µL)	427±81	501±44	469±34
WBC	5.7±2.0	5.1±0.3	3.9±1.2

Supplemental Table 2: Embryo Hematological Parameters. Hematological parameters of E18.5 embryos from dams with different iron states. Data are presented as mean ± SD. RBC, red blood cell count; Hb, hemoglobin concentration; HCT, hematocrit; MCV, mean corpuscular volume; MCH, mean corpuscular hemoglobin; Plt, platelet count; WBC, white blood cell count. Statistical differences between groups were determined by one-way ANOVA for normally distributed values followed by Holm-Sidak method for multiple comparisons versus iron-replete control group (***P<0.001) or one-way ANOVA on ranks followed by Dunn's method for multiple comparisons versus iron-replete control group (#P<0.05).

Supplemental Table 3. Maternal Hematologic Parameters						
	Iron-deficient (short-term)			**Iron-loaded (10K ppm diet)**		
	Non-Preg (n=2)	E18.5 (n=5)	*P*-value	Non-Preg (n=4)	E18.5 (n=4)	*P*-value
RBC (10^6/μL)	9.0±0.7	7.3±0.2	0.250*	9.0±0.2	7.3±0.6	**0.029***
Hb (g/dL)	12.9±0.9	8.7±0.3	0.655	13.1±0.4	11.1±0.5	0.0585
HCT (%)	42.9±4.2	33.0±1.7	**0.005**	42.6±3.3	35.3±4.2	0.289
MCV (fL)	47.6±1.1	45.5±2.0	**0.009**	47.5±2.7	48.3±3.3	0.587
MCH (pg)	13.6±0.1	11.9±0.2	**0.002**	14.6±0.4	15.2±0.7	0.125
Plt (10^3/μL)	616±113	1500±379	0.275	841±118	869±250	0.889
WBC	1.9±0.5	3.0±1.2	0.894	3.4±1.1	3.1±0.5	0.369

Supplemental Table 3: Maternal hematological parameters in alternative mouse models of iron depletion and iron loading. Hematological parameters of short-term iron-depleted dams and 10 Kppm iron-loaded dams. Data are presented as mean ± SD. RBC, red blood cell count; Hb, hemoglobin concentration; HCT, hematocrit; MCV, mean corpuscular volume; MCH, mean corpuscular hemoglobin; Plt, platelet count; WBC, white blood cell count. Statistical analysis compares E18.5 pregnancy values for iron-deficient short-term versus long-term or ironloading diet versus iron dextran using two-tailed Student's t-test for normally distributed values or Mann-Whitney rank sum test for non-normally distributed values (indicated by an asterisk following *P*-value).

Supplemental Table 4. Embryo Hematologic Parameters				
	Iron-deficient (short-term)	*P*-value	Iron-loaded (10Kppm diet)	*P*-value
	E18.5 (n=8)		E18.5 (n=14)	
RBC (10^6/μL)	1.6±0.4	0.118	2.7±0.2	0.594
Hb (g/dL)	3.1±0.8	0.397	9.3±0.6	0.272
HCT (%)	12.8±3.1	0.071	35.2±3.6	0.114
MCV (fL)	78.3±5.2	0.100*	133.7±27.1	**0.019**
MCH (pg)	19.0±1.4	0.050	33.9±2.3	0.535
Plt (10^3/μL)	324±108	**0.022**	411±42	**0.005**
WBC	7.4±1.5	0.142	13.8±10.5	**0.003***

Supplemental Table 4: Embryo hematological parameters in alternative models of iron depletion or iron loading. Hematological parameters of E18.5 embryos from short-term iron-depleted dams and 10 Kppm ironloaded dams. Data are presented as mean ± SD. RBC, red blood cell count; Hb, hemoglobin concentration; HCT, hematocrit; MCV, mean corpuscular volume; MCH, mean corpuscular hemoglobin; Plt, platelet count; WBC, white blood cell count. Statistical analysis compares values for iron-deficient short-term versus long-term or iron-loading diet versus iron dextran using two-tailed Student's t-test for normally distributed values or Mann-Whitney rank sum test for non-normally distributed values (indicated by an asterisk following *P*-value).

Supplemental Table 5. qPCR Primers		
Species	Gene	Sequence
Mouse	*Hprt*	Fwd: 5'-CTG GTT AAG CAG TAC AGC CCC AA-3'
		Rev: 5'-CAG GAG GTC CTT TTC ACC AGC-3'
	Hamp	Fwd: 5'-TTG CGA TAC CAA TGC AGA AGA- 3'
		Rev: 5'-GAT GG GCTT CTA GGC TAT GTT-3'
	Tfr1	Fwd: 5'-TCA TGA GGG AAA TCA ATG ATC-3'
		Rev: 5'-GCC CCA GAA GAT ATG TCG GAA-3'
	Fpn1	Fwd: 5'-ATG GGA ACT GTG GCC TTC AC-3'
		Rev: 5'-TCC AGG CAT GAA TAC GGA GA-3'
	Fpn1A	Fwd: 5'-AAA GAA GAC CCC GTG ACA GC-3'
		Rev: 5'-TCC CCG TGT TTG TTC TGA TG-5'
	Fpn1B	Fwd: 5'-GCC GGT TGG AGT TTC AAT GT-3'
		Rev: 5'-TCC CCG TGT TTG TTC TGA TG-3'
	Zc3h12A/Regnase-1	Fwd: 5'-CGA GAG GCA GGA GTG GAA AC-3'
		Rev: 5'-CTT ACG AAG GAA GTT GTC CAG GCT AG-3'
	Dmt1	Fwd: 5'-CGC TCG GTA AGC ATC TCG AA-3'
		Rev: 5'-TGT TGC CAC CGC TGG TAT CT-3'
	Hfe	Fwd: 5'-CCA CCG CGT TCA CAT TCT CT-3'
		Rev: 5'-CTG GTC ATC CAC ATA GCC CC-3'
	Hephl1	Fwd: 5'-GCA TCG GAA GTG AAG TGG AC-3'
		Rev: 5'-GGT TTG AAA TGT CCC AGG AA-3'
	Flvcr1/Mfsd7b	Fwd: 5'-TTT CCT TTG TGC CTG GAT GT-3'
		Rev: 5'-GCC CGG TGT TTA TAT TGT GC-3'
	Il6	Fwd: 5'-CTC TGC AAG AGA CTT CCA TCC AGT-3'
		Rev: 5'-CGT GGT TGT CAC CAG CAT CA-3'
	Saa1	Fwd: 5'-AGT CTG GGC TGC TGA GAA AA-3'
		Rev: 5'-ATG TCT GTT GGC TTC CTG GT-3'
Human	*FPN1 variant I*	Fwd: 5'-TTT TGC CCA AGG CTG TTG TG-3'
		Rev: 5'-TCA TGA CAC TAG GCG ACC C-3'
	FPN1 variant IIB	Fwd: 5'-ATG TAG GAT CCA CTA CCA GGG-3'
		Rev: 5'-TCA TGA CAC TAG GCG ACC C-3'
	ZC3H12A/REG1	Fwd: 5' – CGA CAC ATA CCG TGA CCT CC – 3'
		Fwd: 5' – TCA GGG GGC ATA AAC TTG TCA – 3'

Supplemental Table 5: qPCR Primers

Supplemental Table 6. Antibodies	
Target protein	**Primary antibody**
Mouse FPN	Rat monoclonal antibody IC7 (western and immunofluorescence), Amgen
Human FPN	Human monoclonal antibodies 38G6 (western), 38C8 (immunofluorescence), Amgen
Hepcidin ELISA	Mouse monoclonal antibodies Ab2B10 and Ab2H4-HRP, Amgen
Mouse and human TFR1	Monoclonal antibody H68.4, ThermoFisher Scientific
Mouse and human ferritin heavy chain	Rabbit monoclonal antibody D1D4, Cell Signaling
Mouse ferritin light chain	Goat polyclonal antibody NBP1-06986, Novus
Mouse and human β-actin	Monoclonal antibody-peroxidase AC-15, SIGMA
Mouse GAPDH	Rabbit monoclonal antibody 14C10, Cell Signaling
Mouse and human electron transport chain	Total OXPHOS Rodent WB Antibody Cocktail ab110413, Abcam
Secondary antibodies:	
Anti-mouse IgG HRP (Cell Signaling #7076)	
Anti-rabbit IgG HRP (Cell Signaling #7074)	
Anti-rat IgG HRP (AbCam #ab102213)	
Pierce high sensitivity neutravidin-HRP (ThermoFisher #31030)	
Goat-anti-mouse-AF488 (ThermoFisher #A32723)	
Goat-anti-mouse-AF594 (ThermoFisher #A11032),	
Streptavidin-AF555 (ThermoFisher #S21381)	
Donkey-anti-rat-AF488 (ThermoFisher #A21208)	

Supplemental Table 6: Antibodies. 38G6 and 38C8 were biotinylated using EZ-Link Sulfo-NHS-LC-LC Biotin (Thermo 21338). FPN antibody validation is provided in Supplemental Figure 10.

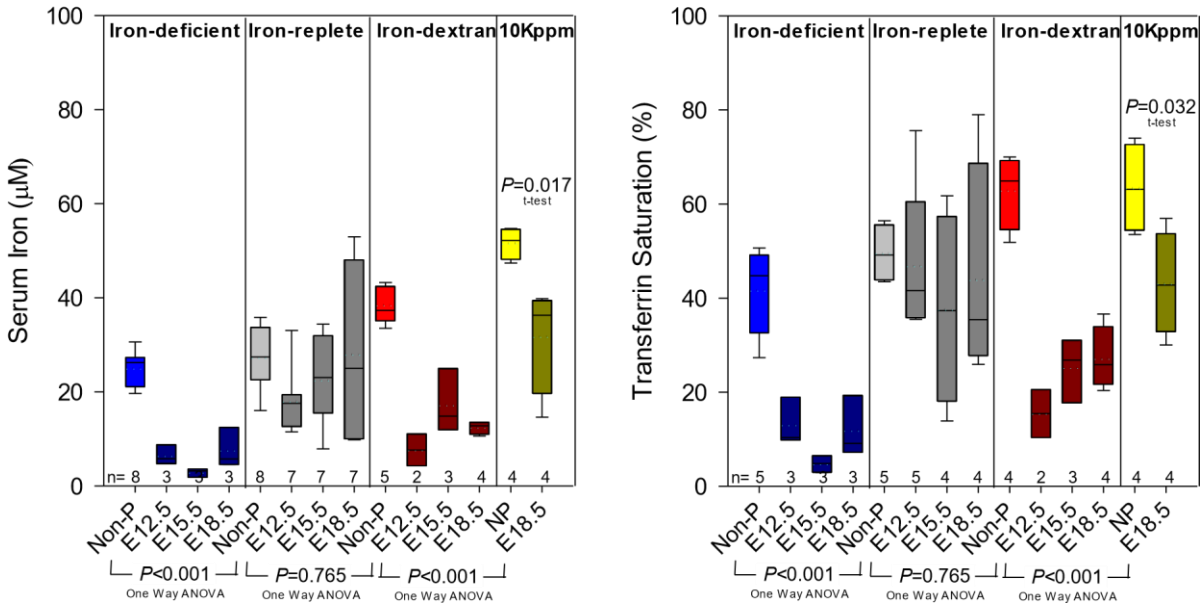

Supplemental Figure 1: Maternal transferrin saturation. Females were fed standard chow (185 ppm iron) or low iron diet (4ppm iron) or high iron diet (10,000 ppm iron) 2 weeks prior to and throughout the pregnancy or were injected with 20 mg iron dextran at time of mating. Pregnant females were analyzed at E12.5, 15.5 and 18.5. Nonpregnant (Non-P) females were subjected to an equivalent iron treatment. Serum iron of the same samples is shown for comparison.

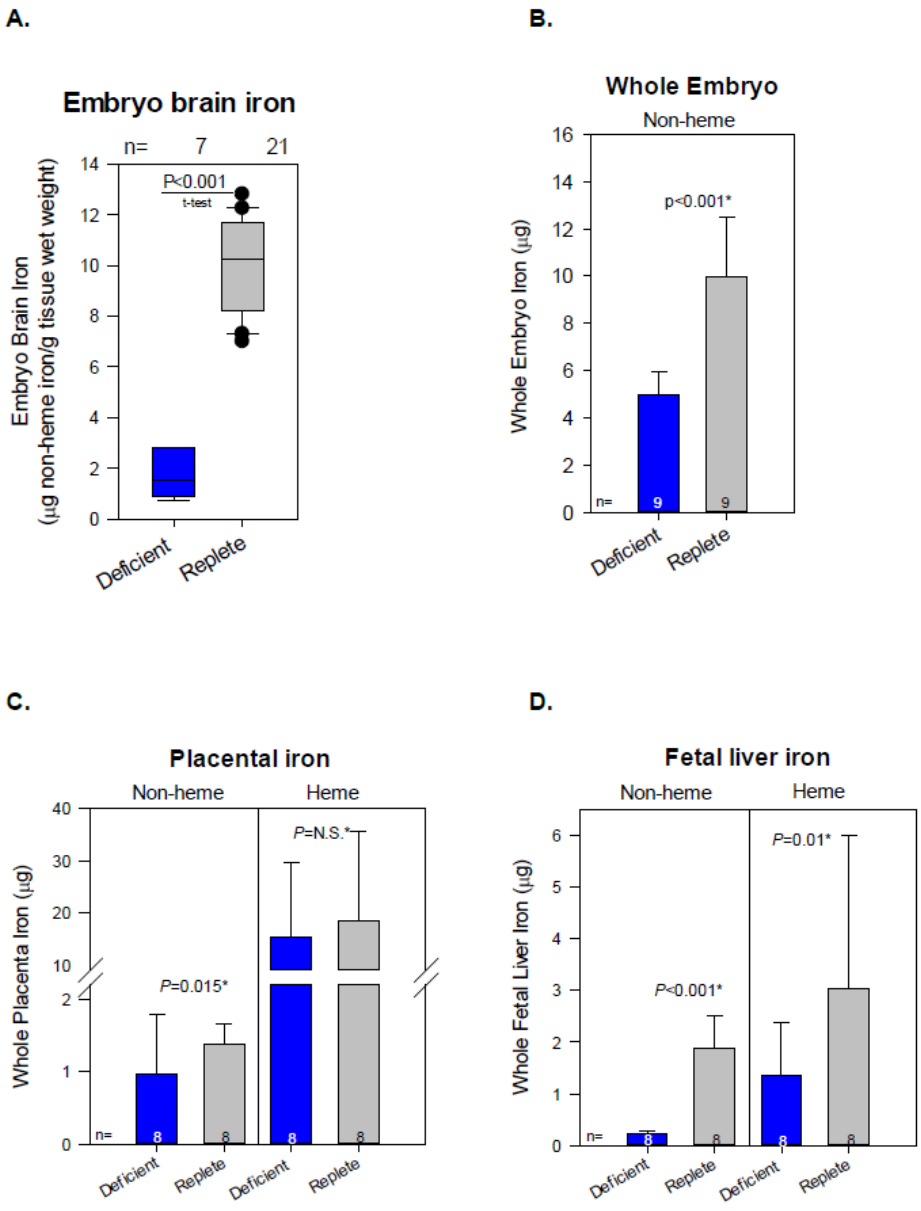

Supplemental Figure 2: The effect of maternal iron deficiency on placental and fetal iron at E18.5 compared to iron-replete pregnancy. (A) Embryo brain non-heme iron concentration. **(B)** Whole embryo non-heme iron. **(C)** Non-heme and heme iron content of whole placentas. **(D)** Non-heme and heme iron content of whole fetal livers. Statistical analyses were performed using two-tailed Student's t-test for normally distributed values or Mann- Whitney rank sum test (*) for non-normally distributed values.

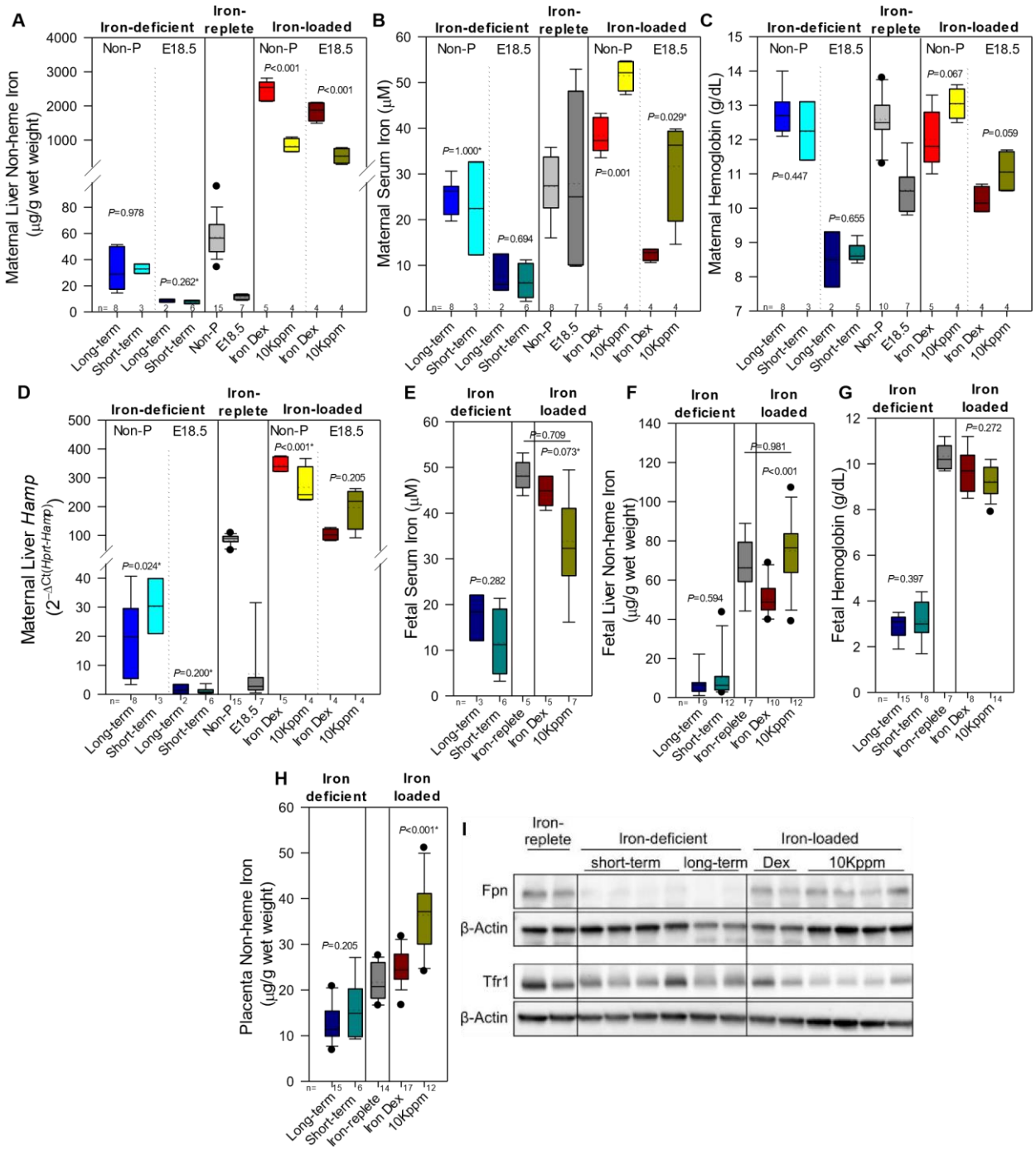
A
Iron-deficient
Iron-replete
Iron-loaded
Non-P
E18.5
Maternal Liver Non-heme Iron (μg/g wet weight)
P=0.978
P=0.262*
P<0.001
P<0.001
Long-term
Short-term
Iron Dex
10Kppm
B
Maternal Serum Iron (μM)
P=1.000*
P=0.694
P=0.001
P=0.029*
C
Maternal Hemoglobin (g/dL)
P=0.447
P=0.655
P=0.067
P=0.059
D
Maternal Liver Hamp (2^-ΔCt(Hprt-Hamp))
P=0.024*
P=0.200*
P<0.001*
P=0.205
E
Iron deficient
Iron loaded
Fetal Serum Iron (μM)
P=0.282
P=0.709
P=0.073*
Iron-replete
F
Fetal Liver Non-heme Iron (μg/g wet weight)
P=0.594
P=0.981
P<0.001
G
Fetal Hemoglobin (g/dL)
P=0.397
P=0.272
H
Placenta Non-heme Iron (μg/g wet weight)
P=0.205
P<0.001*
I
Iron-replete
Iron-deficient
Iron-loaded
short-term
long-term
Dex
10Kppm
Fpn
β-Actin
Tfr1
β-Actin

Supplemental Figure 3: Comparison of different models of iron deficiency and iron loading in pregnant mice. *Iron depletion*: long-term versus short-term iron depletion was achieved by starting females on low iron diet 2 weeks prior to pregnancy versus at mating. The diet was continued through the pregnancy. *Iron loading*: females received a single intraperitoneal injection of 20mg iron dextran at mating, or 10,000ppm iron diet 2 weeks prior to mating and throughout gestation (10Kppm). Non-pregnant animals were subjected to the same regimens and analyzed at the same time point. (**A-D**) Maternal parameters: liver iron (**A**), serum iron (**B**), hemoglobin (**C**), and hepcidin mRNA (**D**). (**E-G**) Fetal parameters: serum iron (**E**), liver iron (**F**) and hemoglobin (**G**). (**H-I**) Placental parameters: tissue non-heme iron (**H**), and Fpn and TfR1 protein levels (**I**). Statistical analyses were performed using two-tailed Student's t-test for normally distributed values or Mann-Whitney rank sum test for non-normally distributed values (indicated by an asterisk). Data for iron-deficient long-term, iron-replete and iron dextran are replicated from Figure 1 but are provided for ease of understanding.

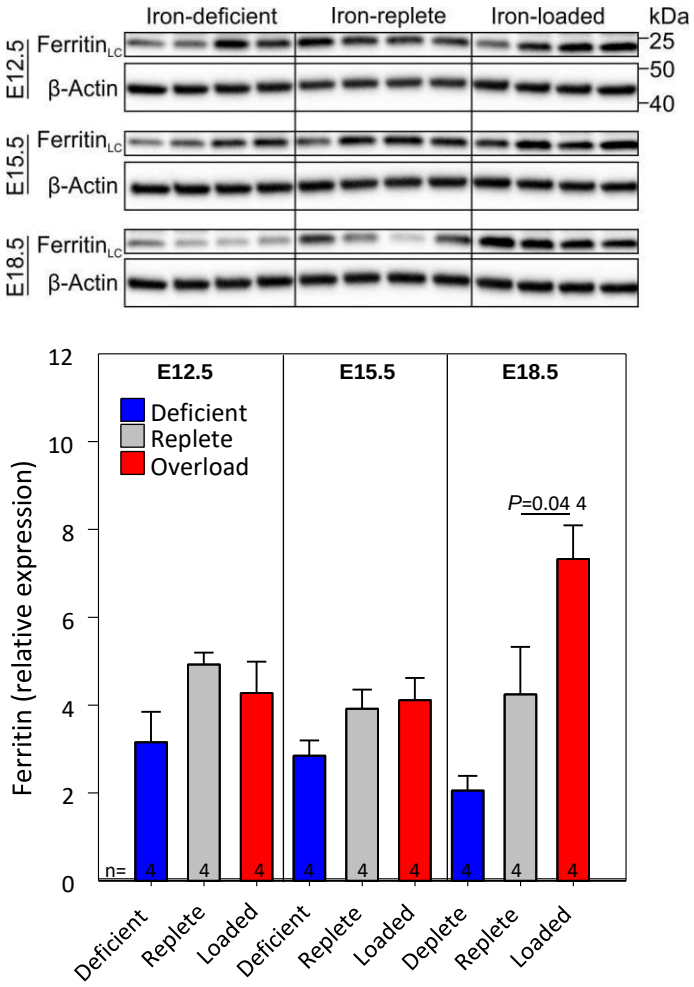

Supplemental Figure 4: Placental ferritin increases with elevated maternal iron status. Mouse placentas from Figure 1 were analyzed by western blotting to determine protein concentration of ferritin. β-Actin was used for normalization (the image is the same as in Figure 2C but included here for convenience). Bar graph shows means +/- SE. Statistical differences between groups were determined by one-way ANOVA for normally distributed values followed by Holm-Sidak method for multiple comparisons versus iron-replete control group.

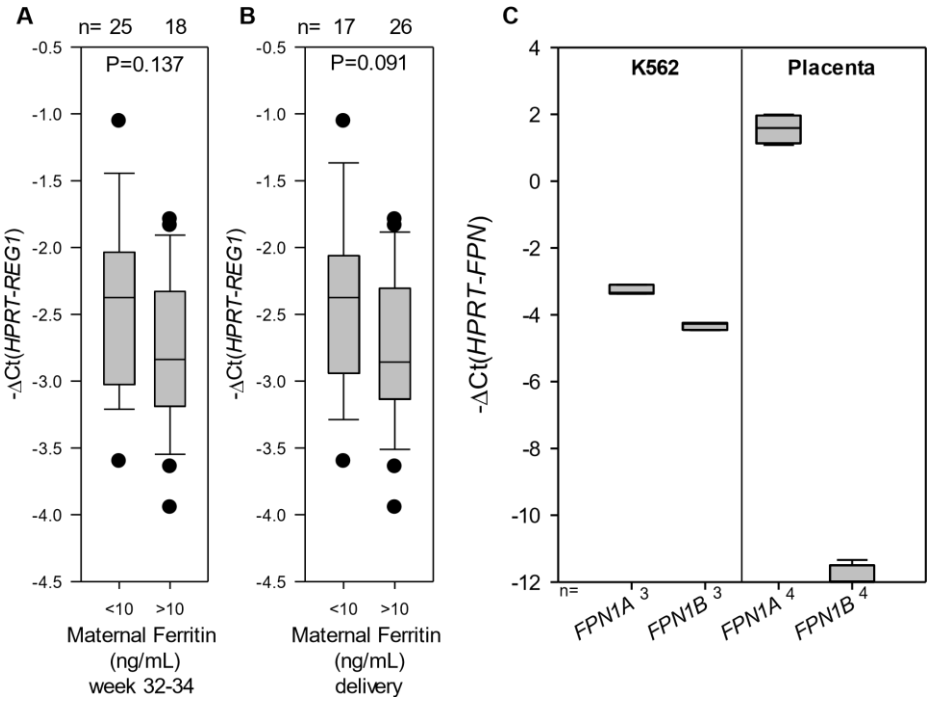

Supplemental Figure 5: *REG1* mRNA expression and *FPN* mRNA isoforms in human placenta. (**A-B**) Placentas from uncomplicated human pregnancies were analyzed by qPCR for *REG1* mRNA expression according to maternal ferritin at week 32-34 or at delivery. (**C**) FPN splicing variant "*FPN1A"* (also known as *FPN variant I* (1)) contains 5'IRE, and "*FPN1B"* (also known as FPN *variant IIB* (1, 2)) does not contain 5'IRE. The isoforms were measured by qPCR in human placental samples. *HPRT* was used as a housekeeping gene. K562 cells were used as a control sample in which a comparable amount of *FPN1A* and *1B* was reported (1).

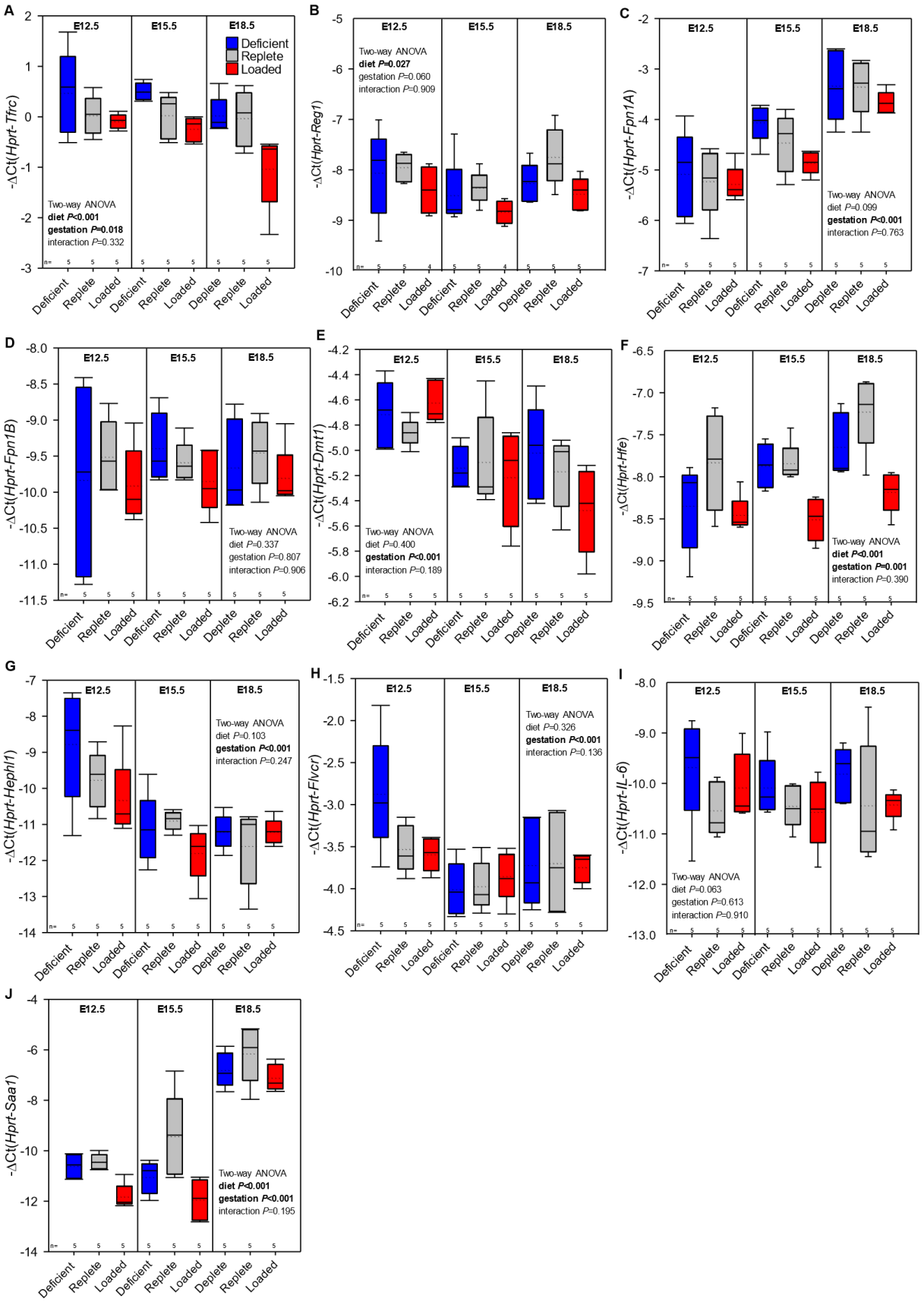
A
E12.5
E15.5
E18.5
Deficient
Replete
Loaded
-ΔCt(Hprt-Tfrc)
Two-way ANOVA
diet P<0.001
gestation P=0.018
interaction P=0.332
B
-ΔCt(Hprt-Reg1)
Two-way ANOVA
diet P=0.027
gestation P=0.060
interaction P=0.909
C
-ΔCt(Hprt-Fpn1A)
Two-way ANOVA
diet P=0.099
gestation P<0.001
interaction P=0.763
D
-ΔCt(Hprt-Fpn1B)
Two-way ANOVA
diet P=0.337
gestation P=0.807
interaction P=0.906
E
-ΔCt(Hprt-Dmt1)
Two-way ANOVA
diet P=0.400
gestation P<0.001
interaction P=0.189
F
-ΔCt(Hprt-Hfe)
Two-way ANOVA
diet P<0.001
gestation P=0.001
interaction P=0.390
G
-ΔCt(Hprt-Hephl1)
Two-way ANOVA
diet P=0.103
gestation P<0.001
interaction P=0.247
H
-ΔCt(Hprt-Flvcr)
Two-way ANOVA
diet P=0.326
gestation P<0.001
interaction P=0.136
I
-ΔCt(Hprt-IL-6)
Two-way ANOVA
diet P=0.063
gestation P=0.613
interaction P=0.910
J
-ΔCt(Hprt-Saa1)
Two-way ANOVA
diet P<0.001
gestation P<0.001
interaction P=0.195
Deficient
Replete
Loaded
Deplete

Supplemental Figure 6: Placental mRNA expression of *Tfrc* and *Fpn* in mouse pregnancies with varying maternal iron status. E12.5, 15.5 and 18.5 placentas from iron-deficient, iron-replete and iron-loaded mouse pregnancies were analyzed by qPCR to determine mRNA expression of *Tfrc* (**A**), its regulator regnase-1 (*Reg-1*) (**B**), *Fpn1* splicing variant *Fpn1A* which contains 5'IRE (**C**) and *Fpn1B* which does not contain 5'IRE (**D**), *Dmt1* (**E**), *Hfe* (**F**), *Hephl1* (**G**), *Flvcr1* (**H**), *Il-6* (**I**), *Saa1* (**J**). *Hprt* was used as a housekeeping gene. Statistical differences between groups was determined by two-way ANOVA, P values for diet, gestation and interactions are listed in the graphs along with n number. For Tfrc, diet affects expression levels ($P<0.001$) with significant differences at E18.5 between iron-deficient and iron-loaded ($P=0.005$) and between iron-replete and iron-loaded ($P=0.005$); however, gestational age does not ($P=0.332$) affect Tfrc expression. For Fpn1A, gestational age affects mRNA expression ($P<0.001$) whereas diet has no effect ($P=0.099$).

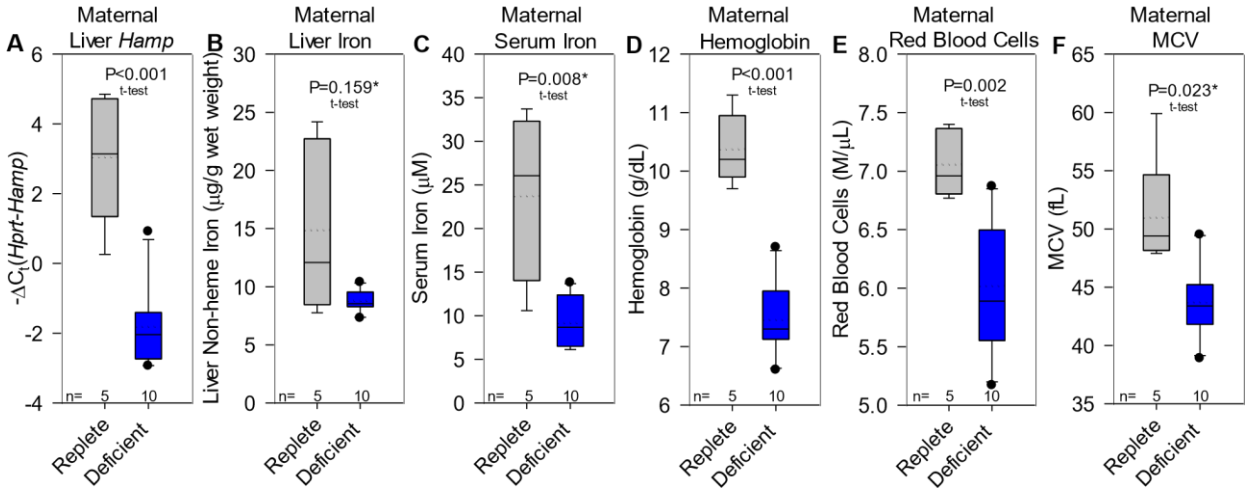

Supplemental Figure 7: Iron and hematological parameters for E18.5 *Hamp*$^{+/-}$ dams. *Hamp*$^{+/-}$ females were mated with *Hamp*$^{+/-}$ males. Females were placed on iron-replete or iron-deficient diet 1 week prior to mating. To confirm sufficient iron depletion, maternal liver hepcidin mRNA (**A**), liver iron (**B**), serum iron (**C**), hemoglobin (**D**), RBC count (**E**), and MCV (**F**) were measured. Statistical differences between groups were determined by two-tailed Student's t-test for normally distributed values or Mann-Whitney rank sum test for non-normally distributed values (indicated by an * following *P*-value).

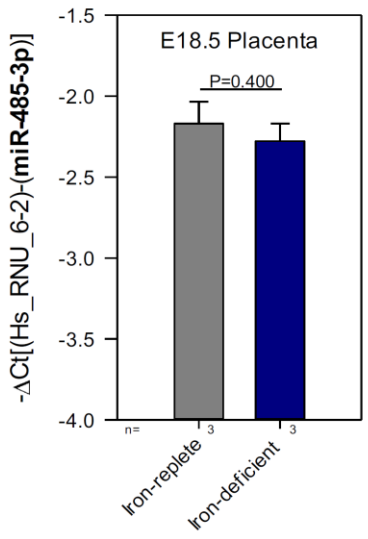

Supplemental Figure 8: miR-485-3p is not responsible for changes in placenta FPN during maternal iron deficiency. Expression levels of miR-485-3p in E18.5 placentas from iron-replete and iron-deficient pregnancies. Data are presented as mean±SE. Statistical differences were determined by Mann-Whitney rank sum test.

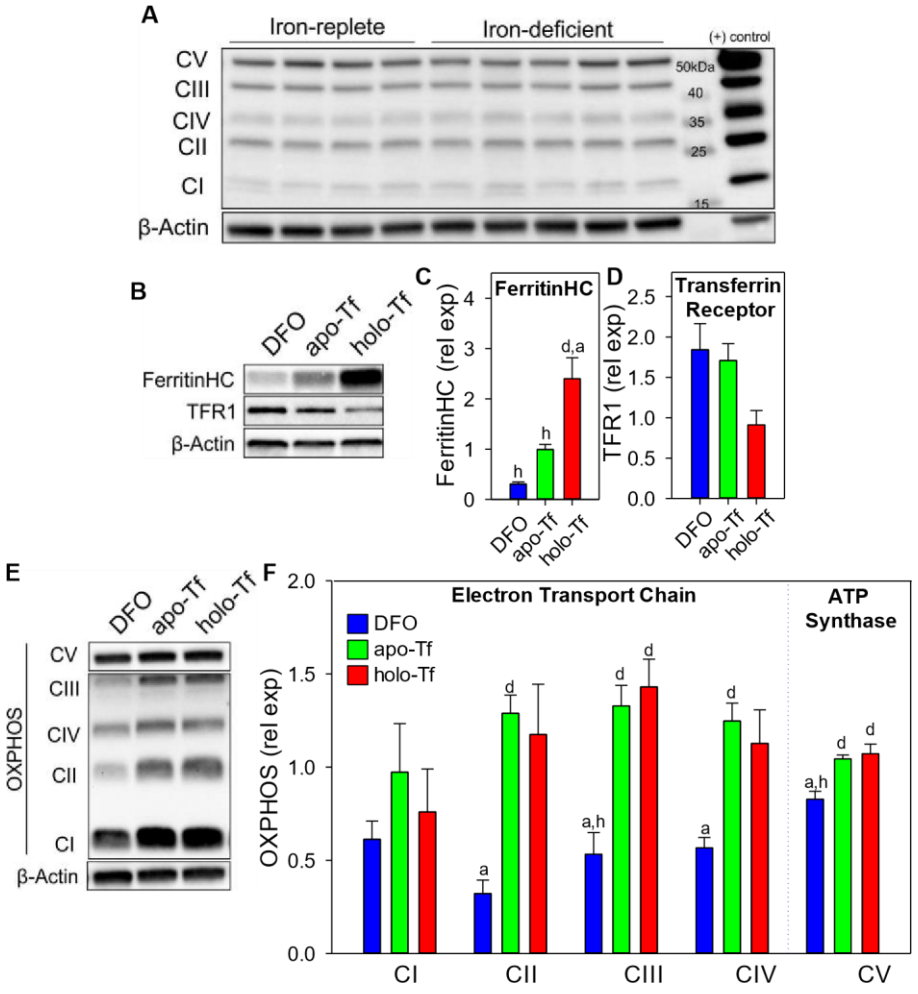

Supplemental Figure 9: Integrity of ETC complexes I-V in E18.5 mouse placentas and BeWo cells under varying iron conditions. (**A**) Placenta lysates from E18.5 iron-replete and iron-deficient pregnancies in Figure 1 were analyzed by western blot for expression of proteins involved in oxidative phosphorylation (OXPHOS): electron transport chain (ETC) complexes I (NDUFB8), II (SDHB), III (UQCRC2), IV (MTCO1) and V (ATP5A). (**B-F**) BeWo cells were treated with DFO, apo-Tf or holo-Tf (100μM each) for 24hr. (**B**) Western blot of FerritinHC and TFR1. βActin was used as a loading control. (**C, D**) Quantitation of ferritinHC and TFR1, relative to an untreated control within each experiment (n=3). (**E**) Western blot of ETC complexes I-V.

(**F**) Quantification of ETC complexes normalized to β-Actin and presented relative to the untreated control for each experiment (n=5). Data are presented as mean±SE. For statistical analysis, the two-tailed 1-sample Student t-test (normally distributed data) was used with 1 as the comparison. Statistical significance, $P<0.05$.

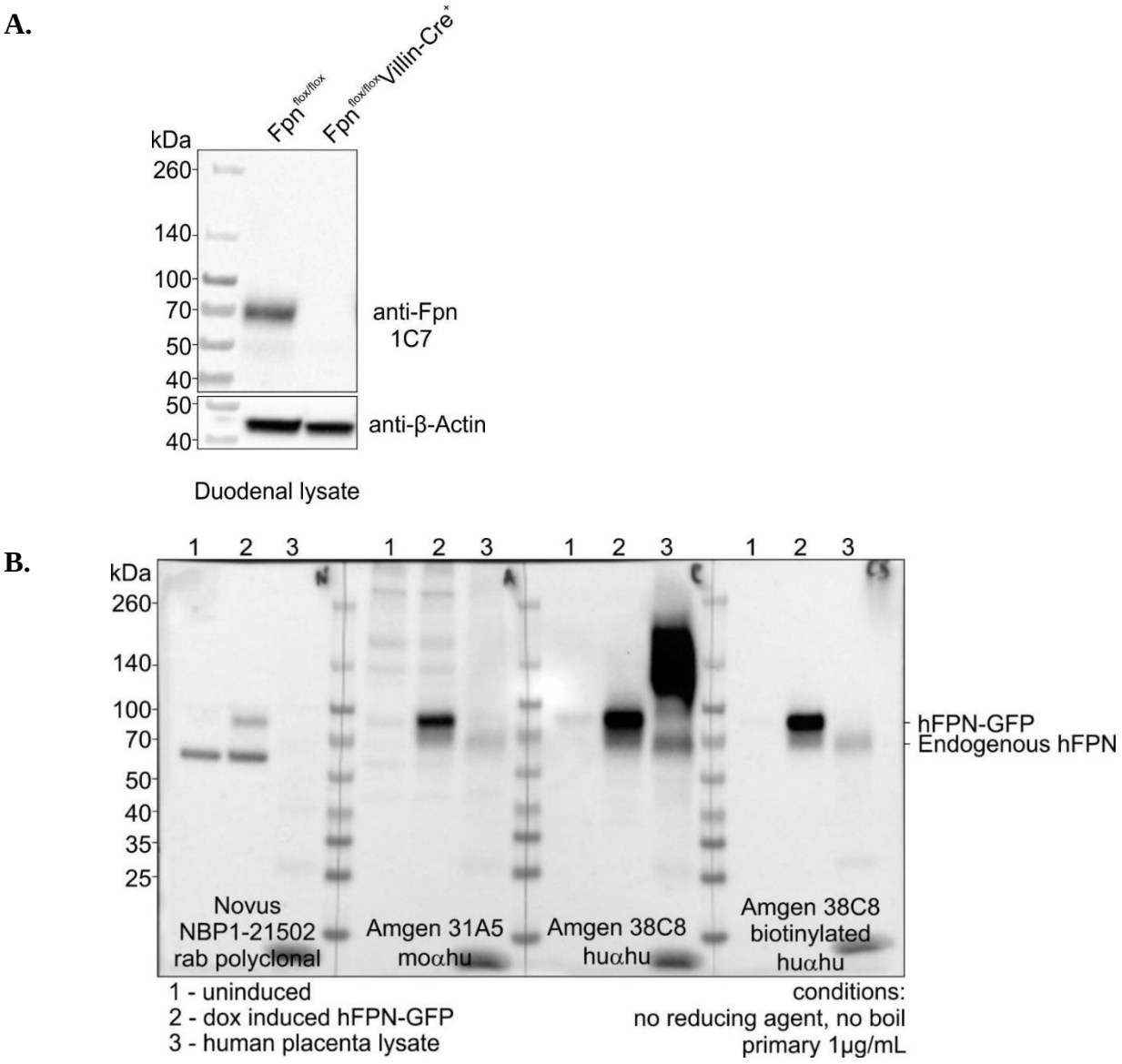

Supplemental Figure 10: FPN antibody validation. (A) Anti-mouse FPN antibody was validated using duodenal epithelium from intestinal-specific FPN knockout mice and their flox littermates. **(B)** Anti-human FPN antibody used in our study is Amgen 38C8 (far right). It was validated using HEK293 cells induced or not to express human FPNGFP (lanes 1 and 2), as well as a human placental lysate expressing endogenous FPN (lane 3). Comparison to additional anti-FPN antibodies is provided.

SUPPLEMENTAL REFERENCES

1. Cianetti L, Segnalini P, Calzolari A, Morsilli O, Felicetti F, Ramoni C, Gabbianelli M, Testa U, and Sposi NM. Expression of alternative transcripts of ferroportin-1 during human erythroid differentiation. *Haematologica.* 2005;90(12):1595-606.

2. Zhang DL, Hughes RM, Ollivierre-Wilson H, Ghosh MC, and Rouault TA. A ferroportin transcript that lacks an iron-responsive element enables duodenal and erythroid precursor cells to evade translational repression. *Cell metabolism.* 2009;9(5):461-73.

CHAPTER 2: MATERNAL HEPCIDIN DETERMINES EMBRYO IRON HOMEOSTASIS (ACCEPTED MANUSCRIPT)

Manuscript accepted in journal *Blood*:

MATERNAL HEPCIDIN DETERMINES EMBRYO IRON HOMEOSTASIS

Veena Sangkhae, Allison L Fisher, Kristine Chua, Peter Ruchala, Tomas Ganz and Elizabeta Nemeth

Abstract

Iron disorders are associated with adverse pregnancy outcomes, yet iron homeostatic mechanisms during pregnancy are poorly understood. In humans and rodents, the iron-regulatory hormone hepcidin is profoundly decreased in pregnant mothers, which is thought to ensure adequate iron availability for transfer across placenta. However, the fetal liver also produces hepcidin, which may regulate fetal iron endowment by controlling placental iron export. To determine the relative contribution of maternal vs embryo hepcidin to the control of embryo iron endowment in iron-sufficient or iron-overloaded mice, we generated combinations of mothers and embryos that had or lacked hepcidin. We found that maternal, but not embryonic hepcidin determined embryo and placental iron endowment in a healthy pregnancy. We further determined that inflammation can counteract pregnancy-dependent suppression of maternal hepcidin. To establish how essential maternal hepcidin suppression is for embryo iron homeostasis, we mimicked the range of maternal hepcidin activity by administering a hepcidin peptide mimetic to pregnant mice. This also allowed us to determine the effect of isolated maternal hepcidin excess on pregnancy, in the absence of other confounding effects of inflammation. Higher doses of hepcidin agonist caused maternal iron restriction and anemia, lower placenta and embryo weight, embryo anemia, and increased embryo mortality. Low agonist doses did not cause maternal anemia but still adversely affected the embryo, causing anemia, tissue iron deficiency including in the brain, and decreased weight. Our studies demonstrate that suppression of maternal hepcidin during pregnancy is essential for maternal and embryo iron homeostasis and health.

Introduction

Systemic iron homeostasis is regulated by the hormone hepcidin[1], which triggers degradation of the only known mammalian iron exporter ferroportin (FPN). Decreased FPN levels prevent iron absorption, recycling and mobilization from storage, thereby decreasing plasma iron levels and iron utilization in tissues[2]. Major stimuli that regulate hepcidin production include iron, erythropoietic activity, pregnancy and inflammation[3,4]. Hepcidin suppression during iron deficiency allows for replenishment of body iron stores, and suppression after an erythropoietic stimulus allows sufficient delivery of iron for compensatory erythropoiesis. Inflammation increases hepcidin production via the IL-6 pathway[5,6], resulting in hypoferremia. Although this host defense mechanism may slow the growth of invading microorganisms, in chronic inflammatory conditions or infections, elevated hepcidin contributes to the development of iron-restricted anemia[7].

During pregnancy, iron is critical for placental growth, fetal development and maternal health[8]. In humans, iron deficiency and its more severe form, iron-deficiency anemia (IDA), have been associated with adverse pregnancy outcomes including increased maternal morbidity and mortality, preterm birth, low birth weight, cognitive defects in newborns and impaired immune function[9-14]. In healthy human[15] and rodent[16,17] pregnancies, maternal hepcidin levels are profoundly decreased in the second and third trimester by an unknown mechanism but are still regulated by maternal iron status[16,18]. Decreased maternal hepcidin allows for increased absorption of dietary iron and mobilization of iron from stores[19], thus increasing the availability of iron for transfer across placenta.

Although maternal hepcidin is low in normal pregnancies, inflammatory disorders could prevent appropriate suppression of hepcidin, potentially compromising iron availability during pregnancy. In addition to causing iron sequestration in the mother, elevated maternal hepcidin could prevent iron absorption from supplements commonly prescribed to pregnant women. A study utilizing

stable iron isotope administration in healthy pregnancies reported that higher maternal hepcidin was associated with lower dietary iron absorption and lower iron transfer to the neonate[20].

Inflammation during pregnancy is common in developing countries with endemic malaria, HIV, tuberculosis or parasitic infestations, whereas in high-resource countries, inflammation occurs in bacterial and viral infections, obesity and diabetes, and less commonly autoimmune diseases or malignancies[21]. It has not been systematically explored whether maternal hepcidin is increased in these conditions, particularly in pregnancies with moderate to severe inflammation, how maternal hepcidin is regulated in the context of co-existing anemia, and whether maternal hepcidin has any effect on neonatal iron homeostasis. In a cross-sectional cohort including both healthy and complicated pregnancies (gestational diabetes mellitus, gestational hypertension, preeclampsia and liver dysfunction), maternal hepcidin correlated with CRP[22] but in healthy human pregnancy maternal serum hepcidin did not correlate with inflammatory markers[15,23,24]. Maternal hepcidin predicted anemia of inflammation in pregnant women with schistosomiasis[25]. In the milder inflammation associated with obesity, some studies reported no difference in maternal hepcidin compared to lean pregnancies in early pregnancy or the third trimester[26-28], whereas other studies found elevated maternal serum hepcidin in obese pregnant women[29-32]. No clear association with neonatal iron status or anemia was reported. Importantly, in human studies utilizing iron parameters measured in cord blood, evaluation of fetal/neonatal iron homeostasis is confounded by the effects of labor and delivery. Indeed, a time-course analysis of perinatal hepcidin expression in mice showed that embryo hepcidin expression is low, but transiently increases at birth until at least P2[33].

In this study, we examined the role and regulation of hepcidin during pregnancy and found that suppression of maternal hepcidin during pregnancy is essential for embryo iron homeostasis and health.

Materials and Methods

Mice – All experiments were approved by the Animal Research Committee at UCLA. Mice were fed a standard diet (PicoLab® Rodent Diet 20, 5053 Irradiated, 185 ppm iron). All mouse strains were on a C57BL/6J background. Wild-type (WT) mice were from The Jackson Laboratory or bred in-house. Hepcidin knockout (KO) mice were originally from Dr. Sophie Vaulont[19] and backcrossed by us onto the C57BL/6J background.

To induce maternal inflammation, pregnant WT mice received a subcutaneous interscapular injection of 0.5 μg/g LPS (*E. coli* serotype O55:B5, MilliporeSigma) or sterile water at E17.5. To model iron-restriction, pregnant C57BL/6J mice were injected subcutaneously with 10 or 50 nmol of minihepcidin (PR73) dissolved in SL220[34,35] (NOF Corporation); controls were injected with the corresponding amount of solvent. Injections were given daily from E12.5-17.5 (6d) or E7.5-17.5 (11d). PR73 (MW 1730 Da) was synthesized as described[35].

Statistical analysis – Statistical analysis was performed using GraphPad Prism 8 or SigmaPlot (Systat Software), details are provided in the Supplemental Data.

Additional methods can be found in the Supplemental Data.

Results

Embryo iron endowment is determined by maternal rather than embryo or placental hepcidin. Maternal hepcidin (*Hamp)* is profoundly suppressed during human[15] and rodent pregnancies[16,17], reaching maximal suppression in the 3rd trimester when iron transfer to the fetus is greatest (reviewed in[36]). However, the fetal liver also produces hepcidin which could control placental iron export through FPN. At embryonic day (E)18.5, maternal liver *Hamp* mRNA was 12-fold lower than in non-pregnant females ($2^{-\Delta Ct}$ 84±18 v 7±10; P<0.001), and embryo liver *Hamp* was another 15-fold lower than maternal *Hamp* ($2^{-\Delta Ct}$ 7±10 v 0.46±0.49; P<0.001) (**Figure 2-1A**). Serum hepcidin was also suppressed in pregnant females and embryos compared to non-pregnant females: 150±37 v 16±16 v 11±7 ng/mL for non-pregnant, pregnant females and embryos respectively (**Figure 2-1B**). Recently, we showed that during *iron deficiency*, embryo iron endowment was not affected by the embryo's hepcidin genotype[16]. However, under high iron conditions, when hepcidin is typically induced[4], embryo hepcidin could limit iron transfer across the placenta. We examined the contribution of maternal and embryo hepcidin to regulating iron transfer from mother to placenta and embryo in normal and iron-loaded pregnancies. The iron-loaded *Hamp* KO and iron-sufficient *Hamp* heterozygous (Het) females were mated with *Hamp*

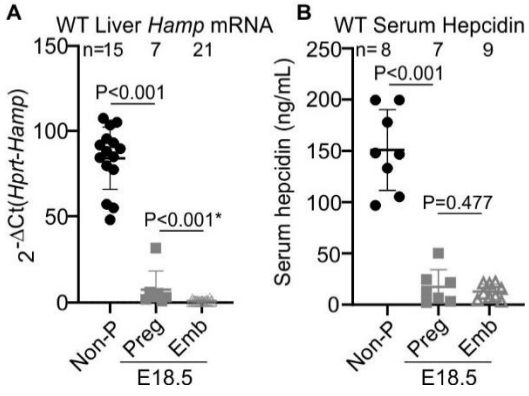

Figure 2-1. Hepcidin expression in non-pregnant and pregnant females and embryos in mice. WT C57BL6/J non-pregnant females are compared to age-matched pregnant females and their embryos at E18.5. **(A)** Hepatic Hamp mRNA and **(B)** serum hepcidin. Statistical differences between groups was determined by two-tailed Student's t-test for normally distributed values or by Mann-Whitney rank-sum test for non-normally distributed values (indicated by * following P-value). Non-P = nonpregnant, Preg = pregnant, Emb = embryos.

Het males to generate genetically mixed litters of *Hamp* KO, Het and WT embryos. *Hamp* KO females were significantly more iron-loaded than Het females at E18.5: serum iron, 45±2 v 20±8 ng/mL (P=0.036, **Figure 2-2A**) and liver non-heme iron, 417±131 v 13±6 µg/g (P=0.003, **Figure 2-2B**). We then compared the iron status of embryos and their placentas at E18.5 within each of the maternal genotypes. Although embryo *Hamp* mRNA was generally low in all genotype groups at E18.5, statistically significant differences were detected in liver *Hamp* expression between WT, Het and KO embryos (**Supplemental Figure 2-1A**). These variations in expression were not functionally relevant, as there was no difference in embryo serum iron, embryo liver non-heme iron, and placental non-heme iron concentrations (P=0.95, P=0.75, and P=0.88) between embryo *Hamp* genotypes derived from Het mothers, nor between embryos derived from KO mothers (P=0.08, P=0.29, P=0.17) (**Figure 2-2C-E**). These data demonstrate that even under high iron conditions, embryo hepcidin has no effect on embryo iron endowment.

By contrast, there was a highly significant effect of maternal *Hamp* genotype on embryo iron endowment. Maternal hepcidin deficiency significantly increased concentration of embryo liver non-heme iron (P<0.001 for maternal v P=0.377 for embryo *Hamp* genotype), and increased placenta non-heme iron (P<0.001 for maternal v P=0.391 for embryo *Hamp* genotype) (**Figure 2-2D, E**). Similar to results at E18.5, analysis of neonatal liver non-heme iron at P1 demonstrated a highly significant effect from maternal but not pup genotype (P<0.001 for maternal v P=0.915 for pup *Hamp* genotype) (**Supplemental Figure 2-1B**). Our data in the mouse model demonstrate that the degree of maternal hepcidin suppression rather than embryo or placental hepcidin determines embryo iron endowment.

Placental FPN levels are a possible target of placental and embryo hepcidin but we found no difference in placental FPN in relation to either embryo genotype (P=0.219) or maternal *Hamp*

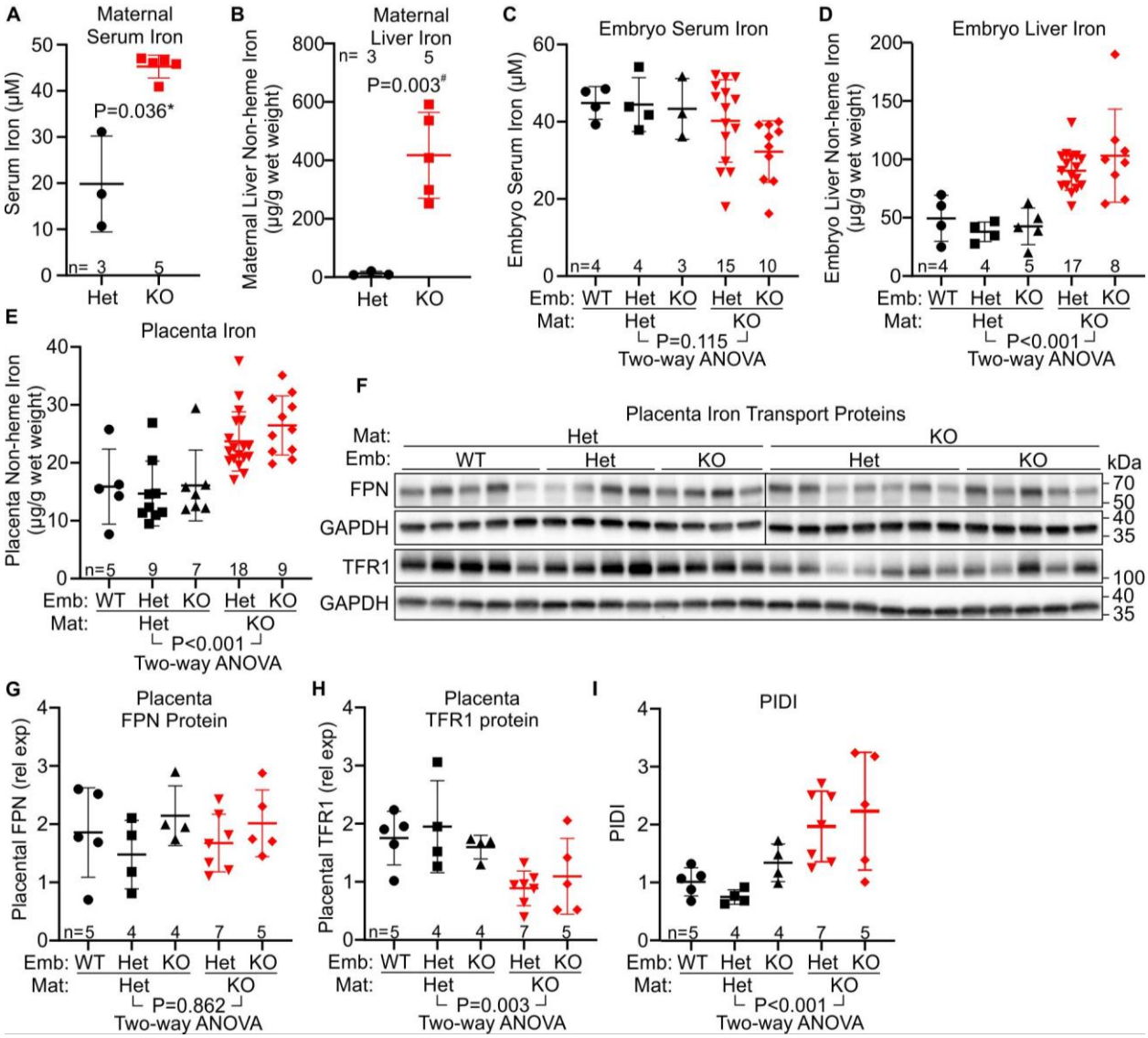

Figure 2-2. Maternal rather than embryo hepcidin determines embryo iron endowment. To determine the relative contribution of maternal versus embryo hepcidin to the regulation of embryo iron endowment, Hamp Het and KO females were mated with Hamp Het males to generate Hamp WT, Het and KO embryos. Mothers and embryos were analyzed on E18.5. **(A)** Maternal serum iron and **(B)** liver non-heme iron concentrations. Statistical comparisons were performed by two-tailed Mann-Whitney rank-sum test for non-normally distributed value (indicated by * following P-values) or for normally distributed but non-equal variance data sets, a two-tailed t-test with Welch's correction was performed (indicated by (#) after the P-value). **(C)** Embryo serum iron, **(D)** embryo liver non-heme iron and **(E)** placenta non-heme iron. **(F)** Western blot for FPN and TFR1 from E18.5 Hamp WT, Het and KO placentas, derived from either Hamp Het mothers and Hamp KO mothers. GAPDH was used as a loading control. FPN was run on two separate blots, as indicated by a line; TFR1 was run on a single blot. **(G)** Quantification of placental FPN across different maternal and embryo genotypes. FPN was normalized to GAPDH for loading. To normalized FPN levels between blots, four samples from each of the two blots were re-run together on a separate blot. **(H)** Quantification of placental TFR1 across different maternal and embryo genotypes. TFR1 was normalized to GAPDH. **(I)** Calculated Placental Iron Deficiency Index (PIDI): the ratio of placental FPN to TFR1 protein. **(C-E, G-I)** Statistical differences between groups was determined by two-way ANOVA for embryo versus mother Hamp genotype.

genotype (P=0.862) (**Figure 2-2F, G**). In contrast, TFR1 was decreased in placentas from *Hamp* KO dams (P=0.003), with no difference observed between embryo *Hamp* genotypes (P=0.993) (**Figure 2-2F, H**). The decrease in placental TFR1 is likely mediated by the IRE-IRP system in response to increased placenta iron concentration.

We previously conceived the placental iron deficiency index (PIDI), the ratio of placental FPN to TFR1 protein concentrations, as a sensitive indicator of placental iron status[16]. In that study, we reported that PIDI was decreased in placentas from iron-deficient compared to iron-adequate mothers. We now show that PIDI increased with placental iron loading and was higher in placentas from *Hamp* KO compared to Het dams (P<0.001), with no effect of embryo Hamp genotype (P=0.337) (PIDI in **Figure 2-2I,** placental iron in **2-2E**).

There was no difference in embryo brain iron regardless of embryo or maternal genotype (P=0.878 and P=0.852) (**Supplemental Figure 2-1C**).

Maternal inflammation induces maternal hepcidin. To assess whether inflammation could counteract the physiological suppression of maternal hepcidin during pregnancy, C57BL/6J females at E17.5 and non-pregnant controls were injected subcutaneously with 0.5 µg/g LPS for

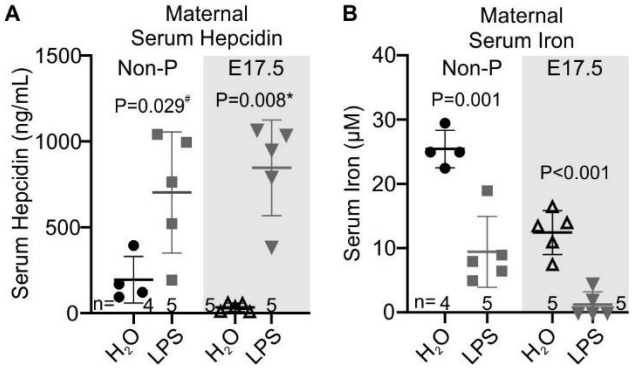

Figure 2-3. Systemic inflammation induces maternal hepcidin and severe hypoferremia during pregnancy. Age-matched non-pregnant and pregnant (E17.5) WT C57BL/6J females received a single subcutaneous injection of water or 0.5µg/g LPS and were analyzed 6 hours later. **(A)** Maternal serum hepcidin and **(B)** maternal serum iron. Statistical comparisons were performed by two-tailed Student's t-test for normally distributed values, by two-tailed Mann-Whitney rank-sum test for non-normally distributed value (indicated by * following P-values), or for normally distributed but non-equal variance data sets, a two-tailed t-test with Welch's correction was performed (indicated by (#) after the P-value).

6h. LPS treatment of dams is known to rapidly increase the concentrations of the cytokine IL-6[37], a potent inducer of hepcidin. In non-pregnant females, LPS induced hepcidin 3.5-fold compared to water-injected controls (198±136 to 706±352 ng/mL, P=0.029, **Figure 2-3A**). In E17.5 pregnant females, serum hepcidin was lower at baseline than in non-pregnant females as expected, but was induced 23-fold after LPS injection (37±25 to 849±279 ng/mL, P=0.008), reaching levels observed in LPS-injected non-pregnant females (P=0.496 for pregnant vs non-pregnant LPS-injected groups) (**Figure 2-3A**).

Following the hepcidin increase, we observed a 2.5-fold decrease in serum iron in non-pregnant LPS-treated females (25.5±2.9 to 9.5±5.5 µM, P=0.001) (**Figure 2-3B**). In pregnant females, baseline serum iron was lower compared to non-pregnant females and was decreased further 9.5-fold from 12.5±3.4 to 1.3±2.0 µM following LPS treatment (P<0.001, **Figure 2-3B**). Inflammatory hypoferremia is predominantly mediated by elevated hepcidin concentrations[38] although direct suppression of *Fpn* mRNA expression by inflammation[39] may also contribute. We next explored the effect of such severe hypoferremia on maternal, placental and fetal health, apart from other effects of inflammation.

Elevated maternal hepcidin results in maternal iron-restriction. Maternal infection and inflammation are associated with adverse pregnancy outcomes[40,41] but whether hepcidin-mediated hypoferremia contributes to those outcomes is unknown. To isolate the effect of elevated maternal hepcidin on pregnancy from other effects of inflammation, we injected pregnant mice with a hepcidin peptide mimetic PR73[34,42]. To first determine whether PR73 crosses the placenta, mothers received a single subcutaneous injection of 100 nmol PR73 or solvent, and maternal and embryo sera were collected after 6h for an in vitro bioassay[43]. HEK293T-FPN-GFP cells were treated with

10% of maternal or embryo serum in DMEM, and FPN levels determined by flow cytometry and compared to PR73 and hepcidin-25 standard curves (**Supplemental Figure 2-2A, B**). Maternal serum from PR73-injected mothers caused degradation of FPN but embryo serum from the same mothers did not, indicating that PR73 does not appreciably cross the placenta.

To examine pregnancy outcomes after a prolonged increase in hepcidin activity, WT pregnant females received daily subcutaneous injections of minihepcidin PR73 as follows: a high short-term dose ("50-6d", 50 nmol/day for 6 days from E12.5-E17.5), a high long-term dose ("50-11d", 50 nmol/day for 11 days from E7.5-E17.5), and a low long-term dose ("10-11d", 10 nmol/day for 11 days from E7.5-E17.5). Pregnant female controls were injected on the same schedule with solvent. Analyses were performed at E18.5.

To estimate how much endogenous hepcidin the PR73 treatment is equivalent to, we assessed FPN degradation with the in vitro bioassay using maternal serum from the 50-6d treatment group (**Supplemental Figure 2-2C**) and compared it to the hepcidin-25 standard curve. We calculated the average activity in maternal serum using the equation in Supplemental Figure 2A and accounting for the use of 10% serum. The activity in 50-6d maternal serum was functionally equivalent to approximately 700 ng/mL of hepcidin-25, which is comparable to endogenous maternal hepcidin levels observed in LPS-treated females (**Figure 2-3**). We also assessed FPN degradation by western blotting after treating FPN-GFP cells with maternal and embryo serum from our "50-6d" and "10-11d" treatment groups (**Supplemental Figure 2-2D**). We found that maternal serum caused much greater FPN degradation than embryo serum, further indicating that PR73 did not appreciably cross the placenta in these treatment groups. We did not have sufficient material to analyze maternal and embryo sera from the 50-11d treatment group and thus cannot rule out that minihepcidins entered the embryo circulation in this group.

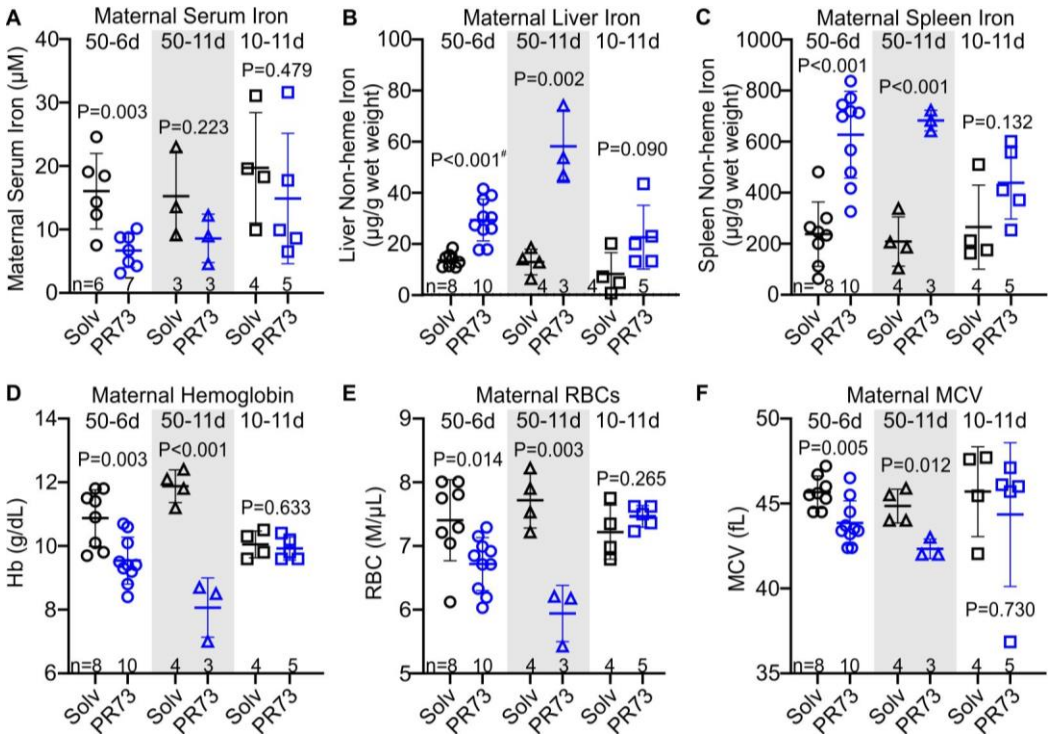

Figure 2-4. Effects of hepcidin-mediated iron restriction during pregnancy on maternal iron status and hematological parameters. Pregnant C57BL/6J dams received daily subcutaneous PR73 injections of 50 nmol/day for 6 days from E12.5-18.5 ("50-6d"), 50 nmol/day for 11 days from E7.5-17.5 ("50-11d"), 10 nmol/day for 11 days from E7.5-17.5 ("10-11d"), or the equivalent amount of solvent. Iron status and hematological parameters were measured at E18.5. Maternal iron parameters: **(A)** serum iron, **(B)** liver non-heme iron, and **(C)** spleen non-heme iron. Maternal hematological parameters: **(D)** hemoglobin, **(E)** red blood cell count, and **(F)** mean corpuscular volume (MCV). Statistical comparisons were performed by two-tailed Student's t-test for normally distributed values or for normally distributed but non-equal variance data sets, a two-tailed t-test with Welch's correction was performed (indicated by (#) after the P-value).

We next assessed the effect of increased hepcidin activity during pregnancy on maternal iron and hematological parameters. Minihepcidin treatment tended to decrease maternal serum iron concentrations in all groups, although because of measurement variability and limited sample sizes, statistical significance was only reached in the 50-6d group (**Figure 2-4A**). PR73 did cause a dose- and time-dependent iron sequestration in the maternal liver and spleen (**Figure 2-4B, C**), with the strongest effect seen in the 50-11d group. The same 50-11d group had the most severe anemia, with significantly decreased Hgb, RBC count and MCV (**Figure 2-4D-F**). The effect on

maternal iron and hematology was less pronounced in the 10-11d group that received the low dose of PR73, where dams did not develop anemia.

To evaluate the maternal response to iron restriction and anemia in the 50 nmol/day injection groups, we first confirmed that PR73 treatment did not induce inflammation, as reflected by the stable liver serum amyloid A1 (*Saa1*) mRNA (**Supplemental Figure 2-3A**). Endogenous maternal liver *Hamp* mRNA was further suppressed, particularly in the 50-11d group (P=0.044) (**Supplemental Figure 2-3B**), likely as a feedback response to iron restriction. To evaluate the erythropoietic response, we measured mRNA expression of maternal bone marrow glycophorin A (*Gypa*) and erythroferrone (*Erfe*) (**Supplemental Figure 2-3C, D**). *Erfe*, but not *Gypa* was significantly elevated in 50-6d and 50-11d groups, suggesting an ineffectual erythropoietic response to anemia. Our data show that despite adequate dietary iron, elevated maternal hepcidin activity during pregnancy caused maternal iron restriction and maternal anemia.

Effects of hepcidin-mediated maternal iron-restriction on the placenta. Placentas were analyzed at E18.5 to determine the consequences of maternal iron restriction on placenta development and iron status. In the 50-6d treatment group, injections started at E12.5, after placental development is complete[44]. There was no difference in placenta weight (P=0.691, **Figure 2-5A**) nor in non-heme iron concentration (P=0.164, **Figure 2-5B**) between minihepcidin-treated and control pregnancies. In the 50-11d treatment group, where injections started at E7.5, before complete placental development, placental weights at E18.5 were 20% lower in the minihepcidin-treated group (P<0.001, **Figure 2-5A**). Decreased placental weight suggests impaired placental development, which may impair nutrient transport to the embryo, not limited to iron. Additionally, placental non-heme iron concentrations were significantly lower in this group (P=0.047, **Figure**

2-5B), despite adaptive alterations in expression of iron transporters TFR1 and FPN (see below).

In the 10-11d treatment group, despite injections starting prior to placental maturation, there was

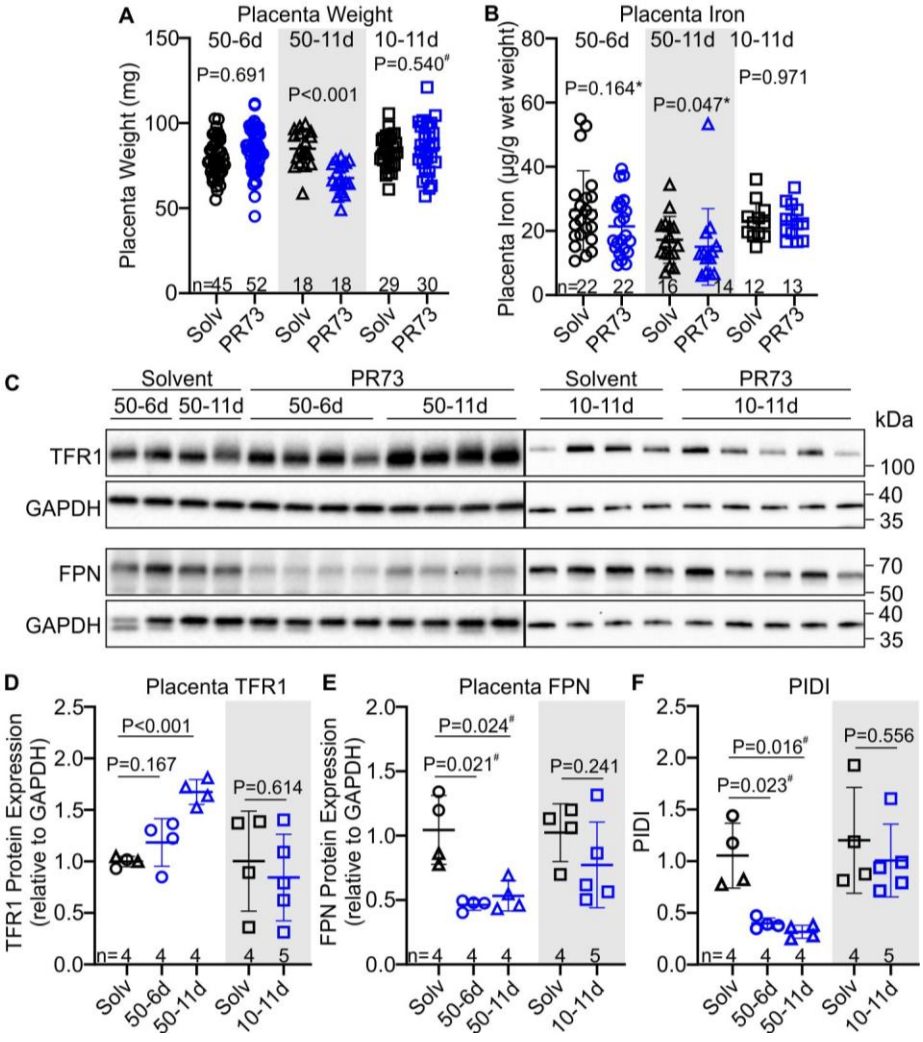

Figure 2-5. Effects of hepcidin-mediated maternal iron restriction on the placenta. Placentas from the three minihepcidin treatment groups from Figure 4 were analyzed at E18.5 for weight and iron content. **(A)** Placental weight was used as a surrogate measure for placental development. **(B)** Placental non-heme iron content. **(C)** Western blot of total placental TFR1 and FPN protein for the 50-6d and 50-11d treatment groups (left panel), and 10-11d treatment group (right panel). Quantification of western blot results for **(D)** TFR1 and **(E)** FPN protein relative to GAPDH. **(F)** Calculated Placental Iron Deficiency Index (PIDI): the ratio of placental FPN to TFR1 protein. Statistical comparisons were performed by two-tailed Student's t-test for normally distributed values, by two-tailed Mann-Whitney rank-sum test for non-normally distributed value (indicated by * following P-values), or for normally distributed but non-equal variance data sets, a two-tailed t-test with Welch's correction was performed (indicated by (#) after the P-value).

no difference in placental weight or placental non-heme iron concentration (**Figure 2-5A, B**), indicating that the level of iron-restriction was insufficient to affect placental development.

We previously reported that during maternal iron deficiency, placental iron transporters are regulated to maintain placental iron homeostasis[16]. As placental tissue becomes iron deficient, placental IRP-1 mediates an increase in TFR1 and decrease in FPN protein, protecting placental tissues from iron deficiency[16]. Maternal iron restriction resulted in similar regulation of placental iron transporters (**Figure 2-5C-E**). In the most severely iron-restricted group (50-11d), TFR1 significantly increased (P<0.001) (**Figure 2-5C, D**) and FPN decreased (P=0.024) (**Figure 2-5C, E**). PIDI (the FPN/TFR1 ratio) was significantly decreased in the 50-6d and 50-11d PR73 groups indicating the placentas 'sensed' iron restriction and responded by altering the transporter expression (**Figure 2-5F**). These transporter changes, however, were not sufficient to prevent placental non-heme iron decrease in the face of severe maternal iron restriction. In the shorter term 50-6d group, only FPN significantly decreased (P=0.021), which was sufficient to maintain normal placental non-heme iron levels. In the 10-11d group, neither TFR1, FPN, nor PIDI differed significantly between the solvent and minihepcidin groups, consistent with the mild iron restriction (**Figure 2-5D-F**).

Hepcidin-mediated maternal iron restriction causes adverse embryo outcomes. Embryos from minihepcidin- and solvent-treated mothers were analyzed at E18.5. In the most severe 50-11d group, in which placental development was also perturbed, 40% of embryos were dead and resorbing, and surviving embryos exhibited marked pallor (**Figure 2-6A**). Such severe adverse outcomes highlight the detrimental effects of maternal iron restriction on pregnancy and may result not only from iron deficiency in the embryo but also the indirect effects of iron restriction via

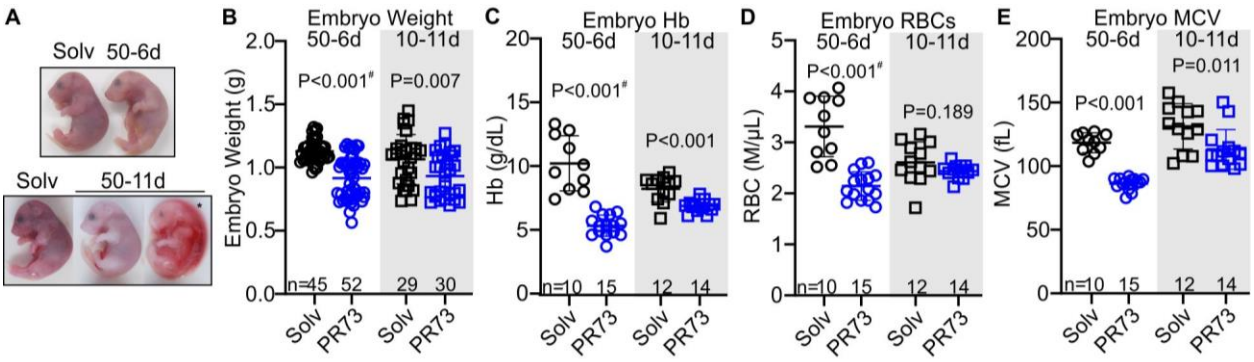

Figure 2-6. Effects of hepcidin-mediated maternal iron restriction on embryo outcome and hematological parameters. Embryos from PR73- and solvent-injected pregnancies from Figure 4 were analyzed at E18.5. **(A)** Embryos were visibly anemic, with increased mortality and resorption in the more severe 50-11d group. Panels B-E: Analysis of embryos from the 50-6d and 10-11d groups. **(B)** Embryo weight. **(C)** blood hemoglobin concentration, **(D)** RBC count and **(E)** mean corpuscular volume MCV. Statistical comparisons were performed by two-tailed Student's t-test for normally distributed values, or for normally distributed but non-equal variance data sets, a two-tailed t-test with Welch's correction was performed (indicated by (#) after the P-value).

maternal anemia or placental insufficiency. Because of frequent embryo death in this group, further analyses were performed in the embryos from the milder 50-6d and 10-11d minihepcidin groups. Embryos weighed significantly less in both the 50-6d and 10-11d groups compared to the solvent groups (50-6d: 1.13±0.08 v 0.92±0.16 g, P<0.001; 10-11d: 1.07±0.19 v 0.93±.017 g, P=0.007) (**Figure 2-6B**), indicating that embryos are much more susceptible to the detrimental effect of iron restriction than the mothers or placentas. Furthermore, both treatments caused embryo anemia, with a stronger effect in the 50-6d group. Embryo Hb, RBC number and MCV were significantly lower in PR73 compared to solvent group (all P<0.001, **Figure 2-6C-E**). In the 10-11d groups, embryo Hb and MCV were significantly lower (P<0.001 and P=0.011, **Figure 2-6C** and **E**); but RBC counts did not statistically differ (P=0.189, **Figure 2-6D**).

We next assessed iron status of embryos. Embryos were hypoferremic in both groups: in the 50-6d group, serum iron decreased more than 3-fold (39.7±8.6 v 12.4±12.0 µM, P=0.010), and in the 10-11d group serum iron decreased from 41.3±12.3 to 26±14.2 µM (P<0.05) (**Figure 2-7A**). Additionally, iron stores assessed by embryo liver non-heme iron concentration were significantly

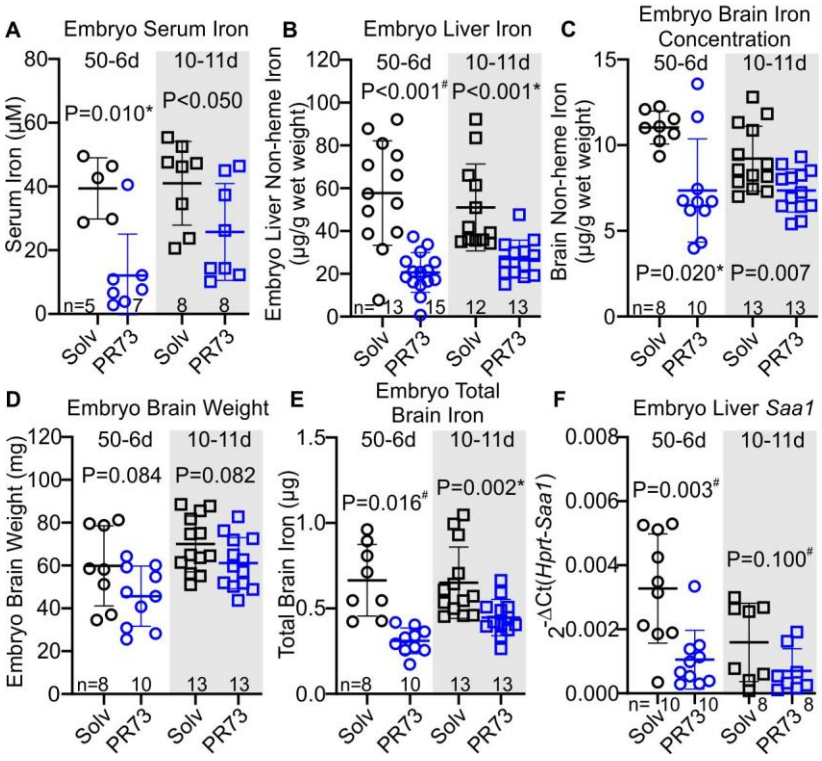

Figure 2-7. Effects of hepcidin-mediated maternal iron restriction on embryo iron status. Embryos from PR73- and solvent-injected pregnancies from Figure 4 were analyzed at E18.5. **(A)** Serum iron. **(B)** Embryo liver non-heme iron. **(C)** Embryo brain non-heme iron concentration. **(D)** Embryo brain weight. **(E)** Total embryo brain non-heme iron content. **(F)** Embryo liver Saa1 mRNA expression. Statistical comparisons were performed by two-tailed Student's t-test for normally distributed values, by two-tailed Mann-Whitney rank-sum test for non-normally distributed value (indicated by * following P-values), or for normally distributed but non-equal variance data sets, a two-tailed t-test with Welch's correction was performed (indicated by (#) after the P-value).

decreased: 50-6d, 58±23 to 21±9 µg/g (P<0.001), and 10-11d, 51±19 to 27±8 µg/g (P<0.001) (**Figure 2-7B**). Brain non-heme iron concentration was also significantly decreased following maternal iron restriction (**Figure 2-7C**). The slight trend for lower brain weight in the iron-restricted groups was not statistically significant (**Figure 2-7D**). Taking into account embryo brain weight, total brain iron was also significantly decreased in embryos from iron-restricted mothers (**Figure 2-7E**). There was no evidence of embryo inflammation in the minihepcidin-treated group as measured by embryo liver *Saa1* mRNA (**Figure 2-7F**). **Supplemental Figure 4** provides a graphical summary of the consequences of elevated maternal hepcidin. Our data in the mouse model demonstrate that even modest hepcidin-mediated iron restriction, which did not substantially alter maternal iron and hematological status or placental homeostasis, still had a detrimental effect on embryos, manifested as growth restriction, anemia, and tissue iron deficiency including in the brain.

Discussion

The iron supply to the developing fetus is essential for its development and is entirely dependent on placental transfer of iron from the maternal circulation. Plasma iron levels are controlled by the iron regulatory hormone hepcidin. Maternal hepcidin is profoundly decreased starting in the second trimester and until delivery in humans[45] and rodents[16,17], presumably to mobilize maternal iron for transfer to the fetus. The relative contribution of maternal, fetal and placental hepcidin to iron regulation in the mother and in the placentofetal unit during physiologic pregnancy is still not completely understood. In embryos with transgenic hepcidin overexpression under the control of the transthyretin promoter that is active as early as E9.5, severe embryo anemia was observed, with perinatal mortality[46]. Similarly, in *Tmprss6-/-* embryos, hepcidin was elevated by E17.5, and was associated with iron deficiency and anemia in embryos and pups[47] but no embryonic lethality[48]. Of note, dams in Tmprss6 studies were heterozygous for *Tmprss6* deletion, as homozygosity causes infertility in females[48]. Conversely, in mice with targeted disruption of the hepcidin gene both genders were fertile, hepcidin knockout pups were born at the expected Mendelian ratios and appeared normal[19]. These genetic mouse models established that elevated embryo hepcidin is detrimental whereas absence of embryo hepcidin does not cause obvious developmental defects. However, the regulatory role of embryonic hepcidin in physiologic pregnancy had not been determined.

During maternal iron loading, we assessed whether a physiological induction of embryonic hepcidin could be functionally important to prevent embryo iron overload in utero. We found no effect of embryo nor placental hepcidin on embryo iron endowment in either iron-sufficient or iron-overloaded dams. Taken together with our previous finding that neither embryo nor placental hepcidin plays a role during maternal iron deficiency[16], we surmise that maternal hepcidin is a key

determinant of embryo iron endowment. This is further evidenced by increased embryo iron endowment, regardless of embryo hepcidin genotype, when maternal hepcidin was absent and mothers were iron-loaded. The importance of maternal hepcidin in determining embryo iron endowment is also supported by our previous findings that in WT dams with high maternal iron stores, maternal hepcidin was proportionally increased, limiting the release of stored maternal iron and preventing embryo iron overload[16]. It is important to note however that in pathological pregnancies embryo hepcidin *can* be increased, resulting in dysregulated iron homeostasis[47,49]. In mice, maternal systemic inflammation induced by LPS injection also caused fetal hepcidin increase and hypoferremia within 24 h[49]. In rhesus macaques, intraamniotic injection of LPS similarly induced fetal hepcidin and hypoferremia, without any effect on maternal hepcidin[49]. In human pregnancies, antenatal exposure to intraamniotic infections resulted in elevated cord blood hepcidin and accompanying hypoferremia[49]. The strong regulation of fetal hepcidin by inflammation may have evolved as a conserved host defense mechanism against microbial infection of the fetoplacental unit. Taken together, data from our mouse models demonstrate that in healthy pregnancies or those with maternal iron loading, maternal hepcidin is the primary physiological controller of embryo iron endowment, but that in certain genetic conditions (e.g. *Tmprss6* mutations) or with exposure to inflammation, fetal hepcidin can contribute to fetal iron regulation.

In the current study, inflammation in pregnant dams robustly induced maternal hepcidin despite signals that suppress maternal hepcidin during normal pregnancy. In humans, inflammatory markers during pregnancy correlated with maternal hepcidin expression in some studies that included complicated pregnancies[22,50,51], but the association was attenuated in pregnancies with mild inflammation such as caused by obesity[26-32]. Another study documented an

approximately 15-fold increase of hepcidin in a subgroup with anemia of chronic inflammation compared to normal pregnancy[52]. However, no effect of elevated maternal hepcidin on neonatal outcomes has yet been conclusively demonstrated. Increased maternal hepcidin was reported in the 1st trimester spontaneous abortion although it is unclear if the increase is a cause or consequence of spontaneous abortion[18]. Currently, multiple factors limit our understanding of the pathophysiology of hepcidin induction by inflammation in human pregnancy, including exclusion of pregnant women with severe infection or inflammation, inadequate definition of the normal range and interpretation of inflammatory biomarkers in pregnancy, and the complexity of hepcidin regulation in the setting of inflammation and pregnancy coexisting with iron deficiency and anemia. In our mouse model, LPS administration caused >20-fold induction of maternal hepcidin which was accompanied by severe hypoferremia, raising the possibility that increased maternal hepcidin during inflammation could contribute to the known adverse effects of maternal inflammation on the fetus. In human pregnancy, inflammation has been linked to increased maternal and neonatal mortality and morbidity, with adverse outcomes including spontaneous abortion, preterm birth, intrauterine growth restriction, and neurodevelopmental impairment[53].

To differentiate the effects of elevated maternal hepcidin from the other effects of inflammation on embryo development, pregnant dams were treated daily with injections of the hepcidin mimetic, PR73. Other models of elevated hepcidin were not suitable as female mice deficient in matriptase-2 (Tmprss6), a negative regulator of hepcidin, are infertile[54]. Elevated maternal hepcidin activity resulted in maternal iron restriction and detrimental effects on the pregnancy. The higher PR73 dose regimens (50-6d and 50-11d treatments) caused iron sequestration in maternal liver and spleen, and hypochromic, microcytic anemia in dams. Unsurprisingly, embryos were also affected. Compared to the solvent groups, embryos were

smaller, anemic and iron-deficient. The most severe iron restriction (50-11d) also resulted in decreased placental weight and death of 40% of embryos. At this dose, it is possible that placental dysfunction impaired general nutrient delivery to the embryo, contributing to the negative embryo outcomes. Likewise, maternal anemia and decreased oxygen delivery may have affected placental function. Remarkably, even at a low PR73 dose (10-11d treatment) that did not cause any appreciable change in maternal hematological parameters or placental development, we still observed adverse effects on embryos, with decreased embryo weight, anemia and iron deficiency, highlighting the sensitivity of the embryo to maternal iron restriction. Our data suggest that elevated maternal hepcidin and consequent maternal iron restriction may be an unrecognized pathogenic factor in inflamed pregnancies that could contribute to fetal harm or demise.

Fetal brain development is highly influenced by the maternal environment. Maternal inflammation during pregnancy is associated with increased risk of neurodevelopmental disorders in offspring[55]. Similarly, maternal iron deficiency is also associated with increased risk of neurobehavioral impairments[11,56]. Whether iron-restriction consequent of inflammation mimics iron deficiency thus resulting in impaired brain development has not been investigated. Interestingly, in our model of maternal iron restriction from excess maternal hepcidin, embryo brains were significantly smaller and contained less iron. The embryo brains were affected even when maternal iron and hematological parameters were unaffected, suggesting that the brain is particularly sensitive to decreases in iron supply.

We previously reported that during maternal iron deficiency, placental iron transporters are regulated to maintain placental iron homeostasis[16]. In that report, we devised the placental iron deficiency index (PIDI), a biological measure of iron deficiency of the materno-fetal unit. PIDI is the ratio of placenta FPN to TFR1, predominantly located on the fetal-facing and maternal-facing

syncytiotrophoblast membranes, respectively. Lower values of PIDI indicate greater placental iron deficiency, and the index is expected to be less sensitive to changes in placental size, cellular composition, or sampling location than the measurement of a single iron transporter would be. In the 50-6d and 50-11d treatment groups, PIDI was lower in the PR73-treated compared to solvent groups, indicating placental sensing of iron restriction. Importantly, PIDI also changed with placental iron loading, and was increased in placentas from *Hamp* KO compared to *Hamp* Het dams, consistent with the observed increase in placental iron content in *Hamp* KO dams. This demonstrated that PIDI changes across the entire spectrum of placental iron exposure, supporting its utility as a sensitive and biologically relevant indicator of materno-fetal iron status.

Our study demonstrates that the maintenance of appropriate maternal hepcidin levels during pregnancy is essential for embryo iron homeostasis and health. In contrast to maternal hepcidin, embryo and placental hepcidin have no observable role in iron regulation in the absence of embryo inflammation. Future studies in pregnant women should reveal whether the combination of increased maternal serum hepcidin and hypoferremia is a useful marker of embryo iron restriction and its adverse consequences.

Acknowledgments

The work was supported by the National Institutes of Health grant R01HD096863 (to EN); the Executive Advisory Board of the Iris Cantor-UCLA Women's Health Center and NCATS UCLA CTSI Grant Number UL1TR000124 (to EN) and pilot award (to VS); and NIH Ruth L. Kirschstein National Research Service Award T32-5T32HL072752-13 (to VS).

The authors also thank Victoria Gabayan and Erika Valore for their assistance with methods development. Flow cytometry was performed in the UCLA Jonsson Comprehensive Cancer Center (JCCC) and Center for AIDS Research Flow Cytometry Core Facility that is supported by National Institutes of Health awards P30 CA016042 and 5P30 AI028697, and by the JCCC, the UCLA AIDS Institute, the David Geffen School of Medicine at UCLA, the UCLA Chancellor's Office, and the UCLA Vice Chancellor's Office of Research.

Author Contributions

VS designed and performed experiments, analyzed data, and wrote the manuscript. ALF performed experiments and assisted with data interpretation. KC performed experiments. PR synthesized minihepcidins and assisted with interpretation of data. TG and EN conceived the project, analyzed data, and wrote the manuscript.

Disclosure of Conflicts of Interest

TG and EN are shareholders of and scientific advisors for Intrinsic LifeSciences and Silarus Therapeutics and are consultants for Ionis Pharmaceuticals, Protagonist Therapeutics, Akebia, Vifor Pharma and Disc Medicine. Other authors have no conflicts to report.

References

1. Ganz T. Hepcidin and iron regulation, 10 years later. *Blood*. 2011;117(17):4425-4433.
2. Nemeth E, Tuttle MS, Powelson J, et al. Hepcidin regulates cellular iron efflux by binding to ferroportin and inducing its internalization. *Science*. 2004;306(5704):2090-2093.
3. Nemeth E, Ganz T. The role of hepcidin in iron metabolism. *Acta Haematol*. 2009;122(2-3):78-86.
4. Sangkhae V, Nemeth E. Regulation of the Iron Homeostatic Hormone Hepcidin. *Adv Nutr*. 2017;8(1):126-136.
5. Nemeth E, Valore EV, Territo M, Schiller G, Lichtenstein A, Ganz T. Hepcidin, a putative mediator of anemia of inflammation, is a type II acute-phase protein. *Blood*. 2003;101(7):2461-2463.
6. Nemeth E, Rivera S, Gabayan V, et al. IL-6 mediates hypoferremia of inflammation by inducing the synthesis of the iron regulatory hormone hepcidin. *J Clin Invest*. 2004;113(9):1271-1276.
7. Ganz T, Nemeth E. Hepcidin and disorders of iron metabolism. *Annu Rev Med*. 2011;62:347-360.
8. Cao C, O'Brien KO. Pregnancy and iron homeostasis: an update. *Nutr Rev*. 2013;71(1):35-51.
9. Stoltzfus RJ. Iron deficiency: global prevalence and consequences. *Food Nutr Bull*. 2003;24(4 Suppl):S99-103.
10. McArdle HJ, Gambling L, Kennedy C. Iron deficiency during pregnancy: the consequences for placental function and fetal outcome. *Proc Nutr Soc*. 2014;73(1):9-15.
11. Georgieff MK. Long-term brain and behavioral consequences of early iron deficiency. *Nutr Rev*. 2011;69 Suppl 1:S43-48.

12. Cogswell ME, Parvanta I, Ickes L, Yip R, Brittenham GM. Iron supplementation during pregnancy, anemia, and birth weight: a randomized controlled trial. *Am J Clin Nutr*. 2003;78(4):773-781.
13. Scanlon KS, Yip R, Schieve LA, Cogswell ME. High and low hemoglobin levels during pregnancy: differential risks for preterm birth and small for gestational age. *Obstet Gynecol*. 2000;96(5 Pt 1):741-748.
14. Scholl TO, Reilly T. Anemia, iron and pregnancy outcome. *J Nutr*. 2000;130(2S Suppl):443S-447S.
15. van Santen S, Kroot JJ, Zijderveld G, Wiegerinck ET, Spaanderman ME, Swinkels DW. The iron regulatory hormone hepcidin is decreased in pregnancy: a prospective longitudinal study. *Clin Chem Lab Med*. 2013;51(7):1395-1401.
16. Sangkhae V, Fisher AL, Wong S, et al. Effects of maternal iron status on placental and fetal iron homeostasis. *J Clin Invest*. 2019.
17. Millard KN, Frazer DM, Wilkins SJ, Anderson GJ. Changes in the expression of intestinal iron transport and hepatic regulatory molecules explain the enhanced iron absorption associated with pregnancy in the rat. *Gut*. 2004;53(5):655-660.
18. Guo Y, Zhang N, Zhang D, et al. Iron homeostasis in pregnancy and spontaneous abortion. *Am J Hematol*. 2019;94(2):184-188.
19. Lesbordes-Brion JC, Viatte L, Bennoun M, et al. Targeted disruption of the hepcidin 1 gene results in severe hemochromatosis. *Blood*. 2006;108(4):1402-1405.
20. Young MF, Griffin I, Pressman E, et al. Maternal hepcidin is associated with placental transfer of iron derived from dietary heme and nonheme sources. *J Nutr*. 2012;142(1):33-39.
21. Gangopadhyay R, Karoshi M, Keith L. Anemia and pregnancy: a link to maternal chronic

diseases. *Int J Gynaecol Obstet*. 2011;115 Suppl 1:S11-15.

22. Rehu M, Punnonen K, Ostland V, et al. Maternal serum hepcidin is low at term and independent of cord blood iron status. *Eur J Haematol*. 2010;85(4):345-352.
23. Gyarmati B, Szabo E, Szalay B, et al. Serum maternal hepcidin levels 3 days after delivery are higher compared to those measured at parturition. *J Obstet Gynaecol Res*. 2011;37(11):1620-1624.
24. Simavli S, Derbent AU, Uysal S, Turhan NO. Hepcidin, iron status, and inflammation variables among healthy pregnant women in the Turkish population. *J Matern Fetal Neonatal Med*. 2014;27(1):75-79.
25. Abioye AI, Park S, Ripp K, et al. Anemia of Inflammation during Human Pregnancy Does Not Affect Newborn Iron Endowment. *J Nutr*. 2018;148(3):427-436.
26. Vega-Sanchez R, Tolentino-Dolores MC, Cerezo-Rodriguez B, Chehaibar-Besil G, Flores-Quijano ME. Erythropoiesis and Red Cell Indices Undergo Adjustments during Pregnancy in Response to Maternal Body Size but not Inflammation. *Nutrients*. 2020;12(4).
27. Flynn AC, Begum S, White SL, et al. Relationships between Maternal Obesity and Maternal and Neonatal Iron Status. *Nutrients*. 2018;10(8).
28. Koenig MD, Klikuszowian E, O'Brien KO, et al. Prepregnancy Obesity Is Not Associated with Iron Utilization during the Third Trimester. *J Nutr*. 2020.
29. Flores-Quijano ME, Vega-Sanchez R, Tolentino-Dolores MC, et al. Obesity Is Associated with Changes in Iron Nutrition Status and Its Homeostatic Regulation in Pregnancy. *Nutrients*. 2019;11(3).
30. Anelli GM, Cardellicchio M, Novielli C, et al. Mitochondrial content and hepcidin are increased in obese pregnant mothers. *J Matern Fetal Neonatal Med*. 2018;31(18):2388-2395.

31. Cao C, Pressman EK, Cooper EM, Guillet R, Westerman M, O'Brien KO. Prepregnancy Body Mass Index and Gestational Weight Gain Have No Negative Impact on Maternal or Neonatal Iron Status. *Reprod Sci*. 2016;23(5):613-622.
32. Garcia-Valdes L, Campoy C, Hayes H, et al. The impact of maternal obesity on iron status, placental transferrin receptor expression and hepcidin expression in human pregnancy. *Int J Obes (Lond)*. 2015;39(4):571-578.
33. Nicolas G, Bennoun M, Porteu A, et al. Severe iron deficiency anemia in transgenic mice expressing liver hepcidin. *Proc Natl Acad Sci U S A*. 2002;99(7):4596-4601.
34. Preza GC, Ruchala P, Pinon R, et al. Minihepcidins are rationally designed small peptides that mimic hepcidin activity in mice and may be useful for the treatment of iron overload. *J Clin Invest*. 2011;121(12):4880-4888.
35. Ramos E, Ruchala P, Goodnough JB, et al. Minihepcidins prevent iron overload in a hepcidin-deficient mouse model of severe hemochromatosis. *Blood*. 2012;120(18):3829-3836.
36. Koenig MD, Tussing-Humphreys L, Day J, Cadwell B, Nemeth E. Hepcidin and iron homeostasis during pregnancy. *Nutrients*. 2014;6(8):3062-3083.
37. Fricke EM, Elgin TG, Gong H, et al. Lipopolysaccharide-induced maternal inflammation induces direct placental injury without alteration in placental blood flow and induces a secondary fetal intestinal injury that persists into adulthood. *Am J Reprod Immunol*. 2018;79(5):e12816.
38. Arezes J, Jung G, Gabayan V, et al. Hepcidin-induced hypoferremia is a critical host defense mechanism against the siderophilic bacterium Vibrio vulnificus. *Cell Host Microbe*. 2015;17(1):47-57.
39. Drakesmith H, Nemeth E, Ganz T. Ironing out Ferroportin. *Cell Metab*. 2015;22(5):777-787.

40. Adams Waldorf KM, McAdams RM. Influence of infection during pregnancy on fetal development. *Reproduction*. 2013;146(5):R151-162.
41. Cappelletti M, Della Bella S, Ferrazzi E, Mavilio D, Divanovic S. Inflammation and preterm birth. *J Leukoc Biol*. 2016;99(1):67-78.
42. Fung E, Chua K, Ganz T, Nemeth E, Ruchala P. Thiol-derivatized minihepcidins retain biological activity. *Bioorg Med Chem Lett*. 2015;25(4):763-766.
43. Aschemeyer S, Qiao B, Stefanova D, et al. Structure-function analysis of ferroportin defines the binding site and an alternative mechanism of action of hepcidin. *Blood*. 2018;131(8):899-910.
44. Rossant J, Cross JC. Placental development: lessons from mouse mutants. *Nat Rev Genet*. 2001;2(7):538-548.
45. Fisher AL, Nemeth E. Iron homeostasis during pregnancy. *Am J Clin Nutr*. 2017;106(Suppl 6):1567S-1574S.
46. Nicolas G, Bennoun M, Porteu A, et al. Severe iron deficiency anemia in transgenic mice expressing liver hepcidin. *Proc Natl Acad Sci U S A*. 2002;99(7):4596-4601.
47. Willemetz A, Lenoir A, Deschemin JC, et al. Matriptase-2 is essential for hepcidin repression during fetal life and postnatal development in mice to maintain iron homeostasis. *Blood*. 2014;124(3):441-444.
48. Folgueras AR, de Lara FM, Pendas AM, et al. Membrane-bound serine protease matriptase-2 (Tmprss6) is an essential regulator of iron homeostasis. *Blood*. 2008;112(6):2539-2545.
49. Fisher AL, Sangkhae V, Presicce P, et al. Fetal and amniotic fluid iron homeostasis in healthy and complicated murine, macaque, and human pregnancy. *JCI Insight*. 2020.
50. Dao MC, Sen S, Iyer C, Klebenov D, Meydani SN. Obesity during pregnancy and fetal iron

status: is Hepcidin the link? *J Perinatol*. 2013;33(3):177-181.

51. Koenig MD, Tussing-Humphreys L, Day J, Cadwell B, Nemeth E. Hepcidin and iron homeostasis during pregnancy. *Nutrients*. 2014;6(8):3062-3083.
52. Vazenmiller D, Ponamaryova O, Muravlyova L, et al. The Levels of Hepcidin and Erythropoietin in Pregnant Women with Anemia of Various Geneses. *Open Access Maced J Med Sci*. 2018;6(11):2111-2114.
53. Kalagiri RR, Carder T, Choudhury S, et al. Inflammation in Complicated Pregnancy and Its Outcome. *Am J Perinatol*. 2016;33(14):1337-1356.
54. Du X, She E, Gelbart T, et al. The serine protease TMPRSS6 is required to sense iron deficiency. *Science*. 2008;320(5879):1088-1092.
55. Ginsberg Y, Khatib N, Weiner Z, Beloosesky R. Maternal Inflammation, Fetal Brain Implications and Suggested Neuroprotection: A Summary of 10 Years of Research in Animal Models. *Rambam Maimonides Med J*. 2017;8(2).
56. Lozoff B, Georgieff MK. Iron deficiency and brain development. *Semin Pediatr Neurol*. 2006;13(3):158-165.

SUPPLEMENTAL MATERIALS

Supplemental Material and Methods

***Hamp-/-* genotyping** - Genotyping was carried out by PCR of genomic tail DNA. DNA was isolated using a Gentra Puregene Tissue Kit (Qiagen). The PCR conditions used were 1 cycle of 95°C for 5 min; 30 cycles of 94°C for 30s, 55°C for 45s, and 72°C for 30s; and 1 cycle of 72°C for 5 min. PCR products were resolved on 1.5% agarose gels. Product sizes: *Hamp-1* (168 bp) and *Hygro* (322 bp). Primers: *Hamp-1* fwd 5′-CTGTGGAAAATGAAGCATGGTGGG-3′ and rev 5′-CACCTCTGGTCCTTCCTCATTAGAG-3′; *Hygro* fwd 5′-GTGTCACGTTGCAAGACCTG-3′ and rev 5'-ACATTGTTGGAGCCGAAATC-3'.

Complete blood counts (CBCs) - Blood was collected from euthanized mice by cardiac puncture into K_2EDTA containing tubes, blood counts were performed on a Hemavet 950FS hematology system (Drew Scientific).

Iron measurements – Serum, liver, placenta and brain non-heme iron concentrations were measured as previously described[1], using acid treatment followed by a colorimetric assay for iron quantification (Sekisui Diagnostics, 157-30).

Serum hepcidin – High-binding 96-well EIA plates (Corning) were coated overnight at room temperature with 50 µl/well of 3.6 µg/ml Ab2B10 in 0.2 M carbonate-bicarbonate buffer, pH 9.4 (Pierce). Plates were washed twice with wash buffer (0.5% Tween-20 in PBS) and blocked for 45 min with 200 µl/well blocking buffer (1% BSA, 1% normal goat serum, 0.5% Tween-20 in PBS). Samples and standards were added and incubated for 1 h at room temperature. After four washes, plates were incubated for 1hr with 50 µl/well of 130 ng/ml Ab2H4-HRP, washed four times and developed with 100 µl/well Ultra-TMB substrate (Thermo Scientific) for 30 min in the dark at

room temperature. The reaction was stopped by adding 50 µl of 2M sulfuric acid to each well, and absorbance was measured at 450 nm.

qPCR - RNA was prepared using TRIzol reagent according to the manufacturer's instructions (Invitrogen). The cDNA was synthesized using iScript cDNA Synthesis Kit (Bio-Rad). Quantitative PCR was performed with SsoAdvanced SYBR Green Supermix (Bio-Rad) and primers (**Supplemental Table 2-1**), and samples were run in duplicate on a CFXconnect instrument (Bio-Rad).

Western blot – Tissues lysates were obtained by homogenizing tissues in RIPA buffer lysis system (Santa Cruz Biotechnology, sc-24948). Protein was quantified using a BCA Assay (ThermoFisher Pierce, 23225), resolved on 4–20% Mini-PROTEAN® TGX™ gels (Bio-rad), electroblotted onto nitrocellulose using a Trans-Blot Turbo system (Bio-rad) and developed on a ChemiDoc XRS+ (Bio-rad). Membranes were stripped using 0.2N NaOH for 10 minutes at room temperature and reprobed for the loading controls. Quantitation was performed using Image Lab Software, version 5.2.1 (Bio-Rad). Antibodies for western blot include: ferroportin antibodes (rat monoclonal IC7 for mouse or human monoclonal 38C8-biotin for human, Amgen), mouse monoclonal transferrin receptor antibody (H68.4, ThermoFisher), monoclonal HPR-conjugated GAPDH antibody (14C10, Cell Signaling), monoclonal anti-β-actin-peroxidase (AC-15, SIGMA), anti-rat IgG HRP (AbCam, #ab102213), Pierce high sensitivity neutravidin-HRP (ThermoFisher, #31030) and anti-mouse IgG HRP (Cell Signaling, #7076).

Placental iron deficiency index (PIDI) – PIDI was calculated as described[2]. Placental FPN and TFR1 were run on different blots because they require different electrophoresis conditions. FPN

and TFR1 levels were first normalized to their respective housekeeping proteins (GAPDH). PIDI was then generated as the ratio of normalized FPN to normalized TFR1.

Ferroportin degradation assay – HEK293T cells stably expressing doxycycline (Dox)-inducible human FPN-GFP[3] were plated at $2x10^5$ cells/well in DMEM +10% FBS with antibiotics (Cipro and Gentamycin) in poly-D lysine coated 24-well plates. Once cells attached to wells, FPN expression was induced with Dox at 10 ng/mL for 16 h. Cells were then washed 3X with PBS to remove Dox and subsequently treated with either 10% FBS or 10% mouse serum for 24 h, detached with TrypLE (Invitrogen) and analyzed for GFP fluorescence. Fluorescence was quantified on a SORP BD LSRII (IMED) analytic flow cytometer at the UCLA Jonsson Comprehensive Cancer Center (JCCC) and Center for AIDS Research Flow Cytometry Core Facility or FPN determined by western blot.

Data sampling – Not all the analyses include the same set of samples. Only weights for placentas and embryos included all the data points since no further processing was required (Figure 5A and 6B). Serum analyses have the lowest n because serum volume was the most limiting factor in our analyses. Placental Western analysis also included smaller n because of the relatively limited number of samples that could be analyzed side-by-side from different groups. Importantly, even when we included a smaller number of samples in the analysis, the samples were selected from at least 3 different pregnancies and thus represent multiple litters. For other parameters (in Figures 2, 4, 5, 6, 7), an overlapping set of samples was analyzed in all graphs, but some assays included additional samples that were randomly selected for inclusion. This did not introduce bias as the sub-analysis using only overlapping samples yielded identical conclusions but with lower power.

Statistical analysis – Statistical methods for multiple comparisons included one-way ANOVA for normally distributed values followed by the Holm-Sidak method for multiple comparison. To compare two groups, a Shapiro-Wilk test was performed (SigmaPlot) to determine normality and an equal variance test was performed. For normally distributed data with equal variance, a parametric test was performed (two-tailed student t-test, GraphPad). For non-normally distributed data, a non-parametric test was performed (two-tailed Mann-Whitney rank sum test, GraphPad) and indicated by a (*) after the P-value. For normally distributed but non-equal variance data sets, a two-tailed t-test with Welch's correction was performed (GraphPad), indicated by ($^{\#}$) after the P-value. Two-way ANOVAs were performed using SigmaPlot software to compare differences due to maternal or fetal genotype, P-values for difference in mean values among the different levels of maternal genotype are included in figures.

Supplemental References

1. Fisher AL, Sangkhae V, Presicce P, et al. Fetal and amniotic fluid iron homeostasis in healthy and complicated murine, macaque, and human pregnancy. *JCI Insight*. 2020.
2. Sangkhae V, Fisher AL, Wong S, et al. Effects of maternal iron status on placental and fetal iron homeostasis. *J Clin Invest*. 2019.
3. Qiao B, Sugianto P, Fung E, et al. Hepcidin-induced endocytosis of ferroportin is dependent on ferroportin ubiquitination. *Cell Metab*. 2012;15(6):918-924.

Supplemental Table 2-1: Mouse specific qRT-PCR primer sequences

Gene	Sequence
Hprt	Fwd: 5'-CTG GTT AAG CAG TAC AGC CCC AA-3'
	Rev: 5'-CAG GAG GTC CTT TTC ACC AGC-3'
Hamp	Fwd: 5'-TTG CGA TAC CAA TGC AGA AGA- 3'
	Rev: 5'-GAT GG GCTT CTA GGC TAT GTT-3'
Saa1	Fwd: 5'-AGT CTG GGC TGC TGA GAA AA-3'
	Rev: 5'-ATG TCT GTT GGC TTC CTG GT-3'
Gypa	Fwd: 5'-ATG GCA GGG ATT ATC GGA AC-3'
	Rev: 5'-CAC CCT CAG GAG ATT GGA TG-3'
Erfe	Fwd: 5'-ATG GGG CTG GAG AAC AGC-3'
	Rev: 5'-TGG CAT TGT CCA AGA AGA CA-3'

Supplemental Figures

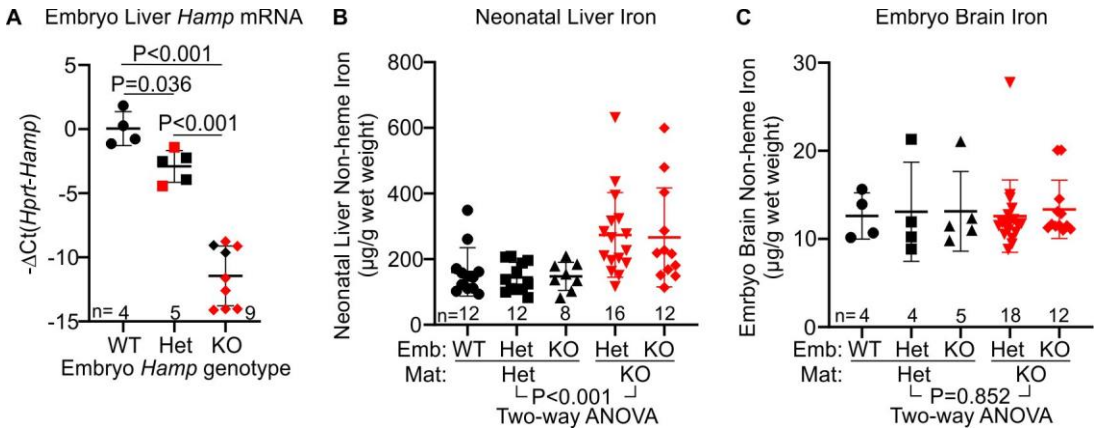

Supplemental Figure 2-1. Embryo hepcidin, neonatal liver iron, and embryo brain iron.

(**A**) Embryo liver *Hamp* mRNA levels were measured in E18.5 *Hamp* WT, Het and KO embryos (an independent set of embryos from that in Figure 2). Black = embryos from *Hamp* Het mothers; red = embryos from *Hamp* KO mothers. Statistical differences were determined one-way ANOVA for normally distributed values followed by the Holm-Sidak method for multiple comparison. (**B**) Liver non-heme iron concentrations were measured in neonates at P1. (**C**) Brain non-heme iron concentrations were measured in E18.5 embryos from Figure 2. (**B, C**) Statistical differences between groups were determined by two-way ANOVA for embryo and mother *Hamp* genotype. P-values below graphs are for differences between maternal genotype.

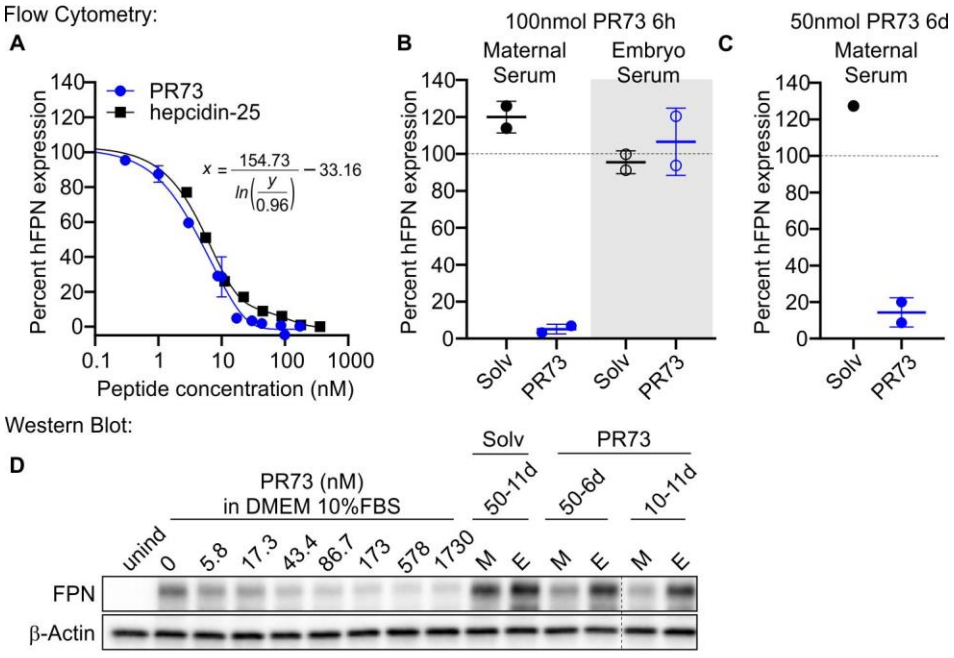

Supplemental Figure 2-2: Minihepcidin PR73 does not cross the placenta. In vitro FPN degradation bioassay, quantified by (**A-C**) flow cytometry or (**D-E**) western blot. (**A**) Standard curves for PR73 and hepcidin-25 activity. Equation is for hepcidin-25 standard curve. Molecular weights: PR73 = 1730 Da; hepcidin-25 = 2789 Da. (**B**) FPN degradation after incubation with 10% serum from E18.5 mothers or embryos after a single subcutaneous injection of 100 nmol solvent or PR73 for 6h. (**C**) FPN degradation after treatment with 10% serum from the "50-6d" maternal group. Serum was collected 24 h after last injection. (**D**) Western blot for FPN after treatment with known concentrations of PR73 or maternal or embryo serum from the "50-6d" or "10-11d" treatment groups, sera were collected 24 h after last injection. Unind: uninduced, M: maternal, E: embryo, Solv: solvent. The dotted line indicates splicing of different parts of the gel for ease of viewing. For embryo measurements, serum from at least 3 embryos from the same treatment group were combined to generate sufficient volume for testing.

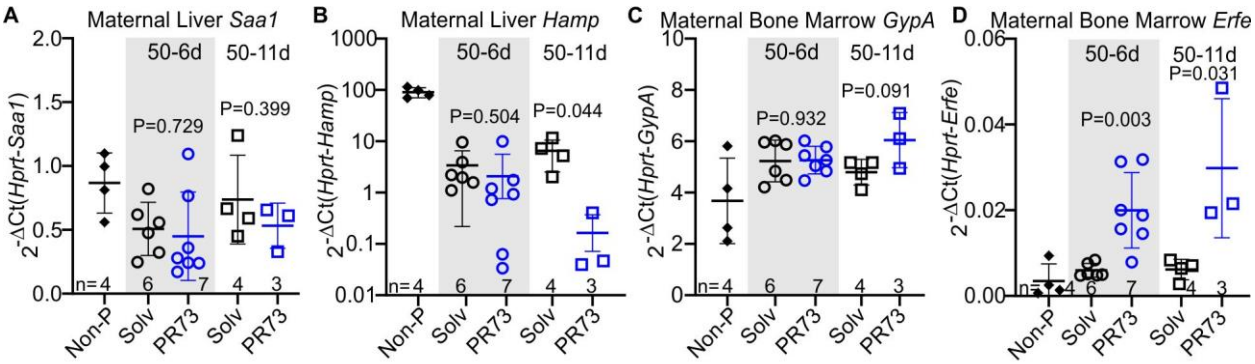

Supplemental Figure 2-3: Maternal response to minihepcidin-induced iron restriction and anemia. (**A**) Maternal liver *Saa1* mRNA expression. (**B**) Maternal liver *Hamp* mRNA expression. (**C**) Maternal bone marrow mRNA expression of the erythroid surface marker glycophorin A (*Gypa).* (**D**) Maternal bone marrow *Erfe* mRNA expression. Statistical differences between groups were determined by two-tailed Student's *t*-test. Non-P: non-pregnant, Solv: solvent.

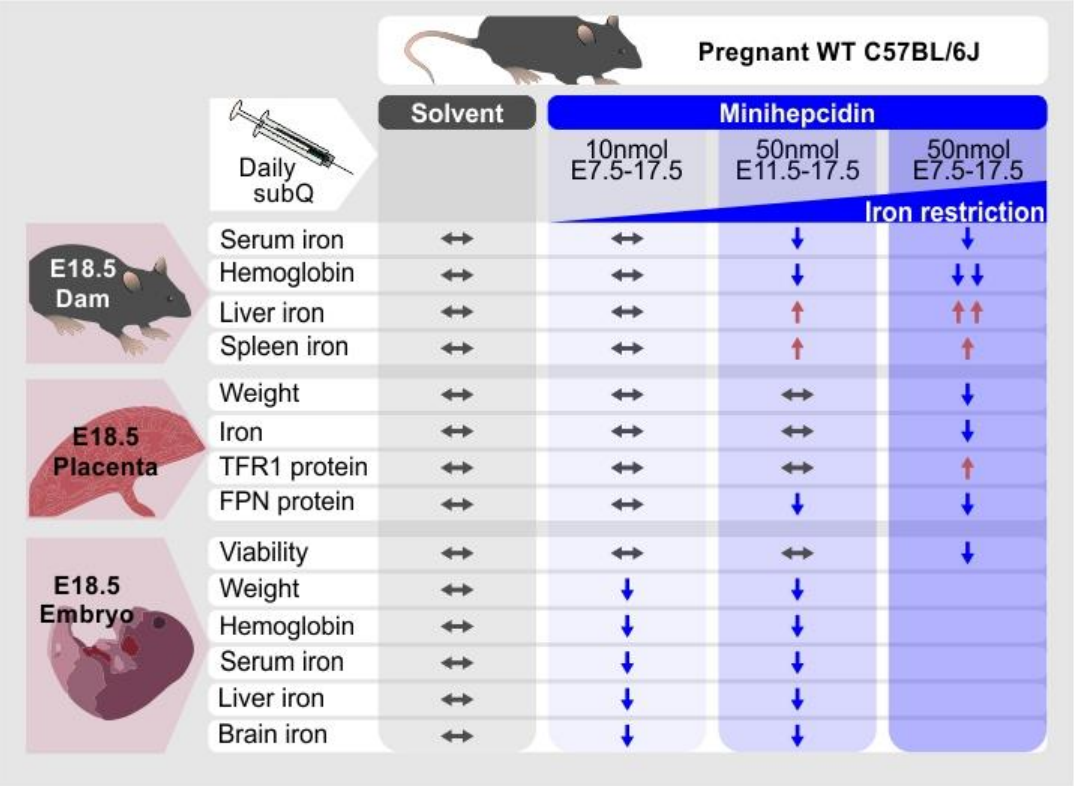

Supplemental Figure 2-4: Graphical summary of the consequences of elevated maternal hepcidin. Pregnant WT C57BL/6J dams received daily injections of minihepcidin PR73 or solvent to mimic elevated maternal hepcidin. Adverse embryo outcomes were observed even with mild maternal iron restriction whereas placenta and the mother were affected only by more severe maternal iron restriction.

CHAPTER 3: FETAL AND AMNIOTIC FLUID IRON HOMEOSTASIS IN HEALTHY AND COMPLICATED MURINE, MACAQUE, AND HUMAN PREGNANCY

JCI insight

RESEARCHARTICLE

Fetal and amniotic fluid iron homeostasis in healthy and complicated murine, macaque, and human pregnancy

Allison L. Fisher,[1,2] Veena Sangkhae,[2] Pietro Presicce,[3] Claire A. Chougnet,[4,5] Alan H. Jobe,[5,6] Suhas G. Kallapur,[3] Sammy Tabbah,[7] Catalin S. Buhimschi,[8] Irina A. Buhimschi,[8] Tomas Ganz,[2] and Elizabeta Nemeth[2]

[1]Molecular, Cellular and Integrative Physiology Graduate Program, Graduate Programs in Bioscience, [2]Center for Iron Disorders, and [3]Neonatal-Perinatal Medicine, Department of Pediatrics, Department of Medicine, David Geffen School of Medicine, UCLA, Los Angeles, California, USA. [4]Division of Immunobiology, Cincinnati Children's Hospital Research Foundation. [5]University of Cincinnati College of Medicine, Cincinnati, Ohio, USA. [6]Division of Neonatology/Pulmonary Biology, Cincinnati Children's Hospital Research Foundation, Cincinnati, Ohio, USA. [7]Cincinnati Fetal Center, Cincinnati Children's Hospital Medical Center and Department of Obstetrics and Gynecology, University of Cincinnati College of Medicine, Cincinnati, Ohio, USA. [8]Department of Obstetrics and Gynecology, University of Illinois at Chicago College of Medicine, Chicago, Illinois, USA.

Adequate iron supply during pregnancy is essential for fetal development. However, how fetal or amniotic fluid iron levels are regulated during healthy pregnancy, or pregnancies complicated by intraamniotic infection or inflammation (IAI), is unknown. We evaluated amniotic fluid and fetal iron homeostasis in normal and complicated murine, macaque, and human pregnancy. In mice, fetal iron endowment was affected by maternal iron status, but amniotic fluid iron concentrations changed little during maternal iron deficiency or excess. In murine and macaque models of inflamed pregnancy, the fetus responded to maternal systemic inflammation or IAI by rapidly upregulating hepcidin and lowering iron in fetal blood, without altering amniotic fluid iron. In humans, elevated cord blood hepcidin with accompanying hypoferremia was observed in pregnancies with antenatal exposure to IAI compared with those that were nonexposed. Hepcidin was also elevated in human amniotic fluid from pregnancies with IAI compared with those without IAI, but amniotic fluid iron levels did not differ between the groups. Our studies in mice, macaques, and humans demonstrate that amniotic fluid iron is largely unregulated but that the rapid induction of fetal hepcidin by inflammation and consequent fetal hypoferremia are conserved mechanisms that may be important in fetal host defense.

Conflict of interest: TG and EN are shareholders of and scientific advisors for Intrinsic LifeSciences and Silarus Therapeutics and consultants for Ionis Pharmaceuticals, Protagonist, and Vifor. TG is a consultant for Akebia.

Submitted: November 27, 2019 Accepted: January 22, 2020
Published: February 27, 2020.

Reference information: *JCI Insight*.
2020;5(4):e135321. https://doi.org/10.1172/jci. insight.135321.

Introduction

In healthy humans and animals, iron in plasma is bound to the carrier protein transferrin (TF). When iron supply to plasma increases, such as in iron overload disorders or with iron supplementation, or when iron utilization decreases, such as with erythropoietic suppression, TF may become saturated, causing "free" or non–TF-bound iron (NTBI) to appear in circulation (1). In humans, NTBI is detectable in amniotic fluid and fetal serum during the first trimester (2) and the beginning of the second trimester (3), when TF levels are low, but is expected to decrease with gestational age (4), as TF concentration increases in amniotic fluid (5, 6) Unlike iron-TF, NTBI is highly reactive, has the potential to catalyze the generation of reactive oxygen species in both the extracellular fluid and tissues in which it is taken up (7), and promotes the rapid growth of Gram-negative bacteria (8).

Since humans and animals cannot excrete excess iron, mechanisms have evolved to prevent iron accumulation and minimize the potential for oxidative damage or spread of certain infections. Hepcidin, a peptide hormone produced in the liver, regulates plasma iron levels and tissue iron distribution (9) by occluding ferroportin, the hepcidin receptor and only known iron exporter, and causing its degradation. In turn, this results in iron sequestration in target cells and decreased iron transport into plasma (10, 11). Hepcidin is feedback regulated by iron concentrations and erythropoietic activity and potently induced by inflammation (12–16).

During pregnancy, iron is critical for the development of the fetus and placenta and for maternal erythropoietic expansion (17, 18). To accommodate these changes, maternal hepcidin is suppressed to nearly undetectable levels in the second and third trimesters (19–22); this is thought to facilitate increased dietary iron absorption, release of iron from stores, and iron transfer to the fetus (23). Thus, inappropriately elevated maternal hepcidin, as would be expected during inflammation, could be detrimental by compromising iron availability for placental uptake and transfer to the fetus.

In addition to maternal hepcidin, fetal hepcidin could also determine placental iron transfer during pregnancy because ferroportin is localized on the basal side of placental syncytiotrophoblast, facing fetal circulation (24, 25). Indeed, a transgenic mouse model of hepcidin overexpression confirmed that fetal hepcidin is capable of regulating placental ferroportin, causing severe fetal iron deficiency and decreased viability (26, 27). Under normal physiological conditions, endogenous fetal hepcidin expression is low (26, 27) and does not affect iron transfer across the placenta (22). However, certain clinical conditions, such as intraamniotic infection or inflammation (IAI), can induce fetal hepcidin (28). Whether hepcidin regulates iron homeostasis in amniotic fluid and fetal blood has not been explored.

Here, we evaluated amniotic fluid and fetal iron homeostasis in normal and complicated murine, rhesus macaque, and human pregnancy. We found that amniotic fluid iron was not strongly regulated by fetal hepcidin or by maternal iron status but that fetal plasma iron during inflammation or infection was regulated by fetal hepcidin, which may be an important protective mechanism for fetal host defense.

Results

Effect of maternal iron status on fetal and amniotic fluid iron homeostasis in mice. To evaluate amniotic fluid iron homeostasis during normal pregnancy, we compared amniotic fluid iron levels during normal mouse gestation from E12.5 to E18.5. Iron concentrations in amniotic fluid were similar between E12.5 and E16.5 and increased sharply before term at E18.5 ($P < 0.001$) (Figure 1A). We next determined how changes in maternal iron status alter iron concentrations in fetal serum and amniotic fluid by comparing E18.5 iron-replete pregnancies (those with normal iron stores) to iron-deficient (diet-induced) and iron-loaded (hepcidin knockout) pregnancies. We confirmed changes in maternal iron status by showing that serum iron concentrations were lower in iron-deficient dams and higher in iron-loaded dams compared with iron-replete controls and that liver iron concentrations were increased in iron-loaded dams (Table 1). Hemoglobin, hematocrit, mean corpuscular volume, and mean corpuscular hemoglobin were all lower in iron-deficient dams and higher in iron-loaded dams compared with iron-replete controls (Table 1).

In fetal serum, iron concentrations were lower with maternal iron deficiency and higher with maternal iron overload compared with those from iron-replete mothers (Figure 1B) (both $P < 0.001$). Compared with fetal serum, iron concentrations in amniotic fluid were relatively spared from changes in maternal iron status (Figure 1C). In all dams, fetal serum iron correlated with maternal serum iron concentrations ($r = 0.846$, $P < 0.001$) (Figure 1D), but amniotic fluid iron concentrations showed only weak nonsignificant correlation with maternal serum iron ($r = 0.465$, $P = 0.110$) (Figure 1E). Fetal serum iron strongly correlated with amniotic fluid iron ($r = 0.657$, $P < 0.001$) (Figure 1F).

Table 1. E18.5 maternal iron and hematological parameters in murine pregnancy

	Iron deficient	*P* value	Iron replete	*P* value	Iron loaded
	E18.5 (*n* = 4)	Iron deficient vs. replete	E18.5 (*n* = 5)	Iron replete vs. loaded	E18.5 (*n* = 5)
Serum iron (μM)	5.84 ± 0.78	*P* = 0.002	21.59 ± 9.73	*P* < 0.001	48.67 ± 1.71
Liver (μg/g)	7.83 ± 0.13	*P* = 0.991	8.59 ± 2.95	*P* < 0.001	476.0 ± 171.95
RBC (10^6/μL)	7.57 ± 0.19	*P* = 0.064	7.66 ± 0.12	*P* = 0.064	7.80 ± 0.08
Hb (g/dL)	9.40 ± 0.35	*P* = 0.009	10.22 ± 0.52	*P* < 0.001	12.20 ± 0.25
HCT (%)	36.25 ± 1.00	*P* < 0.001	40.40 ± 1.58	*P* < 0.001	45.48 ± 0.95
MCV (fL)	47.90 ± 0.74	*P* < 0.001	52.70 ± 1.78	*P* < 0.001	58.28 ± 1.03
MCH (pg)	12.40 ± 0.36	*P* = 0.011	13.32 ± 0.58	*P* < 0.001	15.64 ± 0.34

Iron and hematological parameters of E18.5 pregnant iron-deficient WT dams (fed low-iron diet), iron-replete WT dams (fed standard diet), and iron-loaded hepcidin knockout dams (fed standard diet). Data are presented as mean ± SD. Hb, hemoglobin; HCT, hematocrit; MCV, mean corpuscular volume; MCH, mean corpuscular hemoglobin. Statistical differences between groups were determined by 1-way ANOVA followed by Holm-Sidak method for multiple comparisons.

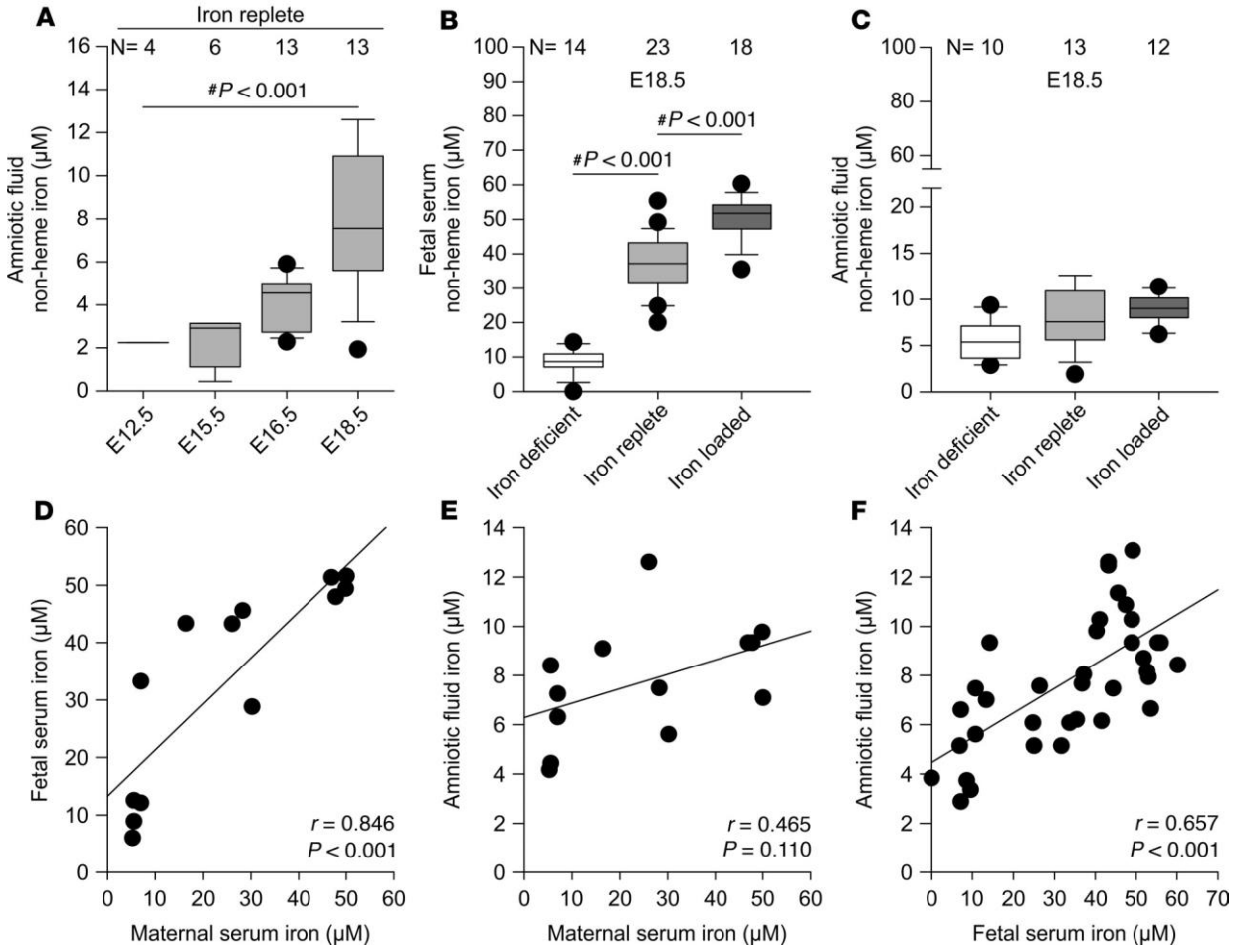

Figure 1. Effect of maternal iron status on fetal and amniotic fluid iron parameters in mice. Maternal iron deficiency was induced by feeding low-iron diet to WT dams starting on E10.5 until analysis at E18.5. Iron-loaded dams were hepcidin-deficient mice fed standard chow. Both iron-deficient and iron-loaded dams were compared with iron-replete WT dams fed standard chow. **(A)** Amniotic fluid iron concentrations from iron-replete dams from E12.5 to E18.5. **(B and C)** Fetal serum and amniotic fluid iron from iron-deficient, iron-replete, and iron-loaded dams on E18.5. **(D–F)** Pearson correlations between maternal serum iron, fetal serum iron, and amniotic fluid iron on E18.5. For **D** and **E**, maternal serum iron was correlated to the litter average for fetal serum iron or amniotic fluid iron. Statistical differences between groups were determined by 1-way ANOVA on ranks followed by Dunn's method for multiple comparisons (as indicated by #). The number of animals is indicated above the box plot for each panel.

To assess whether the fetus or amniotic fluid could be vulnerable to infection because of NTBI, we evaluated whether maternal iron status alters TF concentrations and TF saturations (TSATs) in the fetus and amniotic fluid. Comparing the 3 compartments in iron-replete mouse pregnancy — maternal serum, fetal serum, and amniotic fluid — we found the highest TF concentrations in maternal serum and lowest in amniotic fluid ($P < 0.001$) (Figure 2A). As a result, fetal serum and amniotic fluid had much higher TSAT (60%–70%) than maternal serum (Figure 2B) ($P = 0.007$).

Considering the effect of maternal iron status on maternal iron parameters, TF concentrations were similar between iron-deficient, iron-replete, and iron-loaded dams (Figure 2C). As expected, maternal serum TSAT was lower with iron deficiency ($P = 0.023$) and higher with iron overload ($P < 0.001$) (Figure 2D), reflecting changes in serum iron (Table 1).

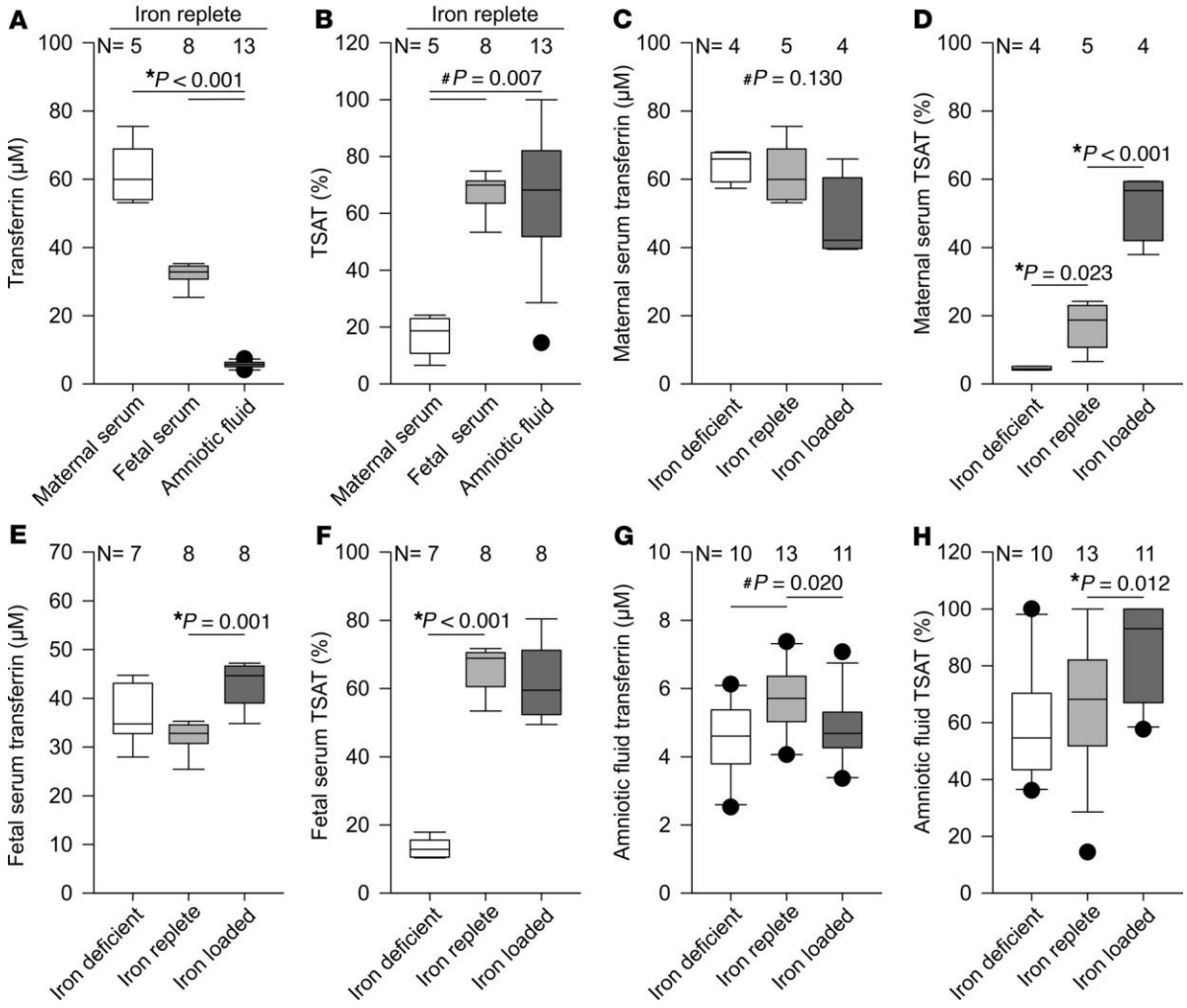

Figure 2. Effect of maternal iron status on fetal and amniotic fluid transferrin and transferrin saturation in mice. Maternal iron deficiency was induced by feeding low-iron diet to WT dams starting on E10.5 until analysis at E18.5. Iron-loaded dams were hepcidin-deficient mice fed standard chow. Both iron-deficient and iron-loaded dams were compared with iron-replete WT dams fed standard chow. **(A and B)** Transferrin concentrations and TSAT in maternal serum, amniotic fluid, and fetal serum on E18.5 in iron-replete pregnancy. **(C and D)** Maternal transferrin concentration and TSAT and **(E–H)** fetal serum and amniotic fluid transferrin concentration and TSAT from iron-deficient, iron-replete, and iron-loaded pregnancies on E18.5. Statistical differences between groups were determined by 1-way ANOVA for normally distributed values followed by Holm-Sidak method for multiple comparisons (as indicated by *) or 1-way ANOVA on ranks followed by Dunn's method for multiple comparisons (as indicated by #). The number of animals is reported above the box plot for each panel.

In fetal serum (Figure 2, E and F), TSAT was lower in iron-deficient pregnancy ($P < 0.001$) due to low serum iron concentrations (Figure 1B). TSATs were similar between iron-loaded and iron-replete groups, despite the difference in fetal serum iron (Figure 1B), because of increased fetal TF levels in iron-loaded pregnancy ($P < 0.001$).

In amniotic fluid, TF levels were slightly lower in iron-deficient and iron-loaded pregnancy compared with iron-replete pregnancy (both $P = 0.02$) (Figure 2G), but TSAT was relatively high in all the groups, particularly in the iron-loaded group ($P = 0.012$) (Figure 2H).

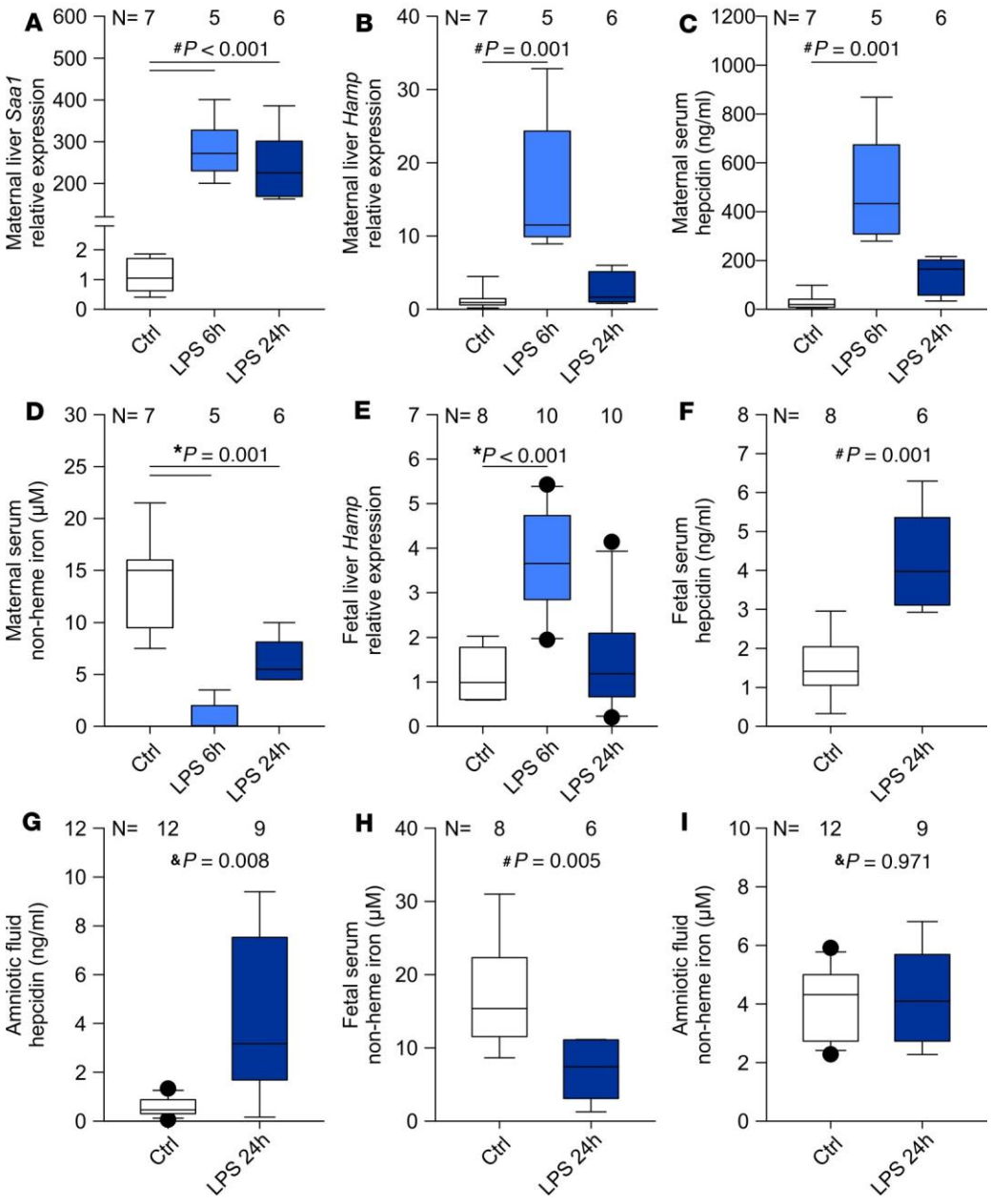

Figure 3. Effect of maternal systemic inflammation on fetal iron homeostasis in mice. To induce maternal systemic inflammation during pregnancy, iron-replete WT dams received a single subcutaneous injection of 0.5 μg/g LPS on E15.5 for 6 or 24 hours. **(A)** Maternal liver serum amyloid A-1 (*Saa1*) and **(B)** hepcidin (*Hamp*) mRNA expression normalized to *Hprt*. Measurements in maternal serum: **(C)** hepcidin and **(D)** iron. Fetal **(E)** liver hepcidin mRNA expression normalized to *Rpl4*, **(F)** serum hepcidin, and **(G)** serum iron. Amniotic fluid **(H)** hepcidin and **(I)** iron. Statistical differences between groups were determined by 1-way ANOVA for normally distributed values followed by Holm-Sidak method for multiple comparisons (as indicated by *), 2-tailed Student's *t* test for normally distributed values (as indicated by #), or Mann-Whitney *U* test (as indicated by &). The number of animals is reported above the box plot for each panel.

Our data demonstrate that, in mouse pregnancy, amniotic fluid iron concentrations are less affected by maternal iron status than fetal serum iron. Although amniotic fluid iron concentrations are relatively low, TSAT of the fluid is high, a condition known to be associated with the presence of NTBI. Fetal serum also had high TSAT under iron-replete conditions, increasing the risk of NTBI generation.

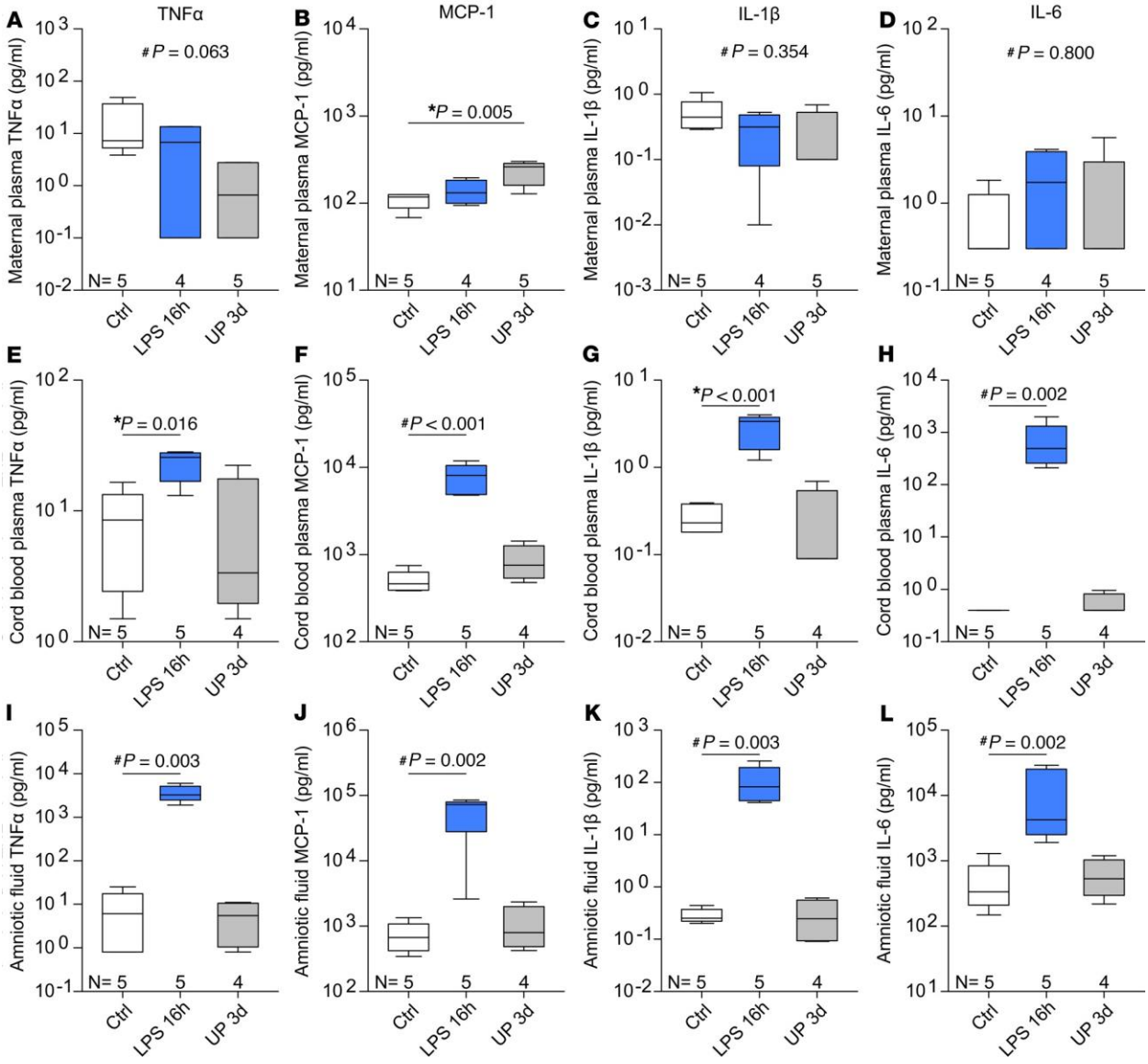

Figure 4. Cytokines in maternal plasma, cord blood plasma, and amniotic fluid during IAI in rhesus macaques. Pregnant rhesus macaques at 130 days gestation received a single intraamniotic injection of LPS (1 mg) for 16 hours or *Ureaplasma parvum* serovar 1 (1×10^7 CFU) for 3 days. Cytokines TNF-α, MCP-1, IL-1β, and IL-6 were measured in **(A–D)** maternal plasma, **(E–H)** cord blood plasma, and **(I–L)** amniotic fluid at delivery. Statistical differences between groups were determined by 1-way ANOVA for normally distributed values followed by Holm-Sidak method for multiple comparisons (as indicated by *) or 1-way ANOVA on ranks followed by Dunn's method for multiple comparisons (as indicated by #). A subset of these data was previously reported (30, 44). The number of animals is reported on the *x* axis of each panel.

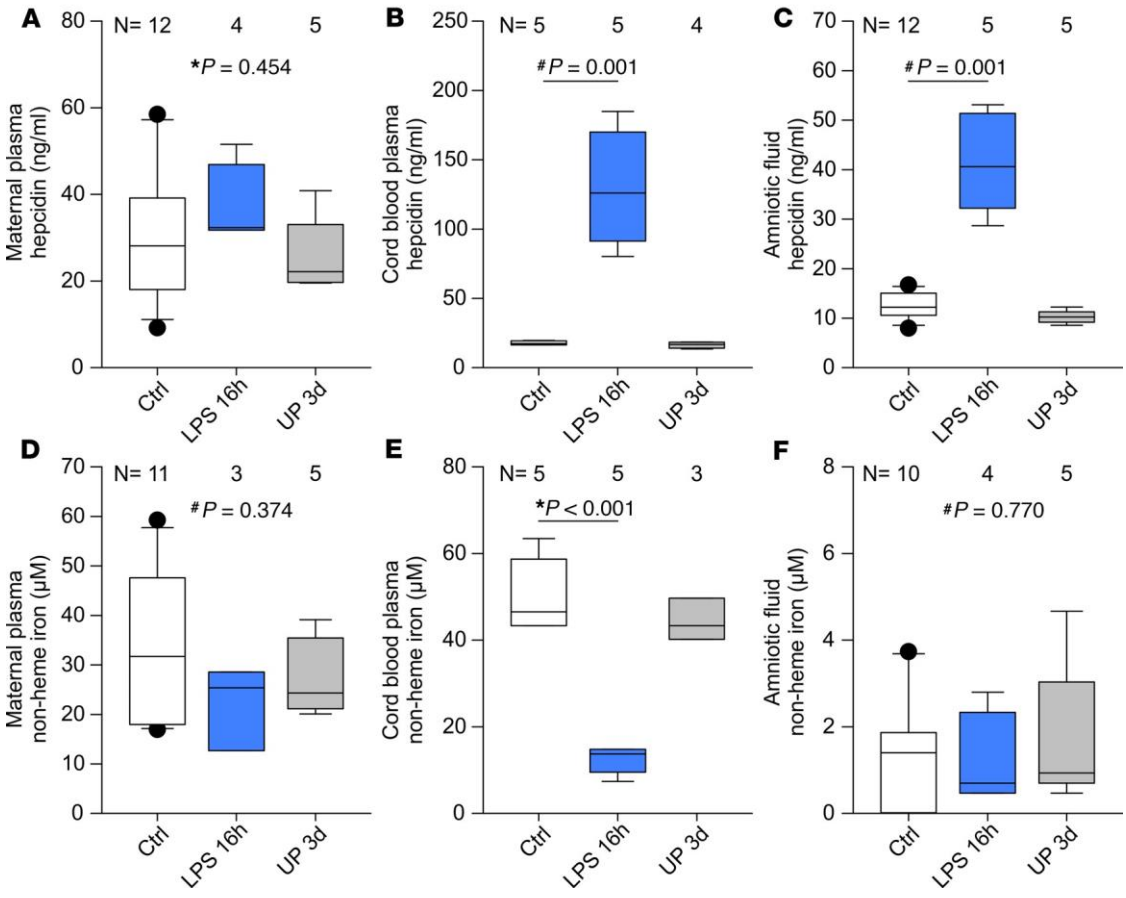

Figure 5. Iron parameters in maternal plasma, cord blood plasma, and amniotic fluid during IAI in rhesus macaques. Pregnant rhesus macaques received a single intraamniotic injection of LPS (1 mg) for 16 hours or *Ureaplasma parvum* serovar 1 (1×10^7 CFU) for 3 days. **(A–C)** Hepcidin and **(D–F)** iron measurements in maternal plasma, cord blood plasma, and amniotic fluid. The control group included samples taken before injection or after saline injection (there was no difference between the 2 groups). The saline group included only samples at delivery after saline injection. Statistical differences between groups were determined by 1-way ANOVA for normally distributed values followed by Holm-Sidak method for multiple comparisons (as indicated by *) or 1-way ANOVA on ranks followed by Dunn's method for multiple comparisons (as indicated by #). The number of animals is reported above the box plot for each panel.

Effect of maternal systemic inflammation on fetal iron homeostasis in mice. Fetal hepcidin expression can be induced by IAI (28), but whether fetal hepcidin can regulate iron homeostasis in the amniotic fluid or fetal circulation is unknown. We evaluated the contribution of fetal hepcidin to the fetal and amniotic iron homeostasis in the presence of maternal inflammation. We induced systemic maternal inflammation in mice by injecting pregnant, iron-replete WT dams with a single subcutaneous dose of LPS on E15.5 (~80% gestation) for 6 or 24 hours. As expected, LPS treatment induced mRNA expression of inflammatory marker serum amyloid A-1 (*Saa-1*) in maternal liver ($P < 0.001$) (Figure 3A). Furthermore, LPS treatment transiently induced maternal hepatic hepcidin (*Hamp*) mRNA and maternal hepcidin protein in serum (both $P = 0.001$) and caused maternal hypoferremia ($P < 0.001$) (Figure 3, B–D). In response to maternal LPS treatment, fetal hepatic hepcidin expression transiently increased within 6 hours and returned to normal levels within 24 hours ($P < 0.001$) (Figure 3E). Following induction of hepcidin synthesis by the fetal liver, both fetal serum hepcidin ($P < 0.001$) and amniotic fluid hepcidin ($P = 0.008$) were elevated 24 hours after maternal LPS injection (Figure 3, F and G). Amniotic fluid hepcidin strongly correlated with fetal serum hepcidin ($r = 0.913$, $P = 0.002$) (Supplemental Figure 1; supplemental material available online with this article; https://doi.org/10.1172/jci.insight.135321DS1). However, hypoferremia occurred only in fetal serum ($P = 0.005$), whereas amniotic fluid iron concentrations were similar between control and LPS-injected groups (Figure 3, H and I). Therefore, fetal hepcidin is responsive to acute inflammation, causing hypoferremia in fetal circulation but not in amniotic fluid.

Fetal iron homeostasis during IAI in rhesus macaques. We evaluated the fetal response to intraamniotic rather than systemic maternal inflammation using a rhesus macaque model of IAI. On gestational day 130 (80% of the duration of pregnancy), pregnant dams received a single intraamniotic injection of LPS for 16 hours or *Ureaplasma* for 3 days. In these models with intraamniotic injections, the inflammation is largely localized to the intrauterine compartment, including the fetus (29, 30). To evaluate maternal systemic inflammation, we measured cytokines TNF-α, MCP-1, IL-1β, and IL-6 in maternal plasma (Figure 4, A–D). We did not detect increases in any cytokines with LPS injection and, with *Ureaplasma* infection, only MCP-1 was elevated ($P = 0.005$). Consistent with the lack of significant increases in cytokines, we did not detect any changes in maternal plasma hepcidin or iron with intraamniotic LPS or *Ureaplasma* (Figure 5, A and D).

In rhesus macaque cord blood plasma, following intraamniotic LPS injection, we detected increased TNF-α ($P = 0.016$), MCP-1 ($P < 0.001$), IL-1β ($P < 0.001$), and IL-6 ($P = 0.002$) (Figure 4, E–H). In amniotic fluid, LPS similarly induced TNF-α ($P = 0.003$), MCP-1 ($P = 0.002$), IL-1β ($P = 0.003$), and IL-6 ($P = 0.002$) (Figure 4, I–L), confirming that inflammation was restricted to the fetal compartment.

Furthermore, LPS strongly induced fetal hepcidin in cord blood plasma and amniotic fluid (both $P = 0.001$) (Figure 5, B and C). Similar to that in mice, amniotic fluid hepcidin strongly correlated with cord blood hepcidin in rhesus macaques ($r = 0.992$, $P < 0.001$) (Supplemental Figure 2). Induction of fetal hepcidin by intraamniotic LPS resulted in profound hypoferremia in cord blood plasma ($P < 0.001$) but not amniotic fluid (Figure 5, E and F). Cord blood plasma hepcidin correlated with cord blood cytokines TNF-α ($r = 0.731$, $P = 0.003$), MCP-1 ($r = 0.739$, $P = 0.003$), IL-1β ($r = 0.809$, $P < 0.001$), and IL-6 ($r = 0.808$, $P < 0.001$) (Supplemental Figure 3, A–D). Amniotic fluid hepcidin correlated with amniotic fluid cytokines TNF-α ($r = 0.910$, $P < 0.001$), MCP-1 ($r = 0.906$, $P < 0.001$), IL-1β ($r = 0.723$, $P = 0.003$), and IL-6 ($r = 0.622$, $P = 0.018$) (Supplemental Figure 3, E–H). We did not detect any changes in iron, hepcidin, or cytokines in cord blood plasma or amniotic fluid with intraamniotic *Ureaplasma* infection.

Thus, similar to the mouse model, fetal hepcidin in rhesus macaques was induced by acute inflammation, causing hypoferremia in fetal circulation, without altering iron concentrations in amniotic fluid.

Amniotic fluid and cord blood iron homeostasis in healthy and complicated human pregnancy. We next evaluated amniotic fluid iron and hepcidin in human pregnancies associated with IAI. All samples were collected at amniocentesis before 32 weeks of gestation (Table 2). The samples were eventually analyzed in the following 4 groups: pregnancies with IAI and with preterm delivery (PosIAI/PTB, $n = 72$), pregnancies without IAI and with preterm delivery (NegIAI/PTB, $n = 22$), pregnancies without IAI and with term delivery (NegIAI/TB, $n = 20$), and pregnancies without IAI but with maternal systemic inflammatory response syndrome (SIRS) and term delivery (NegIAI/TB/SIRS, $n = 10$). Adjusting for gestational age, amniotic fluid hepcidin was significantly different between the groups ($P = 0.008$) and was higher in those positive for IAI and lower in those without IAI (Table 2). Amniotic fluid IL-6 was also elevated in the PosIAI/PTB group ($P < 0.001$) (Table 2). Despite differences in hepcidin, amniotic fluid iron concentrations were similar between all the groups (Table 2). Furthermore, TSAT remained under 20% in all the groups (Table 2).

Although iron is not regulated by inflammation or infection in human amniotic fluid, we next addressed whether the human fetus can upregulate its own hepcidin during inflammation to regulate iron homeostasis in fetal blood. To address this question we used a separate cohort, where umbilical vein cord blood plasma was sampled at delivery from singleton preterm human fetuses (<34 weeks of gestation) with or without antenatal exposure to IAI, as determined by elevated IL-6 in cord blood plasma ($P < 0.001$). In this cohort we confirmed that exposure to IAI resulted in elevated fetal hepcidin and IL-6 in cord blood plasma (both $P < 0.001$) (Figure 6, A and B). Coinciding with elevated hepcidin in circulation, exposure to IAI also resulted in lower cord blood plasma iron concentrations and lower TSAT compared with those in healthy fetuses ($P < 0.001$ and $P = 0.002$) (Figure 6, C and D). Thus, samples from human fetuses with antenatal exposure to IAI demonstrated induction of fetal hepcidin and hypoferremia, similar to responses seen in our animal models.

Discussion

During pregnancy, adequate delivery of iron is essential for normal development of the fetus and placenta. Moreover, tight control of iron concentrations may be protective against certain infections. However, whether fetal or amniotic fluid iron levels are

Table 2. Amniotic fluid iron homeostasis in healthy and complicated human pregnancy

	PosIAI/PTB *n* = 72	NegIAI/TB/SIRS *n* = 10	NegIAI/PTB *n* = 22	NegIAI/TB *n* = 20	*P* value by factorial ANCOVA
IAI	Yes	No	No	No	
GA at amniocentesis (mean ± SD)	26.6 ± 2.9	31.5 ± 3.6	30.5 ± 2.4	29.03 ± 4.0	
GA at delivery (mean ± SD)	26.8 ± 2.9	39.3 ± 1.2	31.2 ± 2.3	38.9 ± 1.1	
AF hepcidin (ng/mL)	8.9	5.7	3.7[A]	2.0[B]	*P* = 0.008
AF IL-6 (pg/mL)	67.0	4.4[A]	5.1[C]	1.5[C]	*P* < 0.001
AF non-heme iron (μM)	2.2	2.4	2.4	2.1	*P* = 0.981
AF TSAT (%)	9.2	14.2	13.1	10.6	*P* = 0.309

Amniotic fluid was sampled at amniocentesis from women that presented with clinical indication of intraamniotic infection. Amniotic fluid was collected by ultrasound-guided amniocentesis from mothers that ultimately delivered preterm with intraamniotic infection (PosIAI/PTB) or without intraamniotic infection (NegIAI/PTB), mothers that ultimately delivered at term but with systemic inflammatory response syndrome (NegIAI/TB/SIRS), or healthy mothers that delivered at term (NegIAI/TB). Differences between groups were analyzed by 1-way factorial ANCOVA after adjusting for gestational age at amniocentesis. IAI, intraamniotic infection or inflammation; PTB, preterm birth; SIRS, systemic inflammatory response syndrome; TB, term birth; AF, amniotic fluid; GA, gestational age; TSAT, transferrin saturation. The values in the table are means adjusted for gestational age at amniocentesis. AP < 0.05; BP < 0.01; CP < 0.001. P value by ANCOVA compared with PosIAI/PTB.

regulated during healthy or complicated pregnancy has not been reported. In this study, we describe amniotic fluid and fetal iron homeostasis in healthy and complicated murine, rhesus macaque, and human pregnancy.

In humans, iron concentrations in amniotic fluid were reported to be approximately 2–3 times lower than those in maternal plasma (31–33). In non-iron–supplemented pregnant women, iron concentrations in amniotic fluid do not correlate with those in maternal blood when assessed at 17 weeks of gestation (32). However, in iron-supplemented women in the second trimester, concentrations of iron in amniotic fluid were linearly correlated to concentrations in maternal blood (31), suggesting that iron in amniotic fluid can be increased through iron supplementation. Using mouse models, we evaluated whether changes in maternal iron status during pregnancy alter fetal and amniotic fluid iron homeostasis. We found that, while fetal serum iron endowment was strongly dependent on maternal iron status, amniotic fluid iron was less affected by either maternal iron deficiency or excess. Compared with maternal serum from normal mouse pregnancy, both fetal serum and amniotic fluid had relatively high TSAT, even under iron replete conditions (~60% in fetal serum/amniotic fluid vs. <20% in maternal serum). Although maternal iron overload did not significantly increase amniotic fluid iron concentrations (which were generally low), TSAT approached 100%, suggesting that maternal iron supplementation could cause the appearance of NTBI in amniotic fluid.

Under normal conditions, iron in plasma is bound to TF with very high affinity, with TSAT ranging from 20% to 50%. Although very few bacterial species can use TF-bound iron, iron availability to microbes increases when NTBI appears in circulation in iron overload diseases or with iron supplementation. In our study, compared with murine amniotic fluid TSAT of >60%, human amniotic fluid collected between 21 and 36 weeks of gestation had TSAT under 20% and human cord blood had TSAT under 40%, suggesting that there is sufficient apoTF to bind iron and decrease the risk of NTBI appearance. Several earlier studies in human amniotic fluid report inhibition of bacterial growth of E. coli, Staphylococcus aureus, and Bacillus subtilis in amniotic fluid with excess apoTF concentrations (4, 34–36), suggesting an important role of the iron-binding capacity of TF to limit iron availability to bacteria.

Inflammation has a potent effect on iron homeostasis. Known as hypoferremia of inflammation, the cytokine-driven increase in hepcidin (13) decreases iron transport into plasma, so that NTBI is not available to stimulate the growth of certain pathogenic bacteria. We investigated whether the fetus shows a hypoferremic response to inflammation in utero. In our mouse model of systemic maternal inflammation, the fetuses responded by acutely increasing mRNA synthesis of hepcidin in the liver and serum hepcidin within 6–24 hours and lowering serum iron within 24 hours. LPS treatment of pregnant mice, however, also induced maternal inflammation, hepcidin, and hypoferremia, raising the question of the relative contribution of fetal versus maternal inflammation to the regulation of fetal serum iron. In our rhesus macaque model of LPS- or Ureaplasma-induced IAI, only fetuses, but not dams, had detectable inflammation. Nevertheless, rhesus macaque fetal hepcidin was increased and fetal plasma iron was decreased, confirming the role of fetal, rather than maternal hepcidin, in regulating fetal plasma iron levels. In both mouse and

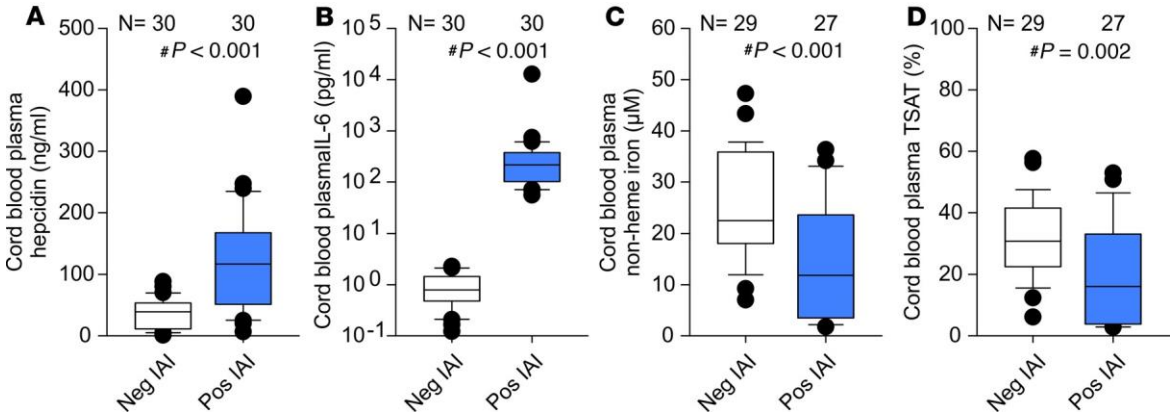

Figure 6. Cord blood iron homeostasis in healthy and complicated human pregnancy. Cord blood from the umbilical vein was sampled at the time of delivery from singleton preterm human fetuses (<34 weeks of gestational age) with or without antenatal exposure to intraamniotic infection. Measurements at time of delivery in cord blood plasma: **(A)** hepcidin, **(B)** IL-6, **(C)** non-heme iron, and **(D)** transferrin saturation. Statistical differences between groups were determined by 1-way ANOVA on ranks followed by Dunn's method for multiple comparisons (as indicated by #). The number of samples are reported above the box plot for each figure panel.

rhesus macaque models, despite detectable increases in amniotic fluid hepcidin, amniotic fluid iron was relatively low and stable, presumably because fetal iron is not exported into the fluid by the organs that contribute to amniotic fluid formation. Iron may even be absorbed from the amniotic fluid by iron transporters in the fetal intestine and possibly lung, which may be advantageous during rapid fetal growth. Hepcidin accumulation in amniotic fluid is likely a result of filtration or excretion of fetal plasma hepcidin by the kidneys. Indeed, we observed a strong correlation between fetal hepcidin and matching amniotic fluid hepcidin in mice and macaques.

Recently described as "intrauterine inflammation or infection or both (Triple I)," chorioamnionitis is a common cause of preterm birth and adverse neonatal and perinatal outcomes in humans (37, 38). In humans, *Ureaplasma* is commonly isolated bacteria from amniotic fluid in the setting of preterm birth with or without clinical chorioamnionitis (39–41), yet a significant percentage of cases with intraamniotic detection of *Ureaplasma* show no histological inflammation (42). In our macaque model, we did not observe any induction in inflammatory cytokines or hepcidin in maternal plasma, cord blood plasma, or amniotic fluid when measured 3 days after intraamniotic inoculation, indicating the absence of strong inflammation in that model. However, using LPS as a stronger inflammatory stimulus, our mouse and rhesus macaque models show that both systemic inflammation and IAI stimulate hepcidin production in the fetus, which in turn lowers iron levels in fetal blood but not amniotic fluid. Although our animal models were treated with exogenous LPS, we observed a similar fetal response to IAI in human pregnancy. Human fetuses exposed antenatally to IAI had elevated cord blood plasma hepcidin levels and consequently lower plasma iron concentrations and TSAT. Amniotic fluid from human fetuses exposed to IAI showed no changes in iron concentrations, despite higher levels of amniotic fluid hepcidin. The ability of the fetus to respond to inflammatory signals by decreasing iron concentration in fetal circulation and sequestering iron away from bacteria may be an important protective mechanism during intraamniotic infections. However, with chronic inflammation, prolonged fetal hepcidin induction and hypoferremia could become detrimental by causing iron restriction in the fetus, leading to decreased iron availability to fetal tissues and possibly anemia.

Our data indicate that iron concentrations in amniotic fluid are much lower than in fetal or maternal circulation in all species examined (mice, macaques, and humans). Interestingly, although TSAT was high in mouse amniotic fluid, it was low in human amniotic fluid from the end of second and third trimester. Thus, although unregulated, low TSAT in humans indicates a low risk of NTBI generation in amniotic fluid, and this may be an important protective factor during intraamniotic infections. The rapid induction of fetal hepcidin by inflammation and consequent hypoferremia in all 3 species (mice, rhesus macaques, and humans) demonstrates a conserved mechanism that may be important in fetal host defense.

Methods

Mouse experiments. WT C57BL/6J mice were obtained from The Jackson Laboratory or bred in the UCLA vivarium. Hepcidin-1–knockout (*Hamp*$^{-/-}$) mice were originally provided to our laboratory by Sophie Vaulont (Institut Cochin, Université Paris Descartes, Paris, France) (43) and were backcrossed to C57BL/6J mice. Mice were housed in a barrier facility under standard laboratory conditions. Unless otherwise specified, mice were maintained on a laboratory chow diet containing 185 ppm iron as ferrous carbonate (Rodent Diet 20 5053, PicoLab). This group was referred to as "iron-replete" (having normal iron stores).

To model iron deficiency during pregnancy, WT mice were fed a purified low-iron diet containing 4 ppm carbonyl iron (TD.80396, Envigo-Teklad) starting at E10.5 and for the duration of pregnancy. To assess the condition of iron overload, we used *Hamp*$^{-/-}$ mice, which become naturally iron loaded when fed standard chow. Iron-deficient and iron-loaded dams were compared with iron-replete WT controls fed standard chow. For these studies, samples were harvested at E18.5. Complete blood counts in maternal blood were performed using a Hemavet 950FS automated analyzer (Drew Scientific). Three to five fetuses from each litter were selected for analysis.

To induce maternal systemic inflammation, pregnant iron-replete WT mice at E15.5 (80% of term gestation) were weighed and injected subcutaneously in the interscapular area with a single dose of 0.5 μg/g LPS (*E. coli* serotype O55:B5, MilliporeSigma) or sterile water. At the indicated times, mice were euthanized by isoflurane overdose and tissues were collected for analysis. For these studies, fetal serum from the entire litter was pooled to generate sufficient volume for analysis.

Mouse amniotic fluid was collected by syringe from individual gestational sacs (50–100 μL per fetus) either at E16.5 (inflammation studies) or E18.5 (iron studies).

Terminology. In literature related to mouse pregnancy studies, the term "embryo" is used to define all stages of murine development in utero. However, because we studied 3 different species in this manuscript, for simplicity we used the term "fetus" for all the species, including the mouse.

Nonhuman primate studies. Adult female rhesus macaques (*Macaca mulatta*) were maintained at the California National Primate Research Center at the University of California, Davis (UCD). To induce IAI, time-mated pregnant rhesus macaques at 130 days gestation (80% of term pregnancy) received by ultrasound-guided intraamniotic injection either 1 mL saline for 16 hours (n = 5), 1 mg LPS (MilliporeSigma Sigma) in 1 mL saline solution (n = 5) for 16 hours, or *Ureaplasma parvum* serovar 1 (1×10^7 CFU) (n = 5) for 3 days. Some animals had maternal blood and amniotic fluid drawn before injections, and those samples were included in the control group. At the indicated times, pregnant dams were surgically delivered, and samples were collected for analysis. Infection and inflammation were confirmed histologically by the presence of neutrophil infiltration. There were no spontaneous deaths or preterm labor in all groups. Some of the animals used in this study were previously reported (30, 44).

Human samples. We studied 124 human amniotic fluid samples from women that were tested because of clinical suspicion of IAI, independent of the research protocol. Clinical suspicion of IAI included preterm labor with contractions persistent despite tocolysis, advanced cervical dilation, and/or preterm prelabor rupture of the membranes. Gestational age at amniotic fluid sampling as well as gestational age at delivery are shown in Table 2. In all cohorts, amniotic fluid was collected by ultrasound-guided amniocentesis. Amniotic fluid was cultured for aerobic and anaerobic bacteria, *Ureaplasma urealyticum* and *Mycoplasma hominis*. IAI was defined by positive culture or positive Gram stain. Additional clinical laboratory tests were performed to confirm or rule-out IAI. Cord blood was not available for analysis. Preterm labor was defined as the presence of regular uterine contractions and documented cervical effacement and/or dilation in patients under 37 weeks of gestation.

The amniotic fluid samples were analyzed in 4 groups: PosIAI/PTB (n = 72), NegIAI/PTB (n = 22), NegIAI/TB (n = 20), and NegIAI/TB/SIRS (n = 10).

In a separate human cohort with available cord blood but not amniotic fluid, we evaluated 60 human cord blood samples from singleton preterm infants with or without antenatal exposure to IAI. Cord blood was obtained by aseptic puncture of the clamped umbilical vein at the time of delivery (30.6 ± 2.8 weeks of gestation, range: 24.1–33.6). The fetal exposure to IAI was defined by IL-6 as previously described (38, 45, 46).

Non-heme iron measurement. Maternal liver iron was measured as previously described (Iron-SL 157-30, Sekisui Diagnostics) (8). Serum was obtained from maternal and fetal mouse blood by centrifugation at 2,700 *g* for 10 minutes. Serum iron concentration was measured by colorimetric spectrophotometry using an iron calibrator. Serum iron in mouse samples and plasma iron in human samples was measured using the Sekisui Diagnostics Iron-SL kit (catalog 157-30): 260 μL R1 reagent was added to 20 μL standard,

blank, or sample. Absorbance at 595 nm (A1) was measured before adding 60 μL R2 for 5 minutes, after which absorbance at 595 nm was remeasured (A2). Plasma iron in rhesus macaque samples was measured using the Genzyme iron total kit (catalog 102-25): 150 μL R1 reagent was added to 20 μL standard (DC-Cal Se-035, Sekisui), blank, or sample. Absorbance at 560 nm (A1) was measured before adding 50 μL R2 and remeasured at 560 nm (A2) after addition of R2. Plasma, serum, or amniotic fluid iron were calculated in μM as = (Δsample A2 – A1/Δstandard A2 – A1) × standard concentration.

TF and TSAT measurement. TF concentrations in human and mouse samples were determined by ELISA according to the manufacturer's instructions (TF ELISA kit, Alpha Diagnostics, 1210 human, 6390 mouse). TF concentrations measured in ng/mL were converted to μM using the molecular weight of TF (~80 kDa), and total iron binding capacity (TIBC) was calculated by multiplying TF in μM by 2 to account for the 2 iron binding sites. TIBC was used in combination with serum iron measurements to calculate TSAT. TSAT (%TSAT) = (serum iron/TIBC) × 100. This method could not accurately and reproducibly determine TF concentrations in rhesus macaque samples.

Hepcidin assays. For human and rhesus macaque samples, hepcidin protein concentrations in plasma and amniotic fluid were measured by ELISA according to the manufacturer's instructions (rhesus macaque, Intrinsic Hepcidin IDx; Human amniotic fluid, DRG Diagnostics; human cord blood, Intrinsic Hepcidin IDx). Hepcidin protein concentration in mouse serum and amniotic fluid was determined by ELISA using Ab2B10 (capture) and Ab2H4-HRP (detection) antibodies provided by Amgen, and synthetic mouse hepcidin-25 was used to generate standard curves ranging from 400 to 3.2 pg/mL (47).

Inflammation assays. In mouse studies, presence of inflammation was assessed by mRNA expression of serum amyloid A-1 (*Saa-1*) (48) and hepcidin (*Hamp*) in maternal liver. In macaque studies, concentrations of cytokines TNF-α, MCP-1, IL-1β, and IL-6 in amniotic fluid, maternal plasma, and cord blood plasma were determined by Luminex using non-human primate multiplex kits (MilliporeSigma). In human samples, concentrations of IL-6 in amniotic fluid and cord blood plasma samples were measured by ELISA (Pierce-Endogen).

Gene expression quantification by qRT-PCR. Frozen mouse liver pieces were homogenized in TRIzol Reagent (Life Technologies). Total RNA was isolated by chloroform extraction, and 1 μg RNA was reverse transcribed using the iScript cDNA Synthesis Kit (Bio-Rad). Quantitative real-time PCR was performed on cDNA using SsoAdvanced SYBER Green Supermix (Bio-Rad) on the CFX Real-Time PCR Detection System (Bio-Rad). Samples were measured in duplicate and normalized to *Hprt* or *Rpl4* using the following primer sequences: *Hprt* forward 5′-CTGGTTAAGCAGTACAGCCCCAA-3′ and reverse 5′-CAGGAGGTCCTTTTCACCAGC-3′, *Rpl4* forward 5′-TGAAAAGCCCAGAAATCCAA-3′ and reverse 5′-AGTCTTGGCGTAAGGGTTCA-3′; *Saa1* forward 5;-AGTCTGGGCTGCTGAGAAAA-3′ and reverse 5′-ATGTCTGTTGGCTTCCTGGT-3′, *Hamp1* forward 5′-AAGCAGGGCAGACATTGCGAT-3′ and reverse 5′-CAGGATGTGGCTCTAGGCTATGT-3′. Data are expressed as $2^{-\Delta\Delta Ct\ (housekeeping\text{-}target)}$.

Statistics. All data are presented as box-and-whisker plots. The box portion indicates the upper 75th and lower 25th percentile, whiskers indicate variability outside the upper 90th and lower tenth percentile, and individual points represent outliers. The solid line within the box indicates the median. Statistical analysis was performed using SigmaPlot version 12.5 (Systat Software). Statistical differences between groups were determined by 1-way ANOVA followed by Holm-Sidak for multiple comparisons for normally distributed values, 1-way ANOVA on ranks followed by Dunn's method for multiple comparisons of nonparametric values, 2-tailed Student's *t* test for normally distributed values, or Mann-Whitney *U* test for nonparametric values. Adjustment for gestational age and comparison of groups in human amniotic fluid samples was done using factorial and 1-way ANOVA (VassarStats). The number of animals in each group is indicated in the graphs. *P* values of less than 0.05 were considered significant.

Study approval. All animal studies were approved by the Institutional Animal Care and Use Committees at UCLA (for mouse studies) and UCD (for macaque studies) and were carried out in accordance with the *Guide for the Care and Use of Laboratory Animals* (National Academies Press, 2011). Human studies were approved by the Institutional Review Boards at Yale University and The Ohio State University, where the samples were collected, and all women signed informed consent.

Author contributions

ALF designed and performed experiments, analyzed data, and wrote the manuscript. VS and PP performed experiments and assisted with data interpretation. SGK, CAC, and AHJ provided rhesus macaque samples and assisted with data interpretation. ST measured amniotic fluid hepcidin concentration in human amniotic fluid samples, collected cord blood samples from the first cohort, and assisted with data interpretation. CSB enrolled human subjects, collected specimens, abstracted human data, and assisted with data

interpretation. IAB provided human samples and assisted with data interpretation. TG and EN conceived the project, analyzed data, and wrote the manuscript. All authors contributed edits to the manuscript and approved the final version.

Acknowledgments

This study was supported by National Center for Advancing Translational Sciences UCLA Clinical and Translational Science Institute grants UL1TR000124, UL1TR001881, and R01 HD096863 (to EN), NIH Ruth L. Kirschstein National Research Service Awards T32GM065823 and F31HD097931 (to AF), NIH grants R21HD90856 and R01HD 98389 (to SGK), NIH grant U01 ES029234, a Burroughs Wellcome grant, and Cincinnati Children's Hospital Medical Center Perinatal Infection and Inflammation Collaborative (to CAC).

Address correspondence to: Elizabeta Nemeth, 10833 LeConte Ave., CHS 43-229, Los Angeles, California 90095, USA. Phone: 310.825.2841; Email: enemeth@mednet.ucla.edu.

References

1. Breuer W, Ronson A, Slotki IN, Abramov A, Hershko C, Cabantchik ZI. The assessment of serum nontransferrin-bound iron in chelation therapy and iron supplementation. *Blood*. 2000;95(9):2975–2982.
2. Evans P, Cindrova-Davies T, Muttukrishna S, Burton GJ, Porter J, Jauniaux E. Hepcidin and iron species distribution inside the first-trimester human gestational sac. *Mol Hum Reprod*. 2011;17(4):227–232.
3. Gazzolo D, et al. Non protein bound iron concentrations in amniotic fluid. *Clin Biochem*. 2005;38(7):674–677.
4. Hattori Y, et al. Catalytic ferrous iron in amniotic fluid as a predictive marker of human maternal-fetal disorders. *J Clin Biochem Nutr*. 2015;56(1):57–63.
5. Legge M. Second trimester amniotic fluid ferritin and transferrin levels in normal and anencephalic pregnancies. *J Obstet Gynaecol (Lahore)*. 1983;4(1):14–15.
6. Larsen B, Snyder IS, Galask RP. Transferrin concentration in human amniotic fluid. *Am J Obstet Gynecol*. 1973;117(7):952–954.
7. Emerit J, Beaumont C, Trivin F. Iron metabolism, free radicals, and oxidative injury. *Biomed Pharmacother*. 2001;55(6):333–339.
8. Stefanova D, et al. Endogenous hepcidin and its agonist mediate resistance to selected infections by clearing non-transferrin-bound iron. *Blood*. 2017;130(3):245–257.
9. Park CH, Valore EV, Waring AJ, Ganz T. Hepcidin, a urinary antimicrobial peptide synthesized in the liver. *J Biol Chem*. 2001;276(11):7806–7810.
10. Nemeth E, et al. Hepcidin regulates cellular iron efflux by binding to ferroportin and inducing its internalization. *Science*. 2004;306(5704):2090–2093.
11. Aschemeyer S, et al. Structure-function analysis of ferroportin defines the binding site and an alternative mechanism of action of hepcidin. *Blood*. 2018;131(8):899–910.
12. Ganz T. Hepcidin and iron regulation, 10 years later. *Blood*. 2011;117(17):4425–4433.
13. Nemeth E, et al. IL-6 mediates hypoferremia of inflammation by inducing the synthesis of the iron regulatory hormone hepcidin. *J Clin Invest*. 2004;113(9):1271–1276.
14. Nicolas G, et al. The gene encoding the iron regulatory peptide hepcidin is regulated by anemia, hypoxia, and inflammation. *J Clin Invest*. 2002;110(7):1037–1044.
15. Nemeth E, Valore EV, Territo M, Schiller G, Lichtenstein A, Ganz T. Hepcidin, a putative mediator of anemia of inflammation, is a type II acute-phase protein. *Blood*. 2003;101(7):2461–2463.
16. Pigeon C, et al. A new mouse liver-specific gene, encoding a protein homologous to human antimicrobial peptide hepcidin, is overexpressed during iron overload. *J Biol Chem*. 2001;276(11):7811–7819.
17. Bothwell TH. Iron requirements in pregnancy and strategies to meet them. *Am J Clin Nutr*. 2000;72(1 Suppl):257S–264S.
18. Fisher AL, Nemeth E. Iron homeostasis during pregnancy. *Am J Clin Nutr*. 2017;106(Suppl 6):1567S–1574S.
19. Bah A, et al. Serum hepcidin concentrations decline during pregnancy and may identify iron deficiency: analysis of a longitudinal pregnancy cohort in The Gambia. *J Nutr*. 2017;147(6):1131–1137.
20. van Santen S, Kroot JJ, Zijderveld G, Wiegerinck ET, Spaanderman ME, Swinkels DW. The iron regulatory hormone hepcidin is decreased in pregnancy: a prospective longitudinal study. *Clin Chem Lab Med*. 2013;51(7):1395–1401.
21. Rehu M, et al. Maternal serum hepcidin is low at term and independent of cord blood iron status. *Eur J Haematol*. 2010;85(4):345–352.
22. Sangkhae V, et al. Effects of maternal iron status on placental and fetal iron homeostasis. *J Clin Invest*. 2020;130(2):625–640.
23. Young MF, et al. Maternal hepcidin is associated with placental transfer of iron derived from dietary heme and nonheme sources. *J Nutr*. 2012;142(1):33–39.
24. Bastin J, Drakesmith H, Rees M, Sargent I, Townsend A. Localisation of proteins of iron metabolism in the human placenta and liver. *Br J Haematol*. 2006;134(5):532–543.
25. Sangkhae V, Nemeth E. Placental iron transport: The mechanism and regulatory circuits. *Free Radic Biol Med*. 2019;133:254–261.
26. Nicolas G, et al. Severe iron deficiency anemia in transgenic mice expressing liver hepcidin. *Proc Natl Acad Sci USA*. 2002;99(7):4596–4601.
27. Willemetz A, et al. Matriptase-2 is essential for hepcidin repression during fetal life and postnatal development in mice to maintain iron homeostasis. *Blood*. 2014;124(3):441–444.
28. Tabbah SM, et al. Hepcidin, an iron regulatory hormone of innate immunity, is differentially expressed in premature fetuses with early-onset neonatal sepsis. *Am J Perinatol*. 2018;35(9):865–872.

29. Presicce P, et al. Neutrophil recruitment and activation in decidua with intra-amniotic IL-1beta in the preterm rhesus macaque. *Biol Reprod.* 2015;92(2):56.
30. Presicce P, et al. IL-1 signaling mediates intrauterine inflammation and chorio-decidua neutrophil recruitment and activation. *JCI Insight*. 2018;3(6):98306.
31. Silberstein T, Saphier M, Mashiach Y, Paz-Tal O, Saphier O. Elements in maternal blood and amniotic fluid determined by ICP-MS. *J Matern Fetal Neonatal Med*. 2015;28(1):88–92.
32. Tamura T, et al. Relationship between amniotic fluid and maternal blood nutrient levels. *J Perinat Med*. 1994;22(3):227–234.
33. Kocyłowski R, et al. Evaluation of essential and toxic elements in amniotic fluid and maternal serum at birth. *Biol Trace Elem Res*. 2019;189(1):45–54.
34. Thadepalli H, Gangopadhyay PK, Maidman JE. Amniotic fluid analysis for antimicrobial factors. *Int J Gynaecol Obstet*. 1982;20(1):65–72.
35. Oka K, Hagio Y, Tetsuoh M, Kawano K, Hamada T, Kato T. The effect of transferrin and lysozyme on antibacterial activity of amniotic fluid. *Biol Res Pregnancy Perinatol*. 1987;8(1 1ST Half):1–6.
36. Evans HE, Levy E, Glass L. Effect of amniotic fluid on bacterial growth. *Obstet Gynecol*. 1977;49(1):35–37.
37. Peng CC, Chang JH, Lin HY, Cheng PJ, Su BH. Intrauterine inflammation, infection, or both (Triple I): A new concept for cho-rioamnionitis. *Pediatr Neonatol*. 2018;59(3):231–237.
38. Tita AT, Andrews WW. Diagnosis and management of clinical chorioamnionitis. *Clin Perinatol*. 2010;37(2):339–354.
39. Cassell GH, Waites KB, Watson HL, Crouse DT, Harasawa R. Ureaplasma urealyticum intrauterine infection: role in prematurity and disease in newborns. *Clin Microbiol Rev*. 1993;6(1):69–87.
40. Kasper DC, et al. The bacterial load of Ureaplasma parvum in amniotic fluid is correlated with an increased intrauterine inflammatory response. *Diagn Microbiol Infect Dis*. 2010;67(2):117–121.
41. Cox C, et al. The common vaginal commensal bacterium Ureaplasma parvum is associated with chorioamnionitis in extreme preterm labor. *J Matern Fetal Neonatal Med*. 2016;29(22):3646–3651.
42. Revello R, et al. Prediction of chorioamnionitis in cases of intraamniotic infection by ureaplasma urealyticum in women with very preterm premature rupture of membranes or preterm labour. *J Matern Fetal Neonatal Med*. 2018;31(14):1839–1844.
43. Lesbordes-Brion JC, et al. Targeted disruption of the hepcidin 1 gene results in severe hemochromatosis. *Blood*. 2006;108(4):1402–1405.
44. Senthamaraikannan P, et al. Intra-amniotic Ureaplasma parvum-induced maternal and fetal inflammation and immune responses in rhesus macaques. *J Infect Dis*. 2016;214(10):1597–1604.
45. Romero R, Yoon BH, Kenney JS, Gomez R, Allison AC, Sehgal PB. Amniotic fluid interleukin-6 determinations are of diagnostic and prognostic value in preterm labor. *Am J Reprod Immunol*. 1993;30(2-3):167–183.
46. Romero R, et al. A comparative study of the diagnostic performance of amniotic fluid glucose, white blood cell count, interleukin-6, and gram stain in the detection of microbial invasion in patients with preterm premature rupture of membranes. *Am J Obstet Gynecol*. 1993;169(4):839–851.
47. Kim A, et al. A mouse model of anemia of inflammation: complex pathogenesis with partial dependence on hepcidin. *Blood*. 2014;123(8):1129–1136.
48. Gabay C, Kushner I. Acute-phase proteins and other systemic responses to inflammation. *N Engl J Med*. 1999;340(6):448–454.

SUPPLEMENTAL MATERIALS

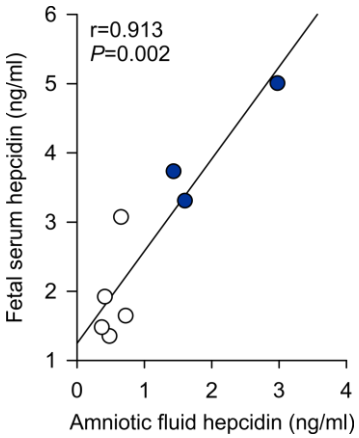

Supplemental Figure 1. Correlation between hepcidin in fetal serum and amniotic fluid in mice. Pregnant iron-replete WT dams received a single subcutaneous injection of 0.5 μg/g LPS or water on E15.5 for 24 h. The values represent the litter averages for serum hepcidin or amniotic fluid hepcidin. White circles = control group, blue circles = LPS group. Statistical analysis was done using Pearson correlation.

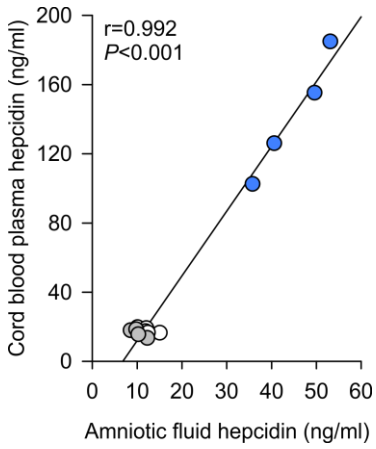

Supplemental Figure 2. Correlation between hepcidin in cord blood plasma and amniotic fluid in rhesus macaques. Pregnant rhesus macaques received a single intraamniotic injection of LPS for 16 h or *Ureaplasma* for 3 days. Pearson correlation was used to compare hepcidin in cord blood plasma versus hepcidin in amniotic fluid. White circles = controls, grey circles = *Ureaplasma* group, blue = LPS group.

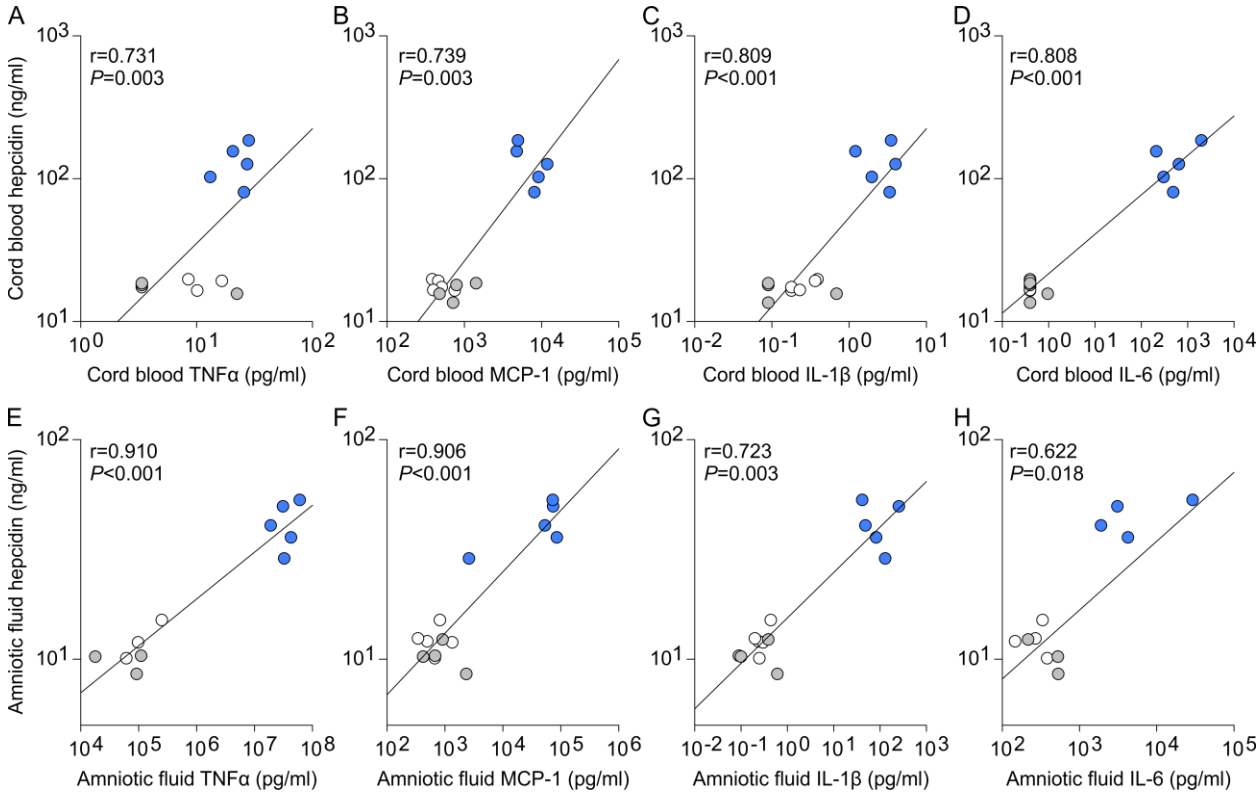

Supplemental Figure 3. Correlations between hepcidin and cytokines in cord blood plasma and amniotic fluid in rhesus macaques. Pregnant rhesus macaques received a single intraamniotic injection of LPS for 16 h or *Ureaplasma* for 3 days. Pearson correlations between hepcidin and cytokines TNF-α, MCP-1, IL-1β, and IL-6 in (A-D) cord blood plasma and (E-H) amniotic fluid at delivery are shown. White circles = controls, grey circles = *Ureaplasma* group, blue = LPS group.

CHAPTER 4: IRON-DEPENDENT APOPTOSIS CAUSES EMBRYOTOXICITY IN INFLAMED AND OBESE PREGNANCY

(**SUBMITTED MANUSCRIPT)**

Manuscript submitted:

IRON-DEPENDENT APOPTOSIS CAUSES EMBRYOTOXICITY IN INFLAMED AND OBESE PREGNANCY

Allison L Fisher, Veena Sangkhae, Kamila Balušíková, Nicolaos J Palaskas, Tomas Ganz, Elizabeta Nemeth

ABSTRACT

Because iron is essential for a healthy pregnancy, iron supplementation during pregnancy is nearly universally recommended, regardless of maternal iron status. A signal of potential harm is the U-shaped association between maternal ferritin, a marker of iron stores, and risk of adverse pregnancy outcomes. However, ferritin is also induced by inflammation and so may overestimate iron stores during inflammation or infection. We used mouse models to determine whether maternal iron loading, inflammation, or their interaction caused poor pregnancy outcomes. Only maternal exposure to both iron excess and inflammation caused embryo malformations and demise. Maternal iron excess potentiated embryo injury during both LPS-induced acute inflammation and obesity-induced chronic mild inflammation. The adverse interaction was dependent on TNFα signaling, caused apoptosis of the placental and embryo endothelium, and was prevented by anti-TNFα or antioxidant treatment in vivo. Our findings raise important questions about the safety of indiscriminate iron supplementation during pregnancy.

INTRODUCTION

Iron is an essential micronutrient required by all tissues for metabolic and cellular processes. Iron requirements increase substantially over the course of pregnancy to support growth of the fetus and placenta and for maternal erythropoietic expansion (Fisher and Nemeth, 2017). To meet these demands, both dietary iron absorption and mobilization of iron from stores must increase, and this is mediated by a decrease in maternal hepcidin, the iron-regulatory peptide hormone produced in the liver (Sangkhae et al., 2020).

Severe iron deficiency and associated anemia is detrimental for both mother and fetus (Breymann, 2015) which has led to the policy of universal iron supplementation even without screening for preexisting iron deficiency in most countries, including the United States. In developed countries, most women of reproductive age have adequate iron stores, and less than 25% of pregnant women have mild iron deficiency and anemia (Le, 2016; WHO, 2001), prompting considerations of the potential risks of indiscriminate iron supplementation.

Although iron is essential for cell function and viability, excess iron can be toxic. In iron overload conditions, high iron concentrations in plasma exceed the iron-binding capacity of transferrin, and non-transferrin-bound iron (NTBI) appears in circulation, damaging cells and tissues through the generation of reactive oxygen species (Breuer et al., 2000; Emerit et al., 2001). How elevated transferrin saturation and/or the presence of NTBI in maternal circulation affects placental and fetal tissues is unknown. Pregnancies associated with iron excess include patients with hereditary hemochromatosis or β-thalassemia, the latter having well-documented complications including prematurity, abortion, and intrauterine fetal death (Fozza et al., 2017; Tuck et al., 1998). However, even normal pregnancies may be exposed to excess iron and NTBI when iron-supplemented (Baron et al., 2008), in part because of decreased maternal hepcidin

allowing for highly efficient iron absorption. High iron status is associated with gestational diabetes and impaired fetal growth (Guo et al., 2019; HOU et al., 2000; Khambalia et al., 2016; Lao et al., 2001; Rawal et al., 2017; Scholl, 2005; Scholl and Reilly, 2000). Furthermore, large epidemiological studies show a U-shaped association between maternal ferritin, a marker of iron stores, and risk of adverse outcomes such as low birthweight, stillbirth, preterm birth (<37 weeks), very preterm birth (<32 weeks' gestation), and neonatal asphyxia (Gonzales et al., 2009; Khambalia et al., 2015; Knottnerus et al., 1990; Lao et al., 2000; Mamun et al., 2006; Scanlon et al., 2000; Stephansson et al., 2000; Xiao et al., 2002). However, these harms are not necessarily caused by iron excess as ferritin is also increased by inflammation and may not accurately reflect iron stores in the presence of inflammation or infection.

Maternal systemic inflammation is independently associated with adverse outcomes including increased risk of schizophrenia, autism, and other psychiatric disorders (Allswede et al., 2020; Jones et al., 2017). This was observed with acute inflammation during bacterial or viral infectious episodes (Atladottir et al., 2010; Ginsberg et al., 2019) and in milder chronic conditions such as obesity (Catalano and Shankar, 2017; Sanchez et al., 2018). Animal models that investigated the underlying mechanisms implicated proinflammatory cytokines as a cause of abnormal fetal brain development and autism-associated behaviors in offspring (Choi et al., 2016; Garay et al., 2013; Hsiao and Patterson, 2011; Wu et al., 2017b). In humans, maternal serum tumor necrosis factor α (TNFα) is elevated in pathologic pregnancies (Gücer et al., 2001) and in first trimester loss (Kaislasuo et al., 2019). Moreover, elevated interleukin (IL) 8, TNFα, and C-reactive protein are associated with risk of schizophrenia in offspring (Brown et al., 2004; Buka et al., 2001; Canetta et al., 2014).

Since high ferritin is a marker of both high iron and inflammation, it is unclear if adverse birth outcomes associated with high maternal ferritin are caused by high iron, inflammation, or a combination of both. To address this question, we developed and examined mouse models of maternal iron excess and systemic inflammation during pregnancy and discovered a dramatic adverse synergy: only the presence of both resulted in embryotoxicity. Embryotoxicity was observed in an LPS-induced sepsis model and with chronic mild inflammation occurring with diet-induced obesity. The underlying mechanism is dependent on iron-induced oxidative stress sensitizing endothelium in the placenta and embryo to TNFα-mediated apoptosis. These findings are surprising in view of the remarkable resistance of mouse models to tissue injury from massive iron overload induced by dietary or genetic manipulations. Synergistic toxicity of iron and inflammation expands our understanding of the potential effects of iron supplementation not only in pregnant women but also during other inflammatory conditions.

RESULTS

Maternal iron overload and systemic inflammation synergize to cause embryotoxicity. To model iron supplementation, wildtype C57BL/6 females were fed high-iron diet (2500-5000ppm carbonyl iron) for 1-3 weeks prior to and during pregnancy (4 to 6 weeks total, gestation in C57BL/6 mice is ~19 days). In addition, we used a genetic model of iron excess: C57BL/6 mice deficient in the iron-regulatory hormone hepcidin (hepcidin KO) which accumulate iron naturally on standard chow (185ppm iron). Control iron-adequate dams were fed standard chow. Non-pregnant females were age- and diet-matched to pregnant females. As expected, in both models of iron loading, pregnant females had higher hepatic iron compared to iron-adequate dams at embryonic day (E) 15.5 and 18.5 (all $P<0.001$) (**Supplemental Figure 4-1A**). Serum iron was significantly elevated in hepcidin KOs but not in dietary-loaded WT dams which express hepcidin **(Supplemental Figure 4-1B)**. Embryos were relatively protected from iron overload on E15.5, but by E18.5, embryos liver iron stores and serum iron were significantly higher in both iron-loading models relative to iron-adequate controls **(Supplemental Figure 4-1D).** Of note, the severity of embryo liver iron loading was much lower than in the dams. Placenta iron concentration was increased in both iron loading groups at E15.5 and 18.5 (both $P<0.001$) **(Supplemental Figure 4-1E)**.

Acute systemic maternal inflammation was induced by a single subcutaneous injection of LPS (*E. coli* serotype O55:B5) on E8.5 or 15.5 in the three group of dams: those on iron-adequate or high-iron diet and hepcidin KOs. Control dams in each group were injected with solvent. Neither iron loading nor inflammation altered litter size **(Supplemental Figure 4-1F,G)** but inflammation altered sex ratio independently of iron status. Litters from dams treated with E8.5 LPS had more

male embryos (P<0.01), suggesting that female embryos are more susceptible to inflammation-induced lethality **(Supplemental Figure 4-1H)**.

After the E8.5 injection, embryo outcome was evaluated on E18.5 **(Figure 4-1A)**. Injection of solvent did not cause embryo loss or abnormalities in any groups except a single stillborn litter in dietary iron-loaded dams at E18.5 (n=1 out of 12 dams) (**Figure 4-1,B-E**). Thus, iron loading by itself did not cause severe embryo damage. E8.5 LPS injection in iron-adequate pregnancies caused embryo loss by E18.5 in 29% of pregnancies (n=2 out of 7 dams) but surviving embryos appeared normal, with subcutaneous hemorrhaging and edema in only 3% of embryos (n=1 out of 36 embryos) **(Figure 4-1,B-E)**. Remarkably, when dams were *both* iron-loaded and LPS-injected, we observed a striking synergistic effect: adverse outcomes (embryo loss or malformation) were observed in all hepcidin KO (fed standard chow) and dietary iron-loaded dams, indicating that elevated maternal iron was the pathogenic factor synergizing with inflammation, rather than diet composition, maternal microbiome, or the lack of hepcidin. Embryo loss was noted in 62% of dietary iron-loaded pregnancies (n=10 out of 16 dams, P=0.019) and in 63% of hepcidin KO pregnancies (n=5 out of 8 dams, P=0.008) **(Figure 4-1B,C)**. Of the remaining iron-loaded inflamed pregnancies that did not resorb embryos, most embryos were severely malformed: 67% of dietary iron-loaded embryos (n=32 out of 47 embryos) and 75% of hepcidin KO embryos (n=19 out of 25 embryos) (both P<0.001) **(Figure 4-1B)**. Embryonic malformations most commonly included anencephaly and anophthalmia, subcutaneous hemorrhaging, and less commonly hernia and cleft palate **(Figure 4-1B, D-E)**.

Since E8.5 LPS injection caused embryo loss in iron-loaded dams, this limited the availability of embryo tissue for analysis. We thus injected LPS or solvent on E15.5 and analyzed outcomes after 24h **(Figure 4-1F)**. Solvent injections did not cause preterm birth or embryo

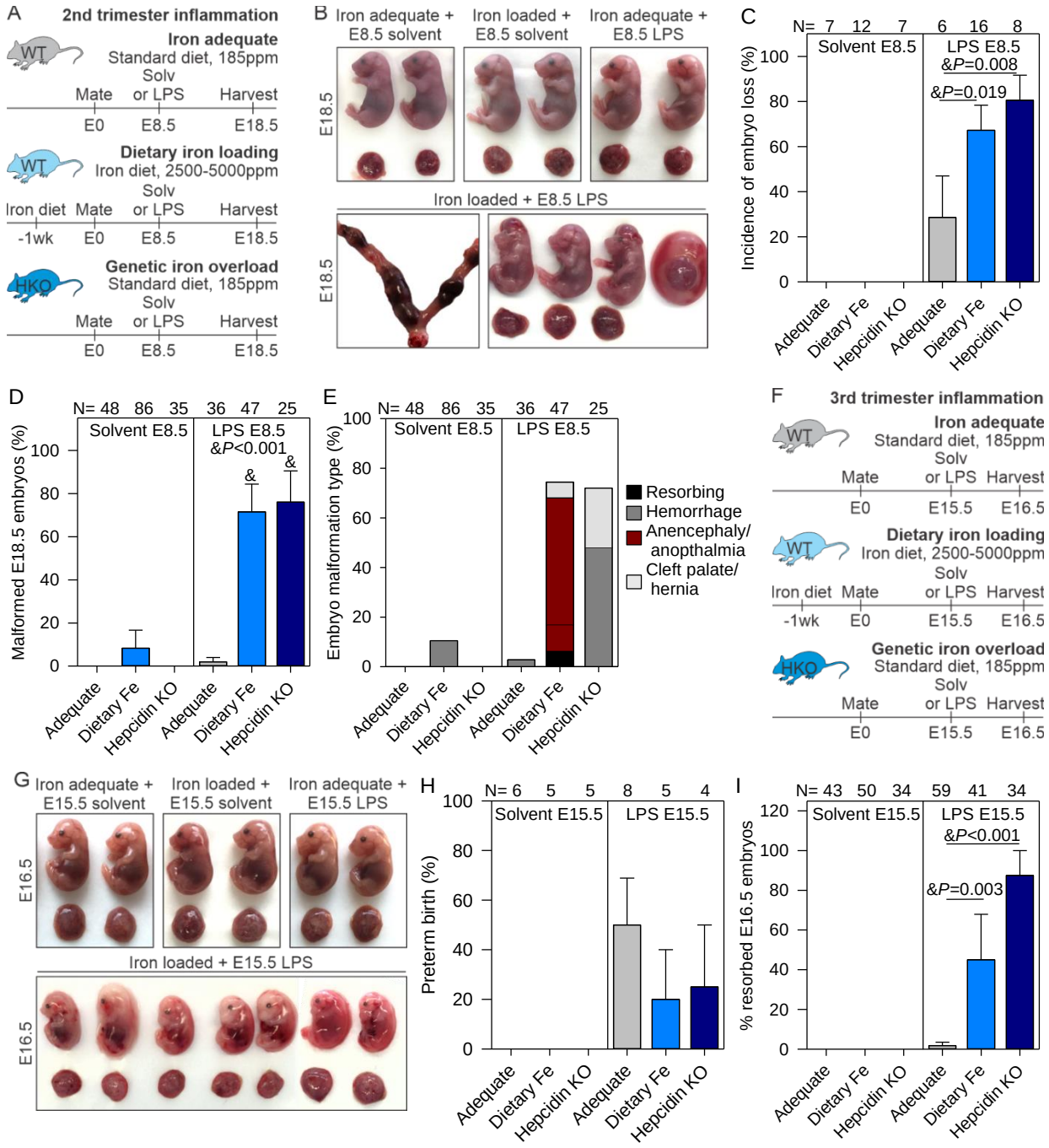

Figure 4-1. Maternal iron overload and systemic inflammation synergize to cause embryotoxicity. Dietary iron loading was achieved by feeding WT mice a high iron diet (2500-5000 ppm iron) for 1-3 weeks before mating and during pregnancy. Hepcidin KO dams, a model of genetic iron loading, were fed standard diet (185pppm iron). Both dietary and genetic iron loaded pregnancies were compared to iron-adequate pregnancies (WT females fed standard diet) under normal conditions and with maternal inflammation. **(A)** Maternal systemic inflammation was induced in the second trimester (E8.5) by a single subcutaneous injection of 0.5µg/g LPS in the interscapular area and dams were euthanized on E18.5: **(B)** embryo gross morphology, **(C)** incidence of embryo loss and **(D)** embryo malformation. **(E)** Incidence of embryo malformation by type. **(F)** Maternal systemic inflammation was induced in the third trimester (E15.5) by a single subcutaneous injection of 0.5µg/g LPS for 24h: **(G)** embryo gross morphology, **(H)** incidence of preterm birth and **(I)** embryo resorption. Statistical differences were determined by two-way ANOVA followed by Holm-Sidak method for multiple comparisons.

resorption in any groups, confirming that maternal iron loading by itself does not cause severe damage to embryos. In dams with normal iron status, E15.5 LPS injection caused preterm birth in 50% of dams, but embryos appeared normal with only 2% lethality (n=1 out of 59 embryos) **(Figure 4-1,G-I)**. In iron-loaded dams, LPS injection on E15.5 induced preterm birth in ~20% of dietary and genetic iron-loaded pregnancies, but embryonic lethality was much higher: 42% in dietary iron-loaded dams (n=17 out of 41 embryos, P=0.003), and 85% in hepcidin KO dams (n=29 out of 34 embryos) (P<0.001) **(Figure 4-1,G-I)**. Collectively, these data show that maternal iron excess, elicited by dietary or genetic means, potentiates the adverse effects of systemic inflammation during pregnancy.

LPS is a component of Gram-negative bacteria but numerous viral and bacterial infections during pregnancy are known to cause adverse outcomes (Adams Waldorf and McAdams, 2013; Racicot and Mor, 2017). We tested if high maternal iron potentiates adverse outcomes in dams injected with different pathogen-associated molecules (PAMPs). Iron-adequate WT and hepcidin KO dams were treated with polyinosinic:polycytidylic acid, lipoteichoic acid, pam3csk4, or flagellin on E15.5, and outcomes were analyzed on E16.5 **(Supplemental Table 4-1)**. In order to study synergy with iron excess, we chose doses that were lower than those previously reported to trigger preterm birth in iron-adequate mice (Ilievski et al., 2007), but most were sufficient to induce maternal inflammation comparable to the LPS group as measured by liver *Saa1* expression **(Supplemental Table 4-1)**. However, unlike LPS which adversely affected even iron-adequate pregnancies, these PAMPS had no detectable effects on mouse pregnancy. No preterm birth was observed in iron-adequate dams, nor adverse embryo outcomes in iron-loaded dams. It remains to be determined if this is related to different cytokine profiles induced by different PAMPs, and whether higher PAMP doses or live infections would synergize with iron excess.

To address the underlying mechanisms of adverse synergy observed in the LPS model, we examined if maternal iron loading augments the inflammatory response in the dam, placenta and embryo. LPS was undetectable in embryo serum after subcutaneous injection in the dam on E17.5 when placental permeability is greatest **(Supplemental figure 4-2A)**, indicating that LPS did not directly cause embryo lethality. We performed a multiplex analysis of 32 cytokines in maternal serum and although most cytokines were induced by LPS within 6h, the induction was similar between iron-adequate and -loaded dams (either dietary-loaded or hepcidin KOs), including TNFα, IL6, IL1β and IL10 (all $P<0.001$, **Figure 4-2,A-D)**, as well as IL-2, -3, -9, -12 (p.40/70), -13, -15, IFNγ, GCSF, GMCSF, MCSF, MCP1, Eotaxin, IP10, MIP1α/β, MIG, LIF, KC, and RANTES (not shown). Serum IL1α, IL-4, -5, -7, -17, LIX, MIP2, and Vegf were not induced by LPS in any dams (not shown). In the placenta, *Tnf* and *Il6* expression increased 6h after LPS **(Figure 4-2,E-F,** $P<0.001$). To obtain enough volume for embryo serum cytokine analysis, a separate cohort of iron-adequate and iron-loaded dams were injected with LPS on E17.5 for 6h and embryo serum was pooled from each litter. Out of 32 cytokines measured, only IL6 **(Figure 4-2G)** and GCSF (not shown) increased in embryo serum but this was independent of maternal iron status. We did not detect any increases in embryo serum TNFα, IL1β, or IL10 **(Figure 4-2,H-J)**.

Collectively, our data show that LPS injection induces acute, transient inflammation that is primarily restricted to the dam and placenta and is independent of maternal iron status. Thus, differential activation of maternal inflammatory pathways is not responsible for the synergistic effects observed with maternal iron excess and systemic inflammation.

We assessed the contribution of a maternal hormonal response to adverse outcomes by measuring progesterone, as premature progesterone withdrawal triggers preterm birth in mice (Dudley et al., 1996). LPS treatment induced progesterone withdrawal within 6h regardless of iron

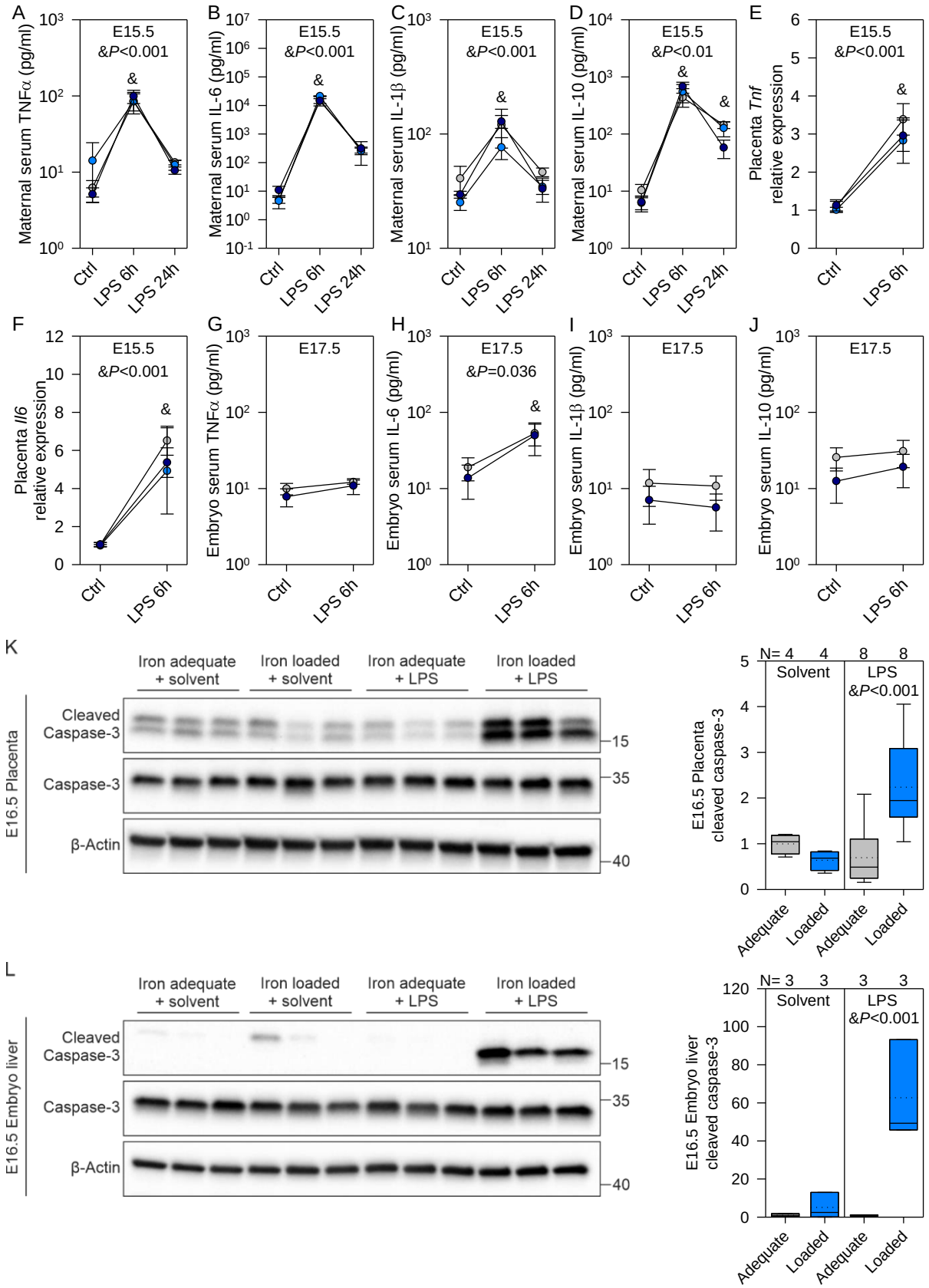
A
Maternal serum TNFα (pg/ml)
E15.5
&P<0.001
Ctrl
LPS 6h
LPS 24h
B
Maternal serum IL-6 (pg/ml)
E15.5
&P<0.001
C
Maternal serum IL-1β (pg/ml)
E15.5
&P<0.001
D
Maternal serum IL-10 (pg/ml)
E15.5
&P<0.01
E
Placenta Tnf relative expression
E15.5
&P<0.001
F
Placenta Il6 relative expression
E15.5
&P<0.001
G
Embryo serum TNFα (pg/ml)
E17.5
H
Embryo serum IL-6 (pg/ml)
E17.5
&P=0.036
I
Embryo serum IL-1β (pg/ml)
E17.5
J
Embryo serum IL-10 (pg/ml)
E17.5
K
Iron adequate + solvent
Iron loaded + solvent
Iron adequate + LPS
Iron loaded + LPS
E16.5 Placenta
Cleaved Caspase-3
Caspase-3
β-Actin
15
35
40
N= 4 4 8 8
Solvent
LPS
&P<0.001
E16.5 Placenta cleaved caspase-3
Adequate
Loaded
L
E16.5 Embryo liver
N= 3 3 3 3
E16.5 Embryo liver cleaved caspase-3

Figure 4-2. Maternal iron excess potentiates inflammation-induced apoptosis in embryo tissues. Maternal systemic inflammation was induced in iron-adequate and iron-loaded dams at E15.5 by a single subcutaneous injection of 0.5μg/g LPS. **(A-D)** Cytokines TNFα, IL6, IL1β, and IL10 in maternal serum 6 and 24h after LPS treatment. Grey circles: iron-adequate group (N=11,7,8 for contorl, 6h and 24h groups respectively), light blue circles: dietary iron group (N=9,3,7), dark blue circles: hepcidin KO group (N=10,5,4). **(E-F)** Placenta mRNA expression of *Tnf* and *Il6* normalized to *Rpl4* 6h after maternal LPS injection. Grey circles: iron-adequate group (N=13,13 for control and 6h groups respectively), light blue circles: dietary iron group (N=4,4), dark blue circles: hepcidin KO group (N=12,8). **(G-J)** Embryo serum TNFα, IL6, IL1β, and IL10 6h after maternal LPS treatment on E17.5, in a separate cohort where embryo blood was pooled from each litter to obtain sufficient serum for analysis. Grey circles: iron-adequate group (N=4,5), dark blue circles: hepcidin KO group (N=4,4). **(K)** Western blot of whole placenta and **(L)** embryo liver for apoptotic marker cleaved caspase-3, 24 h after LPS injection (N=3-8/group). β-Actin was used as a loading control. Statistical differences were determined by two-way ANOVA followed by Holm-Sidak method for multiple comparisons.

status **(Supplemental Figure 4-2B)**, consistent with the incidence of preterm birth observed in **Figure 4-1H**. Additionally, since high iron is associated with oxidative stress, we measured malondialdehyde (MDA) in maternal serum. There was no difference in MDA between iron-adequate and iron-loaded groups at baseline or 6 h after LPS. MDA was elevated in iron-loaded dams 24h after LPS treatment **(Supplemental Figure 4-2C)**, the time point when embryos were actively resorbing, suggesting the increase in MDA is not a causative factor leading to embryo demise. These data suggest that neither maternal progesterone changes nor maternal systemic oxidative stress are responsible for adverse synergy between iron excess and inflammation.

Adverse synergy between maternal iron excess and inflammation targets placental and embryo endothelium to cause its apoptosis. We performed a screen of activated cell death pathways in placentas and embryo tissues. We did not detect any iron-dependent difference in protein levels of pyroptotic markers IL1β or cleaved caspase-1, mRNA for the NLRP3 component of inflammasome, lipid peroxidation marker MDA, or putative ferroptosis marker *Ptgs2* **(Supplemental Figure 4-2,D-K)**. To assess oxidative stress, we measured expression of the NRF2 target gene *Nqo1,* as a marker of antioxidant pathway activation. *Nqo1* expression in embryo liver

did not differ between iron-adequate and loaded groups **(Supplemental Figure 4-2L)**. In whole placentas, *Nqo1* was moderately increased in the iron-loaded group 6 and 24h after LPS treatment **(Supplemental Figure 4-2M)**. Similarly, *Hmox1* was moderately increased 24h after LPS treatment **(Supplemental Figure 4-2N)**, suggesting that iron loading and inflammation synergize to induce placental oxidative stress.

To examine apoptosis, we measured cleaved caspase-3, a canonical marker of programmed cell death. We did not detect a significant increase in placental cleaved caspase-3 6h after maternal LPS injection **(Supplemental Figure 4-2O)**. However, 24h after maternal LPS injection, cleaved caspase-3 protein dramatically increased in placenta and embryo liver in iron-loaded, inflamed pregnancies **(Figure 4-2,K-L)**. TUNEL staining of placental sections confirmed increased cell death in the labyrinth layer only when the dam was both iron-loaded and LPS-injected **(Figure 4-3A)**, with a distribution pattern suggesting endothelial cell death. Co-staining of placental and whole embryo sections for cleaved caspase-3 and endothelial marker CD31 demonstrated colocalization of the two proteins in the placenta, embryo lung, heart, liver, and umbilical cord only in iron-loaded, inflamed pregnancy **(Figure 4-3,B-E, Supplemental Figure 4-3A)**, indicating that the adverse synergy targets the placental and embryo endothelial cells and causes their apoptosis.

To identify the mechanisms leading to endothelial apoptosis, we used human umbilical vein endothelial cells (HUVEC), primary fetal endothelial cells from the umbilical cord, a tissue that was affected by endothelial apoptosis in the mouse model. HUVECs were treated with ferric ammonium citrate (FAC) to induce iron loading (confirmed by ferritin immunoblotting), then stimulated with cytokines IL6, IFNγ, IL1α, IL1β, and TNFα **(Figure 4-3F)**. All of these except IL1α were elevated in maternal circulation 6h after LPS treatment, independently of the dam iron

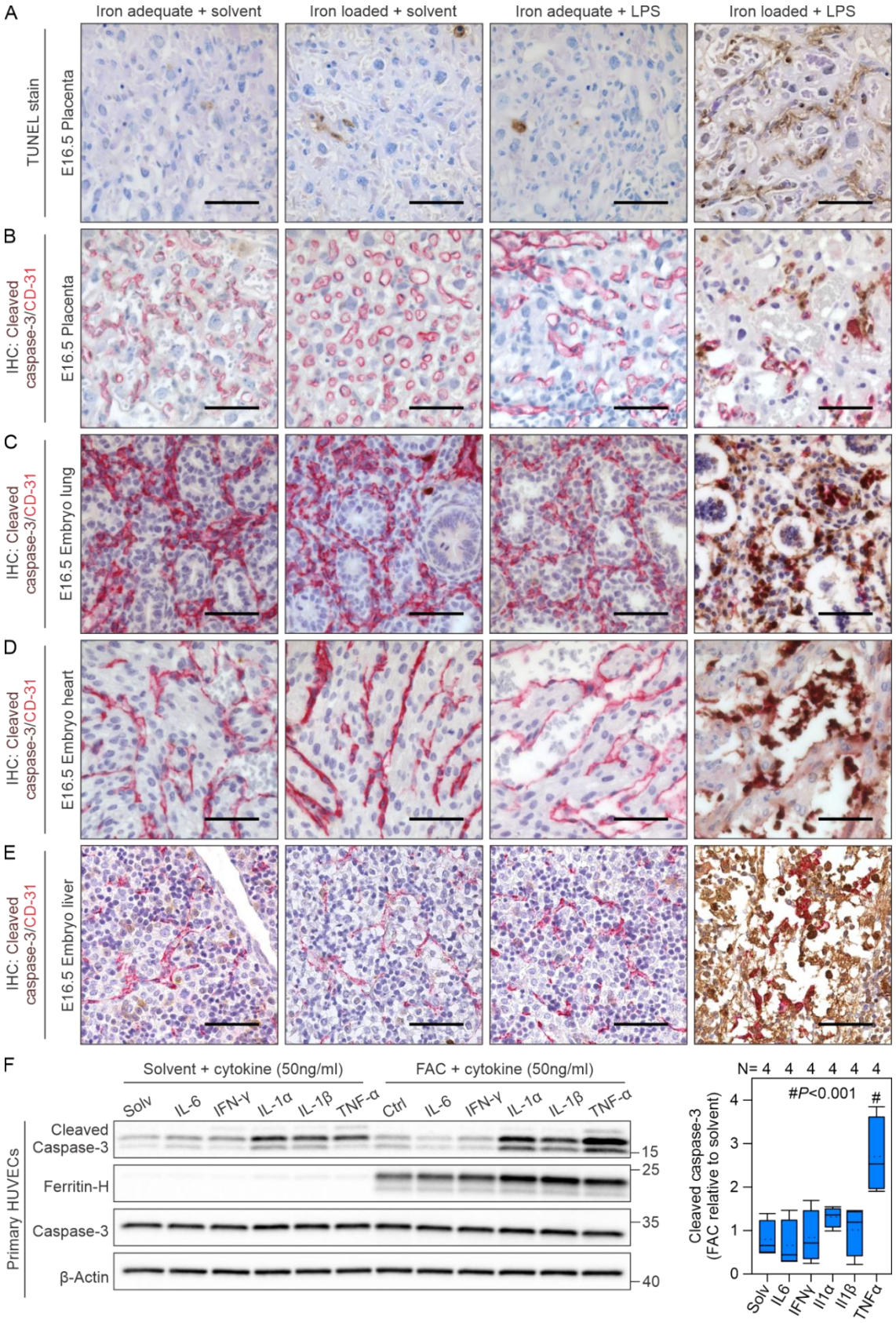
A
Iron adequate + solvent
Iron loaded + solvent
Iron adequate + LPS
Iron loaded + LPS
TUNEL stain
E16.5 Placenta
B
IHC: Cleaved caspase-3/CD-31
E16.5 Placenta
C
IHC: Cleaved caspase-3/CD-31
E16.5 Embryo lung
D
IHC: Cleaved caspase-3/CD-31
E16.5 Embryo heart
E
IHC: Cleaved caspase-3/CD-31
E16.5 Embryo liver
F
Solvent + cytokine (50ng/ml)
FAC + cytokine (50ng/ml)
Solv
IL-6
IFN-γ
IL-1α
IL-1β
TNF-α
Ctrl
IL-6
IFN-γ
IL-1α
IL-1β
TNF-α
Primary HUVECs
Cleaved Caspase-3
Ferritin-H
Caspase-3
β-Actin
15
25
35
40
N= 4 4 4 4 4 4
#P<0.001
#
Cleaved caspase-3 (FAC relative to solvent)
0
1
2
3
4
Solv
IL6
IFNγ
Il1α
Il1β
TNFα

Figure 4-3. Adverse synergy between maternal iron excess and inflammation targets placental and embryo endothelium to cause its apoptosis. Maternal systemic inflammation was induced in iron-adequate and iron-loaded dams in the third trimester (E15.5) by a single subcutaneous injection of 0.5μg/g LPS for 24h. **(A)** TUNEL stain of placental sections. **(B)** Immunohistochemistry for cleaved caspase-3 (brown) and endothelial marker CD31 (red) in paraffin-embedded placenta, **(C)** embryo lung, **(D)** heart, and **(E)** liver sections. Representative images of N=3-5 sections/group. Scale bar= 50μm. **(F)** Primary HUVECs were treated with 100μM ferric ammonium citrate (FAC) for 24h prior to being stimulated with IL6, IFNγ, IL1α, IL1β, or TNFα (all 50ng/ml) in solvent or FAC-supplemented media for 16h. Western blot (left) and quantitation (right) for cleaved caspase-3 normalized to β-Actin, representative image of N=4 independent experiments. Ferritin-H is a marker of cellular iron loading. Statistical differences were determined by one-way ANOVA followed by Holm-Sidak method for multiple comparisons.

status. In HUVECs, IL6 and IFNγ did not induce cleaved caspase-3 in either solvent or iron-treated cells, whereas IL1α and IL1β did induce cleaved caspase-3 but similarly in solvent or iron-treated groups. Only the induction of cleaved caspase-3 by TNFα was strongly potentiated by iron loading (P<0.001, **Figure 4-3F)**. LPS treatment did not induce HUVEC cleaved caspase-3 **(Supplemental Figure 4-3B)**, confirming that the direct action of LPS does not cause apoptosis. To assess if the adverse interaction with TNFα was specific to iron, we treated HUVECs with other metals. Only iron but not copper or zinc potentiated TNFα induction of cleaved caspase-3 **(Supplemental Figure 4-3C)**. Conversely, co-treating HUVECs with FAC and iron chelator deferoxamine completely prevented TNFα-mediated apoptosis **(Supplemental Figure 4-3D)**.

Collectively, our data show that iron accumulation sensitizes endothelial cells to TNFα-induced cell death.

Synergistic toxicity of iron and inflammation is mediated by maternal TNFα. Pathways leading to apoptosis are categorized into the extrinsic or death receptor pathway, and the intrinsic or mitochondrial pathway (Elmore, 2007), but both lead to caspase-3 cleavage. We did not detect

any iron-dependent differences in cleaved caspase-9 or mitochondrial oxidative phosphorylation complexes in HUVECs treated with FAC and TNFα, or in placenta lysates from the iron-loaded, inflamed group **(Supplemental Figure 4-4A,B)**, further suggesting that the synergistic action of iron excess and inflammation acts through the extrinsic apoptotic pathway.

We examined the contribution of TNFα in mediating embryo demise in vivo by treating pregnant iron-loaded hepcidin KO dams with TNFα-neutralizing antibody or control IgG antibody targeting trinitrophenol, prior to LPS treatment on E15.5 **(Figure 4-4A)**. The specificity of TNFα-neutralizing antibody was confirmed in vitro in HUVECs treated with FAC and IL1α, IL1β, and TNFα. In iron-loaded cells, treatment with TNFα-neutralizing antibody prevented cleaved caspase-3 induction by TNFα but not IL1α or IL1β **(Supplemental Figure 4-5A)**. In pregnant hepcidin KO mice, neutralizing TNFα in maternal circulation had no effect on LPS-induced hepatic expression of serum amyloid A1 (*Saa-1*), *Il6*, *Ccl2*, *Il1b*, *Cxcl2*, or *Cxcl10*, but reduced *Cxcl9* expression **(Figure 4-4,C-E, Supplemental Figure 4-5,B-E)**. Despite comparable maternal inflammation, neutralizing TNFα prevented embryo resorption and demise (P=0.002, **Figure 4-4B)**. Placentas from dams treated with anti-TNFα therapy had lower expression of *Tnf*, *Il6*, *Il1b*, and *Cxcl9* (all P<0.001) **(Figure 4-4,F-I)**, showing that anti-TNFα therapy attenuates placental inflammation. Importantly, neutralizing TNFα prevented placenta and embryo apoptosis as reflected by reduced caspase-3 cleavage in placentas (P=0.009) and embryo livers (P=0.029), and decreased TUNEL staining in placental sections **(Figure 4-4,J-L)**. Co-staining shows that anti-TNFα therapy prevented apoptosis of endothelial cells in the placenta, embryo heart, lung, and liver **(Figure 4-4M)**. These data confirm that maternal TNFα is the pathogenic factor causing endothelial apoptosis and embryo demise.

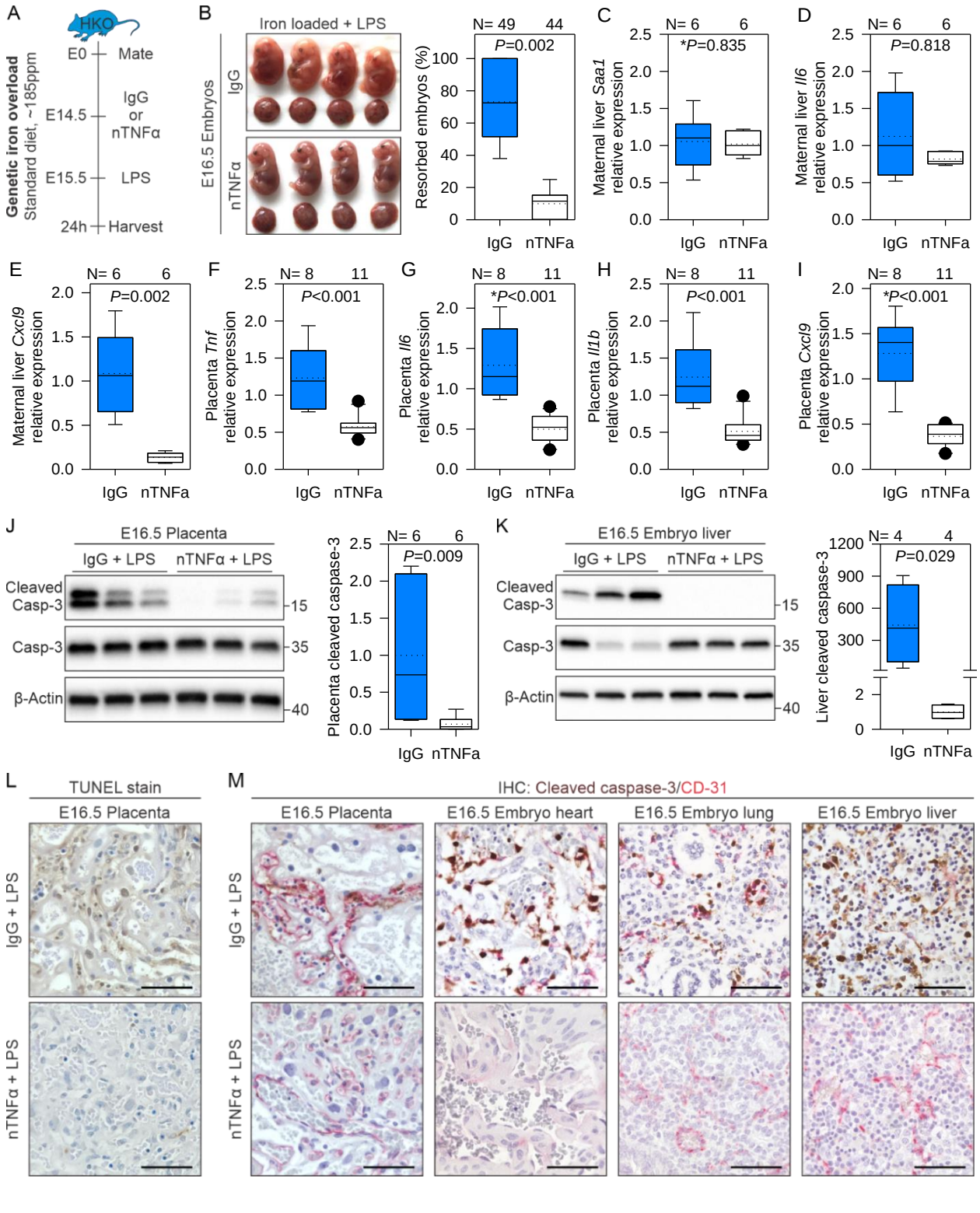
A
HKO
Genetic iron overload
Standard diet, ~185ppm
E0
Mate
E14.5
IgG or nTNFα
E15.5
LPS
24h
Harvest
B
Iron loaded + LPS
E16.5 Embryos
IgG
nTNFα
N= 49 44
P=0.002
Resorbed embryos (%)
IgG nTNFa
C
N= 6 6
*P=0.835
Maternal liver Saa1 relative expression
D
N= 6 6
P=0.818
Maternal liver Il6 relative expression
E
N= 6 6
P=0.002
Maternal liver Cxcl9 relative expression
F
N= 8 11
P<0.001
Placenta Tnf relative expression
G
N= 8 11
*P<0.001
Placenta Il6 relative expression
H
N= 8 11
P<0.001
Placenta Il1b relative expression
I
N= 8 11
*P<0.001
Placenta Cxcl9 relative expression
J
E16.5 Placenta
IgG + LPS
nTNFα + LPS
Cleaved Casp-3
Casp-3
β-Actin
15
35
40
N= 6 6
P=0.009
Placenta cleaved caspase-3
K
E16.5 Embryo liver
IgG + LPS
nTNFα + LPS
Cleaved Casp-3
Casp-3
β-Actin
15
35
40
N= 4 4
P=0.029
Liver cleaved caspase-3
L
TUNEL stain
E16.5 Placenta
IgG + LPS
nTNFα + LPS
M
IHC: Cleaved caspase-3/CD-31
E16.5 Placenta
E16.5 Embryo heart
E16.5 Embryo lung
E16.5 Embryo liver
IgG + LPS
nTNFα + LPS

Figure 4-4. Synergistic toxicity of iron and inflammation is mediated by maternal TNFα. (A) Iron-loaded hepcidin KO dams were treated intravenously via the retroorbital sinus with 500μg neutralizing TNFα antibody (nTNFα) or isotype control IgG (IgG) neutralizing trinitrophenol 15h prior to subcutaneous injection of LPS (0.5μg/g) for 24h. **(B)** Incidence of resorbing embryos. **(C-E)** Maternal liver expression of inflammatory markers *Saa1*, *Il6*, and *Cxcl9* normalized to *Hprt.* **(F-I)** Placental mRNA expression of inflammatory markers *Tnf*, *Il6*, *Il1b*, and *Cxcl9* normalized to *Rpl4*. **(J-K)** Western blots and quantitation of whole placenta or embryo liver lysates for cleaved caspase-3 expression normalized to β-Actin. **(L)** TUNEL stain of placental sections. **(M)** Immunohistochemistry for cleaved caspase-3 (brown) and CD31 (red) in paraffin-embedded placenta, embryo heart, lung, and liver. Representative image of N=3 sections/group. Scale bar= 50μm. Statistical differences between groups were determined by Mann-Whitney *U* or Student's *t*-test (denoted by *).

Synergistic toxicity of iron and inflammation is mediated by endothelial oxidative stress and prevented by α-Tocopherol treatment. To determine why endothelial cells from iron-loaded pregnancies are more susceptible to inflammation-induced apoptosis, we performed RNA-Seq of isolated placental endothelial cells from iron-adequate WT and iron-loaded hepcidin KO dams 6h after solvent or LPS treatment **(Figure 4-5A)**. Isolation of endothelial cells was confirmed by 80-fold enrichment of *Cd31* mRNA ($P<0.001$) **(Supplemental Figure 4-5F)**. Placental endothelial cells from hepcidin KO dams had lower expression of iron-importer transferrin receptor (*Tfrc*) compared to placental endothelial cells from iron-adequate dams ($P=0.014$), indicative of cellular iron loading **(Figure 4-5B).** Ingenuity pathway analysis of differentially expressed genes showed upregulation of reactive oxygen species and canonical inflammatory signaling pathways in endothelial cells from hepcidin KO dams compared to WT dams **(Figure 4-5C)**. After LPS treatment, endothelial cells from hepcidin KO dams compared to LPS-treated WT dams showed further enrichment in genes in oxidative stress pathways, namely reactive oxygen species, Nrf2-oxidative stress, and Hmgb1 signaling **(Figure 4-5D)**. These data suggest that iron loading sensitizes endothelial cells to injury through oxidative stress and enhanced inflammatory signaling. In agreement, treatment of HUVECs with different forms of iron including non-transferrin bound iron and iron-rich ferritin induced oxidative stress as reflected by over 2-fold induction in *NQO1*

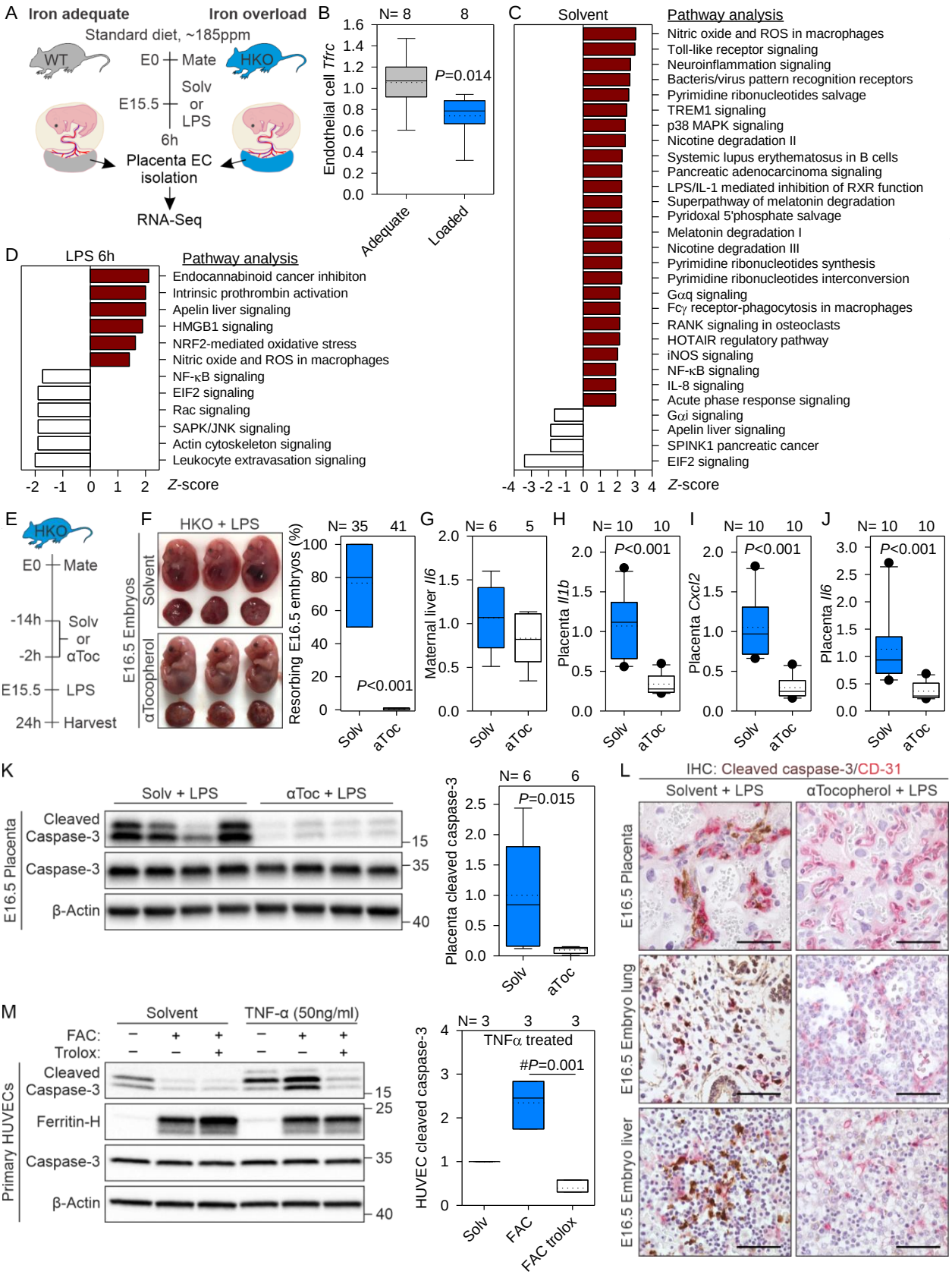
A
Iron adequate
Iron overload
Standard diet, ~185ppm
WT
HKO
E0
Mate
E15.5
Solv or LPS
6h
Placenta EC isolation
RNA-Seq
B
N= 8 8
Endothelial cell Tfrc
P=0.014
Adequate
Loaded
C
Solvent
Pathway analysis
Nitric oxide and ROS in macrophages
Toll-like receptor signaling
Neuroinflammation signaling
Bacteris/virus pattern recognition receptors
Pyrimidine ribonucleotides salvage
TREM1 signaling
p38 MAPK signaling
Nicotine degradation II
Systemic lupus erythematosus in B cells
Pancreatic adenocarcinoma signaling
LPS/IL-1 mediated inhibition of RXR function
Superpathway of melatonin degradation
Pyridoxal 5'phosphate salvage
Melatonin degradation I
Nicotine degradation III
Pyrimidine ribonucleotides synthesis
Pyrimidine ribonucleotides interconversion
Gαq signaling
Fcγ receptor-phagocytosis in macrophages
RANK signaling in osteoclasts
HOTAIR regulatory pathway
iNOS signaling
NF-κB signaling
IL-8 signaling
Acute phase response signaling
Gαi signaling
Apelin liver signaling
SPINK1 pancreatic cancer
EIF2 signaling
Z-score
D
LPS 6h
Pathway analysis
Endocannabinoid cancer inhibiton
Intrinsic prothrombin activation
Apelin liver signaling
HMGB1 signaling
NRF2-mediated oxidative stress
Nitric oxide and ROS in macrophages
NF-κB signaling
EIF2 signaling
Rac signaling
SAPK/JNK signaling
Actin cytoskeleton signaling
Leukocyte extravasation signaling
Z-score
E
HKO
E0
Mate
-14h
Solv or αToc
-2h
E15.5
LPS
24h
Harvest
F
HKO + LPS
E16.5 Embryos
Solvent
αTocopherol
Resorbing E16.5 embryos (%)
N= 35 41
P<0.001
Solv
aToc
G
N= 6 5
Maternal liver Il6
H
N= 10 10
P<0.001
Placenta Il1b
I
N= 10 10
P<0.001
Placenta Cxcl2
J
N= 10 10
P<0.001
Placenta Il6
K
Solv + LPS
αToc + LPS
E16.5 Placenta
Cleaved Caspase-3
Caspase-3
β-Actin
15
35
40
N= 6 6
P=0.015
Placenta cleaved caspase-3
L
IHC: Cleaved caspase-3/CD-31
Solvent + LPS
αTocopherol + LPS
E16.5 Placenta
E16.5 Embryo lung
E16.5 Embryo liver
M
Solvent
TNF-α (50ng/ml)
FAC:
Trolox:
Primary HUVECs
Cleaved Caspase-3
Ferritin-H
Caspase-3
β-Actin
15
25
35
40
N= 3 3 3
TNFα treated
#P=0.001
HUVEC cleaved caspase-3
Solv
FAC
FAC trolox

Figure 4-5. Synergistic toxicity of iron and inflammation is mediated by endothelial oxidative stress and prevented by αTocopherol treatment. (A) Iron-adequate and iron-loaded dams were treated with subcutaneous LPS (0.5μg/g) on E15.5 for 6h. Placentas from solvent and LPS-treated mice were collected for endothelial cell isolation by magnetic separation using CD31 beads and total RNA was analyzed by RNA-Seq. **(B)** Endothelial cell *Tfrc* relative to *Rpl4*. **(C-D)** RNA-Seq Ingenuity Pathway Analysis of significantly downregulated (white bars) and enriched (red bars) genes (*Z*-score < and > than ±1.5) from placental endothelial cells comparing hepcidin KO and WT mice at **(C)** baseline and **(D)** 6h after LPS injection. **(E-L)** Hepcidin KO dams were treated with subcutaneous αTocopherol (αToc: vitamin E) 14 and 2h prior to LPS treatment on E15.5 for 24h: **(F)** incidence of resorbing embryos; **(G)** maternal liver *Il6* expression; **(H-J)** placental *Il1b*, *Cxcl2*, and *Il6* expression. **(K)** Western blot (left) and quantitation (right) of cleaved caspase-3 in whole placentas normalized to β-Actin. **(L)** Immunohistochemistry for cleaved caspase-3 (brown) and CD31 (red) in paraffin-embedded placenta, embryo lung and liver (representative image of N=3 sections/group). Scale bar= 50μm. **(M)** Primary HUVECs were treated with 100μM ferric ammonium citrate (FAC) with and without vitamin E analog Trolox (300μM) for 24h prior to being stimulated with TNFα (50ng/ml) for 16h. Western blot (left) and quantitation (right) of cleaved caspase-3 normalized to β-Actin (representative image of N=3 independent experiments). Statistical differences were determined by Mann-Whitney *U* or one-way ANOVA followed by Holm-Sidak method for multiple comparisons (denoted by #).

Iron supplementation potentiates embryonic malformation and placental apoptosis in a mouse model of Western diet-induced obesity. To investigate if maternal iron excess adversely interacts with chronic inflammation during pregnancy, we used a mouse model of diet-induced obesity in WT and hepcidin KOs **(Figure 4-6A)**. WT C57BL/6 females were fed an iron-adequate Western diet (100ppm iron) for 8 weeks, then half of the mice continued on the same Western diet (iron-adequate group), and the other half were switched to a high-iron Western diet (3700ppm carbonyl iron) for 1-3 weeks (dietary iron loading group), then mated and fed the same diet in pregnancy. The third group (genetic iron loading) consisted of hepcidin KO females maintained on the iron-adequate Western diet for the same duration. Dams in all three Western diet groups weighed ~40% more at mating than their respective controls fed non-obesogenic standard diet or high iron diet **(Figure 4-6B)**. At E18.5, compared to iron-adequate dams, hepcidin KOs were most iron-loaded with >20-fold higher liver iron and >2-fold higher serum iron (both $P<0.001$), whereas dietary iron-loaded dams had ~6-fold higher liver iron ($P<0.001$) but no increase in serum iron **(Supplemental Figure 4-6A,B)**. Placental iron increased in both dietary-loaded and hepcidin KO groups ($P=0.001$) **(Supplemental Figure 4-6C).** Embryos were completely protected from iron

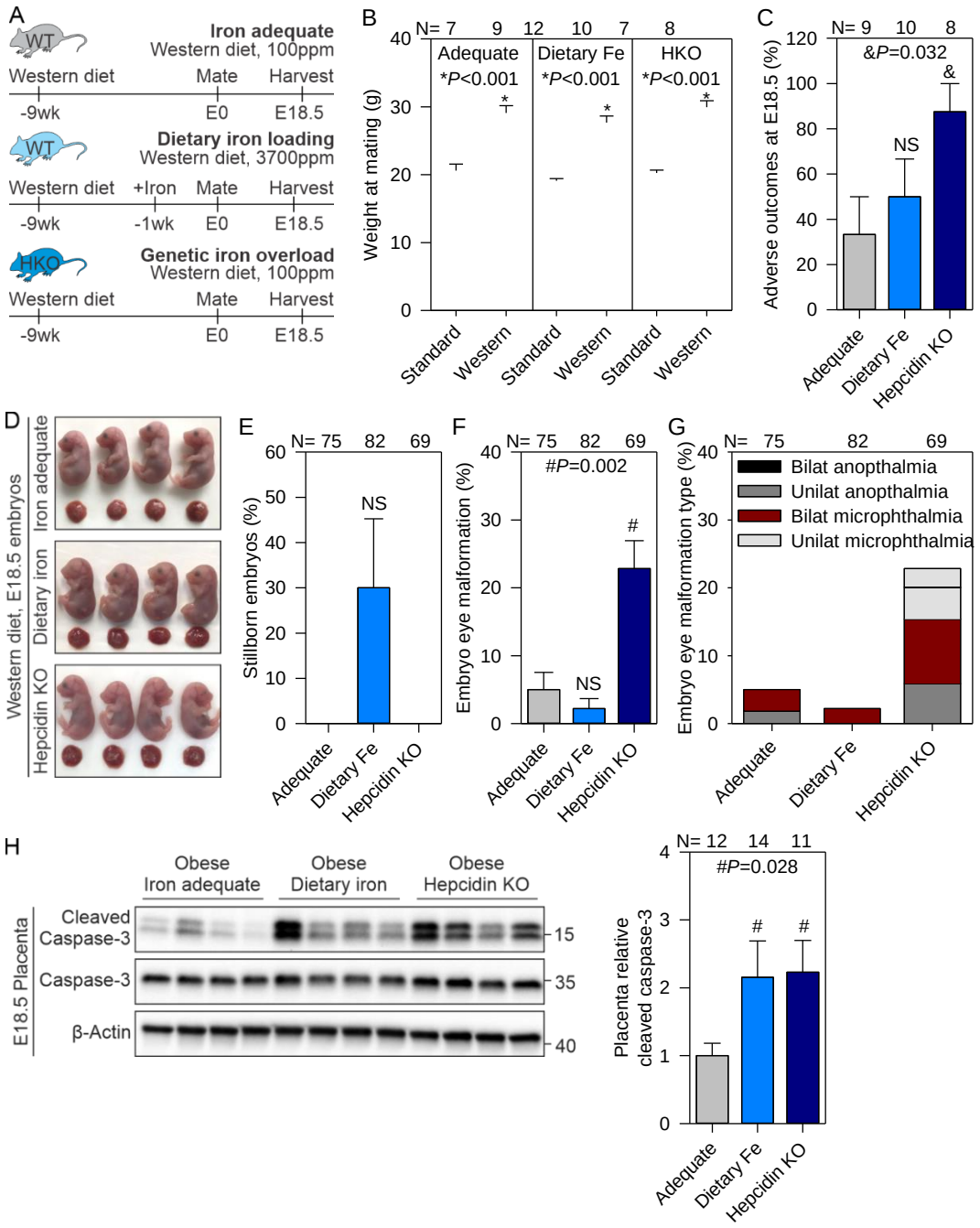

Figure 4-6. Iron supplementation potentiates embryonic malformation and placental apoptosis in a mouse model of Western diet-induced obesity. (A) Starting at 3 weeks of age, wild-type C57BL/6 (iron-adequate) or hepcidin KO (genetic iron overload) females were fed an iron-adequate Western diet (100ppm iron) for 8 weeks. After 8 weeks, half of the WT mice were switched to a high-iron Western diet (5,000ppm carbonyl iron, dietary iron loading) for 1-3 weeks, while the other mice continued on Western diet. Mice were mated and continued their respective diets during pregnancy. Iron adequate dams were compared to dietary or genetic iron-loaded dams. **(B)** Maternal weight at mating in dams fed a Western diet compared to those fed non-obesogenic diet. **(C)** Incidence of adverse outcomes at E18.5 in obese pregnancies. **(D)** Embryo gross morphology. **(E)** Incidence of stillborn embryos, **(F-G)** incidence of embryo eye malformations. **(H)** Western blot of whole placentas for cleaved caspase-3 and quantification normalized to β-Actin. Statistical differences were determined by Student's *t*-test (denoted by *), one-way ANOVA on ranks followed by Dunn's method for multiple comparisons (denoted by #), or Mann-Whitney *U* test (indicated by &).

loading and had liver iron and serum iron concentrations comparable to embryos from iron-adequate dams **(Supplemental Figure 4-6D,E)**. Litter size was similar between the groups, but embryo sex ratio was skewed towards fewer female embryos in obese pregnancies, similarly to the LPS model **(Supplemental Figure 4-6F,G)**.

Obesity in iron-adequate dams caused adverse outcomes in one-third of pregnancies (N=3 out of 9 dams) **(Figure 4-6C)**, although few embryos were affected in each litter (~5% had eye malformations) **(Figure 4-6,D-F)**. Dietary iron loading of obese dams resulted in a more variable phenotype where 50% of litters were normal and 50% of litters were afflicted by fatal subcutaneous hemorrhaging and uncommonly eye malformations **(Figure 4-6,C-G)**. Obesity in the most iron-loaded hepcidin KO dams caused adverse pregnancy outcomes in over 80% of pregnancies **(Figure 4-6C)**, with embryo eye malformations in over 20% of embryos (P=0.002, **Figure 4-6,C-F)**. Embryo eye malformations included anophthalmia and microphthalmia **(Figure 4-6G)**. Similar to our acute LPS model, in placental lysates we observed an increase in cleaved caspase-3 in iron-loaded obese dams (P=0.028) **(Figure 4-6H)**, suggesting similarities in the pathogenic mechanism between our acute and chronic inflammation models.

Neutralizing maternal TNFα is protective against embryonic malformation induced by the combination of high maternal iron and Western diet. We evaluated if maternal exposure to high iron while on an obesogenic diet affected inflammation, as both obese humans and animal models are reported to have elevated TNFα and IL6 (Aronson et al., 2004; Katsuki et al., 1998; Roytblat et al., 2000). Clustering analysis of Luminex 32-plex cytokine panel in maternal serum from obese and lean mouse pregnancies with and without iron loading identified the most severe group - obese hepcidin KO dams - as having a distinct cytokine profile compared to the other

groups, and showed increases in TNFα and related cytokines **(Figure 4-7A)**. Elevated TNFα levels were confirmed in obese hepcidin KO dams (P=0.017), but not in others **(Figure 4-7B)**. No difference in TNFα levels were found in sera from their embryos or amniotic fluid, or in placental *Tnf* expression **(Figure 4-7,C-E)**, suggesting that maternal TNFα is the driver of embryonic complications. Thus, we treated hepcidin KO dams maintained on Western diet with neutralizing TNFα antibody or isotype control IgG antibody throughput pregnancy (E5.5, E8.5, E12.5, and E15.5) and analyzed embryo outcome at E18.5 **(Figure 4-7F)**. We observed eye malformations in embryos from obese hepcidin KO dams treated with IgG control **(Figure 4-7G)**, whereas neutralizing TNFα reduced the incidence of embryo eye malformations (P<0.01) **(Figure 4-7H,I)**, confirming the role of maternal TNFα in mediating adverse embryo outcomes in iron-loaded, obese pregnancies.

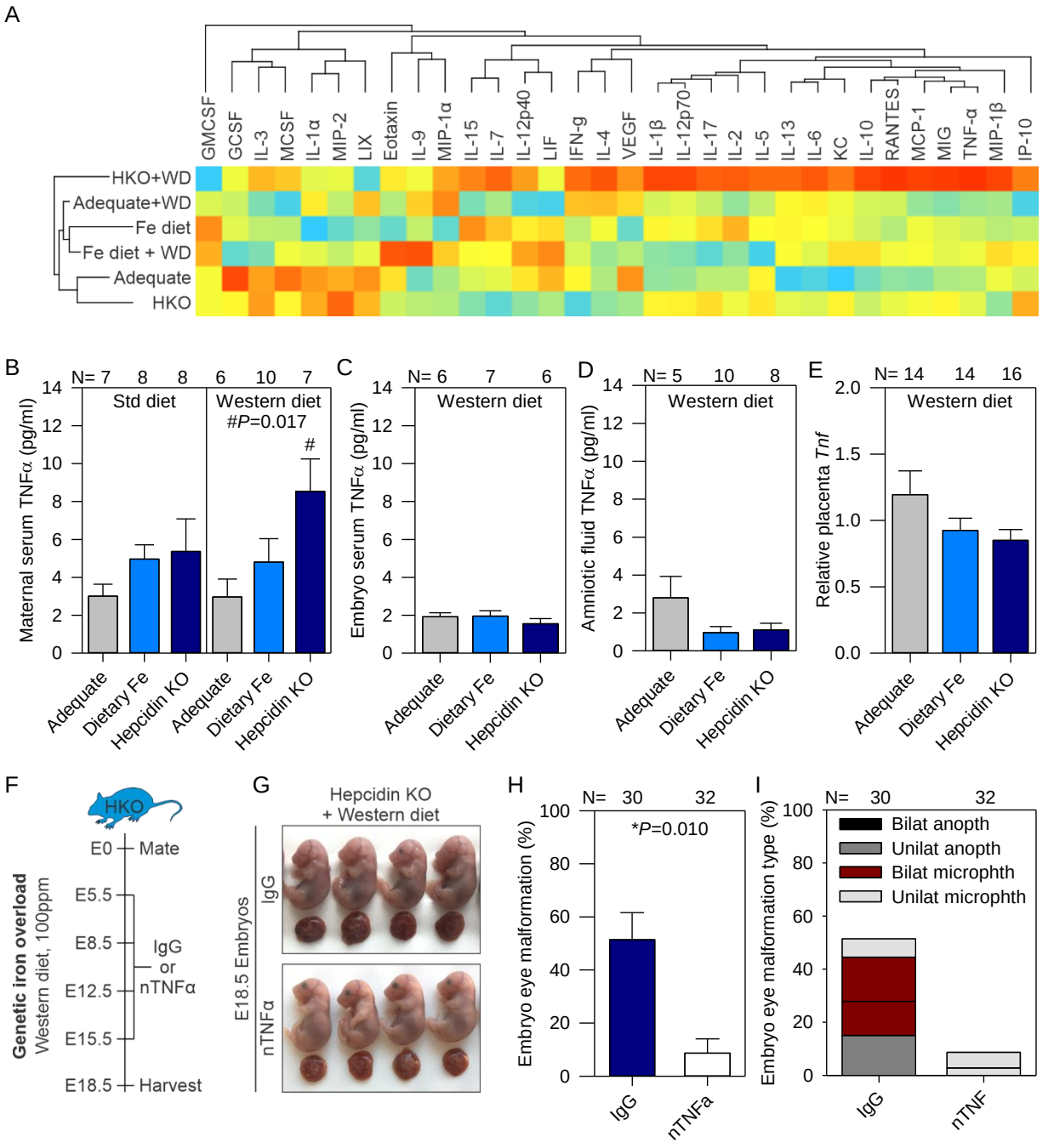

Figure 4-7. Neutralizing maternal TNFα is protective against embryonic malformation induced by the combination of high maternal iron and Western diet. (A) Clustering analysis of 32-plex cytokine panel in maternal serum from iron-adequate, dietary iron-loaded (Fe diet), and genetically iron-loaded hepcidin KO (HKO) dams fed standard or Western diet (WD). **(B-E)** E18.5 TNFα measurements in **(B)** maternal serum, **(C)** embryo serum, **(D)** amniotic fluid, and **(E)** placental *Tnf* gene expression. **(F)** Hepcidin KO females were fed Western diet (100ppm iron) starting at 3 weeks of age and were mated after 9 weeks. Pregnant dams received intravenous injections of neutralizing TNFα antibody or isotype IgG targeting trinitrophenol as a control (250µg/injection) on E5.5, E8.5, E12.5, and E15.5, and embryo outcome was evaluated at E18.5. **(G)** Embryo gross morphology. **(H-I)** Incidence of eye malformations. Statistical differences were determined by one-way ANOVA on ranks followed by Dunn's method for multiple comparisons (denoted by #), or Student's *t*-test (denoted by *).

DISCUSSION

While the WHO recommends that all pregnant women take daily iron supplements (WHO, 2016), the US Preventive Services Task Force concluded that there are insufficient data to assess the balance of benefits and harms of iron supplementation during pregnancy (Siu and Force, 2015). In developed countries, most women have sufficient iron stores, but women are still advised to take 30-60mg elemental iron daily starting at the first prenatal visit (Breymann, 2015), even without screening for iron deficiency. We recently showed that the maternal homeostatic adaptations during pregnancy include suppression of the iron-regulatory hormone hepcidin (Sangkhae et al., 2020), which would promote the rapid absorption of iron supplements, potentially exposing pregnant women to iron excess.

Maternal serum ferritin, a marker of body iron stores, shows a U-shaped risk curve where both low and high ferritin are associated with adverse pregnancy outcomes. However, ferritin is also induced by inflammation and does not accurately reflect iron stores in the setting of inflammation or infection. Thus, association of high ferritin with adverse outcomes could reflect the pathogenic role of iron excess or inflammation, or the combination of both. We addressed this question using mouse models and identified a novel interaction between iron excess and inflammation. Our study is the first to demonstrate iron-dependent apoptotic injury in mouse models.

The interaction between iron overload and inflammation is even more surprising because uninflamed mice are resistant to tissue injury from even massive iron overload. To analyze the consequences of pure iron excess in the setting of pregnancy, we modeled two modes of iron loading: one based on feeding mice high iron diet during pregnancy and the other used hepcidin KO mice, a model of genetic hemochromatosis. Both genetic and dietary maternal iron loading

resulted in higher placental iron and embryo iron stores. Although consequences of fetal iron excess in humans are not understood, it has been suggested that excessive iron supplementation of infants may have adverse effects on growth, risk of infections, cognition, and brain development (Domellof, 2010). In the hepcidin KO model, we did not see any phenotypic effect of maternal genetic iron loading on embryo development, and hepcidin KO mice are viable, survive until adulthood, and are fertile. In our dietary iron-loading model, we observed a small but insignificant increase in the incidence of embryo fatal subcutaneous hemorrhaging and stillbirth. In this regard, additional studies are needed to better determine the long-term effects on offspring of excess iron supplementation during pregnancy.

When both iron excess and inflammation were present in pregnant animals, we found a dramatic adverse synergy that resulted in dire consequences for the fetus. In our LPS model of acute inflammation, both dietary and genetic loading were associated with high incidence of embryo mortality or malformations. In our model of diet-induced obesity, representing a milder chronic inflammatory state, we similarly observed that dietary iron loading caused embryo subcutaneous hemorrhaging or malformations. Our data question the safety of iron supplementation in women with acute or chronic inflammation.

Importantly, we defined the mechanism underlying the adverse synergy between acute inflammation and maternal iron excess. Our animal models show that maternal iron excess increased oxidative stress in the whole placenta and specifically in placental endothelial cells, which was further exacerbated in the presence of inflammation. Iron-induced oxidative stress sensitizes endothelium in the placenta and embryo to inflammation-induced apoptosis, ultimately resulting in fetal death or malformations. Although also iron-dependent, this mechanism is distinct from ferroptosis as it does not involve iron-dependent changes in markers of lipid peroxidation,

Ptgs2 or MDA. Of note, treating dams with vitamin E isomer α-Tocopherol prior to the inflammatory insult completely prevented endothelial apoptosis and fetal demise, likely due to the attenuation of placental inflammation. Vitamin E exerts its cytoprotective effects as an antioxidant by scavenging reactive oxygen species and more broadly by inhibiting caspase activity (Uemura et al., 2002; Wu et al., 2017a), and reducing inflammation (Devaraj and Jialal, 2005; Huey et al., 2008; Li et al., 2012; Wu et al., 2010). Although the WHO reports no beneficial effect of routine vitamin E supplementation for women with or without a high risk of adverse pregnancy outcomes (Rumbold et al., 2015), our study suggests that acute vitamin E therapy may be beneficial in iron supplemented pregnancies with underlying inflammation. We speculate that the mechanism of iron-dependent apoptosis and its prevention by vitamin E supplementation could apply beyond pregnancy, to broader clinical problems associated with endothelial dysfunction, oxidative stress, and inflammation, and iron loading conditions could similarly worsen outcomes in hypertension, sickle cell disease, renal failure, and other cardiovascular and metabolic diseases.

We demonstrated that TNFα was the pathogenic factor synergizing with maternal iron excess. TNFα is a pleiotropic cytokine that regulates diverse biological functions including cell growth, viral replication, septic shock, inflammation, and autoimmunity (Aggarwal et al., 2012), and aberrant TNFα production is associated with many inflammatory diseases in humans. Although both our acute inflammatory LPS model and chronic inflammatory obesity model resulted in similar adverse embryo outcomes and placental apoptosis, there seem to be differences in how iron excess alters TNFα signaling in acute and chronic inflammatory settings. In acute inflammation caused by LPS injection, there was no difference in maternal TNFα production between iron-adequate and iron-loaded dams. Thus, iron excess in our acute inflammatory model alters downstream TNFα signaling rather than TNFα production. In contrast, in our obesity model,

genetic iron loading increased circulating TNFα levels in the dam but not in placentas or embryos, suggesting that maternal iron excess did modulate TNFα production. TNFα is produced by adipose tissue and its secretion correlates with the degree of adiposity (Tzanavari et al., 2010), suggesting that iron excess may further promote TNFα production by adipose tissue in obesity.

Notably, maternal anti-TNFα therapy was sufficient to prevent embryotoxicity in iron-loaded pregnancies in either the acute LPS inflammatory model, or in obese mice. The development of anti-TNFα therapy has been indispensable for the treatment of several inflammatory-mediated autoimmune conditions (Berns and Hommes, 2016; Dretzke et al., 2011). Monoclonal anti-TNFα antibodies are considered safe during pregnancy, although they are actively transported across the placenta particularly in the third trimester (Kane and Acquah, 2009; Mahadevan et al., 2013), and are detectable in newborns until 6 months post-partum (Esteve-Solé et al., 2017; Julsgaard et al., 2016; Mahadevan et al., 2013). Despite measurable levels in offspring, studies report no association between anti-TNFα concentrations in infants at birth and risk of infection or in reaching developmental milestones in the first year of life (Julsgaard et al., 2016; Mahadevan et al., 2014).

In summary, we investigated the consequences of excess maternal iron during healthy and inflamed pregnancy and discovered a novel adverse interaction. Maternal iron excess, accrued through dietary or genetic means, potentiated the adverse effects of inflammation during pregnancy, causing embryo malformations and demise. We observed this synergy between iron and acute inflammation utilizing a LPS-induced sepsis model and with chronic mild inflammation caused by diet-induced obesity. We provide specific evidence that the interaction between iron excess and inflammation is dependent on TNFα signaling causing lethal apoptotic damage to endothelial cells in the embryo and the placenta which can be prevented by maternal antioxidant

therapy. Our data suggest that pregnant women are at high risk for adverse birth outcomes when the mother is exposed to both high iron levels and systemic inflammation during pregnancy and underscores the importance of screening pregnant women for iron deficiency before recommending iron supplementation. Given the increasing prevalence of inflammatory disorders worldwide, and that iron supplementation of pregnant women is universal, our study raises important questions about the safety of indiscriminate iron supplementation in inflamed pregnancy. Furthermore, future studies will assess whether iron represents a modifiable factor to decrease detrimental effects of inflammation in conditions other than pregnancy.

ACKNOWLEDGEMENTS

The authors thank Victoria Gabayan for her assistance with animal experiments; Emmanuelle Faure-Kumar and the UCLA Integrated Molecular Technologies Core for performing the multiplex cytokine assay; the UCLA Translational Pathology Core Laboratory for histology processing; the UCLA Technology Center for Genomics & Bioinformatics (TCGB) for performing RNA seq. This study was supported by the Executive Advisory Board of the Iris Cantor–UCLA Women's Health Center and National Center for Advancing Translational Sciences UCLA Clinical and Translational Science Institute grants UL1TR0001881 and UL1TR000124 (to EN), NIH grant R01 HD096863 (to EN), NIH Ruth L. Kirschstein National Research Service Awards T32GM065823 and F31HD097931 (to AF).

AUTHOR CONTRIBUTIONS

ALF designed and performed experiments, analyzed data, and wrote the manuscript. VS performed experiments and assisted with data interpretation. KB performed experiments. NJP assisted with data analysis. TG and EN conceived the project, analyzed data, and wrote the manuscript.

DECLARATION OF INTERESTS

TG and EN are shareholders of and scientific advisors for Intrinsic LifeSciences and Silarus Therapeutics and consultants for Ionis Pharmaceuticals, Protagonist, and Vifor. TG is a consultant for Akebia.

MATERIALS AND METHODS

Animals. All animal experiments were approved by the University of California, Los Angeles (UCLA) Institutional Animal Care and Use Committee and were carried out in accordance with the Guide for Care and Use of Laboratory Animals (National Institutes of Health, Bethesda, MD). The following strains of mice were housed in our vivarium under standard laboratory conditions and used for experiments: wild type (WT) C57BL/6J (Jackson Laboratory, Bar Harbor, ME, stock #000664), and hepcidin-1 knockout mice on C57BL/6J background (Lesbordes-Brion et al., 2006). Unless specified, mice received a standard diet (PicoLab Rodent Diet 20, 5053 Irradiated, 185 ppm iron). For purified diets, iron content was determined by ICP-MS (Veterinary Diagnostic Laboratory, Michigan State University).

To model maternal dietary iron overload, female WT mice were fed a purified high iron diet containing 2500-5000ppm carbonyl iron (Envigo Teklad TD. 160249 and TD.08043) for 1-3 weeks prior to mating and for the duration of pregnancy. Non-pregnant controls were subjected to the same iron treatment and were age-matched to pregnant dams.

For maternal obesity studies, female WT and hepcidin KO mice were fed a Western diet containing 100-ppm ferric citrate (Envigo Teklad TD.180722) starting at 3 weeks of age. After 8 weeks, WT mice were fed a Western diet supplemented with 3700-ppm carbonyl iron (Envigo Teklad TD.180723) for one week prior to mating and throughout pregnancy. Dietary iron loaded dams were compared to WT mice (iron adequate, fed standard diet) and hepcidin knockout dams (genetic iron overload) maintained on Western diet. The Western diet contains 0.2% total cholesterol, saturated fat >60% of total fat (42% calories from fat), and high sucrose (43% calories from carbohydrate), and 15% calories from protein.

Maternal Systemic Inflammation Model. For second trimester inflammation, pregnant mice on E8.5 were weighed and received a single subcutaneous injection of 0.5 µg/g LPS (Escherichia coli serotype O55:B5, Sigma-Aldrich L2880) or equivalent volume of sterile solvent as a control. Mice were weighed daily after injection, and mice that lost pregnancy weight gain were euthanized from E11.5-E18.5 to confirm embryo loss (miscarriage or resorption of embryos).

For third trimester inflammation, pregnant mice on E15.5 received a single subcutaneous injection of LPS, 100 µg pam3csk4 (InvivoGen tlrl-pms), 30 µg flagellin (Bacillus subtilis, InvivoGen tlrl-bsfla), or single intravenous injection of 10 µg/g polyinosinic:polycytidylic acid (high molecular weight, InvivoGen tlrl-pic) or 10 µg/g lipotechoic acid (Staph aureus, InvivoGen tlrl-pslta). Preterm birth was recorded as the delivery of at least one pup within 24h of injection. At the indicated times, mice were euthanized by isoflurane overdose and tissues collected for analysis.

For TNFα neutralizing experiments, pregnant E14.5 hepcidin KO dams received a single intravenous injection via the retroorbital sinus of 500 µg rat antibody targeting mouse TNFα (BioXCell) or rat IgG1 isotype control antibody targeting trinitrophenol (BioXCell) prior to LPS injection on E15.5 for 24 h. Pregnant hepcidin knockout dams fed a Western diet received intravenous injections of 250 µg of anti-TNFα or anti-TNP on E5.5, E8.5.5, E12.5, and E15.5, and mice were euthanized on E18.5.

For antioxidant experiments, pregnant hepcidin KO dams received subcutaneous injections of 100 µg/g (±)-α-Tocopherol phosphate disodium salt (Sigma T2020) 14 and 2 h prior to LPS injection on E15.5 for 24 h.

Cytokine and Chemokine Analysis. Cytokine and chemokine analyses were performed by the UCLA Integrated Molecular Technologies Core using a multiplex bead immunoassay (Millipore Milliplex Cytokine/Chemokine 32-plex Kit on Luminex FlexMap3D). Levels of mouse cytokines interleukin (IL)-1α, IL-1β, IL-2, IL-3, IL-4, IL-5, IL-6, IL-7, IL-9, IL-10, IL-12 (p40), IL-12 (p70), IL-13, IL-15, IL-17, leukemia inhibitory factor (LIF), interferon (IFN)-γ, and tumor necrosis factor (TNF)-α; chemokines interferon inducible protein (IP)-10, keratinocyte derived chemokine (KC), LPS-induced CXC chemokine (LIX), monocyte chemotactic protein (MCP)-1, and Eotaxin/CCL11; colony stimulating factors (CSF) macrophage (M)-CSF, monocyte induced by gamma-interferon (MIG), macrophage inflammatory protein (MIP)-1α, MIP-1β, MIP-2, regulated on activation normal T cells expressed and secreted (RANTES), granulocyte (G), granulocyte macrophage (GM)-CSF, and vascular endothelial growth factor (VEGF), were quantified in maternal serum 6 and 24h after E15.5 LPS injection. For embryo serum, a separate cohort of dams were treated on E17.5 for 6h and embryo serum from each litter was pooled to generate sufficient volume for analysis. For Western diet mouse experiments, cytokines in maternal serum collected on E18.5 were determined by the multiplex ELISA, and TNFα in pooled embryo serum and amniotic fluid was determined by a separate ELISA (Biolegend 430901) following the manufacturer's instructions.

Histopathology and Immunohistochemistry. Placentas and whole embryos were fixed in 10% neutral buffered formalin for 48 h at room temperature, rinsed once in distilled water and stored in 70% ethanol until processing. The tissues were paraffin-embedded and sectioned at 4 μm thickness by the UCLA Translational Pathology Core Laboratory. Prior to staining, sections were heated for

45 min at 50°C and deparaffinized through serial changes of xylenes and ethanol and rehydrated to distilled water.

For TUNEL staining, tissue sections were processed using ApopTag Plus Peroxidase in situ Apoptosis Detection Kit (EMD Millipore #S7101) following the manufacturer's instructions.

For immunohistochemistry, antigen retrieval was performed by boiling in Tris-EDTA (10 mM Tris base 1 mM disodium EDTA dihydrate, pH 9.0) for 10 min. Sections were quenched with BLOXALL (Vector Laboratories SP-6000) for 10 min and washed with TBS containing 0.1% Tween-20. Blocking was performed using 2.5% normal horse serum in PBS. Sections were incubated with primary antibodies in blocking buffer at 4°C overnight in a humidified chamber. Negative control sections were incubated with normal IgG from the same species and at the same concentrations as primary antibodies. The secondary reaction was performed using ImmPRESS IgG (Vector Laboratories) conjugated to horseradish peroxidase (HRP) or alkaline peroxidase (AP). HRP and AP were developed using DAB and vector red per the manufacturer's instructions (Vector Laboratories). Sections were counterstained with Gill's hematoxylin. Light microscopy images were captured by a digital camera (Spot Imaging).

Cell Culture. Primary human umbilical vein endothelial cells (HUVECs) pooled from 10 donors were obtained from ATCC (ATCC PCS-100-013) and cultured in complete endothelial cell growth medium (Cell Applications #211-500) at 37°C in a 5% CO2 95% air atmosphere. For experiments, HUVECs were seeded at 1 x 10^5/well on collagen-coated plates (Corning BioCoat). All experiments were performed from passages 3 to 5.

For iron loading experiments, HUVECs were plated in in regular media or media supplemented with 100μM ferric ammonium citrate (FAC) (MP biomedicals #158040), or cupric

chloride (Sigma #C-6917), or zinc sulfate (Fisher #Z-58) for 24h. For iron depletion studies, HUVECs were treated with 100μM FAC with and without 100μM deferoxamine (Sigma D9533) for 24h. The optimal time of culture was based on preliminary concentration and time-dependence studies.

For inflammation studies, HUVECs were treated with solvent, 2mg/ml LPS O55:B5, or 50ng/mL recombinant human IL-6 (R&D Systems #206-IL), IFN-γ (PeproTech #300-02), IL-1α (PeproTech #200-01A), IL-1β (PeproTech #200-01B), or TNFα (Biolegend #570102) for 16h. The optimal time of culture with cytokines was based on preliminary concentration and time-dependence studies.

For TNFα neutralizing experiments, HUVECs were treated with 100μM FAC and 1μg human TNFα neutralizing antibody for 24h and stimulated with 50ng/ml IL-1α, IL-1β, or TNFα for 16h.

RNA-Sequencing. RNA-Sequencing was performed by the UCLA Technology Center for Genomics & Bioinformatics on endothelial cells isolated from mouse placentas. Briefly, 5 placentas/dam were pooled, and endothelial cells were isolated by magnetic separation using the MidiMACS system following the manufacturer's instructions (Miltenyi #130-095-927, #130-097-418). Total RNA was extracted using a RNeasy Micro kit (Qiagen) following the manufacturer's instructions. Expression data were analyzed by comparing cells from the following groups of mice: iron adequate (WT) and iron loaded (HKO) pregnant mice injected on E15.5 with solvent or 0.5μg/g LPS for 6h (N=4 dams/group). Libraries for RNA-Seq were prepared with Nugen Universal plus mRNA-Seq Kit to generate strand-specific RNA-seq libraries. Data were sequenced on Illumina HiSeq 3000 for a single-read 50bp run, and depth of coverage was 2 lanes for >30

million reads/sample. Partek flow and Ingenuity Pathway Analysis (IPA) were used for bioinformatics methods and data analysis, respectively. The reads were mapped to the latest UCSC transcript set using STAR - 2.6.1d. The Partek E/M was used to quantify reads to an annotation model. After obtaining gene counts, the counts were normalized by TPM. The Principal Component Analysis was applied to the transcript counts. The differential gene expressions were examined using DESeq2 algorithm. Canonical pathway analysis was performed by IPA using significantly differentially expressed genes (genes filtered by $P<0.05$).

Non-heme Iron Measurements. Serum was obtained from maternal and embryo blood by centrifugation at 2,700 x g for 10 min. Serum iron concentration was measured by colorimetric spectrophotometry using an iron calibrator (Iron-SL, Sekisui Diagnostics 157-30) (Fisher et al., 2020), excluding hemolyzed samples. For maternal liver iron measurements, 75 µL of whole liver homogenate was weighed and incubated in 1125 µL protein precipitation solution (0.53 N HCl 5.3% tricholoracetic acid) at 100°C for 1 h. For embryo tissue iron measurements, half of each placenta and liver were weighed and homogenized in 1200 µL protein precipitation solution prior to boiling. Samples were centrifuged at 17,000 x g for 10 min and supernatant was analyzed by colorimetric spectrophotometry using an iron standard (1,000-ppm iron in 3% HCl, Ricca Chemical Company).

Serum Endotoxin Assay. Endotoxin in maternal and embryo serum was determined by a limulus amebocyte assay kit following the manufacturer's instructions (BioWhittaker #50-648U).

Serum Progesterone Assay. Progesterone in maternal serum was measured by ELISA according to the manufacturer's instructions (Cayman Chemicals #582601).

Lipid Peroxidation Assay. Lipid peroxidation was quantified in serum and embryonic tissues by colorimetric spectrophotometry using the Thiobarbituric Acid Reactive Substances (TCA Method) Assay Kit (Cayman Chemicals #700870) following the manufacturer's instructions.

Western Blot Analysis. Placenta pieces from pregnant mice treated with LPS or solvent on E15.5 were homogenized in RIPA lysis buffer with freshly added protease inhibitor cocktail (Santa Cruz #24948). For cell culture experiments, HUVECs were lysed in RIPA buffer by mechanical disruption. Tissue and cell lysates were centrifuged at 17,000 x g for 15 min at 4°C and protein concentration was measured by the bicinchoninic acid assay using bovine serum albumin as a standard. Proteins from placentas (30 μg/lane) and HUVECs (20 μg/lane) were separated by SDS-PAGE and transferred to nitrocellulose membranes. Membranes were blocked for 1 hr in 5% w/v dried nonfat milk or bovine serum albumin in TBS with 0.1% Tween-20 and incubated with primary antibodies in blocking buffer overnight at 4°C The secondary reaction was performed using HRP-conjugated anti-rabbit IgG diluted in blocking buffer. Protein blots were visualized by chemiluminescence using the ChemiDoc XRS+ imaging system and quantified using Image Lab software (Bio-RAD).

Antibodies:

Target protein	Primary antibody
Mouse and human cleaved caspase-3	Rabbit monoclonal antibody 9664, Cell Signaling Technology
Mouse and human total caspase-3	Rabbit monoclonal antibody 9662, Cell Signaling Technology
Mouse and human ferritin heavy chain	Rabbit monoclonal antibody 4393, Cell Signaling Technology
Mouse and human β-actin	Monoclonal antibody-peroxidase A3854, Sigma
Mouse IL-1 beta /IL-1F2	Goat polyclonal antibody AF401, R&D Systems
Mouse cleaved caspase-1	Rabbit monoclonal antibody 89332, Cell Signaling Technology
Human caspase-9	Mouse monoclonal antibody 9508, Cell Signaling Technology
Mouse and human electron transport chain	Total OXPHOS Rodent WB Antibody Cocktail ab110413, Abcam
Mouse CD31/PECAM-1	Goat polyclonal antibody AF3628, Novus Biologicals
Secondary antibodies:	
Anti-mouse IgG HRP antibody 7076, Cell Signaling Technology	
Anti-rabbit IgG HRP antibody 7074, Cell Signaling Technology	
Anti-goat IgG HRP antibody 2354, Santa Cruz	
ImmPRESS horse anti-rabbit IgG HRP detection kit MP-7401, Vector Laboratories	
ImmPRESS horse anti-goat IgG AP detection kit MP-5405, Vector Laboratories	
Neutralizing antibodies:	
Human TNFα neutralizing	Rabbit monoclonal antibody 7321, Cell Signaling Technology
Mouse TNFα neutralizing	Rat monoclonal antibody clone XT3.11, BioXcell
Rat IgG isotype control, anti-trinitrophenol	Rat monoclonal antibody clone TNP6A7, BioXcell

Gene Expression Quantification by RT-PCR. Frozen mouse tissues or cell cultures were homogenized in TRIzol Reagent (Life Technologies) and total RNA was isolated by chloroform extraction. One μg (mouse tissues) or 500 ng (cell cultures) of RNA was reverse transcribed using the iScript cDNA Synthesis Kit (Bio-RAD). Quantitative real-time PCR was performed on cDNA using Sso Advance SYBER Green Supermix (Bio-RAD) on the CFX Real-Time PCR Detection System (Bio-RAD). Samples were measured in duplicate and target genes were normalized to *Rpl4 or Hprt*. Data are expressed as $2^{-\Delta\Delta Ct}$ unless otherwise specified.

Primer sequences:

Gene	Sequence
Mouse *Tnf*	Forward: 5'- AAT GGC CTC CCT CTC ATC AG -3' Reverse: 5'- GCT ACG ACG TGG GCT ACA GG -3'
Mouse *Il6*	Forward: 5'- CTC TGC AAG AGA CTT CCA TCC AGT -3' Reverse: 5'- CGT GGT TGT CAC CAG CAT CA -3'
Mouse *Cxcl9*	Forward: 5'- GCC ATG AAG TCC GCT GTT CT -3' Reverse: 5'- TAG GGT TCC TCG AAC TCC ACA -3'
Mouse *Il1b*	Forward: 5'- AAG GAG AAC CAA GCA ACG ACA AAA -3' Reverse: 5'- TGG GGA ACT CTG CAG ACT CAA ACT -3'
Mouse *Nqo1*	Forward: 5'- CAC GGG GAC ATG AAC GTC AT -3' Reverse: 5'- GGA GTG TGG CCA ATG CTG TA -3'
Mouse *Nlrp3*	Forward: 5'- AAA ATG CCT TGG GAG ACT CA -3' Reverse: 5'- AAG TAA GGC CGG AAT TCA CC -3'
Mouse *Ptgs2*	Forward: 5'- TGA GTA CCG CAA ACG CTT CT -3' Reverse: 5'- CAG CCA TTT CCT TCT CTC CTG T -3'
Mouse *Saa1*	Forward: 5'- AGT CTG GGC TGC TGA GAA AA -3' Reverse: 5'- ATG TCT GTT GGC TTC CTG GT -3'
Mouse *Ccl2*	Forward: 5'- AGG TCC CTG TCA TGC TCC TG -3' Reverse: 5'- TCA TTG GGA TCA TCT TGC TG -3'
Mouse *Cxcl2*	Forward: 5'- GAA GTC ATA GCC ACT CTC AAG G -3' Reverse: 5'- CCT CCT TTC CAG GTC AGT TAG C -3'
Mouse *Cxcl10*	Forward: 5'- CCA CGT GTT GAG ATC ATT GCC -3' Reverse: 5'- TCA CTC CAG TTA AGG AGC CC -3'
Mouse *Cxcl1*	Forward: 5'- AGA CCA TGG CTG GGA TTC AC -3' Reverse: 5'- AGT GTG GCT ATG ACT TCG GT -3'
Mouse *Cd31*	Forward: 5'- CAG GAC CAC GTG TTA GTG TT -3' Reverse: 5'- ACT CCT GAT GGG TTC TGA CT -3'
Mouse *Tfrc*	Forward: 5'- TCA TGA GGG AAA TCA ATG AT -3' Reverse: 5'- GCC CCA GAA GAT ATG TCG GAA -3'
Mouse *Hmox1*	Forward: 5'- CCT CAC AGA TGG CGT CAC TT -3' Reverse: 5'- TCT GCA GGG GCA GTA TCT TG -3'
Mouse *Hprt*	Forward: 5'- CTG GTT AAG CAG TAC AGC CCC AA -3' Reverse: 5'- CAG GAG GTC CTT TTC ACC AGC -3'
Mouse *Rpl4*	Forward: 5'- TGA AAA GCC CAG AAA TCC AA -3' Reverse: 5'- AGT CTT GGC GTA AGG GTT CA -3'
Human *HPRT*	Forward: 5'- GCC CTG GCG TCG TG ATTA GT -3' Reverse: 5'- AGC AAG ACG TTC AGT CCT GTC -3'
Human *NQO1*	Forward: 5'- GCT GGT TTG AGC GAG TGT TC -3' Reverse: 5'- CTG CCT TCT TAC TCC GGA AGG -3'
Human *HMOX1*	Forward: 5'- ACC TTC CCC AAC ATT GCC AG -3' Reverse: 5'- CAA CTC CTC AAA GAG CTG GAT -3'

Statistical Analysis. Statistical analysis was performed using SigmaPlot version 12.5 (Systat Software). Data are presented as box-and-whisker plots or bar graphs. For box plots, the box portion represents the upper 75th and lower 25th percentile, whiskers indicate variability outside the upper 90th and lower tenth percentile, and individual points represent outliers. The solid line denotes the median and the dotted line the mean. For bar graphs, data are presented as mean ± SEM unless otherwise specified. Statistical differences between groups were determined by one-way ANOVA followed by Holm-Sidak for multiple comparisons for normally distributed values, one-way ANOVA on ranks followed by Dunn's method for multiple comparisons of non-normally distributed values, two-tailed student's *t*-test for normally distributed values, Mann-Whitney *U* test for non-normally distributed values, or Chi-square test. Statistical test, number of animals in each group, experimental replicates, and *P*-value are indicated in each figure panel or legend. A *P*-value of <0.05 was considered significant.

REFERENCES

Adams Waldorf, K.M., and McAdams, R.M. (2013). Influence of infection during pregnancy on fetal development. Reproduction *146*, R151-R162.

Aggarwal, B.B., Gupta, S.C., and Kim, J.H. (2012). Historical perspectives on tumor necrosis factor and its superfamily: 25 years later, a golden journey. Blood *119*, 651-665.

Allswede, D.M., Yolken, R.H., Buka, S.L., and Cannon, T.D. (2020). Cytokine concentrations throughout pregnancy and risk for psychosis in adult offspring: a longitudinal case-control study. Lancet Psychiatry.

Aronson, D., Bartha, P., Zinder, O., Kerner, A., Markiewicz, W., Avizohar, O., Brook, G.J., and Levy, Y. (2004). Obesity is the major determinant of elevated C-reactive protein in subjects with the metabolic syndrome. Int J Obes Relat Metab Disord *28*, 674-679.

Atladottir, H.O., Thorsen, P., Ostergaard, L., Schendel, D.E., Lemcke, S., Abdallah, M., and Parner, E.T. (2010). Maternal infection requiring hospitalization during pregnancy and autism spectrum disorders. J Autism Dev Disord *40*, 1423-1430.

Baron, J., Ben-David, G., and Hallak, M. (2008). Changes in non-transferrin-bound iron (NTBI) in pregnant women on iron supplements. European journal of obstetrics, gynecology, and reproductive biology *140*, 281-282.

Berns, M., and Hommes, D.W. (2016). Anti-TNF-alpha therapies for the treatment of Crohn's disease: the past, present and future. Expert Opin Investig Drugs *25*, 129-143.

Breuer, W., Ronson, A., Slotki, I.N., Abramov, A., Hershko, C., and Cabantchik, Z.I. (2000). The assessment of serum nontransferrin-bound iron in chelation therapy and iron supplementation. Blood *95*, 2975-2982.

Breymann, C. (2015). Iron Deficiency Anemia in Pregnancy. Seminars in hematology *52*, 339-

347.

Brown, A.S., Hooton, J., Schaefer, C.A., Zhang, H., Petkova, E., Babulas, V., Perrin, M., Gorman, J.M., and Susser, E.S. (2004). Elevated maternal interleukin-8 levels and risk of schizophrenia in adult offspring. Am J Psychiatry *161*, 889-895.

Buka, S.L., Tsuang, M.T., Torrey, E.F., Klebanoff, M.A., Wagner, R.L., and Yolken, R.H. (2001). Maternal cytokine levels during pregnancy and adult psychosis. Brain Behav Immun *15*, 411-420.

Canetta, S., Sourander, A., Surcel, H.-M., Hinkka-Yli-Salomäki, S., Leiviskä, J., Kellendonk, C., McKeague, I.W., and Brown, A.S. (2014). Elevated maternal C-reactive protein and increased risk of schizophrenia in a national birth cohort. The American journal of psychiatry *171*, 960-968.

Catalano, P.M., and Shankar, K. (2017). Obesity and pregnancy: mechanisms of short term and long term adverse consequences for mother and child. BMJ (Clinical research ed) *356*, j1.

Choi, G.B., Yim, Y.S., Wong, H., Kim, S., Kim, H., Kim, S.V., Hoeffer, C.A., Littman, D.R., and Huh, J.R. (2016). The maternal interleukin-17a pathway in mice promotes autism-like phenotypes in offspring. Science *351*, 933-939.

Devaraj, S., and Jialal, I. (2005). Alpha-tocopherol decreases tumor necrosis factor-alpha mRNA and protein from activated human monocytes by inhibition of 5-lipoxygenase. Free Radic Biol Med *38*, 1212-1220.

Domellof, M. (2010). Benefits and harms of iron supplementation in iron-deficient and iron-sufficient children. Nestle Nutr Workshop Ser Pediatr Program *65*, 153-162; discussion 162-155.

Dretzke, J., Edlin, R., Round, J., Connock, M., Hulme, C., Czeczot, J., Fry-Smith, A., McCabe,

C., and Meads, C. (2011). A systematic review and economic evaluation of the use of tumour necrosis factor-alpha (TNF-alpha) inhibitors, adalimumab and infliximab, for Crohn's disease. Health Technol Assess *15*, 1-244.

Dudley, D.J., Branch, D.W., Edwin, S.S., and Mitchell, M.D. (1996). Induction of preterm birth in mice by RU486. Biology of reproduction *55*, 992-995.

Elmore, S. (2007). Apoptosis: a review of programmed cell death. Toxicol Pathol *35*, 495-516.

Emerit, J., Beaumont, C., and Trivin, F. (2001). Iron metabolism, free radicals, and oxidative injury. Biomed Pharmacother *55*, 333-339.

Esteve-Solé, A., Deyà-Martínez, À., Teixidó, I., Ricart, E., Gompertz, M., Torradeflot, M., de Moner, N., Gonzalez, E.A., Plaza-Martin, A.M., Yagüe, J., *et al.* (2017). Immunological Changes in Blood of Newborns Exposed to Anti-TNF-α during Pregnancy. Frontiers in Immunology *8*.

Fisher, A.L., and Nemeth, E. (2017). Iron homeostasis during pregnancy. Am J Clin Nutr *106*, 1567S-1574S.

Fisher, A.L., Sangkhae, V., Presicce, P., Chougnet, C.A., Jobe, A.H., Kallapur, S.G., Tabbah, S.M., Buhimschi, C.S., Buhimschi, I.A., Ganz, T., *et al.* (2020). Fetal and amniotic fluid iron homeostasis in healthy and complicated murine, macaque, and human pregnancy. JCI Insight.

Fozza, C., Asara, M.A., Vacca, N., Caggiari, S., Monti, A., Zaccheddu, F., Capobianco, G., Dessole, S., Dore, F., and Antonucci, R. (2017). Pregnancy Outcome among Women with Beta-Thalassemia Major in North Sardinia. Acta Haematol *138*, 166-167.

Garay, P.A., Hsiao, E.Y., Patterson, P.H., and McAllister, A.K. (2013). Maternal immune activation causes age- and region-specific changes in brain cytokines in offspring throughout development. Brain Behav Immun *31*, 54-68.

Ginsberg, Y., D'Onofrio, B.M., Rickert, M.E., Class, Q.A., Rosenqvist, M.A., Almqvist, C., Lichtenstein, P., and Larsson, H. (2019). Maternal infection requiring hospitalization during pregnancy and attention-deficit hyperactivity disorder in offspring: a quasi-experimental family-based study. J Child Psychol Psychiatry *60*, 160-168.

Gonzales, G.F., Steenland, K., and Tapia, V. (2009). Maternal hemoglobin level and fetal outcome at low and high altitudes. American journal of physiology Regulatory, integrative and comparative physiology *297*, R1477-1485.

Gücer, F., Balkanli-Kaplan, P., Yüksel, M., Sayin, N.C., Yüce, M.A., and Yardim, T. (2001). Maternal serum levels of tumor necrosis factor-α and interleukin-2 receptor in threatened abortion: a comparison with normal and pathologic pregnancies. Fertility and Sterility *76*, 707-711.

Guo, W., Wang, H., Liu, Q., Yuan, Y., Jing, Y., and Yang, X. (2019). Analysis of the correlation of gestational diabetes mellitus and peripheral ferritin with iron levels in early pregnancy. Minerva Endocrinol *44*, 91-96.

HOU, J., CLIVER, S.P., TAMURA, T., JOHNSTON, K.E., and GOLDENBERG, R. (2000). Maternal Serum Ferritin and Fetal Growth. Obstetrics & Gynecology *95*, 447-452.

Hsiao, E.Y., and Patterson, P.H. (2011). Activation of the Maternal Immune System Induces Endocrine Changes in the Placenta via IL-6. Brain Behav Immun *25*, 604-615.

Huey, K.A., Fiscus, G., Richwine, A.F., Johnson, R.W., and Meador, B.M. (2008). In vivo vitamin E administration attenuates interleukin-6 and interleukin-1beta responses to an acute inflammatory insult in mouse skeletal and cardiac muscle. Exp Physiol *93*, 1263-1272.

Ilievski, V., Lu, S.-J., and Hirsch, E. (2007). Activation of Toll-like Receptors 2 or 3 and Preterm Delivery in the Mouse. Reproductive sciences *14*, 315-320.

Jones, K.L., Croen, L.A., Yoshida, C.K., Heuer, L., Hansen, R., Zerbo, O., DeLorenze, G.N., Kharrazi, M., Yolken, R., Ashwood, P., *et al.* (2017). Autism with intellectual disability is associated with increased levels of maternal cytokines and chemokines during gestation. Mol Psychiatry *22*, 273-279.

Julsgaard, M., Christensen, L.A., Gibson, P.R., Gearry, R.B., Fallingborg, J., Hvas, C.L., Bibby, B.M., Uldbjerg, N., Connell, W.R., Rosella, O., *et al.* (2016). Concentrations of Adalimumab and Infliximab in Mothers and Newborns, and Effects on Infection. Gastroenterology *151*, 110-119.

Kaislasuo, J., Simpson, S., Petersen, J.F., Peng, G., Aldo, P., Lokkegaard, E., Paidas, M., Pal, L., Guller, S., and Mor, G. (2019). IL-10 to TNFalpha ratios throughout early first trimester can discriminate healthy pregnancies from pregnancy losses. Am J Reprod Immunol, e13195.

Kane, S.V., and Acquah, L.A. (2009). Placental transport of immunoglobulins: a clinical review for gastroenterologists who prescribe therapeutic monoclonal antibodies to women during conception and pregnancy. Am J Gastroenterol *104*, 228-233.

Katsuki, A., Sumida, Y., Murashima, S., Murata, K., Takarada, Y., Ito, K., Fujii, M., Tsuchihashi, K., Goto, H., Nakatani, K., *et al.* (1998). Serum Levels of Tumor Necrosis Factor-α Are Increased in Obese Patients with Noninsulin-Dependent Diabetes Mellitus1. The Journal of Clinical Endocrinology & Metabolism *83*, 859-862.

Khambalia, A.Z., Aimone, A., Nagubandi, P., Roberts, C.L., McElduff, A., Morris, J.M., Powell, K.L., Tasevski, V., and Nassar, N. (2016). High maternal iron status, dietary iron intake and iron supplement use in pregnancy and risk of gestational diabetes mellitus: a prospective study and systematic review. Diabetic medicine : a journal of the British Diabetic Association *33*, 1211-1221.

Khambalia, A.Z., Collins, C.E., Roberts, C.L., Morris, J.M., Powell, K.L., Tasevski, V., and Nassar, N. (2015). High maternal serum ferritin in early pregnancy and risk of spontaneous preterm birth. Br J Nutr *114*, 455-461.

Knottnerus, J.A., Delgado, L.R., Knipschild, P.G., Essed, G.G., and Smits, F. (1990). Haematologic parameters and pregnancy outcome. A prospective cohort study in the third trimester. J Clin Epidemiol *43*, 461-466.

Lao, T.T., Chan, P.L., and Tam, K.F. (2001). Gestational diabetes mellitus in the last trimester - a feature of maternal iron excess? Diabetic medicine : a journal of the British Diabetic Association *18*, 218-223.

Lao, T.T., Tam, K.-F., and Chan, L.Y. (2000). Third trimester iron status and pregnancy outcome in non-anaemic women; pregnancy unfavourably affected by maternal iron excess. Human Reproduction *15*, 1843-1848.

Le, C.H.H. (2016). The Prevalence of Anemia and Moderate-Severe Anemia in the US Population (NHANES 2003-2012). PLOS ONE *11*, e0166635.

Lesbordes-Brion, J.C., Viatte, L., Bennoun, M., Lou, D.Q., Ramey, G., Houbron, C., Hamard, G., Kahn, A., and Vaulont, S. (2006). Targeted disruption of the hepcidin 1 gene results in severe hemochromatosis. Blood *108*, 1402-1405.

Li, C.-J., Li, R.W., Kahl, S., and Elsasser, T.H. (2012). Alpha-Tocopherol Alters Transcription Activities that Modulates Tumor Necrosis Factor Alpha (TNF-α) Induced Inflammatory Response in Bovine Cells. Gene Regul Syst Bio *6*, 1-14.

Mahadevan, U., Martin, C.F., Chambers, C., Kane, S.V., Dubinsky, M., Sandborn, W., and Sands, B.E. (2014). 1 Achievement of Developmental Milestones Among Offspring of Women With Inflammatory Bowel Disease: The PIANO Registry. Gastroenterology *146*, S-1.

Mahadevan, U., Wolf, D.C., Dubinsky, M., Cortot, A., Lee, S.D., Siegel, C.A., Ullman, T., Glover, S., Valentine, J.F., Rubin, D.T., *et al.* (2013). Placental transfer of anti-tumor necrosis factor agents in pregnant patients with inflammatory bowel disease. Clin Gastroenterol Hepatol *11*, 286-292; quiz e224.

Mamun, A.A., Padmadas, S.S., and Khatun, M. (2006). Maternal health during pregnancy and perinatal mortality in Bangladesh: evidence from a large-scale community-based clinical trial. Paediatr Perinat Epidemiol *20*, 482-490.

Racicot, K., and Mor, G. (2017). Risks associated with viral infections during pregnancy. The Journal of Clinical Investigation *127*, 1591-1599.

Rawal, S., Hinkle, S.N., Bao, W., Zhu, Y., Grewal, J., Albert, P.S., Weir, N.L., Tsai, M.Y., and Zhang, C. (2017). A longitudinal study of iron status during pregnancy and the risk of gestational diabetes: findings from a prospective, multiracial cohort. Diabetologia *60*, 249-257.

Roytblat, L., Rachinsky, M., Fisher, A., Greemberg, L., Shapira, Y., Douvdevani, A., and Gelman, S. (2000). Raised interleukin-6 levels in obese patients. Obes Res *8*, 673-675.

Rumbold, A., Ota, E., Hori, H., Miyazaki, C., and Crowther, C.A. (2015). Vitamin E supplementation in pregnancy. Cochrane Database of Systematic Reviews.

Sanchez, C.E., Barry, C., Sabhlok, A., Russell, K., Majors, A., Kollins, S.H., and Fuemmeler, B.F. (2018). Maternal pre-pregnancy obesity and child neurodevelopmental outcomes: a meta-analysis. Obes Rev *19*, 464-484.

Sangkhae, V., Fisher, A.L., Wong, S., Koenig, M.D., Tussing-Humphreys, L., Chu, A., Lelic, M., Ganz, T., and Nemeth, E. (2020). Effects of maternal iron status on placental and fetal iron homeostasis. J Clin Invest *130*, 625-640.

Scanlon, K.S., Yip, R., Schieve, L.A., and Cogswell, M.E. (2000). High and low hemoglobin levels during pregnancy: differential risks for preterm birth and small for gestational age. Obstet Gynecol *96*, 741-748.

Scholl, T.O. (2005). Iron status during pregnancy: setting the stage for mother and infant. Am J Clin Nutr *81*, 1218S-1222S.

Scholl, T.O., and Reilly, T. (2000). Anemia, iron and pregnancy outcome. J Nutr *130*, 443S-447S.

Siu, A.L., and Force, o.b.o.t.U.S.P.S.T. (2015). Screening for Iron Deficiency Anemia and Iron Supplementation in Pregnant Women to Improve Maternal Health and Birth Outcomes: U.S. Preventive Services Task Force Recommendation Statement. Annals of Internal Medicine *163*, 529-536.

Stephansson, O., Dickman, P.W., Johansson, A., and Cnattingius, S. (2000). Maternal hemoglobin concentration during pregnancy and risk of stillbirth. JAMA *284*, 2611-2617.

Tuck, S.M., Jensen, C.E., Wonke, B., and Yardumian, A. (1998). Pregnancy management and outcomes in women with thalassaemia major. J Pediatr Endocrinol Metab *11 Suppl 3*, 923-928.

Tzanavari, T., Giannogonas, P., and Karalis, K.P. (2010). TNF-alpha and obesity. Curr Dir Autoimmun *11*, 145-156.

Uemura, M., Manabe, H., Yoshida, N., Fujita, N., Ochiai, J., Matsumoto, N., Takagi, T., Naito, Y., and Yoshikawa, T. (2002). Alpha-tocopherol prevents apoptosis of vascular endothelial cells via a mechanism exceeding that of mere antioxidation. Eur J Pharmacol *456*, 29-37.

WHO (2001). Iron Deficiency Anaemia: Assesment, Prevention and Control: a Guide for Programme Managers (World Health Organization).

WHO (2016). WHO Recommendations on Antenatal Care for a Positive Pregnancy Experience (Geneva: World Health Organization).

Wu, D., Jiang, Z., Gong, B., Dou, Y., Song, M., Song, X., and Tian, Y. (2017a). Vitamin E Reversed Apoptosis of Cardiomyocytes Induced by Exposure to High Dose Formaldehyde During Mice Pregnancy. Int Heart J *58*, 769-777.

Wu, D., Luo, X.L., Lin, Y., Fang, Z.F., Luo, X.R., Xu, H.T., and Zeng, W. (2010). Effects of vitamin E on reproductive protection in pregnant mice infected with pseudorabies virus (PRV) via regulating expression of Toll-like receptors (TLRs) and cytokine balance. J Nutr Sci Vitaminol (Tokyo) *56*, 353-363.

Wu, W.-L., Hsiao, E.Y., Yan, Z., Mazmanian, S.K., and Patterson, P.H. (2017b). The placental interleukin-6 signaling controls fetal brain development and behavior. Brain, behavior, and immunity *62*, 11-23.

Xiao, R., Sorensen, T.K., Frederick, I.O., El-Bastawissi, A., King, I.B., Leisenring, W.M., and Williams, M.A. (2002). Maternal second-trimester serum ferritin concentrations and subsequent risk of preterm delivery. Paediatr Perinat Epidemiol *16*, 297-304.

SUPPLEMENTAL MATERIALS

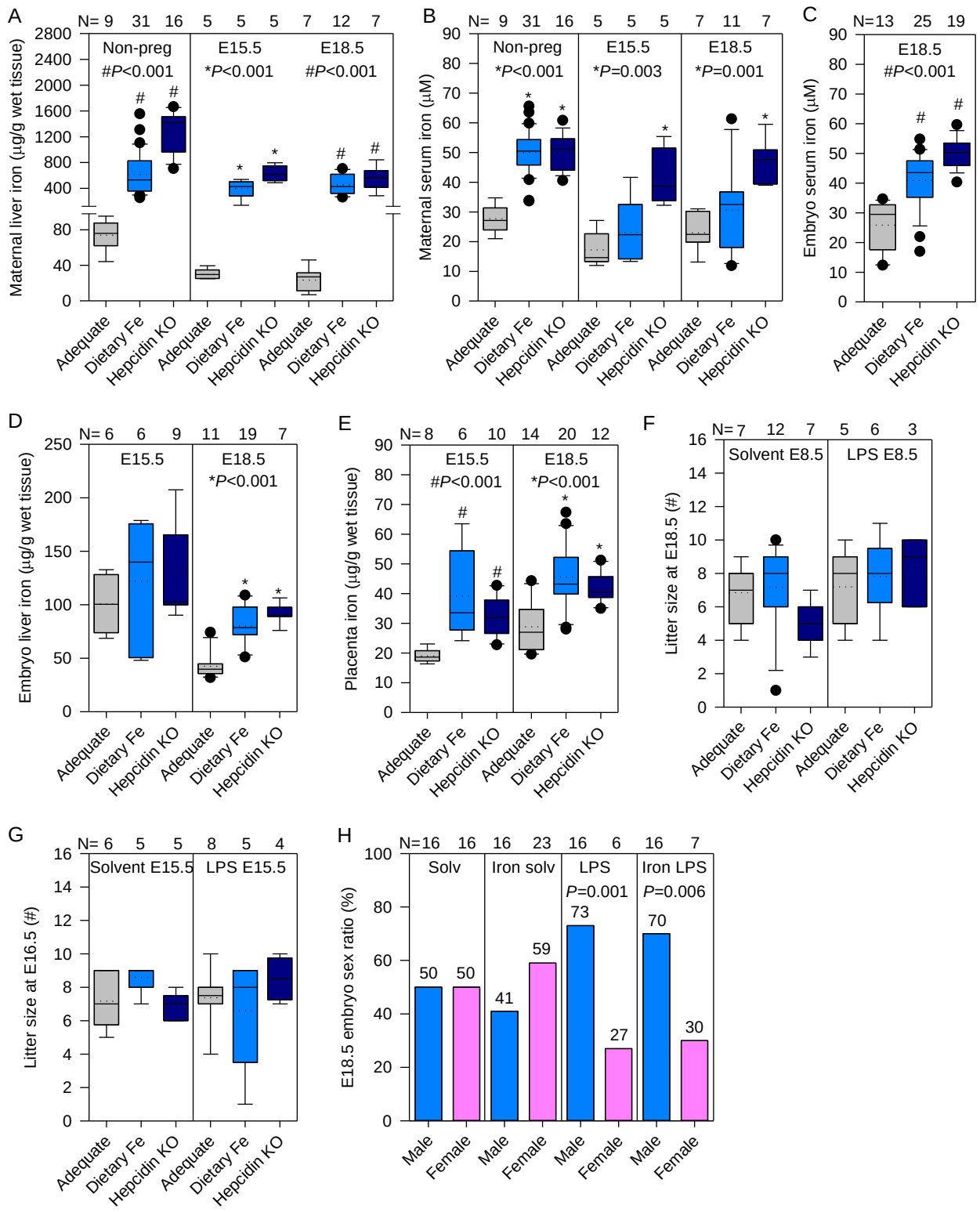

Supplemental Figure 4-1. Maternal, placental, and embryo iron status in dietary and genetic iron overload during pregnancy. Iron-adequate mice were maintained on standard chow (185ppm iron). Dietary iron-loaded dams were fed a high iron diet (2,500-5,000ppm iron) for 1-3 weeks prior to mating and during pregnancy. Genetic iron-loading model were hepcidin-1 KO dams fed standard chow. Non-pregnant females received the same iron treatment and were age-matched to pregnant dams. Pregnant iron-loaded dams were analyzed at E15.5 and E18.5 and compared to iron-adequate controls. **(A-B)** Maternal non-heme iron measurements in liver and serum. **(C-D)** Embryo non-heme iron measurements in serum and liver. Embryo serum was not analyzed at E15.5 due to insufficient volume for analysis. **(E)** Placenta non-heme iron concentrations. **(F-G)** Litter size from iron-adequate and iron-loaded dams treated with a single subcutaneous dose of 0.5µg/g LPS on E8.5 or E15.5 and analyzed at the indicated time points. **(H)** E18.5 embryo sex ratio from iron adequate and iron loaded dams treated with solvent or LPS on E8.5. Statistical differences between groups were determined by one-way ANOVA for normally distributed values followed by Holm-Sidak method for multiple comparisons versus iron-adequate group (denoted by *) or one-way ANOVA on ranks followed by Dunn's method for multiple comparisons versus iron-adequate group (denoted by #), or chi-squared test. *P* values and animal numbers are indicated in each panel.

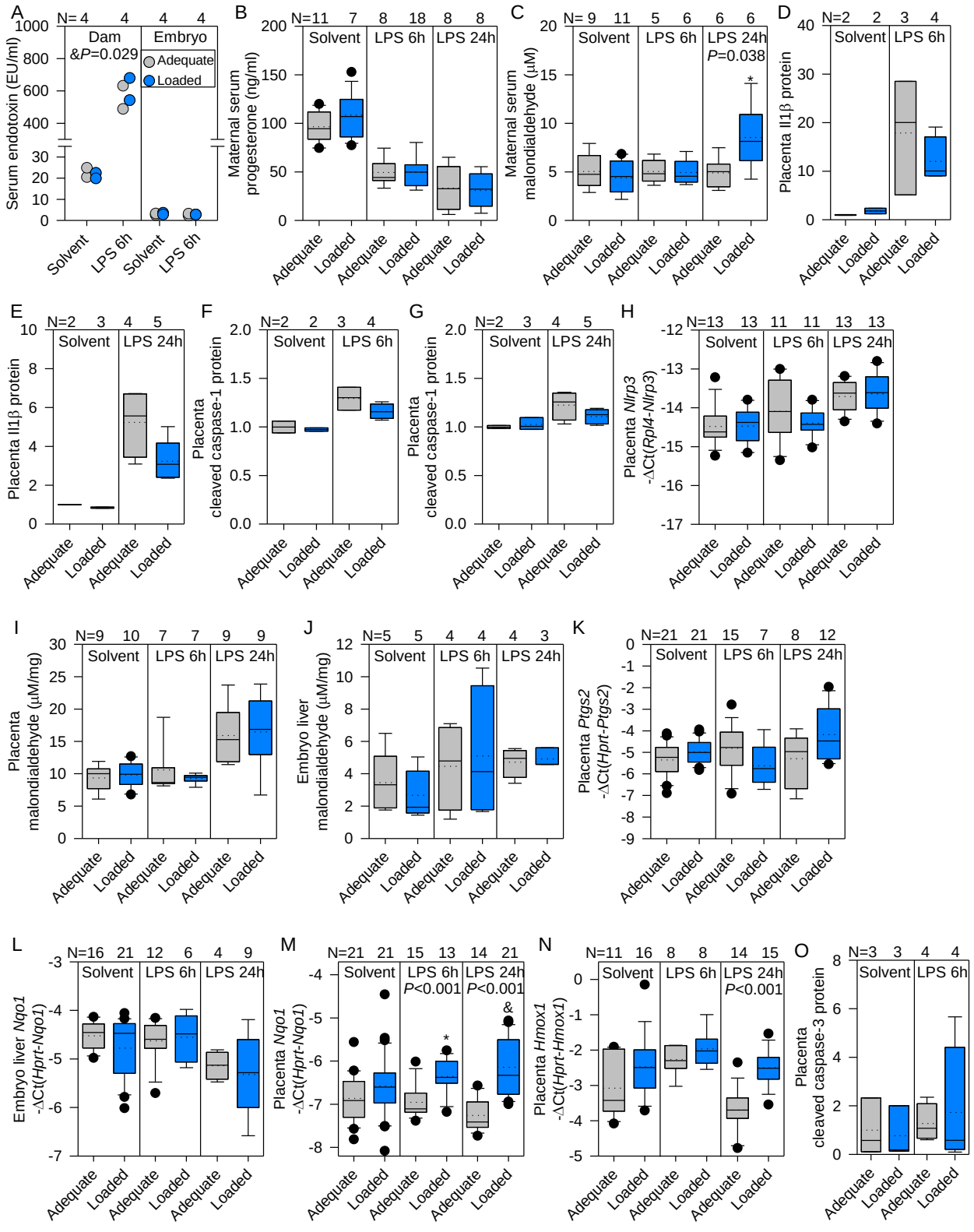
A
N= 4 4 4 4
Dam
Embryo
&P=0.029
Adequate
Loaded
Serum endotoxin (EU/ml)
Solvent
LPS 6h
B
N=11 7 8 18 8 8
Solvent
LPS 6h
LPS 24h
Maternal serum progesterone (ng/ml)
C
N= 9 11 5 6 6 6
Maternal serum malondialdehyde (µM)
P=0.038
D
N=2 2 3 4
Placenta Il1β protein
E
N=2 3 4 5
F
N=2 2 3 4
Placenta cleaved caspase-1 protein
G
N=2 3 4 5
H
N=13 13 11 11 13 13
Placenta Nlrp3 -ΔCt(Rpl4-Nlrp3)
I
N=9 10 7 7 9 9
Placenta malondialdehyde (µM/mg)
J
N=5 5 4 4 4 3
Embryo liver malondialdehyde (µM/mg)
K
N=21 21 15 7 8 12
Placenta Ptgs2 -ΔCt(Hprt-Ptgs2)
L
N=16 21 12 6 4 9
Embryo liver Nqo1 -ΔCt(Hprt-Nqo1)
M
N=21 21 15 13 14 21
P<0.001
Placenta Nqo1 -ΔCt(Hprt-Nqo1)
N
N=11 16 8 8 14 15
Placenta Hmox1 -ΔCt(Hprt-Hmox1)
O
N=3 3 4 4
Placenta cleaved caspase-3 protein
Adequate
Loaded

Supplemental Figure 4-2. Comparison of cell death pathways induced by LPS in placentas and embryos from iron-adequate and iron-loaded pregnancies. (A) Endotoxin in maternal serum and in pooled embryo serum after maternal subcutaneous LPS injection (0.5µg/g) on E17.5 for 6h. **(B-N)** Iron-adequate and iron-loaded dams were treated with subcutaneous LPS (0.5µg/g) on E15.5 for 6 and 24h. **(B)** Maternal serum progesterone and **(C)** serum malondialdehyde. **(D-G)** Quantification of IL-1β and cleaved caspase-1 by Western blot in whole placenta lysates. **(H)** Placental *Nlrp3* mRNA expression. **(I-J)** Malondialdehyde measurements in placenta and embryo livers. **(K)** Placental *Ptgs2* mRNA expression. **(L-M)** Embryo liver and placenta mRNA expression. **(N)** Placenta *Hmox1* mRNA expression. **(O)** Quantification of cleaved caspase-3 by Western blot in whole placenta lysates. Statistical differences between groups were determined by Student's *t*-test for normally distributed values (denoted by *) or Mann-Whitney *U* for non-normally distributed values (denoted by &). *P* values and animal numbers are indicated in each panel.

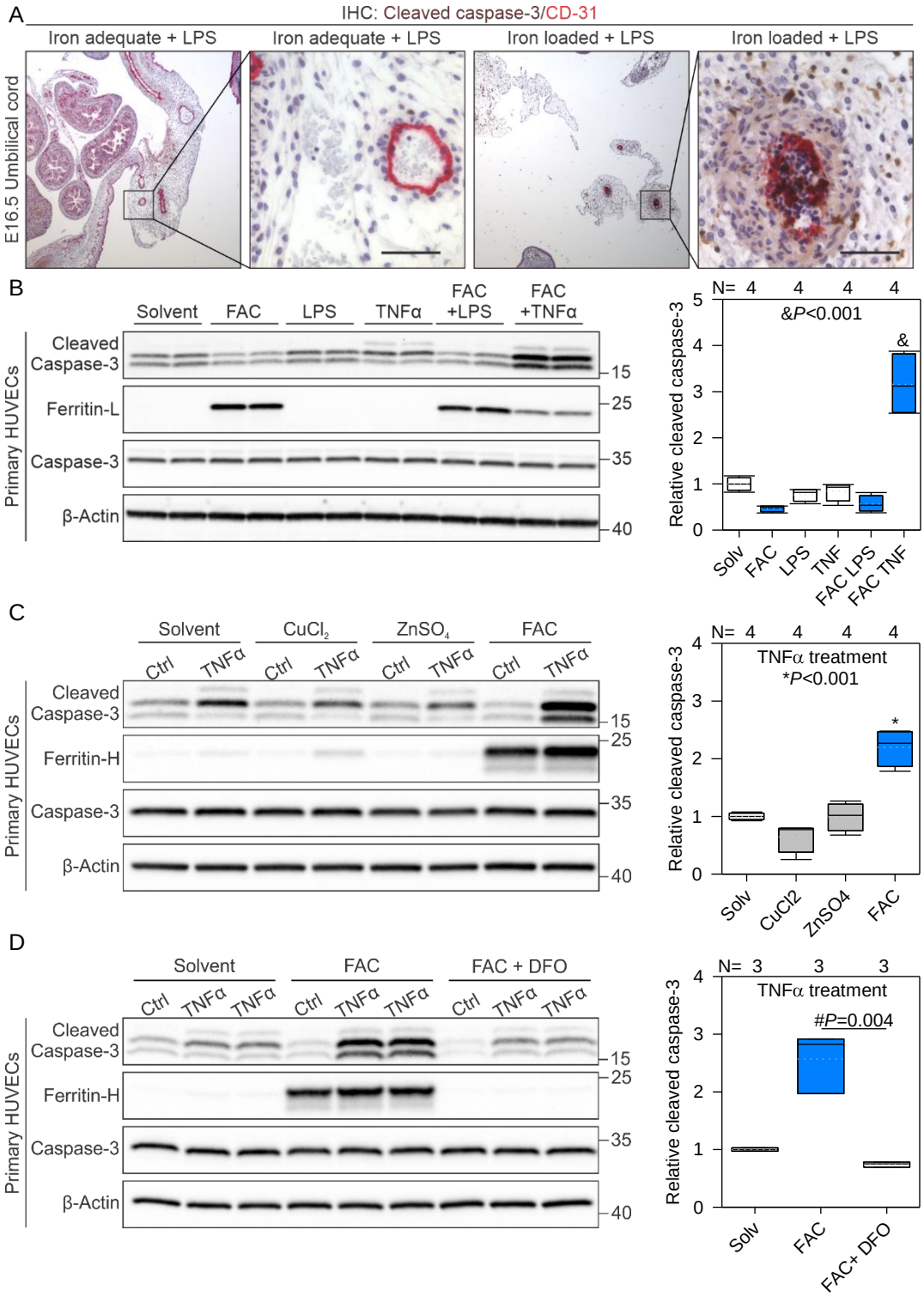
A
IHC: Cleaved caspase-3/CD-31
Iron adequate + LPS
Iron adequate + LPS
Iron loaded + LPS
Iron loaded + LPS
E16.5 Umbilical cord
B
Solvent
FAC
LPS
TNFα
FAC +LPS
FAC +TNFα
Primary HUVECs
Cleaved Caspase-3
Ferritin-L
Caspase-3
β-Actin
15
25
35
40
N= 4 4 4 4
&P<0.001
&
Relative cleaved caspase-3
Solv
FAC
LPS
TNF
FAC LPS
FAC TNF
C
Solvent
CuCl2
ZnSO4
FAC
Ctrl
TNFα
Primary HUVECs
Cleaved Caspase-3
Ferritin-H
Caspase-3
β-Actin
15
25
35
40
N= 4 4 4 4
TNFα treatment
*P<0.001
*
Relative cleaved caspase-3
Solv
CuCl2
ZnSO4
FAC
D
Solvent
FAC
FAC + DFO
Ctrl
TNFα
TNFα
Primary HUVECs
Cleaved Caspase-3
Ferritin-H
Caspase-3
β-Actin
15
25
35
40
N= 3 3 3
TNFα treatment
#P=0.004
Relative cleaved caspase-3
Solv
FAC
FAC+ DFO

Supplemental Figure 4-3. Potentiation of TNFα-induced apoptosis is specific to iron. (A) Immunohistochemistry of paraffin-embedded mouse umbilical cords for cleaved caspase-3 (brown) and CD31 (red) after iron-adequate and iron-loaded dams were treated with LPS on E15.5 for 24h. Scale bar= 50μM. **(B)** HUVECs were treated with solvent or 100μM ferric ammonium citrate (FAC) for 24h and simulated with 2mg/ml LPS or 50ng/ml TNFα for 16h. Western blot (left) and quantitation (right) of cleaved caspase-3 normalized to β-Actin (N=4 independent experiments). **(C)** HUVECs were treated with solvent, 100μM FAC, 100μM copper chloride ($CuCl_2$), or 100μM zinc sulfate ($ZnSO_4$) and stimulated with 50ng/ml TNFα for 16h. Western blot for cleaved caspase-3 (left) and quantitation of N=4 independent experiments (right). β-Actin was used as a loading control. **(D)** HUVECs were treated with 100μM FAC with and without 100μM iron chelator deferoxamine for 24h prior to stimulation with 50ng/ml TNFα for 16h. Western blot for cleaved caspase-3 (left) and quantitation of N=3 independent experiments (right). β-Actin was used as a loading control. Statistical differences between groups was determined by two-way ANOVA with Holm-Sidak method for multiple comparisons (denoted by &), one-way ANOVA for normally distributed values with Holm-Sidak method for multiple comparisons versus solvent group (denoted by *), or one-way ANOVA on ranks with Tukey's method of multiple comparison (denoted by #). *P* values and experimental replicates are indicated in each panel.

A

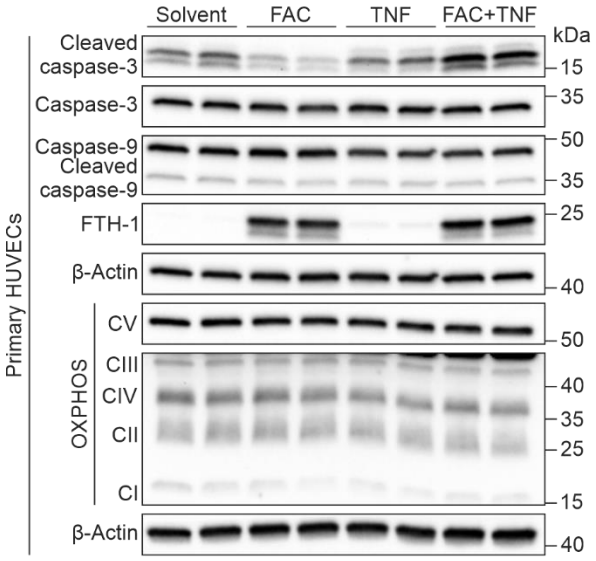
Solvent
FAC
TNF
FAC+TNF
kDa
Primary HUVECs
Cleaved caspase-3
15
Caspase-3
35
Caspase-9
Cleaved caspase-9
50
35
FTH-1
25
β-Actin
40
OXPHOS
CV
50
CIII
CIV
40
35
CII
25
CI
15
β-Actin
40

B

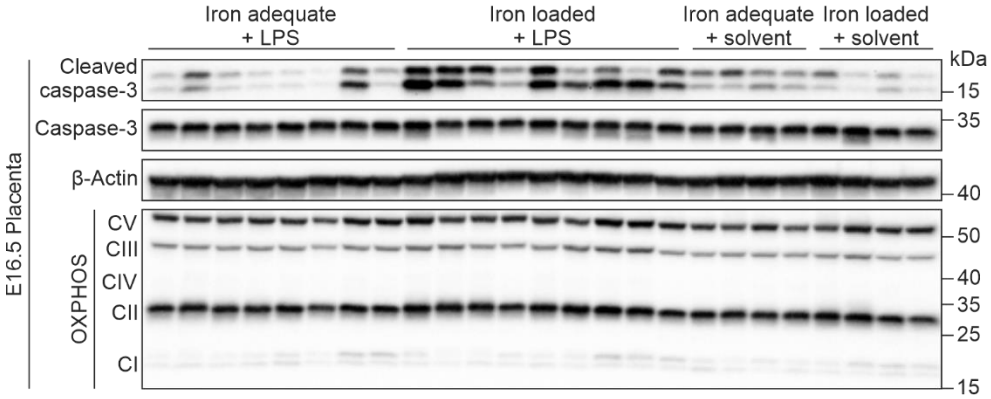
Iron adequate + LPS
Iron loaded + LPS
Iron adequate + solvent
Iron loaded + solvent
kDa
E16.5 Placenta
Cleaved caspase-3
15
Caspase-3
35
β-Actin
40
OXPHOS
CV
50
CIII
CIV
40
35
CII
25
CI
15

Supplemental Figure 4-4. Comparison of the intrinsic and extrinsic pathways in iron-potentiated apoptosis. (A) Primary HUVECs were treated with solvent or 100μM FAC for 24h prior to stimulation with 50ng/ml of TNFα for 16h. Western blot for cleaved caspase-3, -9, and mitochondrial complexes CI-CV (OXPHOS). Ferritin heavy chain (FTH1) is a marker of cellular iron loading. Representative image of N=3 independent experiments. **(B)** Iron-adequate and iron-loaded dams were treated with LPS on E15.5 for 24h (N=4-8 placentas/group). Western blot for cleaved caspase-3 and mitochondrial OXPHOS complexes CI-CV. β-Actin was used as a loading control.

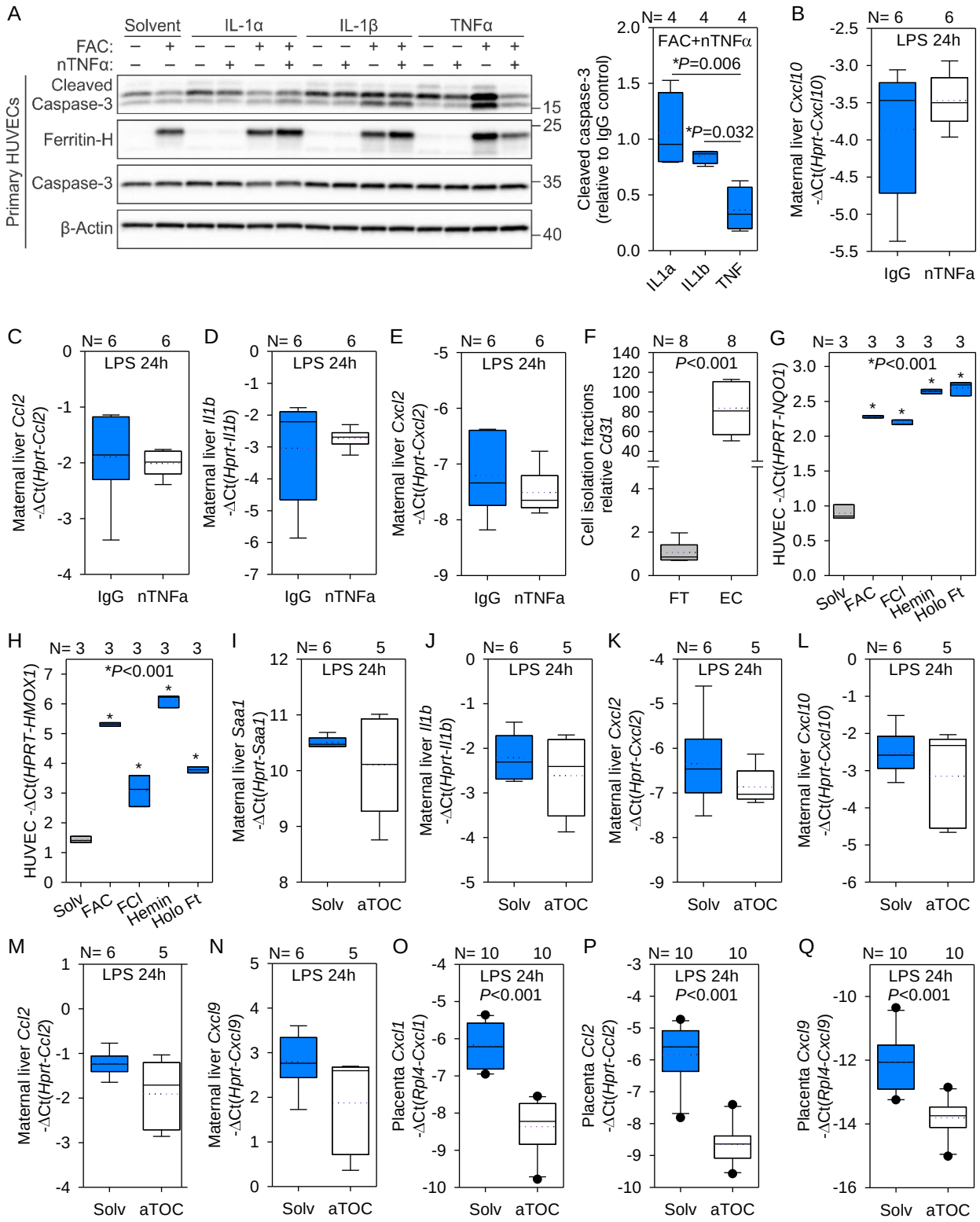
A
Solvent
IL-1α
IL-1β
TNFα
FAC:
nTNFα:
Primary HUVECs
Cleaved Caspase-3
Ferritin-H
Caspase-3
β-Actin
15
25
35
40
Cleaved caspase-3 (relative to IgG control)
N= 4 4 4
FAC+nTNFα
*P=0.006
*P=0.032
IL1a
IL1b
TNF
B
N= 6 6
LPS 24h
Maternal liver Cxcl10 -ΔCt(Hprt-Cxcl10)
IgG nTNFa
C
N= 6 6
LPS 24h
Maternal liver Ccl2 -ΔCt(Hprt-Ccl2)
IgG nTNFa
D
N= 6 6
LPS 24h
Maternal liver Il1b -ΔCt(Hprt-Il1b)
IgG nTNFa
E
N= 6 6
LPS 24h
Maternal liver Cxcl2 -ΔCt(Hprt-Cxcl2)
IgG nTNFa
F
N= 8 8
P<0.001
Cell isolation fractions relative Cd31
FT EC
G
N= 3 3 3 3 3
*P<0.001
HUVEC -ΔCt(HPRT-NQO1)
Solv FAC FCl Hemin Holo Ft
H
N= 3 3 3 3 3
*P<0.001
HUVEC -ΔCt(HPRT-HMOX1)
Solv FAC FCl Hemin Holo Ft
I
N= 6 5
LPS 24h
Maternal liver Saa1 -ΔCt(Hprt-Saa1)
Solv aTOC
J
N= 6 5
LPS 24h
Maternal liver Il1b -ΔCt(Hprt-Il1b)
Solv aTOC
K
N= 6 5
LPS 24h
Maternal liver Cxcl2 -ΔCt(Hprt-Cxcl2)
Solv aTOC
L
N= 6 5
LPS 24h
Maternal liver Cxcl10 -ΔCt(Hprt-Cxcl10)
Solv aTOC
M
N= 6 5
LPS 24h
Maternal liver Ccl2 -ΔCt(Hprt-Ccl2)
Solv aTOC
N
N= 6 5
LPS 24h
Maternal liver Cxcl9 -ΔCt(Hprt-Cxcl9)
Solv aTOC
O
N= 10 10
LPS 24h
P<0.001
Placenta Cxcl1 -ΔCt(Rpl4-Cxcl1)
Solv aTOC
P
N= 10 10
LPS 24h
P<0.001
Placenta Ccl2 -ΔCt(Hprt-Ccl2)
Solv aTOC
Q
N= 10 10
LPS 24h
P<0.001
Placenta Cxcl9 -ΔCt(Rpl4-Cxcl9)
Solv aTOC

Supplemental Figure 4-5. Maternal pretreatment with neutralizing TNFα antibody or αTocopherol does not attenuate LPS-induced maternal inflammation. (A) The specificity of TNFα neutralizing antibody was tested in control and 100μM ferric ammonium citrate (FAC)-loaded HUVECs treated with 50ng/ml of IL-1α, IL-1β, or TNFα with and without 1μg neutralizing TNFα antibody (nTNFα). Western blot for cleaved caspase-3 (left) and quantitation of n=4 independent experiments. β-Actin was used as a loading control. **(B-E)** Hepcidin KO dams were treated intravenously via the retroorbital sinus with 500μg TNFα neutralizing antibody (nTNF) or isotype control IgG antibody targeting trinitrophenol on E14.5, 15h prior to subcutaneous LPS injection (0.5μg/g) on E15.5 for 24h. Inflammatory genes were measured by qRT-PCR in maternal liver: **(B)** *Cxcl10*, **(C)** *Ccl2*, **(D)** *Il1b*, and **(E)** *Cxcl2*. **(F)** Placentas from solvent and LPS-treated mice were collected for endothelial cell isolation by magnetic separation using CD31 beads. *Cd31* mRNA relative to *Rpl4* in the CD31 fraction (endothelial cells, EC) and flow through (FT, non-endothelial cells). **(G-H)** *NQO1* and *HMOX1* expression in primary HUVECs treated with FAC (100μM), ferric chloride (FCl, 100μM), hemin (20μM) or holo-ferritin (FT, 2mg/ml) for 40h. **(I-Q)** Hepcidin KO dams were treated with subcutaneous αTocopherol (vitamin E, 100ug/g) 14 and 2h prior to LPS injection on E15.5 for 24h. Inflammatory genes in maternal liver: **(I)** *Saa1*, **(J)** *Il1b*, **(K)** *Cxcl2*, **(L)** *Cxcl10*, **(M)** *Ccl2*, **(N)** *Cxcl9*; **(O-Q)** placental mRNA expression of *Cxcl1*, *Cxcl10*, and *Cxcl1*. Differences between groups was determined by one-way ANOVA for normally distributed values followed by Holm-Sidak method for multiple comparisons versus control group (denoted by *) or Student's *t*-test. *P* values, experimental replicates, and animal numbers are indicated in each panel.

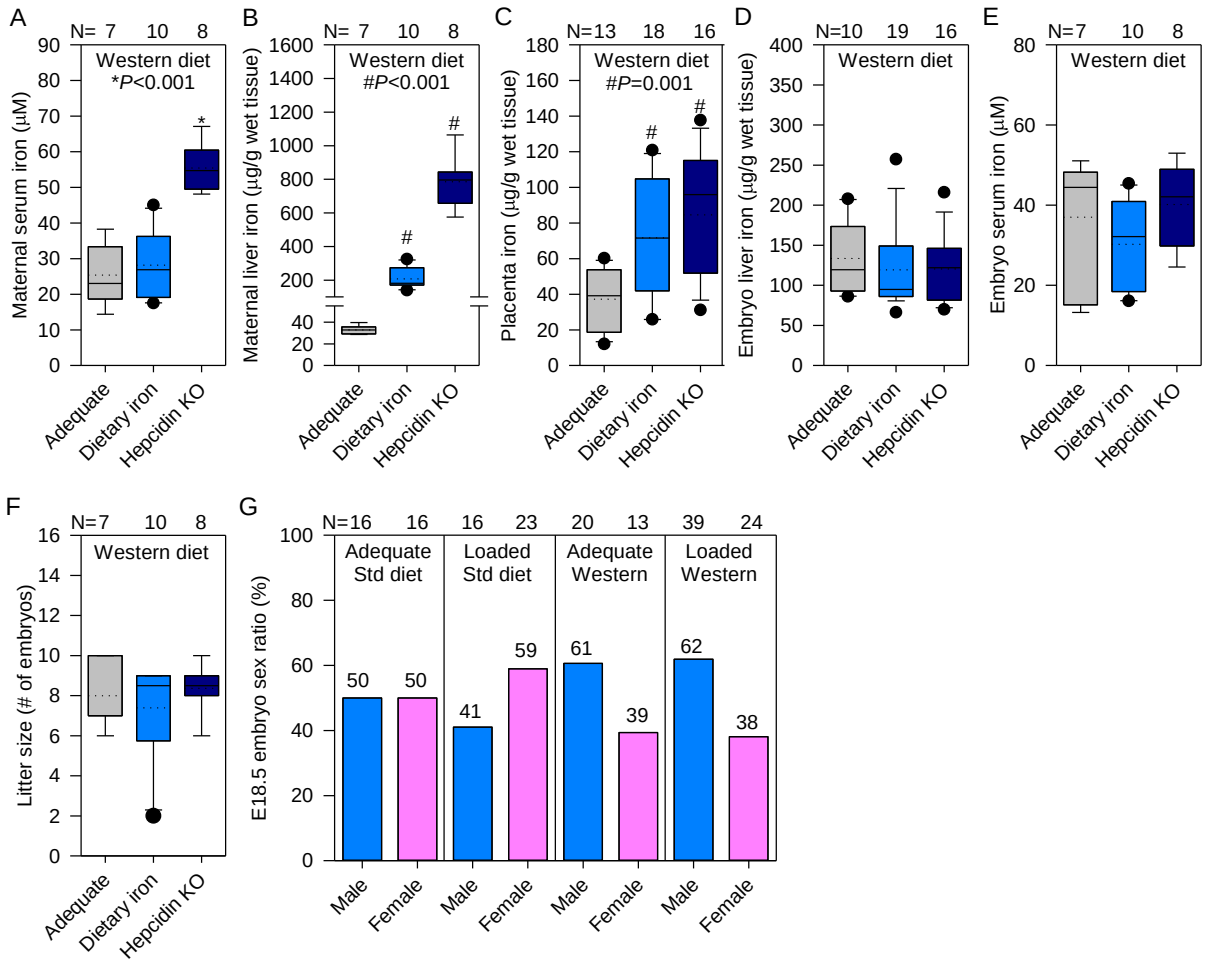

Supplemental Figure 4-6. Iron parameters and embryo malformations in iron-adequate, dietary iron supplemented, and hepcidin KO obese mice. To induce obesity, wild-type C57BL/6 or hepcidin KO mice were fed a Western diet (100ppm iron) starting at 3 weeks of age. Dietary iron-loaded dams were fed a Western diet supplemented with 5,000ppm carbonyl iron for 1 week prior to mating and for the duration of pregnancy. Iron-loaded dams were analyzed at E18.5 and compared to iron-adequate controls. **(A)** Maternal serum iron and **(B)** liver iron concentrations. Iron measurements at E18.5: **(C)** placenta, **(D)** embryo liver iron, and **(E)** embryo serum iron. **(F)** Litter size. **(G)** Sex ratio of E18.5 male and female embryos from iron adequate and iron loaded dams fed standard diet (std) or Western diet (WD). Data for iron-adequate and -loaded dams fed

standard diet are replicated from Supplemental Figure 4-1 but are included for ease of understanding. Statistical differences between groups were determined by one-way ANOVA for normally distributed values followed by Holm-Sidak method for multiple comparisons versus Western diet group (denoted by *) or one-way ANOVA on ranks followed by Dunn's method for multiple comparisons versus Western diet group (denoted by #). *P* values and animal numbers are indicated in each panel.

Supplemental Table 4-1. Interaction of maternal iron excess and PAMPs in pregnancy

PAMP	Mimetic	TLR	Dose/ Route	GD/ time	Iron adequate			Iron loaded		
					N	*Saa1* fold-change v solvent (Mean±SD)	Embryo outcome	N	*Saa1* fold-change v solvent (Mean±SD)	Embryo outcome
LPS *E. coli* O55:B5	Gram-negative bacteria	TLR4	0.5μg/g SQ	E15.5, 24h	8	251 ± 92	Normal	5	284 ± 42	Adverse
Poly I:C	dsDNA virus	TLR3	10μg/g IV	E15.5, 24h	3	289 ± 123	Normal	5	197 ± 38	Normal
LTA (*S. aureus*)	Gram-positive bacteria	TLR2	20μg/g IV	E15.5, 24h	3	227 ± 97	Normal	4	139 ± 33	Normal
Pam3csk4	Triacylated lipopeptide	TLR1/2	100μg SQ	E15.5, 24h	3	229 ± 72	Normal	4	330 ± 167	Normal
Flagellin (*B. subtilis*)	Flagellin	TLR5	30μg SQ	E15.5, 24h	3	76 ± 46	Normal	3	33 ± 19	Normal

Supplemental Table 4-1. Interaction of maternal iron excess and PAMPs in pregnancy. Pregnant iron-adequate WT dams and iron-loaded hepcidin KO dams were treated with the indicated PAMPs on E15.5 to evaluate the interaction of maternal iron excess with inflammatory pathways triggered by a broader spectrum of pathogen-derived molecules from viruses and bacteria. PAMP= pathogen associated molecular patter, LPS= lipopolysaccharide, Poly I:C= polyinosinic:polycytidylic acid, LTA= lipoteichoic acid. TLR= toll like receptor. SQ= subcutaneous, IV=intravenous, GD= gestational day, Saa1= serum amyloid A1.

CHAPTER 5: IRON INDUCES CHOLESTEROL SYNTHESIS AND SENSITIZES ENDOTHELIAL CELLS TO TNFα-MEDIATED APOPTOSIS (SUBMITTED MANUSCRIPT)

Manuscript submitted:

IRON LOADING INDUCES CHOLESTEROL SYNTHESIS AND SENSITIZES ENDOTHELIAL CELLS TO TNFα-MEDIATED APOPTOSIS

Allison L Fisher, Daniel N Srole, Nicolaos J Palaskas, David Meriwether, Srinivasa T Reddy, Tomas Ganz, Elizabeta Nemeth

ABSTRACT

In plasma, iron is normally bound to transferrin, but in conditions of iron overload when the iron-binding capacity of transferrin is exceeded, non-transferrin-bound iron (NTBI) appears in plasma. NTBI is taken up by hepatocytes and other parenchymal cells via NTBI transporters and can cause cellular damage by promoting the generation of reactive oxygen species. However, how NTBI affects endothelial cells, the most proximal cell type exposed to circulating NTBI, has not been explored. We modeled in vitro the effects of systemic iron overload on endothelial cells by treating primary human umbilical vein endothelial cells (HUVECs) with NTBI (ferric ammonium citrate, FAC). Using an unbiased approach, we showed by RNA-Seq that iron loading alters lipid homeostasis in HUVECs by inducing SREBP2-mediated cholesterol biosynthesis. We also determined that FAC increased the susceptibility of HUVECs to apoptosis induced by TNFα. Moreover, we showed that cholesterol biosynthesis contributes to iron-potentiated apoptosis. Treating HUVECs with a cholesterol chelator hydroxypropyl-β-cyclodextrin demonstrated that depletion of cholesterol was sufficient to rescue HUVECs from TNFα-induced apoptosis, even in the presence of FAC. Finally, we showed that FAC or cholesterol treatment modulated the TNFα pathway by inducing novel proteolytic processing of TNFR1 to a short isoform that localizes to lipid rafts. Our study raises the possibility that iron-mediated toxicity in human iron overload disorders is at least in part dependent on alterations in cholesterol metabolism in endothelial cells, increasing their susceptibility to apoptosis.

INTRODUCTION

Iron is an essential micronutrient but can cause tissue damage when in excess. In healthy humans and animals, iron in plasma is bound to the protein transferrin. When the iron-carrying capacity of transferrin is exceeded, such as in iron overload conditions, iron appears in plasma complexed with low molecular weight molecules, collectively referred to as non-transferrin bound iron (NTBI) (1), with ferric citrate reported to be the predominant NTBI species (2,3). NTBI is thought to contribute to organ dysfunction in iron overload conditions through the generation of reactive oxygen species that damage cellular lipids, proteins, and DNA (4), and can also promote susceptibility to certain infections (5). Since humans lack compensatory mechanisms to excrete excess iron, iron absorption is tightly regulated by the hormone hepcidin, which is produced in the liver. Hepcidin acts by binding to its receptor and only known iron exporter, ferroportin, blocking iron transport into plasma, and lowering plasma iron levels (6). Hepcidin deficiency results in iron overload in patients with hereditary iron disorders and ineffective erythropoiesis. Iron overload can also develop in people after repeated blood transfusions, or excessive iron supplementation. Milder iron excess has been linked to metabolic disorders including diabetes (7-10) and nonalcoholic fatty liver disease (11-13).

NTBI accumulation in cells leads to their dysfunction, with specific tissue toxicities dependent on both the rate and extent of NTBI accumulation. The liver is the main storage organ for iron, but also the organ most damaged by chronic iron overload. Iron uptake pathways in hepatocytes include the classical transferrin-transferrin receptor mediated uptake, as well as uptake of NTBI through specific transporters. Hepatocytes take up NTBI at a rapid rate that exceeds their capacity for iron export, resulting in the net accumulation of excess iron when NTBI is chronically elevated (14). Iron accumulation in the liver in iron overload diseases increases the risk of hepatic

fibrosis, cirrhosis, and hepatocellular carcinoma (15). Although most NTBI in plasma is cleared by the liver, NTBI can also be taken up by the pancreas, kidney, and heart (16). Thus, apart from the liver damage, severe iron overload is also known to cause cardiomyopathy, diabetes and other endocrinopathies (17,18). How different cell types take up NTBI is an area of active investigation (19), but ZIP14 was shown to be the NTBI transporter in hepatocytes and pancreatic acinar cells (20,21).

In patients with iron overload, circulating NTBI would come in contact with endothelial cells first, yet the effect of NTBI on endothelial cell function has not been explored. In the liver, endothelial cells have emerged as a cell type with essential roles in iron homeostasis (22,23). In response to liver iron loading, hepatic sinusoidal endothelial cells produce bone morphogenetic proteins, which exert paracrine effects on hepatocytes to induce hepcidin production and thereby modulate systemic iron homeostasis (23). However, how endothelial cells take up and sense iron remains poorly understood.

In this study, we explored how NTBI accumulation affects cultured endothelial cells. Using unbiased RNA-Seq, we determined that iron loading of human umbilical vein endothelial cells (HUVECs) by ferric ammonium citrate (FAC) potently induced lipid biosynthesis through the sterol regulatory element-binding protein (SREBP) pathways, predominantly affecting SREBP2-mediated cholesterol metabolism. We further found that cellular iron loading sensitized HUVECs to apoptotic cell death induced by TNFα and that iron loading altered the TNFα pathway by generating a short isoform of TNFR1 through novel proteolytic cleavage. Evaluating the contribution of cholesterol biosynthesis and TNFR1 cleavage to iron-potentiated apoptosis, we show that pharmacological depletion of cholesterol was sufficient to rescue the apoptotic phenotype even in the presence of excess iron and the presence of the short TNFR1 isoform. Thus,

we provide specific evidence that iron loading alters endothelial cell cholesterol homeostasis and increases their susceptibility to inflammation-mediated apoptosis.

RESULTS

Iron induces cholesterol biosynthesis. We used a cell culture system to model the effects of systemic iron overload on endothelial cells by treating primary human umbilical vein endothelial cells (HUVECs) with non-transferrin-bound iron (NTBI) in the form of ferric ammonium citrate (FAC). We chose prolonged exposures (30-40 h of NTBI) based on preliminary experiments assessing HUVECs rate of iron loading and evidence of cellular damage. To identify global transcriptome changes in endothelial cells in response to NTBI, we performed RNA-Seq analysis of HUVECs treated with 100 μM FAC for 30 h. Principal component analysis of RNA-Seq data showed that solvent- and FAC-treated groups were in distinct clusters, and indicated that the first principal component explains almost 40% of the variability among samples **(Figure 5-1A)**. Volcano plot showed 816 differentially expressed genes, including both downregulated and upregulated genes, between solvent and FAC-treated HUVECs **(Figure 5-1B)**. The gene expression of transferrin receptor 1 (*TFRC*) was among those with highly significant suppression **(Figure 5-1B)**, confirming that cells were effectively iron loaded. Ingenuity pathway analysis of FAC- and solvent-treated cells revealed that FAC primarily stimulates cholesterol biosynthesis pathways **(Figure 5-1C)**. We validated the RNA-Seq findings by measuring mRNA expression of genes involved in cholesterol biosynthesis by qRT-PCR in a separate set of HUVECs, treated with 100 μM FAC for 40 h. The cells were effectively iron-loaded, as reflected by the decrease in *TFRC* mRNA expression ($P<0.001$, *t*-test, **Figure 5-1D**). We confirmed increased expression of sterol regulatory element-binding protein 2 (*SREBP2*), a transcription factor that is a master

regulator of cholesterol synthesis (*P*=0.008, Mann-Whitney *U*). The expression of SREBP2 target genes was likewise upregulated: mevalonate pyrophosphate decarboxylase (*MVD*) (*P*=0.008, Mann-Whitney *U*), low-density lipoprotein receptor *(LDLR*) (*P*=0.008, Mann-Whitney *U*), and 3-Hydroxy-3-Methylglutaryl-CoA Reductase (*HMGCR*) (*P*<0.001, *t*-test) **(Figure 5-1E-H)**. Furthermore, we measured *SREBP2* mRNA expression in HUVECs treated with different forms of iron — NTBI (FAC, ferrous ammonium sulfate, ferric chloride), transferrin-bound iron, holo-

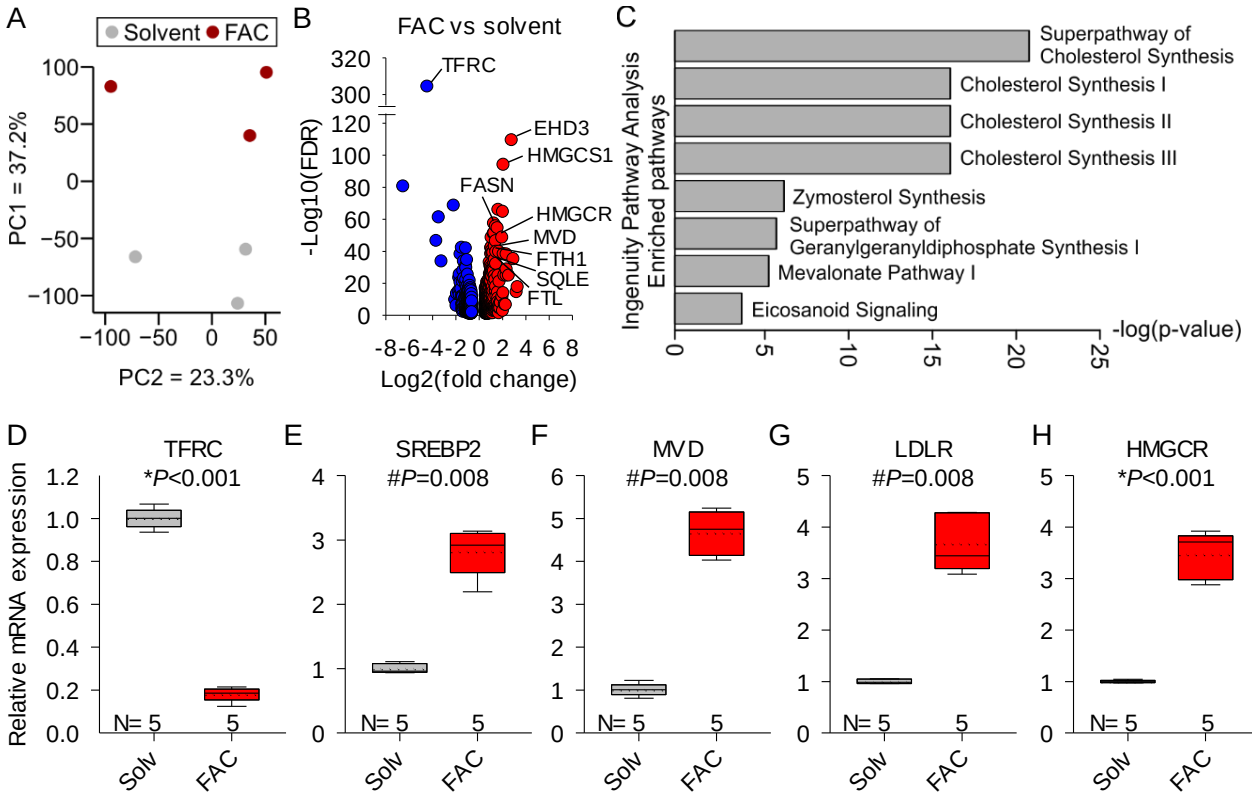

Figure 5-1. Iron induces cholesterol biosynthesis in primary HUVECs. To induce cellular iron loading, primary HUVECs were treated with 100 µM FAC for 30 h, and total RNA was collected for RNA-Seq. **(A)** Principal component scatter plot of gene expression in FAC- versus solvent-treated HUVECs. The percentages of each axis represent the percentage of variation explained by the principal components. **(B)** Volcano plot of 816 differentially expressed genes comparing FAC- versus solvent-treated HUVECs. Differentially expressed genes were identified by fold change of greater or less than ±1.5 and *P*<0.05. Blue circles= downregulated genes, red circles= upregulated genes. **(C)** Ingenuity pathway analysis identifying significantly enriched categories between FAC- and solvent-treated HUVECs (top hits shown, based on *P*<0.001 and *z*-score>2). **(D-H)** Primary HUVECs were treated with 100 µM FAC for 40 h. qPCR analysis of **(D)** iron importer *TFRC* and **(E-H)** cholesterol biosynthesis genes *SREBP2, MVD, LDLR, HMGCR*. Data are shown as $2^{-\Delta\Delta Ct}$. Number of biological replicates are indicated above the *x*-axis. Statistical differences between groups were determined by Student's *t*-test for normally distributed values (indicated by *) or Mann-Whitney *U* for non-normally distributed values (indicated by #).

ferritin and hemin — or with triammonium citrate as a control **(Supplemental Figure 5-1A)**. Most of the iron treatments induced *SREBP2* mRNA whereas triammonium citrate (lacking iron) did not. Expression of *SREBP2* correlated with the degree of cellular iron loading as measured by ferritin heavy chain immunoblotting (r=0.826, *P*=0.012, **Supplemental Figure 5-1B**). This result demonstrated that it is the cellular iron loading, as opposed to the specific form of NTBI, that induces cholesterol synthesis.

We further measured mRNA expression of SREBP transcription factors that control fatty acid biosynthetic pathways. FAC treatment of HUVECs increased expression of *SREBP1* isoforms a and c (both *P*<0.001, *t*-test) and their gene targets acetyl-CoA carboxylase (*ACCA*) (*P*=0.002, *t*-test), and fatty acid synthase (*FASN*) (*P*<0.001, *t*-test) **(Supplemental Figure 5-2A-E)**, suggesting that iron plays a broader role in lipid homeostasis. Taken together, these findings demonstrate that iron loading of endothelial cells induces expression of the SREBP pathway genes that control sterol and fatty acid synthesis.

To assess the effect on lipid synthesis, HUVECs were labeled with [U^{13}C]-D-glucose and treated with FAC for 30 and 40 h, the two time-points used for transcriptional analysis in Figure 1. Using isotopomer spectral analysis we did not detect any changes in the synthesis of saturated fatty acids myristic acid (14:0) or stearic acid (18:0) with FAC treatment **(Figure 5-2A and B)**. FAC treatment mildly increased synthesis of palmitic acid (16:0) (*P*=0.030, one-way ANOVA) and oleic acid (18:1) (*P*=0.034, one-way ANOVA) by 1.5-fold after 40h **(Figure 5-2C and D),** and more strongly induced synthesis of unsaturated fatty acid palmitoleic acid (16:1) by >2-fold at both time points (*P*=0.002 at 30 h, and *P*<0.001 at 40 h, one-way ANOVA) **(Figure 5-2E)**. FAC had the strongest effect on cholesterol biosynthesis, with 4-fold induction achieved by 40 h (**Figure 5-2F**; *P*=0.002 at 30 h and *P*<0.001 at 40 h, one-way ANOVA). Increases in cellular cholesterol

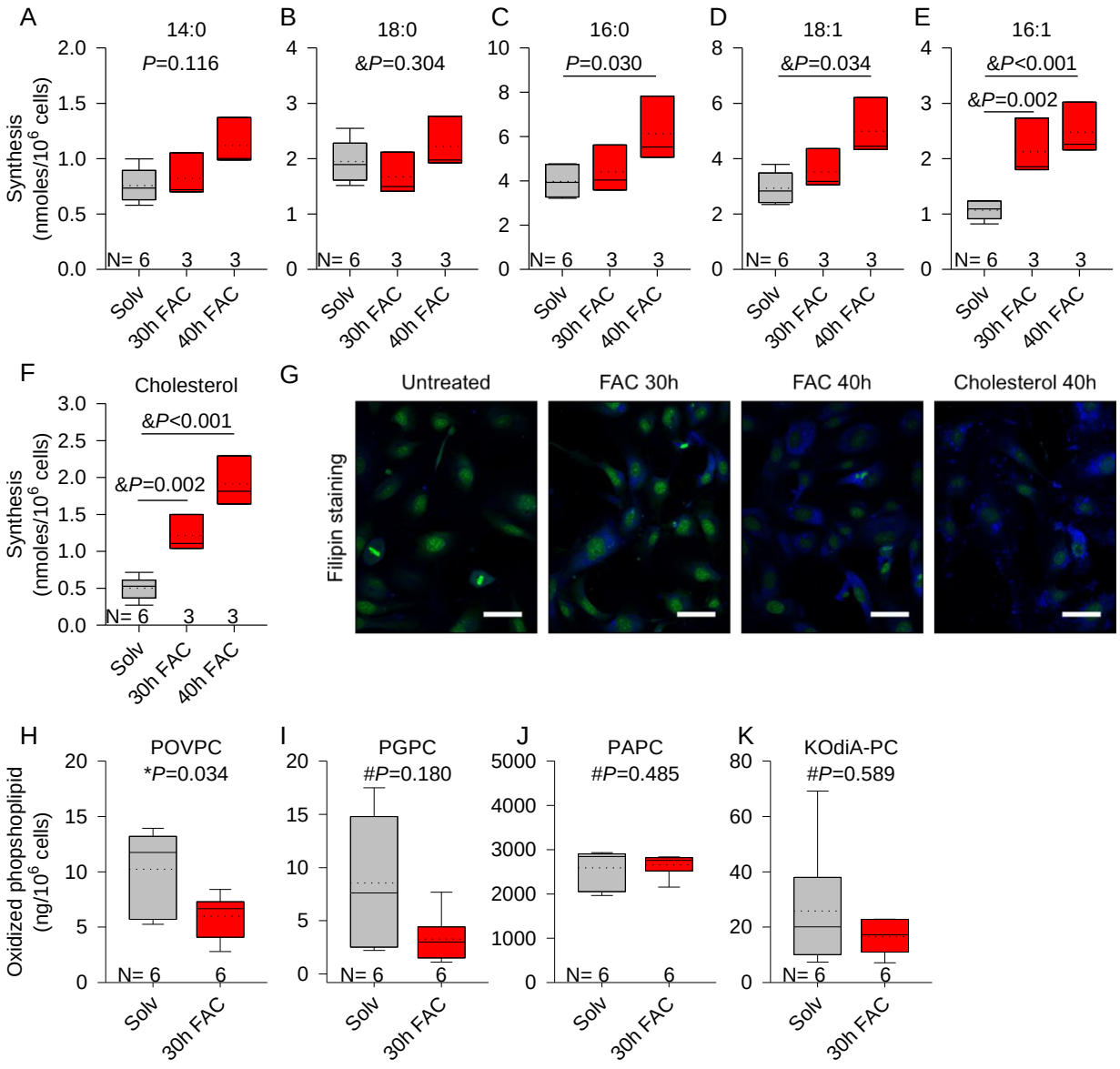

Figure 5-2. Lipid composition in control and iron loaded HUVECs. (A-F) Isotopic spectral analysis of HUVECs treated with 100 µM FAC for 30 or 40 h in the presence of 5 mM [$U^{13}C$]-D-glucose. Lipid synthesis is expressed as nmoles/million cells: cellular **(A)** myristic acid (14:0), **(B)** stearic acid (18:0), **(C)** palmitic acid (16:0), **(D)** oleic acid (18:1), **(E)** palmitoleic acid (16:1), and **(F)** cholesterol. **(G)** Confocal microscopy of filipin staining (blue) of HUVECs treated with 100 µM FAC for 30 or 40 h. HUVECs treated with 50 µM cholesterol-methyl-β-cyclodextrin (MβCD) were used as a positive control. Nuclear stain= Sytox green. Scale bar= 50 µm. **(H-K)** LC-MS analysis of oxidized phospholipids in HUVECs treated with 100 µM FAC for 30h. **(H)** 1-palmitoyl-2-(5-oxovaleroyl)-sn-glycero-3-phosphocholine (POVPC), **(I)** 1-palmitoyl-2-glutaroyl-sn-glycero-3-phosphocholine (PGPC), **(J)** 1-palmitoyl-2-arachidonoyl-sn-glycero-3-phosphocholine (PAPC), and **(K)** 1-(palmitoyl)-2-(5-keto-6-octene-dioyl)phosphatidylcholine (KOdiA-PC). Number of replicates are indicated above the *x*-axis. Statistical differences between groups were determined by one-way ANOVA on ranks with Dunn's method of multiple comparison for non-normally distributed values, one-way ANOVA followed by Holm-Sidak method of multiple comparisons for normally distributed values (indicated by &), Student's *t*-test (indicated by *) or Mann-Whitney *U* for non-normally distributed values (indicated by #).

were also confirmed by staining of HUVECs with the fluorescent cholesterol probe filipin after FAC treatment **(Figure 5-2G),** which revealed cytoplasmic rather than cell surface distribution. Cholesterol-treated HUVECs were used as a control for filipin staining.

Iron can damage cellular membrane integrity by generating hydroxyl radicals through the Fenton reaction that cause peroxidation of membrane phospholipids (24). We considered whether cellular membrane damage mediates the induction in cholesterol biosynthesis by determining whether FAC caused peroxidation of membrane phospholipids. We measured 1-palmitoyl-2-(5-oxovaleroyl)-sn-glycero-3-phosphocholine (POVPC), 1-palmitoyl-2-glutaroyl-sn-glycero-3-phosphocholine (PGPC), and 1-(palmitoyl)-2-(5-keto-6-octene-dioyl)phosphatidylcholine (KOdiA-PC), which are common stable end-products of and biomarkers for lipid peroxidation of palmitoyl arachidonoyl phosphatidylcholine (PAPC) **(Figure 5-2H-K)** (25). We did not detect any major iron-dependent changes in the cellular levels of these phospholipid peroxidation markers. These data indicate that FAC did not damage the cell membranes through peroxidation and suggests that iron stimulates cholesterol biosynthesis independently of membrane damage.

To ascertain whether iron loading of other cell types alters their *SREBP2* mRNA, human cell lines Hep3B (hepatocellular carcinoma) and immortalized endothelial line teloHAEC were treated with 100 μM FAC for 40 h. FAC decreased *TFRC* expression in both Hep3B and teloHAEC, confirming that these cell lines efficiently load FAC **(Supplemental Figure 5-3A)**. Despite this, neither Hep3B nor teloHAEC induced *SREBP2* expression, and Hep3Bs even moderately reduced *SREBP2* expression **(Supplemental Figure 5-3B)**. This result suggests that although iron-dependent changes in cholesterol homeostasis occur in primary endothelial cells, such a cellular response to iron loading is not universal.

Cellular iron loading potentiates apoptosis. In iron overload conditions, NTBI causes toxicity through promoting the formation of free radicals in tissues in which it accumulates. We next evaluated the sensitivity of endothelial cells to iron-mediated cytotoxicity. Caspase-3 is known to be a critical executioner of apoptosis, and its activation requires proteolytic processing of the proenzyme (26,27). We therefore determined the levels of cleaved caspase-3 as a marker of apoptosis in HUVECs treated with 100 µM FAC for 30 h, but FAC treatment alone did not cause apoptosis (**Figure 5-3**). We then assessed the effect of iron loading on apoptosis triggered by TNFα, a canonical apoptotic stimulus. TNFα treatment (5 and 50 ng/ml for 6 h) by itself mildly increased cleaved caspase-3. However, we observed a strong interaction between iron and the inflammatory cytokine, where FAC treatment significantly potentiated cleaved caspase-3 induced by TNFα **(Figure 5-3).** The result indicates that iron loading increases the susceptibility of endothelial cells to inflammatory damage. We did not observe any FAC-dependent potentiation of cleaved caspase-3 by TNFα in immortalized Hep3B or teloHAEC **(Supplemental Figure 5-4**), suggesting that primary endothelial cells are unusually susceptible to iron-potentiated apoptosis.

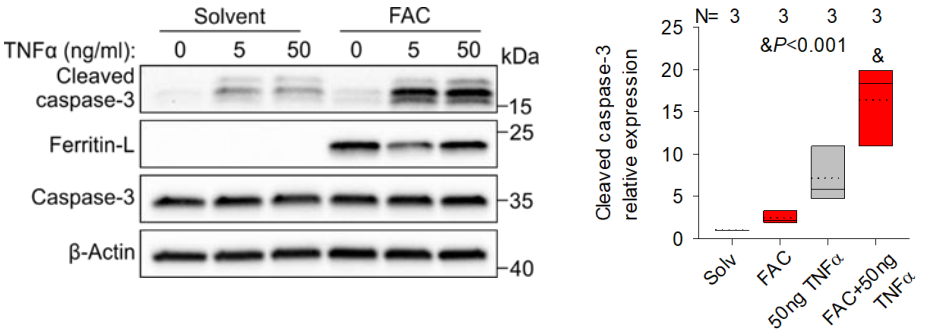

Figure 5-3. Iron loading of HUVECs sensitizes them to apoptosis. Primary HUVECs were treated with 100 µM FAC for 24 h prior to stimulation with 5 or 50 ng/ml TNFα in normal or FAC-supplemented media for 6 h. Western blot for cleaved caspase-3. Representative image of N=3 independent experiments. Quantification of cleaved caspase-3 normalized to β-actin is shown for the 50 ng/ml dose. Statistical differences between groups were determined by one-way ANOVA for normally distributed values (indicated by &).

Iron modulates TNFR1 proteolytic processing. We next evaluated whether iron alters signaling downstream of TNFα, which could increase susceptibility to cell death. TNFα has two main receptors, TNFR1 (or p55) and TNFR2 (or p75), which are expressed on many cell types but belong to different subgroups of the TNFR family. TNFR1 is a death receptor and harbors a death domain in its cytoplasmic portion, which links TNFR1 to apoptosis and necroptosis (28). In comparison, TNFR2 does not contain a death domain. TNFR1 is a 55-kDa transmembrane protein that is shed into circulation as 27- to 30-kDa soluble proteins after extracellular cleavage (29,30), and the soluble form can inhibit TNFα by competing for TNFα binding. We therefore evaluated the effect of iron excess on TNFR1 expression. HUVECs were treated with FAC over a time-course between 0-48 hours and we assessed TNFR1 mRNA and protein expression. FAC treatment did not significantly alter *TNFRSF1A* mRNA expression **(Figure 5-4A)**. However, FAC treatment strongly affected TNFR1 protein composition. Although the longest isoform (55-kDa) was relatively stable with FAC treatment, a novel shorter isoform (35-kDa) was induced 10-fold at 24 and 48 h (P<0.001, one-way ANOVA) **(Figure 5-4B)**. To ensure that the 35-kDa isoform is TNFR1 rather than a result of nonspecific antibody interaction with another protein, we validated the finding by depleting HUVECs of endogenous TNFR1 using control siRNA (siNC) or siRNA targeting TNFR1 (siTNFR1) for 48 h and treating the cells with FAC or solvent for 24 h. Treatment with siTNFR1 reduced the mRNA levels ~5-fold, and reduced protein expression of both the full length and shorter isoform of TNFR1 **(Supplemental Figure 5-5A-B)**, confirming the specificity of the antibody.

We next tested whether the induction of the smaller 35-kD isoform was specifically caused by cellular iron loading. We treated HUVECs with FAC, ferrous ammonium sulfate (FAS), ferric chloride ($FeCl_3$), apo-ferritin (apo-FT, ferritin lacking iron), holo-ferritin (holo-FT, ferritin

containing iron), copper chloride ($CuCl_2$), or zinc sulfate ($ZnSO_4$) for 24 h. Induction of the short TNFR1 isoform was strongest with FAC treatment, occurred to a lesser extent with $FeCl_3$ and holo-

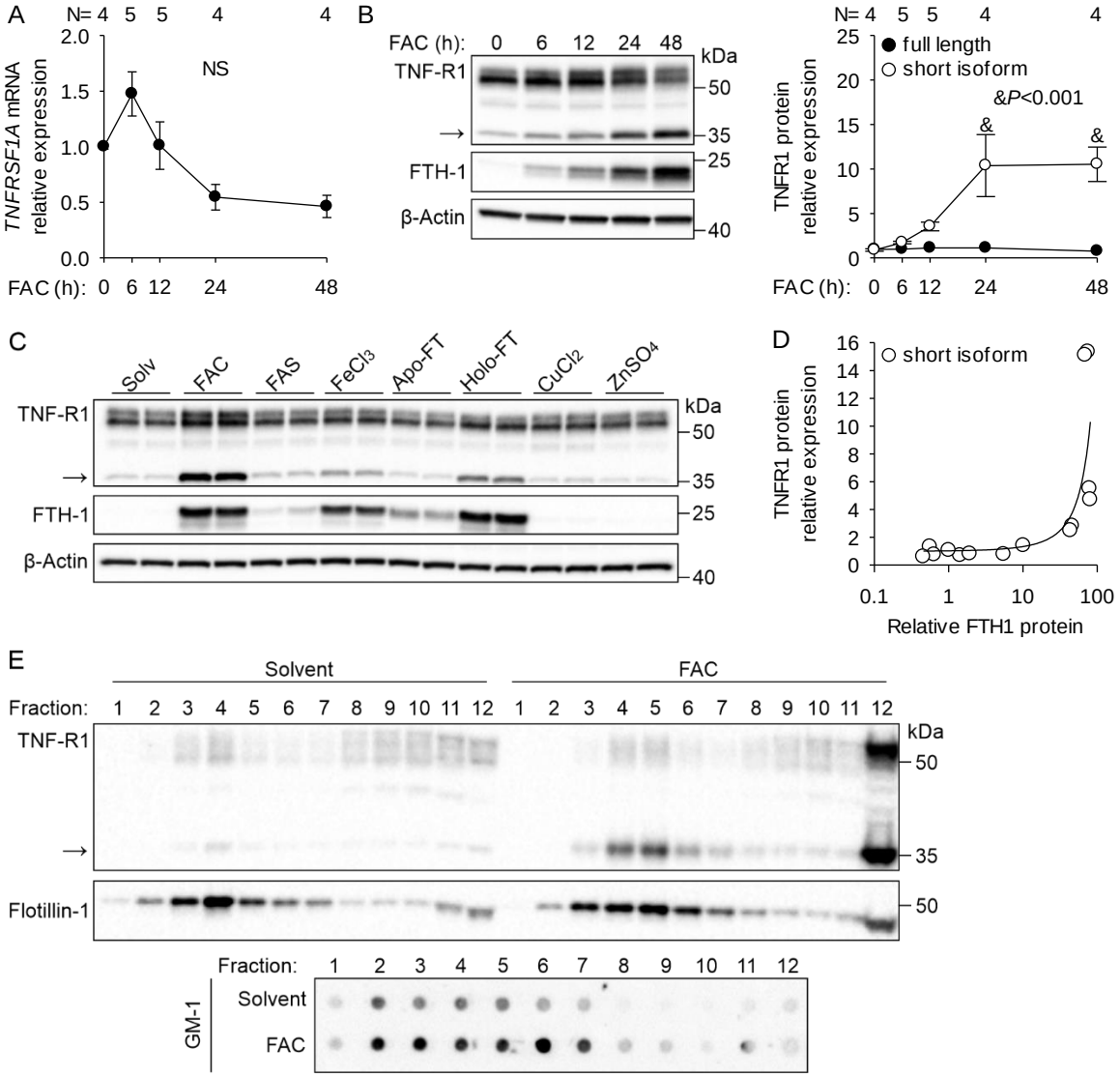

Figure 5-4. In HUVECs, iron loading induces expression of a short isoform of TNFR1 that localizes to lipid rafts. (A) Primary HUVECs were treated with 100 μM FAC for 0-48 h. *TNFRSF1A* mRNA analysis by qRT-PCR normalized to *HPRT* and expressed as $2^{-\Delta\Delta Ct}$. (**B**) Western blot and protein quantification of the full length (55 kDa) and short TNFR1 isoform (35 kDa, indicated by an arrow) normalized to β-actin. **(C)** Western blot for TNFR1 in HUVECs treated with solvent or 100 μM FAC, ferric ammonium sulfate (FAS, 100 μM), ferric chloride ($FeCl_3$, 100 μM), apoferritin (FT, 2 mg/ml), holo-FT (2 mg/ml), copper chloride ($CuCl_2$, 100 μM), or zinc sulfate ($ZnSO_4$, 100 μM) for 24 h. (**D**) Correlation between FTH1 and short TNFR1 isoform normalized to β-actin. **(E)** HUVECs treated with solvent or 100 μM FAC for 24 h were subjected to sucrose density gradient centrifugation to isolate lipid rafts. Proteins from equal volume of collected fractions were separated by SDS-PAGE and analyzed by Western blotting. To analyze the distribution of GM-1, each fraction was dot blotted onto a nitrocellulose membrane and detected using CTx^{HRP}. Statistical differences were determined by one-way ANOVA with Holm-Sidak method of multiple comparisons (indicated by &).

FT, and was not induced by FAS, apo-FT, copper, or zinc **(Figure 5-4C)**. In agreement, the levels of the short TNFR1 isoform correlated with the degree of iron loading as measured by FTH1 expression, with an apparent threshold at FTH1/β-actin of about 30 **(Figure 5-4D)**, whereas the full-length isoform did not correlate with FTH1 expression **(Supplemental Figure 5-6)**.

To determine the cellular localization of the short TNFR1 isoform, we performed membrane enrichment assays. In view of the reported recruitment of TNFR1 to lipid rafts (31), we determined the localization of the short TNFR1 isoform in membrane fractions from HUVECs treated with solvent or FAC for 24 h. Using density-gradient centrifugation, we found that FAC treatment upregulates expression of the short form of TNFR1 in the lipid rafts fractions, as defined by the enrichment of flotillin-1 and ganglioside GM-1 **(Figure 5-4E)**.

We next examined whether iron induces proteolytic processing of TNFR1 to generate the shorter isoform. HUVECs were transduced with lentivirus expressing TNFR1 (pLX304-TNFR1) prior to FAC treatment. Since the lentivirus contains TNFR1 cDNA, any change in TNFR1 would be from post-translational modifications rather than generation of new mRNA isoforms. FAC treatment of HUVECs overexpressing TNFR1 resulted in a strong induction in the short but not full-length TNFR1 isoform **(Figure 5-5A)**, confirming that TNFR1 regulation by iron is a result of proteolytic processing rather than generation of a new mRNA isoform. Considering this, we first evaluated the role of the canonical TNFR1 cleavage pathways in the induction of the short TNFR1 isoform. These pathways have been previously shown to generate a 27-30 kDa soluble fragment (32) and 26-30 kDa cell-associated fragment of TNFR1 (29,33). Treatment of FAC-loaded HUVECs with TAPI2, an ADAM17 (TNFα converting enzyme, TACE) and matrix metalloprotease inhibitor in combination with FAC did not change the amount of the lower TNFR1 isoform despite a reduction in soluble TNFR1 in supernatants **(Figure 5-5B)**. Furthermore,

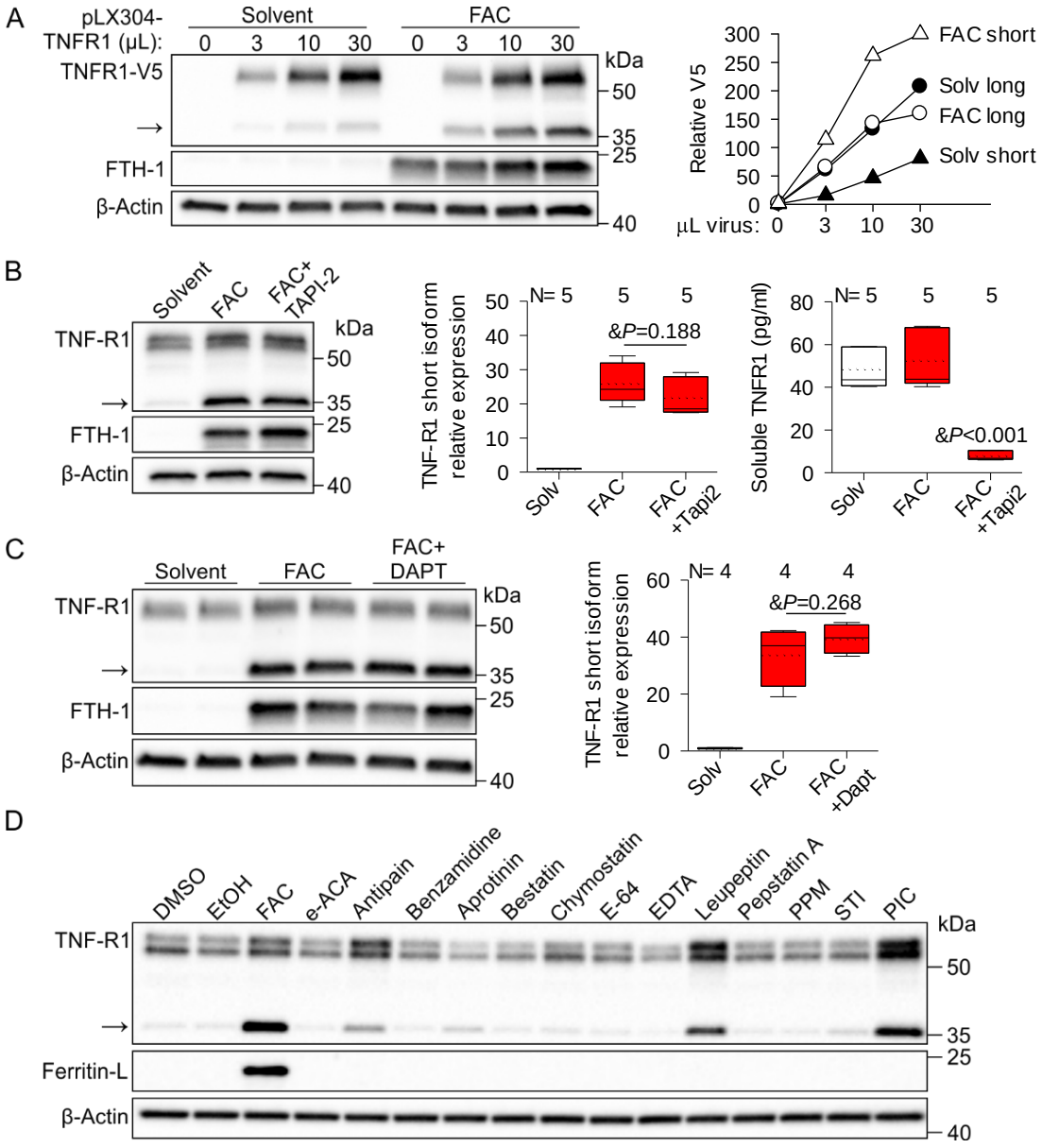

Figure 5-5. Iron induces post-translational modifications of TNFR1. (A) HUVECs were transduced with increasing volume of lentivirus expressing human TNFR1 with a C-terminal V5 tag for 10 h prior to incubation with solvent or 100 µM ferric ammonium citrate (FAC) for 24 h. Western blot using anti-V5 antibody; the short isoform indicated by an arrow. **(B)** HUVECs were treated with 100 µM FAC with and without 25 µM TAPI-2 inhibitor for 24 h and Western blot performed for TNFR1. Representative image showing endogenous TNFR1 (left), quantification of the small TNFR1 isoform (middle), and quantification of soluble TNFR1 in HUVEC supernatants (right). **(C)** Western blot and quantification of small TNFR1 isoform after HUVECs were treated with solvent or 100 µM FAC with and without 1 µM DAPT inhibitor. **(D)** Western blot for TNFR1 in HUVECs treated with a panel of protease inhibitors: 6-aminohexanoic acid (E-ACA, 40 mM), antipain (100 µM), benzamidine HCl (4 mM), aprotinin (1 µM), bestatin (40 µM), chymostatin (100 µM), E-64 (10 µM), EDTA (1 mM), leupeptin (100 µM), pepstatin A (1 µM), phosphoramidon (PPM, 10 µM), soybean trypsin inhibitor (STI, 5 µM), or protease inhibitor cocktail (PIC, 1:200) for 24 h. FAC was used as a positive control. β-actin was used as a loading control. Number of replicates are indicated above the *x*-axis. Statistical differences between groups were determined by one-way ANOVA with Holm-Sidak method for multiple comparisons for normally distributed values (indicated by &).

treatment of HUVECs with DAPT, a γ-secretase inhibitor, prior to iron loading did not alter expression of the short TNFR1 isoform **(Figure 5-5C)**, suggesting that generation of the 35-kDa isoform is independent of the canonical TNFR1 cleavage processes. Further evaluation of proteolytic processing using a panel of protease inhibitors in HUVECs showed that protease inhibitors antipain (serine inhibitor) and leupeptin (serine & thiol inhibitor) increased expression of the short TNFR1 isoform similarly as FAC treatment or treatment with a protease inhibitor cocktail (containing aprotinin, bestatin, E-64, leupeptin, and pepstatin A) **(Figure 5-5D)**, demonstrating that FAC treatment mimics the action of protease inhibitors and thereby suggesting that FAC may antagonize or inactivate one or more serine proteases.

In addition to the known *N*-linked glycosylation sites on TNFR1 (asparagine 54, 145, and 151), we considered whether the 35-kDa isoform may be a result of glycosylation of an even smaller fragment, by treating HUVECs with FAC for 30 h and evaluating *N*- and *O*-linked glycosylation. As expected, the full-length TNFR1 isoform was *N*-linked glycosylated, as treatment with PNGaseF resulted in a downward shift in the molecular weight of full-length TNFR1 compared to untreated and *O*-glycosidase treated lysates **(Supplemental Figure 5-7)**. However, the molecular weight of the short TNFR1 isoform was similar between untreated, *N*- and *O*-deglycosylated lysates **(Supplemental Figure 5-7)**, indicating that the short isoform is not glycosylated. We similarly detected induction of the short TNFR1 isoform with FAC loading in Hep3B and teloHAEC **(Supplemental Figure 5-8)**, suggesting a more common role of iron in TNFR1 processing.

Cellular cholesterol loading potentiates apoptosis and promotes TNFR1 processing. Our data show that iron alters lipid homeostasis and proteolytic processing of TNFR1 in endothelial cells. We next asked whether altered lipid homeostasis or TNFR1 expression contributes to iron-

potentiation of apoptosis. We tested the contribution of high cellular cholesterol on apoptosis by treating HUVECs with 50 µM cholesterol-methyl-β-cyclodextrin (MβCD) for 24 h prior to stimulation with 50 ng/ml TNFα for 16 h, and compared the apoptotic response seen with the combination of FAC and TNFα. Cholesterol-MβCD by itself had no effect on cleaved caspase-3, but co-treatment with TNFα did potentiate cleaved caspase-3 (*P*=0.008, one-way ANOVA), to a similar level as FAC **(Figure 5-6A)**. Interestingly, cholesterol-MβCD also induced expression of the shorter TNFR1 isoform (*P*=0.002, one-way ANOVA) **(Figure 5-6B)**.

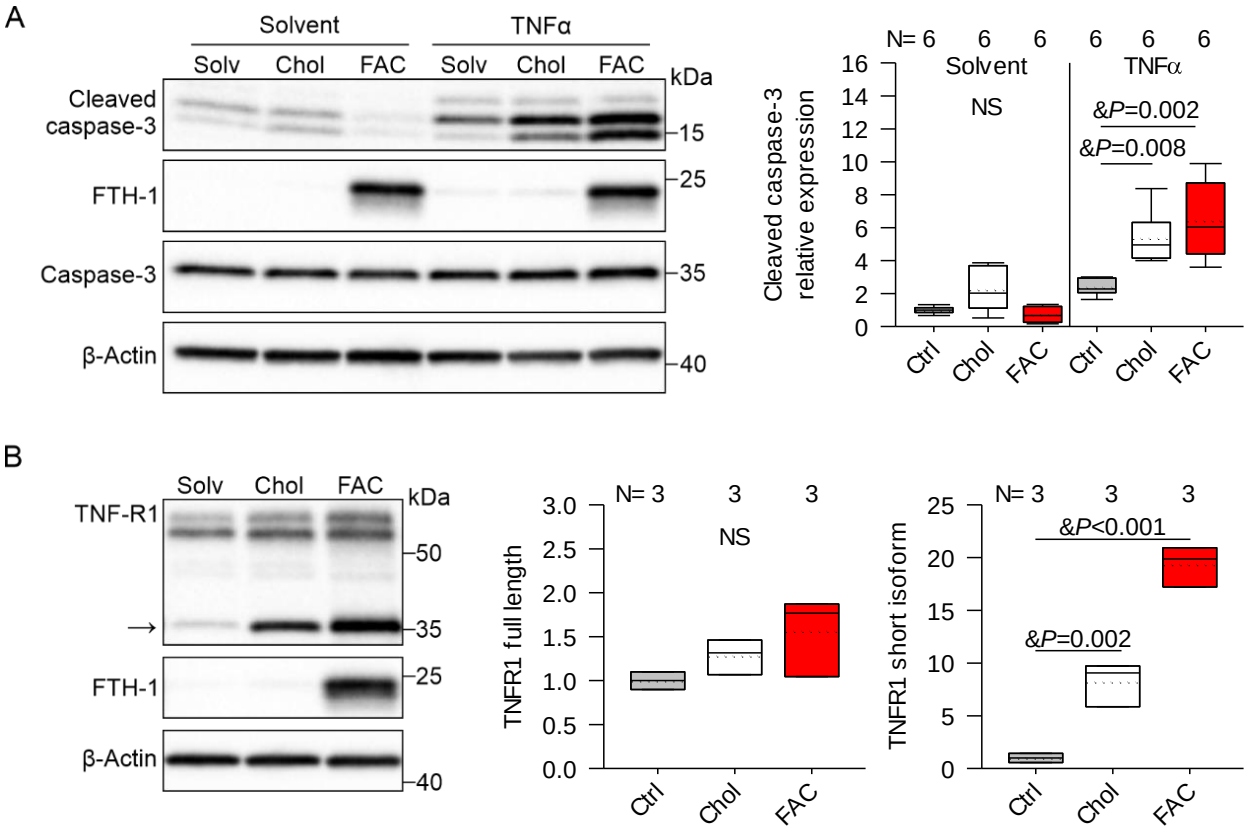

Figure 5-6. Cholesterol treatment potentiates apoptosis and increases TNFR1 short isoform in HUVECs. (A) Cleaved caspase-3 Western blot of HUVECs treated with 100 µM FAC or 50 µM cholesterol-MβCD followed by stimulation with 50 ng/ml TNFα for 16 h. **(B)** Western blot and protein quantification of full length- and TNFR1-short isoform (indicated by an arrow) in HUVECs treated with 100 µM FAC or 50 µM cholesterol-MβCD for 40 h. Representative images of N=3 independent experiments. β-actin was used as a loading control. Statistical differences between groups were determined by one-way ANOVA with Holm-Sidak method for multiple comparisons for normally distributed values (indicated by &).

Modulation of cholesterol metabolism rescues iron-dependent apoptosis. To evaluate the role of lipid metabolism in FAC-potentiated apoptosis, HUVECs were treated with different drugs that

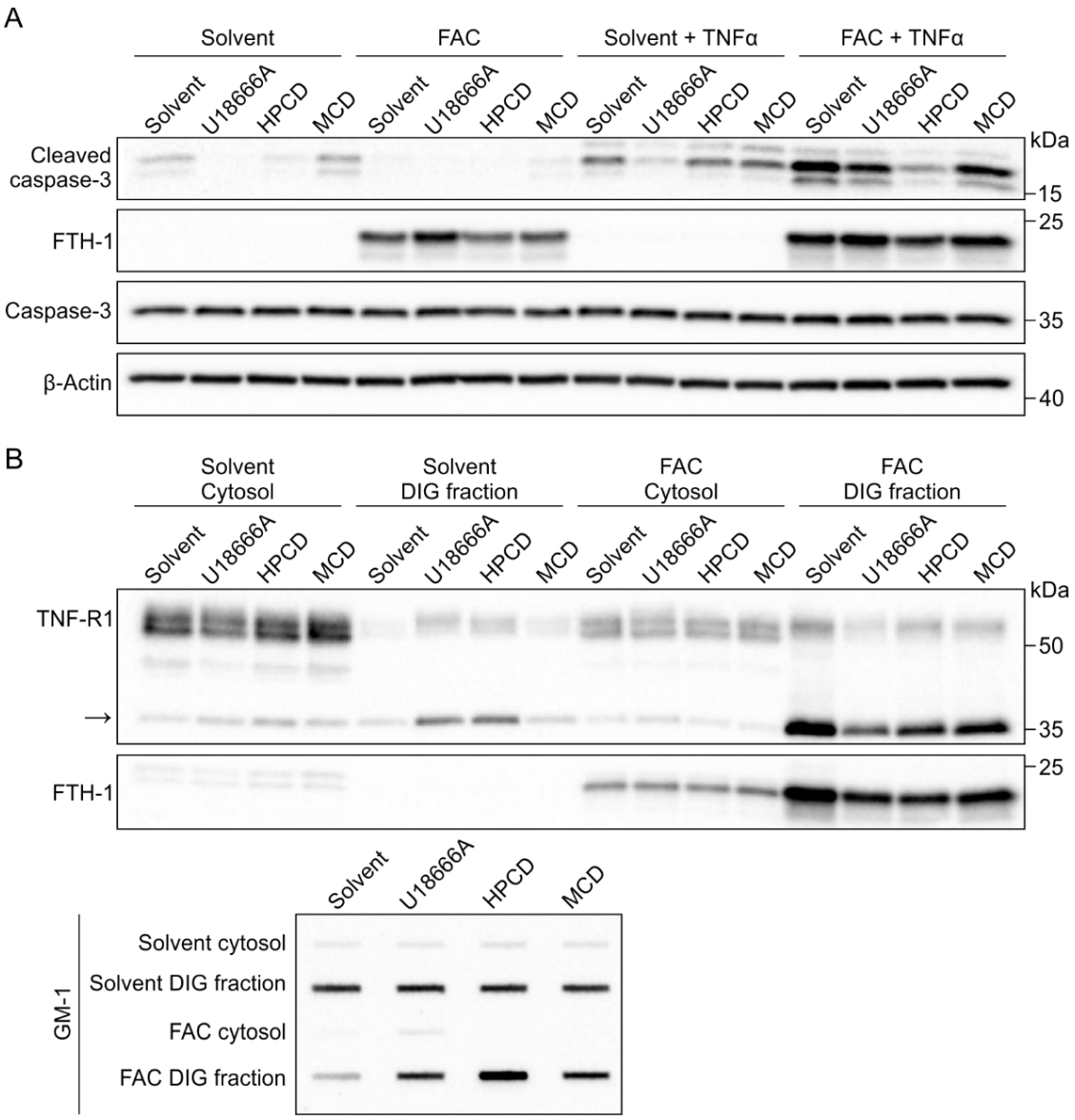

Figure 5-7. Cholesterol depletion rescues apoptosis of HUVECs induced by iron excess independently of TNFR1 short isoform. (A) HUVECs were pharmacologically depleted of cholesterol by treating with 1 μM U18666A, 0.3% HPCD, or 50 μM MCD in the presence of 100 μM FAC for 24 h prior to stimulation with 50 ng/ml TNFα for 16 h. Western blot for cleaved caspase-3. β-Actin was used as a loading control. **(B)** HUVECs were treated with solvent, 1 μM U18666A, 0.3% HPCD, or 50 μM MCD in the presence or absence of 100 μM FAC for 40 h. Detergent soluble (cytosol) and insoluble glycosphingolipid (DIG) fractions were isolated by centrifugation. Proteins from equal volume of collected fractions were separated by SDS-PAGE and analyzed by Western blotting. To analyze the distribution of GM-1, each fraction was dot blotted onto a nitrocellulose membrane and detected using CTx^{HRP}.

alter cellular cholesterol content, then treated with 100 μM FAC and 50 ng/ml TNFα. U18666A (1 μM) was used to inhibit cholesterol movement out of lysosomes, whereas (2-hydroxypropyl)-β-cyclodextrin (HPCD, 0.3%) and methyl-β-cyclodextrin (MCD, 50 μM) were used to deplete cholesterol. As expected, FAC strongly potentiated cleaved caspase-3 expression induced by TNFα **(Figure 5-7A)**. Neither treatment of FAC-loaded cells with U18666A nor MCD was sufficient to rescue apoptosis **(Figure 5-7A)**. However, treatment with HPCD was protective against FAC-potentiated apoptosis **(Figure 5-7A)**. Although MCD and HPCD are both reported to remove membrane cholesterol, it is likely that the MCD dose used (50 μM) was not sufficient to reduce cholesterol levels, as this requires mM concentrations (34,35). Using lipid raft isolation, we evaluated the changes in TNFR1 isoforms after pharmacological lowering of cellular cholesterol. As expected, TNFR1 short isoform expression was strongly potentiated by FAC in the lipid raft fractions; however, neither U18666A, MCD, nor HPCD altered TNFR1 expression **(Figure 5-7B)**. Considering that apoptosis was rescued with HPCD despite prominent TNFR1 short isoform expression, our data suggest that altered lipid metabolism rather than TNFR1 isoform expression is the adverse mediator of iron-potentiated apoptosis.

Taken together, our data suggest that iron loading of endothelial cells alters lipid metabolism, which sensitizes cells to apoptotic death by TNFα. Iron as well as cholesterol loading also induces accumulation of a short isoform of TNFR1. Although the accumulation of the short TNFR1 isoform is not sufficient to induce apoptosis, it remains to be determined whether it is needed in conjunction with changes in cholesterol metabolism to induce this new form of iron-dependent cell death.

DISCUSSION

In diseases of iron overload, the iron-binding capacity of transferrin is exceeded, and non-transferrin-bound iron appears in circulation. Utilizing the ZIP14 transporter, the liver rapidly clears NTBI from plasma to store iron in hepatocytes, but with chronic exposure to NTBI, the liver becomes iron-overloaded, resulting in an increased risk for hepatic fibrosis, cirrhosis, and hepatocellular carcinoma (15). Apart from hepatocytes, several other cell types including cardiomyocytes, pancreatic and pituitary cells can take up NTBI and become iron-overloaded, with consequent organ dysfunction. Before reaching any of those cell types, however, NTBI will first contact endothelial cells, but how iron excess affects endothelial cells has not been explored. We used a primary endothelial cell culture model to mimic the exposure of endothelial cells to NTBI in diseases with systemic iron overload. Using RNA-Seq to determine how endothelial cells respond to iron excess, we first found that iron excess in HUVECs induces cholesterol biosynthesis. Cholesterol has essential functions in mammalian systems and its availability is regulated through homeostatic mechanisms to prevent the pathologic consequences of deficient or excessive cholesterol (36). The SREBPs are transcription factors that have well-defined roles in lipid homeostasis (37). Three SREBP isoforms, SREBP-1a, -1c, and -2, have been identified in mammals. SREBP-1a controls both cholesterol and fatty acid biosynthetic pathways by potently activating all SREBP-responsive genes. SREBP1c preferentially regulates transcription of genes involved in fatty acid synthesis (38), whereas SREBP2 preferentially activates genes involved in cholesterol synthesis (39), although a moderate induction in genes involved in fatty acid synthesis also occurs (40). In our study, we found that iron loading induced mRNA expression of *SREBP1a, c* and *SREBP2,* their gene targets, as well as synthesis of palmitoleic acid and cholesterol, indicating a broader role of iron in modulating lipid homeostasis.

The interaction between iron and cholesterol is not well understood, but increasing evidence associates high iron status with altered cholesterol metabolism, although the data are occasionally conflicting. An early study in rats correlated hepatic iron content with circulating cholesterol levels, although hepatic iron retention was induced by dietary copper deficiency rather than dietary iron loading (41). A more direct comparison was made in dietary iron-loaded rats, where hepatic iron loading correlated with circulating cholesterol, but reduced expression of genes involved in sterol synthesis (42). In contrast, in mice with dietary iron overload, hepatic iron content positively correlated with hepatic cholesterol content but not circulating cholesterol levels, and positively correlated with genes involved in cholesterol biosynthesis (43). Similarly, dietary iron and iron-dextran loaded mice had increased mRNA and enzyme activity of stearoyl-CoA desaturase-1, an enzyme involved in fatty acid metabolism (44). In agreement, we also detected changes in lipid homeostasis in mouse livers after iron perturbation. We had access to microarray data from a published cohort of transferrin receptor 2 (TFR2)-mutant mice susceptible to spontaneous iron overload. The mice were iron-depleted (using iron-deficient diet in combination with phlebotomy) and refed for 1 or 21 days with an iron-sufficient diet (45). Microarray analysis of the liver mRNA showed an increase in cholesterol and fatty acid biosynthesis genes with iron-repletion. Specifically, the microarray MOE 430 2.0 array (Affymetrix) included 25915 unique genes, of which 2254 were annotated as belonging to a biochemical pathway. Out of the annotated pathway genes, 44 increased robustly with iron refeeding, and of those 8 belonged to the cholesterol synthesis pathway ($p<0.000001$). Further studies in iron-loaded mouse models that utilize cell sorting or single-cell RNA-Seq are needed to determine which cell types increase cholesterol biosynthesis in vivo. In our in vitro study, we saw a strong induction of cholesterol biosynthesis genes by iron loading in HUVECs, but not in the hepatic cell line Hep3B, suggesting

that endothelial cells rather than hepatocytes may be responsible for the changes observed in rodent models.

Importantly, we showed that iron interacts with the TNFα pathway. Iron excess worsened TNFα-induced apoptosis, as evidenced by increased levels of cleaved caspase-3. Iron loading further affected the TNFα pathway by inducing novel proteolytic processing of TNFR1 to promote accumulation of a shorter TNFR1 isoform in lipid rafts. In agreement, aberrations in cholesterol-rich lipid rafts are shown to promote apoptosis through TNFR1 (31). Similar to the adverse effects of iron, we noted accumulation of the short TNFR1 isoform after cholesterol treatment of HUVECs, and increased cleaved caspase-3 after co-treatment of HUVECs with cholesterol and TNFα. Examining the interaction of cholesterol and iron excess in HUVECs, we determined that cholesterol depletion was sufficient to rescue iron-potentiated apoptosis, but this occurred even in the presence of the shorter TNFR1 isoform. Interestingly, Hep3Bs and teloHAECs did not show altered susceptibility to apoptosis or cholesterol homeostasis with FAC loading but did demonstrate conservation of the TNFR1 processing mechanism. This implies that the generation of the short TNFR1 isoform is not sufficient to induce apoptosis. We speculate that susceptibility to iron-potentiated apoptosis requires both induction of cholesterol biosynthesis and alterations in the TNFR1 pathway manifested as processing of the short TNFR1 isoform, with endothelial cells being particularly sensitive to iron excess. Although there is a large body of evidence demonstrating that disease susceptibility and response to infection worsens with elevated iron stores (46-48), any interaction between iron and cytokine-driven apoptosis has not previously been reported. Future studies are needed to determine the contribution of iron loading to endothelial apoptosis in inflammatory conditions in vivo, particularly those characterized by increased TNFα.

In this study, we demonstrate how NTBI accumulation affects cultured endothelial cells. Iron loading induces cholesterol biosynthesis, promotes novel TNFR1 proteolytic processing, and sensitizes cells to TNFα-mediated apoptosis. We determined that during iron excess, the contribution of altered cholesterol homeostasis is the driving pathogenic mediator of apoptosis. Our findings have important implications for iron loading conditions, especially when inflammation is present. Altered cholesterol metabolism by iron excess in endothelial cells may contribute to iron-mediated toxicity in human iron overload disorders.

ACKNOWLEDGEMENTS

The authors thank the UCLA Lipidomics core for running the lipid compositional assays; Jeremy Papesh for performing the oxidized phospholipid assays; the UCLA Broad Stem Cell Center Microscopy Core for providing access to and training on confocal microscopes; and Veena Sangkhae for assisting with confocal microscopy. This study was supported by National Center for Advancing Translational Sciences UCLA Clinical and Translational Science Institute grants UL1TR000124, UL1TR001881, and R01 HD096863 (to EN), NIH Ruth L. Kirschstein National Research Service Awards T32GM065823 and F31HD097931 (to AF). The content is solely the responsibility of the authors and does not necessarily represent the official views of the National Institutes of Health.

AUTHOR CONTRIBUTIONS

ALF designed and performed experiments, analyzed data, and wrote the manuscript. DS performed experiments. NJP assisted with data analysis. DM assisted with experiments and data interpretation. STR assisted with data interpretation and edited the manuscript. TG and EN conceived the project, analyzed data, and wrote the manuscript.

MATERIALS & METHODS

Cell culture. Primary human umbilical vein endothelial cells (HUVECs) pooled from 10 donors were obtained from the American Type Culture Collection (ATCC #PCS-100-013). HUVECs were cultured in complete endothelial cell growth media (Cell Applications #211-500) at 37°C in a 5% CO_2 95% air atmosphere. For experiments, HUVECs were plated on collagen and experiments were performed from passages 3-6.

Reagents. Unless otherwise specified, all chemicals were obtained from Sigma-Aldrich. For iron loading studies, HUVECs were treated with 100 μM ferric ammonium citrate (FAC, MP biomedicals #158040), 100 μM ferrous ammonium sulfate (F-1543), 100 μM ferric chloride (#157740), 2 mg/ml apoferritin (#A-3641), 2 mg/ml holoferritin (#F-4503), 100 μM cupric chloride (#C-6917), or 100 μM zinc sulfate (Fisher #Z-58) for the indicated times.

Cholesterol-methylβcyclodextrin complexes were prepared as follows: a 5% w/v solution of methyl-β-cyclodextrin (#C4555) was prepared in water by heating to 70°C and 10 mg/ml cholesterol (#C8667) in 100% ethanol was added dropwise. Cholesterol-MβCD was stirred until the solution was clear, solvent was evaporated overnight by speed-vac, and cholesterol-MβCD was reconstituted in milliQ water to 2.5 mM, filtered, and stored at 4°C. HUVECs were treated with 0-50 μM cholesterol-MβCD for 40 h. For cholesterol depletion studies, HUVECs were treated with 1 μM U18666A (Cayman Chemicals #10009085), 0.3% 2-hydroxypropyl-beta-cyclodextrin (#H107), or 50 μM methylβcyclodextrin for the indicated times. For inflammation studies, HUVECs were treated with 50 ng/ml recombinant human TNFα (Biolegend #570104) for 6 or 16 h. The optimal time of culture with TNFα was based on preliminary studies testing concentration and time-dependence.

For protease inhibitor experiments, HUVECs were treated with 25 μM TAPI2 (Calbiochem, #579052), 1 μM DAPT (Calbiochem, #565770), or protease inhibitors (from Sigma #INHIB1) 6-aminohexanoic acid (E-ACA, 40 mM), antipain (100 μM), benzamidine HCl (4 mM), aprotinin (1 μM), bestatin (40 μM), chymostatin (100 μM), E-64 (10 μM), EDTA (1 mM), leupeptin (100 μM), pepstatin A (1 μM), phosphoramidon (10 μM), soybean trypsin inhibitor (STI, 5 μM), or protease inhibitor cocktail (PIC, 1:200, Sigma P1860) for 24 h.

The specific time of culture with FAC for cholesterol biosynthesis analysis, apoptosis, and TNFR1 processing was based on preliminary time-course experiments to determine iron loading of HUVECs and their susceptibility to apoptosis (see Figure 4B as an example).

RNA sequencing. RNA sequencing was performed by the UCLA Technology Center for Genomics and Bioinformatics Core Facility. Libraries for RNA-seq were prepared with Kapa Standard kit, and data were sequenced on Illumina HiSeq 3000 for a single-read 50bp run. Data quality check was done on Illumina SAV. Demultiplexing was performed with Illumina Bcl2fastq2 v 2.17 program. Total RNA from primary HUVECs was extracted using a RNeasy Micro kit (Qiagen) following the manufacturer's instructions. The reads were mapped to the latest UCSC transcript set using Bowtie2 version 2.1.0[1] and the gene expression level was estimated using RSEM v1.2.15 Trimmed mean of M-values were used to normalize gene expression. Differentially expressed genes were identified using the edgeR program. Expression data were analyzed by comparing control cells treated with solvent (N=3) to cells treated with 100 μM FAC (N=3) for 30 h. Genes identified by RNA sequencing were validated by quantitative real-time PCR.

Gene Expression Quantification by RT-PCR. HUVECs were lysed in TRIzol Reagent (Life Technologies) and total RNA was isolated by chloroform extraction. Five hundred ng of RNA was reverse transcribed using the iScript cDNA Synthesis Kit (Bio-RAD). Quantitative real-time PCR

was performed on cDNA using SsoAdvanced SYBR Green Supermix (Bio-RAD) on the CFX Real-Time PCR Detection System (Bio-RAD). Samples were measured in duplicate and target genes were normalized to *HPRT*. Data are expressed as $2^{-\Delta\Delta Ct}$. Primer sequences are provided in **Table 5-1**.

Lipid analysis. Lipid compositional analysis was performed by the UCLA Lipidomics Core Facility. For stable isotope labeling, HUVECs were cultured in endothelial cell growth media supplemented with 5 mM [$U^{13}C$]-D-glucose with and without 100 μM FAC for 30 or 40 h to assess the time course of cholesterol synthesis. Analysis of fatty acid and cholesterol synthesis in normal and iron-loaded HUVECs were performed on an Agilent 7890B/5977A GC-MS instrument. Data are presented as nmol synthesis/million cells and was estimated using isotopic spectral analysis.

Oxidized phospholipids were extracted from HUVECs treated with 100 μM FAC for 30 h, to determine whether membrane damage precedes cholesterol synthesis, using a biphasic butanol extraction. Cells were washed in PBS and collected in 1-butanol and transferred to a glass tube. 10% NaCl was added to each tube and centrifuged at 2,000 x g for 10-min at room temperature. The upper organic phase was evaporated under argon gas in a 37°C water bath and contents were solubilized in 150 μL methanol. Sample was centrifuged and clear supernatant was stored at -80°C until analysis. Oxidized phospholipids were measured by LC-MS using an internal oxPAPC standard.

Lipid raft isolation. Lipid rafts were isolated using discontinuous sucrose gradient centrifugation as previously described (49). Two 150 mm dishes of cultured HUVECs were combined for each treatment group. Detergent-insoluble membrane (DIG) fractionation was performed as described (50), using HUVECs cultured on 150 mm dishes. Equal volumes of proteins from each fraction

were resolved by SDS-PAGE. To identify the lipid raft and DIG fractions, equal volumes of proteins were dot blotted onto nitrocellulose and probed for ganglioside GM1.

Western Blotting. HUVECs were lysed by mechanical disruption in RIPA lysis buffer with freshly added protease inhibitors (Santa Cruz #SC-24948). Cell lysates were centrifuged at 21,000 x g for 15 min at 4°C and protein concentration was measured by the bicinchoninic acid assay using bovine serum albumin as a standard. Proteins (20 μg/lane) were separated by SDS-PAGE and transferred to nitrocellulose membranes. Membranes were blocked for 1 hr in 5% w/v dried nonfat milk or bovine serum albumin in TBS with 0.1% Tween-20 and incubated with primary antibodies in blocking buffer overnight at 4°C: cleaved caspase 3 (rabbit, 1:2,000, Cell Signaling Technology #9664), total caspase 3 (rabbit, 1:5,000, Cell Signaling Technology #9662), ferritin light chain (goat, 1:5,000, Novus Biologicals #NBP1-06986), ferritin heavy chain 1 (rabbit, 1:25,000, Cell Signaling Technology #4393), TNFR1 (rabbit, 1:5,000, Cell Signaling Technology #3736), Cholera Toxin B subunit peroxidase conjugate (1:10,000, Sigma #C3741) and β-Actin-peroxidase (1:50,000, Sigma A3854). The secondary reaction was performed using HRP-conjugated anti-rabbit or anti-goat IgG diluted 1:5,000 in blocking buffer. Protein blots were visualized by chemiluminescence using the ChemiDoc XRS+ imaging system and quantified using Image Lab software (Bio-RAD).

Filipin staining. Filipin staining was performed using a cholesterol cell-based assay kit following the manufacturer's instructions (Cayman Chemicals 10009779). Sytox green was used as a nuclear counterstain. Images were captured using a Zeiss LSM700 confocal microscope.

Lentivirus generation. Hek293t cells were grown to 70% confluence in 150 mm poly-D-lysine coated plates in 10% FCS with antibiotics. Hek293t cells were transfected with 2 μg C-terminal

V5-tagged TNFR1 pLX304 (DNasu #HsCD00438626), 5 μg pMD2.6 (Addgene #12259), 7.5 μg pMDLg/pRRE (Addgene #12251), and 7.5 μg pRSV-REV (Addgene #12253) using lipofectamine 2000 (ThermoFisher) for 16 h. Supernatant was replaced with fresh DMEM with 10% FCS. Viral supernatant was harvested after 24 and 48 h, pooled, and centrifuged at 300 x g for 5 min to pellet cells. Supernatant was filtered through a 0.45 μM low protein binding filter and stored at 4°C until plasmid digestion. To digest plasmid DNA, supernatant was treated with DNase-1 (Sigma D4527, 10 U per 10 μg of total plasmid DNA) at room temperature for 30 min followed by 4 h at 4°C. Virus was concentrated by ultracentrifugation at 70,000 x g for 2 h at 12°C. Viral pellets resuspended in HBSS were layered on 20% sucrose and centrifuged at 50,000 x g for 2 h at 12°C. Supernatant was snap frozen in liquid nitrogen and stored at -80°C.

For transduction experiments, HUVECs were treated with increasing volume of lentivirus for 10 h prior to incubation with solvent or 100 μM FAC for 24 h. Cell lysates were resolved by SDS-PAGE and probed for the transduced V5-tag.

Statistical Analysis. Data are presented as box and whisker plots, where the box plot indicates the upper 75th and lower 25th percentile, the whiskers indicate the 90th and 10th percentile. Within the box, the solid line indicates the median and the dotted line the mean. Statistical analysis was performed using SigmaPlot version 12.5 (Systat Software). Principal component analysis was performed using R and Transcripts Per kilobase Million values (TPM). Statistical differences between groups were determined by one-way ANOVA followed by Holm-Sidak for multiple comparisons for normally distributed values, one-way ANOVA on ranks followed by Dunn's method for multiple comparisons of nonparametric values, two-tailed Student's *t*-test for normally distributed values, or Mann-Whitney *U* test for non-parametric values. Statistical test, number of

biological replicates, and *P*-value are indicated in each figure panel. A *P*-value of <0.05 was considered significant.

Table 5-1. List of human primers for qRT-PCR

Gene name	Primer sequences
HPRT	Forward: 5'- GCC CTG GCG TCG TG ATTA GT -3' Reverse: 5'- AGC AAG ACG TTC AGT CCT GTC -3'
SREBP2	Forward: 5'- AGG AGA ACA TGG TGC TGA -3' Reverse: 5'- TAA AGG AGA GGC ACA GGA -3'
MVD	Forward: 5'- ATC AAG TAC TGG GGC AAG CG -3' Reverse: 5'- TTC AGC CAA ATC CGG TCC TC -3'
LDLR	Forward: 5'- GGG CTC TGT CCA TTG TCC TC -3' Reverse: 5'- ACC ATC TGT CTC GAG GGG TAG -3'
HMGCR	Forward: 5'- TTC GGT GGC CTC TAG TGA GAT -3' Reverse: 5'- GTC ACT GCT CAA AAC ATC CTC TTC -3'
TFRC	Forward: 5'- AGT TGA ACA AAG TGG CAC GAG -3' Reverse: 5'- AGC AGT TGG CTG TTG TAC CTC -3'
TNFRSF1A	Forward: 5'- CGC TAC CAA CGG TGG AAG TC -3' Reverse: 5'- CAA GCT CCC CCT CTT TTT CAG -3'
SREBP1a	Forward: 5'- TGC TGA CCG ACA TCG AAG AC -3' Reverse: 5'- CCA GCA TAG GGT GGG TCA AA -3'
SREBP1c	Forward: 5'- CCA TGG ATT GCA CTT TCG AA -3' Reverse: 5'- CCA GCA TAG GGT GGG TCA AA -3'
ACCA	Forward: 5'- CTG TAG AAA CCC GGA CAG TAG AAC -3' Reverse: 5'- GGT CAG CAT ACA TCT CCA TGT G -3'
FASN	Forward: 5'- TCG TGG GCT ACA GCA TGG T -3' Reverse: 5'- GCC CTC TGA AGT CGA AGA AGA A -3'

REFERENCES

1. Brissot, P., Ropert, M., Le Lan, C., and Loréal, O. (2012) Non-transferrin bound iron: A key role in iron overload and iron toxicity. *Biochimica et Biophysica Acta (BBA) - General Subjects* **1820**, 403-410
2. Evans, R. W., Rafique, R., Zarea, A., Rapisarda, C., Cammack, R., Evans, P. J., Porter, J. B., and Hider, R. C. (2008) Nature of non-transferrin-bound iron: studies on iron citrate complexes and thalassemic sera. *J Biol Inorg Chem* **13**, 57-74
3. Grootveld, M., Bell, J. D., Halliwell, B., Aruoma, O. I., Bomford, A., and Sadler, P. J. (1989) Non-transferrin-bound iron in plasma or serum from patients with idiopathic hemochromatosis. Characterization by high performance liquid chromatography and nuclear magnetic resonance spectroscopy. *J Biol Chem* **264**, 4417-4422
4. Emerit, J., Beaumont, C., and Trivin, F. (2001) Iron metabolism, free radicals, and oxidative injury. *Biomed Pharmacother* **55**, 333-339
5. Ganz, T. (2018) Iron and infection. *Int J Hematol* **107**, 7-15
6. Nemeth, E., Tuttle, M. S., Powelson, J., Vaughn, M. B., Donovan, A., Ward, D. M., Ganz, T., and Kaplan, J. (2004) Hepcidin Regulates Cellular Iron Efflux by Binding to Ferroportin and Inducing Its Internalization. *Science* **306**, 2090-2093
7. Kishimoto, M., Endo, H., Hagiwara, S., Miwa, A., and Noda, M. (2010) Immunohistochemical findings in the pancreatic islets of a patient with transfusional iron overload and diabetes: case report. *J Med Invest* **57**, 345-349
8. Lu, J. P., and Hayashi, K. (1994) Selective iron deposition in pancreatic islet B cells of transfusional iron-overloaded autopsy cases. *Pathol Int* **44**, 194-199
9. Simcox, J. A., and McClain, D. A. (2013) Iron and diabetes risk. *Cell Metab* **17**, 329-341

10. Ford, E. S., and Cogswell, M. E. (1999) Diabetes and serum ferritin concentration among U.S. adults. *Diabetes Care* **22**, 1978-1983

11. MacDonald, G. A., Bridle, K. R., Ward, P. J., Walker, N. I., Houglum, K., George, D. K., Smith, J. L., Powell, L. W., Crawford, D. H., and Ramm, G. A. (2001) Lipid peroxidation in hepatic steatosis in humans is associated with hepatic fibrosis and occurs predominately in acinar zone 3. *J Gastroenterol Hepatol* **16**, 599-606

12. Fujita, N., Miyachi, H., Tanaka, H., Takeo, M., Nakagawa, N., Kobayashi, Y., Iwasa, M., Watanabe, S., and Takei, Y. (2009) Iron overload is associated with hepatic oxidative damage to DNA in nonalcoholic steatohepatitis. *Cancer Epidemiol Biomarkers Prev* **18**, 424-432

13. Minamiyama, Y., Takemura, S., Kodai, S., Shinkawa, H., Tsukioka, T., Ichikawa, H., Naito, Y., Yoshikawa, T., and Okada, S. (2010) Iron restriction improves type 2 diabetes mellitus in Otsuka Long-Evans Tokushima fatty rats. *Am J Physiol Endocrinol Metab* **298**, E1140-1149

14. Chua, A. C., Drake, S. F., Herbison, C. E., Olynyk, J. K., Leedman, P. J., and Trinder, D. (2006) Limited iron export by hepatocytes contributes to hepatic iron-loading in the Hfe knockout mouse. *J Hepatol* **44**, 176-182

15. Kew, M. C. (2014) Hepatic iron overload and hepatocellular carcinoma. *Liver Cancer* **3**, 31-40

16. Wang, C. Y., and Knutson, M. D. (2013) Hepatocyte divalent metal-ion transporter-1 is dispensable for hepatic iron accumulation and non-transferrin-bound iron uptake in mice. *Hepatology* **58**, 788-798

17. Swaminathan, S., Fonseca, V. A., Alam, M. G., and Shah, S. V. (2007) The Role of Iron in

Diabetes and Its Complications. *Diabetes Care* **30**, 1926

18. Gujja, P., Rosing, D. R., Tripodi, D. J., and Shizukuda, Y. (2010) Iron overload cardiomyopathy: better understanding of an increasing disorder. *J Am Coll Cardiol* **56**, 1001-1012

19. Knutson, M. D. (2019) Non-transferrin-bound iron transporters. *Free Radical Biology and Medicine* **133**, 101-111

20. Jenkitkasemwong, S., Wang, C. Y., Coffey, R., Zhang, W., Chan, A., Biel, T., Kim, J. S., Hojyo, S., Fukada, T., and Knutson, M. D. (2015) SLC39A14 is required for the development of hepatocellular iron overload in murine models of hereditary hemochromatosis. *Cell Metab* **22**, 138-150

21. Liuzzi, J. P., Aydemir, F., Nam, H., Knutson, M. D., and Cousins, R. J. (2006) Zip14 (Slc39a14) mediates non-transferrin-bound iron uptake into cells. *Proc Natl Acad Sci U S A* **103**, 13612-13617

22. Canali, S., Wang, C. Y., Zumbrennen-Bullough, K. B., Bayer, A., and Babitt, J. L. (2017) Bone morphogenetic protein 2 controls iron homeostasis in mice independent of Bmp6. *Am J Hematol* **92**, 1204-1213

23. Canali, S., Zumbrennen-Bullough, K. B., Core, A. B., Wang, C. Y., Nairz, M., Bouley, R., Swirski, F. K., and Babitt, J. L. (2017) Endothelial cells produce bone morphogenetic protein 6 required for iron homeostasis in mice. *Blood* **129**, 405-414

24. Emerit, J., Beaumont, C., and Trivin, F. (2001) Iron metabolism, free radicals, and oxidative injury. *Biomedicine & Pharmacotherapy* **55**, 333-339

25. Meriwether, D., Sulaiman, D., Volpe, C., Dorfman, A., Grijalva, V., Dorreh, N., Solorzano-Vargas, R. S., Wang, J., O'Connor, E., Papesh, J., Larauche, M., Trost, H., Palgunachari, M.

N., Anantharamaiah, G. M., Herschman, H. R., Martin, M. G., Fogelman, A. M., and Reddy, S. T. (2019) Apolipoprotein A-I mimetics mitigate intestinal inflammation in a COX2-dependent inflammatory disease model. *The Journal of Clinical Investigation* **129**, 3670-3685

26. Wolf, B. B., Schuler, M., Echeverri, F., and Green, D. R. (1999) Caspase-3 Is the Primary Activator of Apoptotic DNA Fragmentation via DNA Fragmentation Factor-45/Inhibitor of Caspase-activated DNase Inactivation. *Journal of Biological Chemistry* **274**, 30651-30656
27. Porter, A. G., and Janicke, R. U. (1999) Emerging roles of caspase-3 in apoptosis. *Cell Death Differ* **6**, 99-104
28. Tartaglia, L. A., Ayres, T. M., Wong, G. H., and Goeddel, D. V. (1993) A novel domain within the 55 kd TNF receptor signals cell death. *Cell* **74**, 845-853
29. Reddy, P., Slack, J. L., Davis, R., Cerretti, D. P., Kozlosky, C. J., Blanton, R. A., Shows, D., Peschon, J. J., and Black, R. A. (2000) Functional analysis of the domain structure of tumor necrosis factor-alpha converting enzyme. *J Biol Chem* **275**, 14608-14614
30. Mullberg, J., Durie, F. H., Otten-Evans, C., Alderson, M. R., Rose-John, S., Cosman, D., Black, R. A., and Mohler, K. M. (1995) A metalloprotease inhibitor blocks shedding of the IL-6 receptor and the p60 TNF receptor. *J Immunol* **155**, 5198-5205
31. Legler, D. F., Micheau, O., Doucey, M. A., Tschopp, J., and Bron, C. (2003) Recruitment of TNF receptor 1 to lipid rafts is essential for TNFalpha-mediated NF-kappaB activation. *Immunity* **18**, 655-664
32. Engelmann, H., Aderka, D., Rubinstein, M., Rotman, D., and Wallach, D. (1989) A tumor necrosis factor-binding protein purified to homogeneity from human urine protects cells from tumor necrosis factor toxicity. *Journal of Biological Chemistry* **264**, 11974-11980

33. Chhibber-Goel, J., Coleman-Vaughan, C., Agrawal, V., Sawhney, N., Hickey, E., Powell, J. C., and McCarthy, J. V. (2016) γ-Secretase Activity Is Required for Regulated Intramembrane Proteolysis of Tumor Necrosis Factor (TNF) Receptor 1 and TNF-mediated Pro-apoptotic Signaling. *Journal of Biological Chemistry* **291**, 5971-5985

34. Resnik, N., Repnik, U., Kreft, M. E., Sepčić, K., Maček, P., Turk, B., and Veranič, P. (2015) Highly Selective Anti-Cancer Activity of Cholesterol-Interacting Agents Methyl-β-Cyclodextrin and Ostreolysin A/Pleurotolysin B Protein Complex on Urothelial Cancer Cells. *PLOS ONE* **10**, e0137878

35. Barman, S., and Nayak, D. P. (2007) Lipid raft disruption by cholesterol depletion enhances influenza A virus budding from MDCK cells. *J Virol* **81**, 12169-12178

36. Tabas, I. (2002) Consequences of cellular cholesterol accumulation: basic concepts and physiological implications. *The Journal of clinical investigation* **110**, 905-911

37. Horton, J. D., Goldstein, J. L., and Brown, M. S. (2002) SREBPs: activators of the complete program of cholesterol and fatty acid synthesis in the liver. *The Journal of Clinical Investigation* **109**, 1125-1131

38. Shimano, H., Horton, J. D., Shimomura, I., Hammer, R. E., Brown, M. S., and Goldstein, J. L. (1997) Isoform 1c of sterol regulatory element binding protein is less active than isoform 1a in livers of transgenic mice and in cultured cells. *The Journal of Clinical Investigation* **99**, 846-854

39. Horton, J. D., Shimomura, I., Brown, M. S., Hammer, R. E., Goldstein, J. L., and Shimano, H. (1998) Activation of cholesterol synthesis in preference to fatty acid synthesis in liver and adipose tissue of transgenic mice overproducing sterol regulatory element-binding protein-2. *The Journal of Clinical Investigation* **101**, 2331-2339

40. Horton, J. D., Shah, N. A., Warrington, J. A., Anderson, N. N., Park, S. W., Brown, M. S., and Goldstein, J. L. (2003) Combined analysis of oligonucleotide microarray data from transgenic and knockout mice identifies direct SREBP target genes. *Proceedings of the National Academy of Sciences* **100**, 12027

41. Fields, M., and Lewis, C. G. (1999) Cholesterol-lowering nature of unsaturated fat in rats may be due to its inability to increase hepatic iron. *Metabolism* **48**, 200-204

42. Brunet, S., Thibault, L., Delvin, E., Yotov, W., Bendayan, M., and Levy, E. (1999) Dietary iron overload and induced lipid peroxidation are associated with impaired plasma lipid transport and hepatic sterol metabolism in rats. *Hepatology* **29**, 1809-1817

43. Graham, R. M., Chua, A. C. G., Carter, K. W., Delima, R. D., Johnstone, D., Herbison, C. E., Firth, M. J., O'Leary, R., Milward, E. A., Olynyk, J. K., and Trinder, D. (2010) Hepatic iron loading in mice increases cholesterol biosynthesis. *Hepatology* **52**, 462-471

44. Pigeon, C., Legrand, P., Leroyer, P., Bouriel, M., Turlin, B., Brissot, P., and Loreal, O. (2001) Stearoyl coenzyme A desaturase 1 expression and activity are increased in the liver during iron overload. *Biochim Biophys Acta* **1535**, 275-284

45. Ramos, E., Kautz, L., Rodriguez, R., Hansen, M., Gabayan, V., Ginzburg, Y., Roth, M.-P., Nemeth, E., and Ganz, T. (2011) Evidence for distinct pathways of hepcidin regulation by acute and chronic iron loading in mice. *Hepatology* **53**, 1333-1341

46. Drakesmith, H., and Prentice, A. (2008) Viral infection and iron metabolism. *Nat Rev Microbiol* **6**, 541-552

47. Stefanova, D., Raychev, A., Arezes, J., Ruchala, P., Gabayan, V., Skurnik, M., Dillon, B. J., Horwitz, M. A., Ganz, T., Bulut, Y., and Nemeth, E. (2017) Endogenous hepcidin and its agonist mediate resistance to selected infections by clearing non-transferrin-bound iron.

Blood **130**, 245-257

48. Arezes, J., Jung, G., Gabayan, V., Valore, E., Ruchala, P., Gulig, P. A., Ganz, T., Nemeth, E., and Bulut, Y. (2015) Hepcidin-induced hypoferremia is a critical host defense mechanism against the siderophilic bacterium Vibrio vulnificus. *Cell Host Microbe* **17**, 47-57
49. Gajate, C., and Mollinedo, F. (2017) Isolation of Lipid Rafts Through Discontinuous Sucrose Gradient Centrifugation and Fas/CD95 Death Receptor Localization in Raft Fractions. in *CD95: Methods and Protocols* (Legembre, P. ed.), Springer New York, New York, NY. pp 125-138
50. LEGLER, D. F., DOUCEY, M.-A., CEROTTINI, J.-C., BRON, C., and LUESCHER, I. F. (2001) Selective inhibition of CTL activation by a dipalmitoyl-phospholipid that prevents the recruitment of signaling molecules to lipid rafts. *The FASEB Journal* **15**, 1601-1603

SUPPLEMENTAL MATERIALS

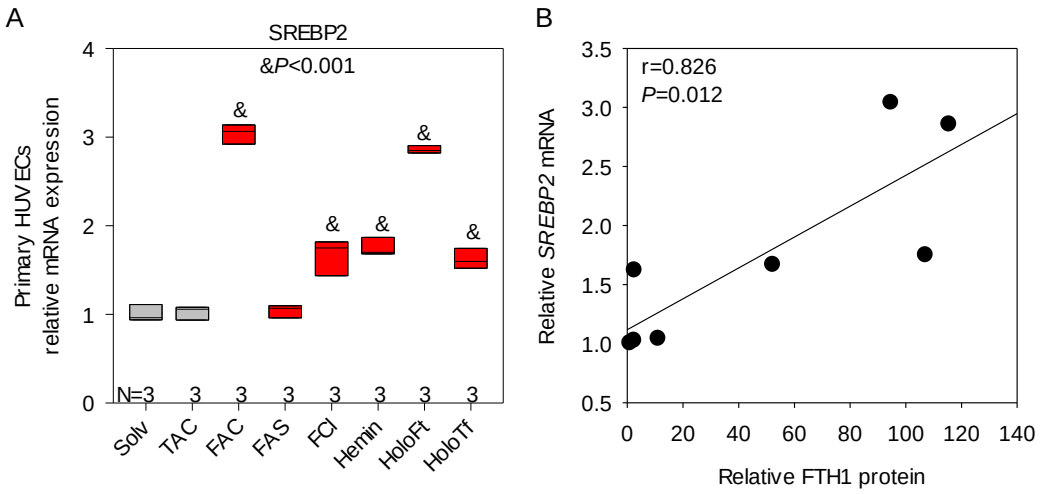

Supplemental Figure 5-1. Cellular iron loading induces *SREBP2* mRNA expression. Primary HUVECs were treated with solvent or triammonium citrate (TAC, 100 μM), ferric ammonium citrate (FAC, 100 μM), ferric ammonium sulfate (FAS, 100 μM), ferric chloride (FCl, 100 μM), hemin chloride (20 μM), holo-ferritin (Ft, 2 mg/ml) or holo-transferrin (Tf, 100 μM) for 40 h. N=3 biological replicates per condition. **(A)** *SREBP2* mRNA expression relative to solvent. Data are expressed as $2^{-\Delta\Delta Ct}$. **(B)** Pearson correlation between *SREBP2* mRNA and ferritin heavy chain 1 (FTH1) protein in HUVECs. Statistical differences between groups were determined by one-way ANOVA with Holm-Sidak method for multiple comparisons for normally distributed values (indicated by &).

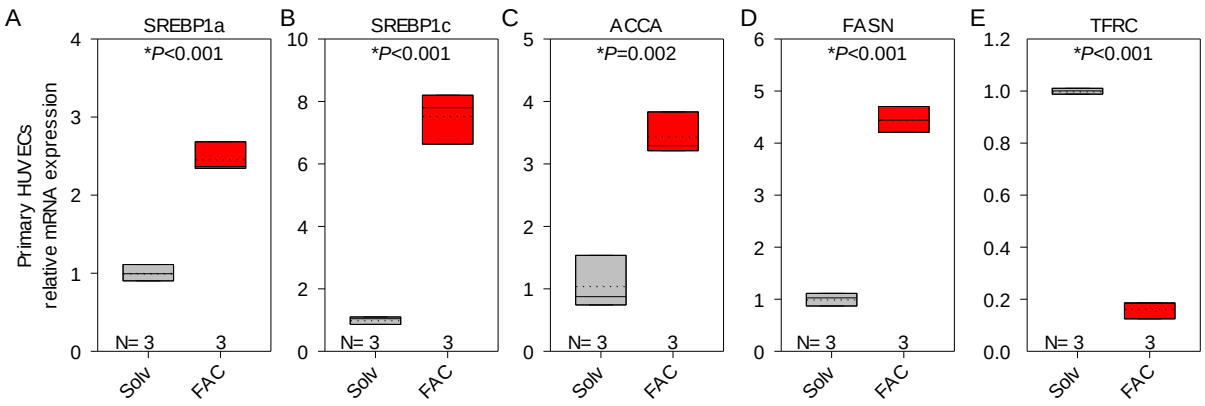

Supplemental Figure 5-2. Iron induces SREBP-1 target genes in HUVECs. Primary HUVECs were treated with solvent or 100 μM ferric ammonium citrate (FAC) for 40 h. **(A-E)** qPCR analysis of fatty acid biosynthesis genes *SREBP1a*, *SREBP1c*, *ACCA*, *FASN*, and iron importer *TFRC*. Data are expressed as $2^{-\Delta\Delta Ct}$. Number of biological replicates are indicated above the *x*-axis. Statistical differences between groups were determined by Student's *t*-test for normally distributed values (indicated by *).

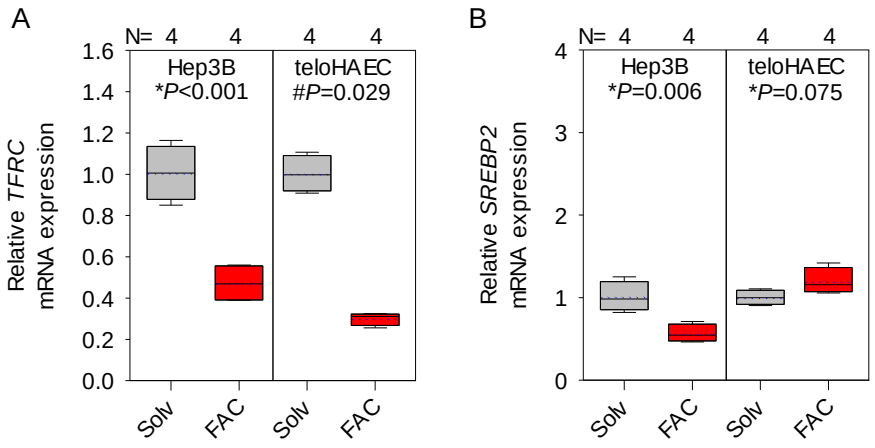

Supplemental Figure 5-3. Cell panel for induction of *SREBP2* by iron loading. Human hepatic cell line Hep3B and immortalized endothelial cells teloHAEC were treated with 100 μM FAC for 40 h. **(A)** *TFRC* and **(B)** *SREBP2* mRNA expression was determined by qRT-PCR and data are shown as $2^{-\Delta\Delta Ct}$. Number of replicates are indicated above the *x*-axis. Statistical differences between groups were determined by Student's *t*-test for normally distributed values (indicated by *) or Mann-Whitney *U* for non-normally distributed values (indicated by #).

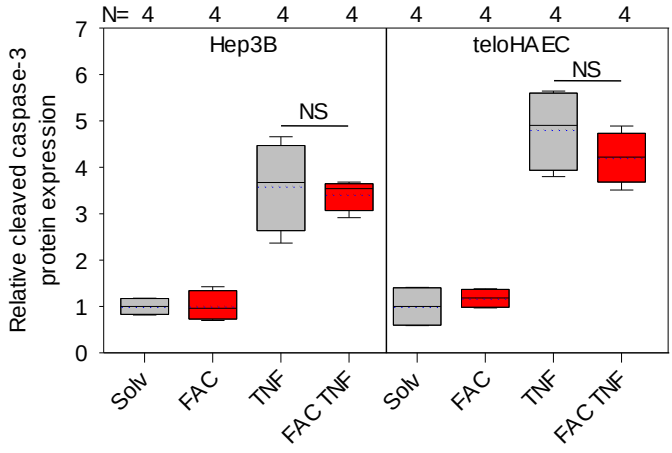

Supplemental Figure 5-4. Cell panel for potentiation of TNFα-induced apoptosis by iron loading. Human cell lines Hep3B and immortalized endothelial teloHAECs were treated with 100 μM FAC for 24 h following stimulation with 50 ng/ml TNFα for 16 h in normal or FAC-supplemented media. Cleaved caspase-3 protein expression was determined by Western blotting and normalized to β-actin. Number of replicates are indicated above the *x*-axis. Statistical differences between groups were determined by one-way ANOVA.

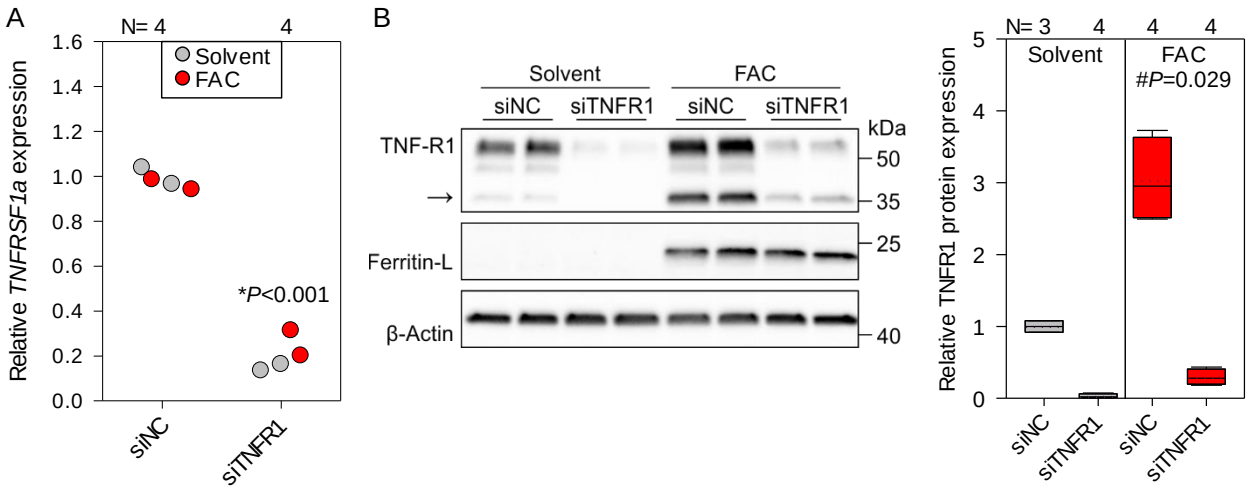

Supplemental Figure 5-5. Validation of TNFR1 antibody in HUVECs. HUVECs were reverse transfected with 12.5 pmol negative control siRNA or siRNA targeting TNFR1 for 48 h and treated with 100 μM FAC for 24h. **(A)** *TNFRSF1A* mRNA expressed as $2^{-\Delta\Delta Ct}$ and **(B)** TNFR1 protein expression by Western blotting. β-actin was used as a loading control. Representative image from N=4 independent experiments. Number of replicates are indicated above the figure panels. Statistical differences between groups were determined by Student's *t*-test for normally distributed values (indicated by *) or Mann-Whitney *U* for non-normally distributed values (indicated by #).

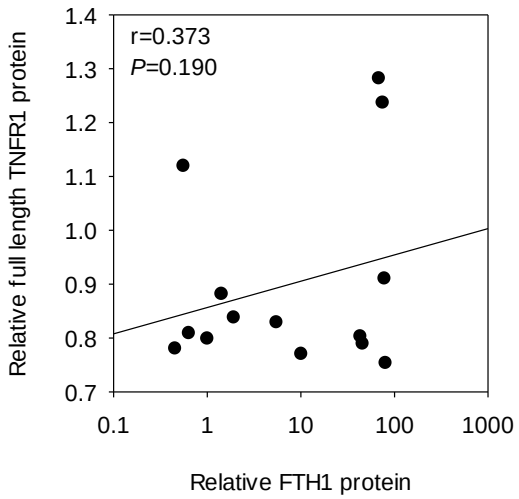

Supplemental Figure 5-6. Full length TNFR1 does not correlate with cellular iron loading in HUVECs. HUVECs were treated with solvent or 100 μM FAC, ferric ammonium sulfate (FAS, 100 μM), ferric chloride ($FeCl_3$, 100 μM), apo-ferritin (FT, 2 mg/ml), holo-FT (2 mg/ml), copper chloride ($CuCl_2$, 100 μM), or zinc sulfate ($ZnSO_4$, 100 μM) for 24 h. Pearson correlation between ferritin heavy chain (FTH1) and TNFR1 protein by Western blotting and normalized to β-actin.

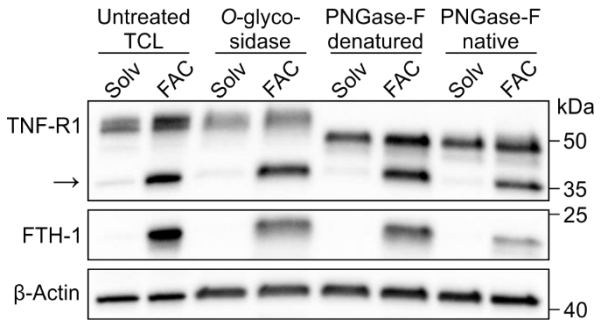

Supplemental Figure 5-7. TNFR1 glycosylation in HUVECs. HUVECs were treated with 100 μM FAC for 30 h. Western blot for full-length and short TNFR1 isoform (indicated by arrow) of solvent and FAC-treated lysates after incubation with or without *O*-glycosidase or PNGase F. β-actin was used as a loading control.

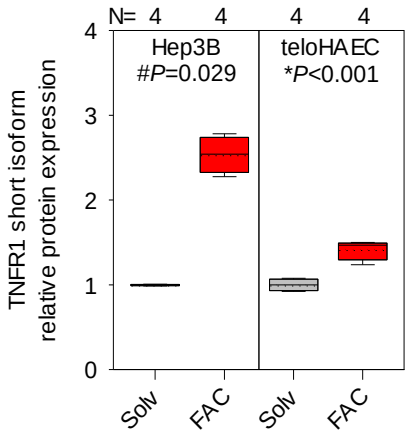

Supplemental Figure 5-8. Induction of a short isoform of TNFR1 with iron loading in different cell lines. Human hepatic cell line Hep3B and immortalized endothelial teloHAECs were treated with 100 μM FAC for 40 h. TNFR1 short isoform protein levels were determined by Western blotting and normalized to β-actin. Number of replicates are indicated above the *x*-axis. Statistical differences between groups were determined by Student's *t*-test for normally distributed values (indicated by *) or Mann-Whitney *U* for non-normally distributed values (indicated by #).

Supplemental materials & methods

Reagents

Unless otherwise specified, all chemicals were obtained from Sigma-Aldrich. For the indicated times, HUVECs were treated with ferric ammonium citrate (FAC, 100 μM), ferrous ammonium sulfate (100 μM), ferric chloride (100 μM), hemin chloride (20 μM, #H-1652), holoferritin (2 mg/ml), holotransferrin (100 μM, Serologicals Corporation #4455-01), or triammonium citrate (100 μM , #A1332) as a control.

siRNA knockdown of TNFR1

SMARTPool siRNA targeting human TNFR1 (Dharmacon SMARTPool L-005197-00-0005) was used to suppress *TNFRSF1A* expression. Non-targeting siRNA was used as a control (Dharmacon D-001810-10-05). Reverse transfection was performed using Lipofectamine RNAiMAX (ThermoFisher) in Opti-MEM media following the manufacturer's protocol to yield a final concentration of 12.5 pmol siRNA per well. HUVECs were reverse transfected for 48 h and treated with 100 μM FAC for 24 h. Knockdown was confirmed by qRT-PCR and immunoblotting.

TNFR1 deglycosylation

HUVECs were treated with 100 μM FAC for 30 h. Cell lysates were digested with O-glycosidase to cleave O-glycans or PNGase F to cleave N-linked glycans following the manufacturer's protocol (New England Biolabs #E0540S). N-linked deglycoslyation was performed under denaturing and non-denaturing conditions.

CHAPTER 6: MATERNAL IRON DEFICIENCY WORSENS INFLAMMATION-INDUCED EMBRYOTOXICITY

INTRODUCTION

Pregnancy is a major challenge to iron homeostasis as 30% of a woman's total body iron is needed to support the development of the placenta and fetus while maintaining maternal health [1, 2]. Pregnancy's large iron requirement predisposes to iron deficiency and women with insufficient iron stores before becoming pregnant have an increased risk of developing iron deficiency anemia, a common global health problem, affecting >20% of pregnant women in developed countries and >60% in some developing countries [3, 4]. In mice, maternal iron deficiency anemia during pregnancy is detrimental to embryo iron endowment [5]. In humans, iron deficiency anemia during pregnancy is associated with increased maternal morbidity and mortality, preterm birth, low birth weight, cognitive defects in newborns and impaired immune function [6-13].

Iron disorders during pregnancy are common. Iron deficiency is characterized by depletion of iron stores, and eventually results in hypoferremia and anemia. Iron restriction on the other hand is characterized by iron sequestration in macrophages and low plasma iron levels, usually as a result of inflammation. Inflammation induces the iron regulatory hormone hepcidin, blocking iron transport into plasma, and lowering plasma iron levels [14, 15]. Although inflammation-induced hypoferremia is important in host [16, 17], it can be maladaptive with chronic inflammation and contribute to iron-restricted anemia [18].

The maternal immune system is important for healthy pregnancy [19, 20], and is involved in implantation, angiogenesis and vascular remodeling at the maternal-fetal interface, and in the development of the fetal immune system. Excessive systemic maternal inflammation, as in complicated pregnancies, is associated with adverse outcomes including spontaneous abortion, preterm labor, intrauterine growth restriction, fetal death, gross developmental abnormalities, and autistic behaviors in offspring [21-24]. How maternal inflammation causes these effects is not well

understood but is likely dependent on the effect of maternal or fetal-derived cytokines on the dam, placenta, and embryo [19, 21, 22, 25-28]. In developing countries, inflammation is common because of endemic infections. In industrialized countries, common conditions associated with chronic inflammation include obesity and autoimmune diseases, and for acute inflammation, infections.

Epidemiological studies show a U-shaped risk curve between iron marker ferritin and pregnancy complications including preterm birth [29-31]. Low serum ferritin occurs with iron deficiency, but high serum ferritin occurs with both iron excess and inflammation. In Chapter 3, we evaluated the right side of the U-shaped curve, and noted an adverse interaction between iron excess and inflammation during pregnancy where the combination of the two caused adverse outcomes including severe embryo malformations and demise. These adverse outcomes did not occur in inflamed dams with normal iron status.

In this Chapter, we evaluated if iron deficiency interacts with inflammation. We used two clinically relevant models of inflammation. Acute maternal inflammation was caused by LPS injection during pregnancy, mimicking a bacterial infection. Chronic mild inflammation was caused by diet-induced obesity. Surprisingly, outcomes in iron-deficient inflamed dams were as or more severe than those with the iron-loading diet. Acute inflammation in iron-deficient dams led to fetal demise, and obesity in iron-deficient dams led to fetal malformations. We demonstrate that maternal iron deficiency potentiates apoptosis in the placental and fetal tissues, primarily affecting endothelial cells. Notably, we found that iron deficiency induces TNFα-receptor 1 (TNFR1) and worsens LPS-induced inflammation in the placenta, suggesting possible mechanisms of adverse fetal outcomes. We extended our study to non-pregnant mice and found that iron deficiency potentiates apoptosis of organs, primarily the lung, suggesting that the mechanism is more common and may be relevant to inflammatory disorders beyond pregnancy. Considering the global

prevalence of iron deficiency, and the increasing occurrence of inflammatory conditions such as obesity, our findings have the potential to explain commonly observed pregnancy complications and could eventually influence the clinical management of pregnant women worldwide.

RESULTS

Maternal iron deficiency potentiates inflammation-induced pregnancy complications. We modeled iron deficiency by feeding C57BL/6J females an iron-poor diet (4 ppm iron) for 1-3 weeks prior to mating and throughout pregnancy. Control females were maintained on an iron-

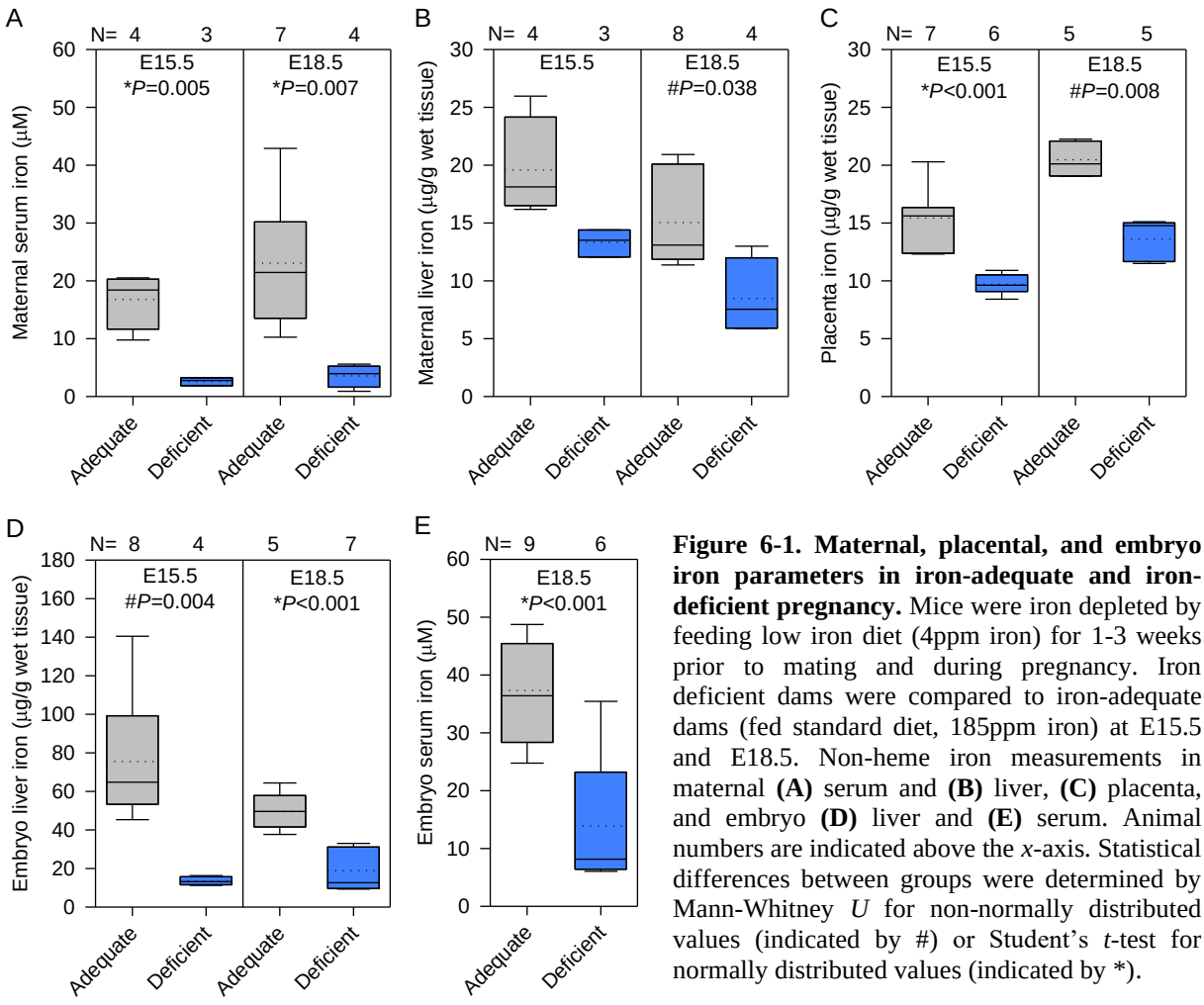

Figure 6-1. Maternal, placental, and embryo iron parameters in iron-adequate and iron-deficient pregnancy. Mice were iron depleted by feeding low iron diet (4ppm iron) for 1-3 weeks prior to mating and during pregnancy. Iron deficient dams were compared to iron-adequate dams (fed standard diet, 185ppm iron) at E15.5 and E18.5. Non-heme iron measurements in maternal **(A)** serum and **(B)** liver, **(C)** placenta, and embryo **(D)** liver and **(E)** serum. Animal numbers are indicated above the *x*-axis. Statistical differences between groups were determined by Mann-Whitney *U* for non-normally distributed values (indicated by #) or Student's *t*-test for normally distributed values (indicated by *).

Table 6-1. Maternal hematological parameters in mouse pregnancy

	Iron-deficient	**Iron-adequate**	***P*-value**	**Iron-deficient**	**Iron-adequate**	***P*-value**
	E15.5 (N=3)	E15.5 (N=4)		E18.5 (N=4)	E18.5 (N=6)	
RBC (10^6/µL)	7.3±0.7	8.3±0.5	*P*=0.089	7.5±0.7	8.1±0.7	*P*=0.215
Hb (g/dL)	9.9±0.9	12.2±0.6	***P*=0.011**	8.5±0.4	11.9±0.6	***P*<0.001**
HCT (%)	28.4±3.3	35.2±1.7	***P*=0.015**	35.0±5.2	40.5±2.8	*P*=0.061
MCV (fL)	38.0±2.9	42.6±0.8	***P*=0.025**	46.6±2.7	50.2±5.0	*P*=0.225
MCH (pg)	13.6±0.2	14.8±0.2	***P*<0.001**	11.5±0.8	14.5±0.7	***P*=0.010**
MCHC (pg/dL)	35.0±1.0	34.7±0.7	*P*=0.629	24.7±3.0	29.0±3.3	*P*=0.066

Table 6-1. Maternal hematological parameters in mouse pregnancy. Hematological parameters of E15.5 and E18.5 pregnant iron-deficient wild type dams (fed low iron diet) and iron-adequate wild type dams (fed standard diet). Data are presented as mean ± SD. RBC, red blood cell; Hb, hemoglobin; HCT, hematocrit; MCV, mean corpuscular volume; MCH, mean corpuscular hemoglobin; MCHC, mean corpuscular hemoglobin concentration. Statistical differences between groups were determined by t-test.

adequate diet (185 ppm iron). Iron-deficient dams were compared to iron-adequate dams on E15.5 and E18.5 of pregnancy. At both gestational ages, pregnant dams on the iron-poor diet had lower serum iron (E15.5, *P*=0.005; E18.5, *P*=0.007) and liver iron concentrations (E18.5, *P*=0.038) **(Figure 6-1A, B)**, and lower hemoglobin concentrations (~2 g/dL lower by E15.5, *P*=0.011 and ~3 g/dL lower by E18.5, *P*<0.001) **(Table 6-1)**, confirming that the dams were iron-deficient and anemic. Placentas from iron-deficient dams were mildly iron deficient with ~25% less iron at E15.5 (*P*<0.001) and E18.5 (*P*=0.008) **(Figure 6-1C)**. Embryos from iron-deficient dams were severely iron deficient, as reflected by ~70% lower liver iron stores (E15.5, *P*=0.004; E18.5, *P*<0.001) **(Figure 6-1D)** and 60% lower serum iron levels (*P*<0.001) **(Figure 6-1E)**.

Maternal systemic inflammation was elicited in iron-adequate and iron-deficient pregnant dams by a single subcutaneous injection of LPS (0.5 µg/g) in the interscapular area during the second trimester on E8.5 **(Figure 6-2A)**. LPS treatment of dams with normal iron status on E8.5 caused embryo loss in 22% of pregnancies (N=9 dams), but surviving embryos were normal **(Figure 6-2B)**. However, when the dam was both iron-deficient and LPS-injected, all pregnancies were aborted (N=3 dams) and we did not obtain live embryos to evaluate **(Figure 6-2B)**. Since

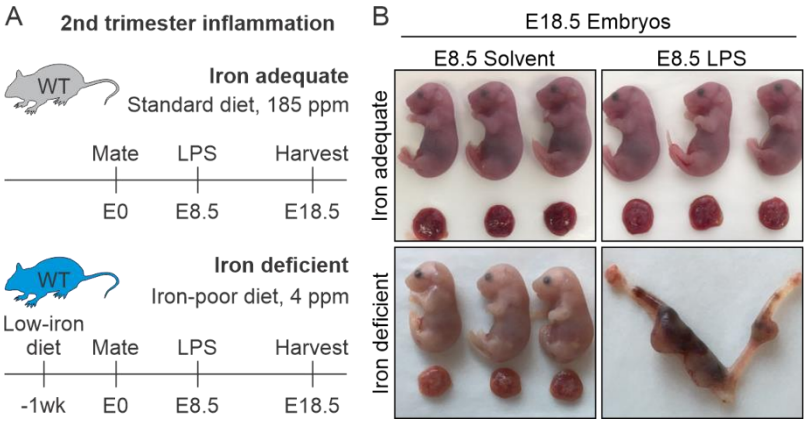

Figure 6-2. Adverse synergy between maternal iron deficiency and acute inflammation in the second trimester. **(A)** Maternal inflammation was induced in the second trimester by a single subcutaneous injection of LPS on E8.5 in pregnant iron-adequate (fed standard diet) and iron-deficient (fed iron-poor diet) dams, and embryos were harvested on E18.5. **(B)** LPS or iron-poor diet alone did not affect embryo development. The combination of iron deficiency and LPS caused embryo loss (uterus with resorptions depicted).

LPS injection in early pregnancy limited embryo analysis, we evaluated the effect of inflammation in later pregnancy. Iron-adequate and iron-deficient pregnant dams were injected with LPS on E15.5 and outcomes were evaluated 24 h later **(Figure 6-3A)**. Consistent with other reports [32], LPS injection caused preterm birth in 50% of dams with normal status (N=8 dams). However, in iron-deficient dams, LPS on E15.5 caused embryonic demise and resorption **(Figure 6-3B)**, affecting 60% of embryos (N=42 embryos from 5 dams) (P<0.001) **(Figure 6-3C)**. Taken together, our data show that maternal iron deficiency potentiates inflammation-induced embryo injury.

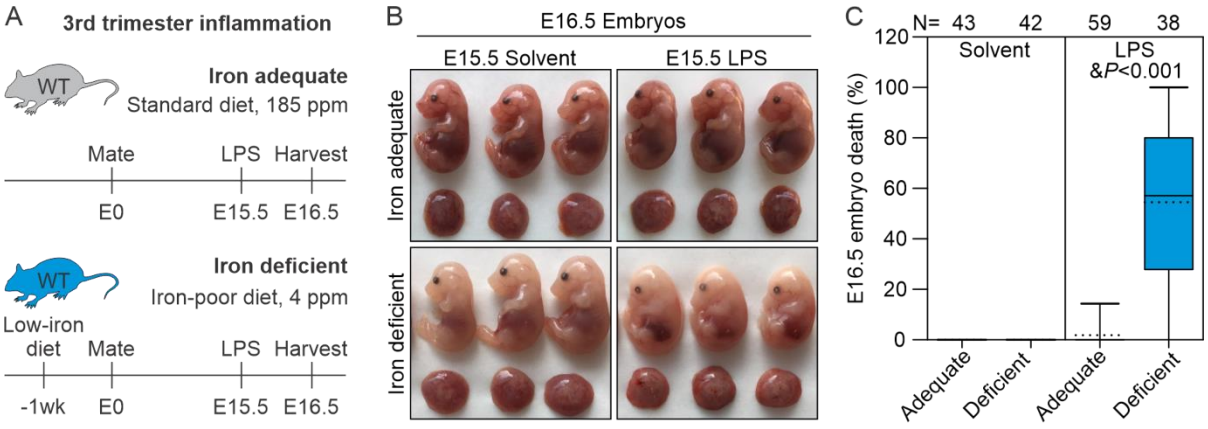

Figure 6-3. Adverse synergy between maternal iron deficiency and acute inflammation in the third trimester. **(A)** Maternal inflammation was induced in the third trimester by a single subcutaneous injection of LPS on E15.5 in iron-adequate (fed standard diet) and iron-deficient (fed iron-poor diet) dams and embryos were evaluated 24 h later. **(B)** LPS or iron-poor diet alone did not affect embryo health. Iron deficiency potentiated LPS-induced embryo death and resorption. Animal numbers are indicated above the *x*-axis. Statistical differences between groups were determined by two-way ANOVA (indicated by &).

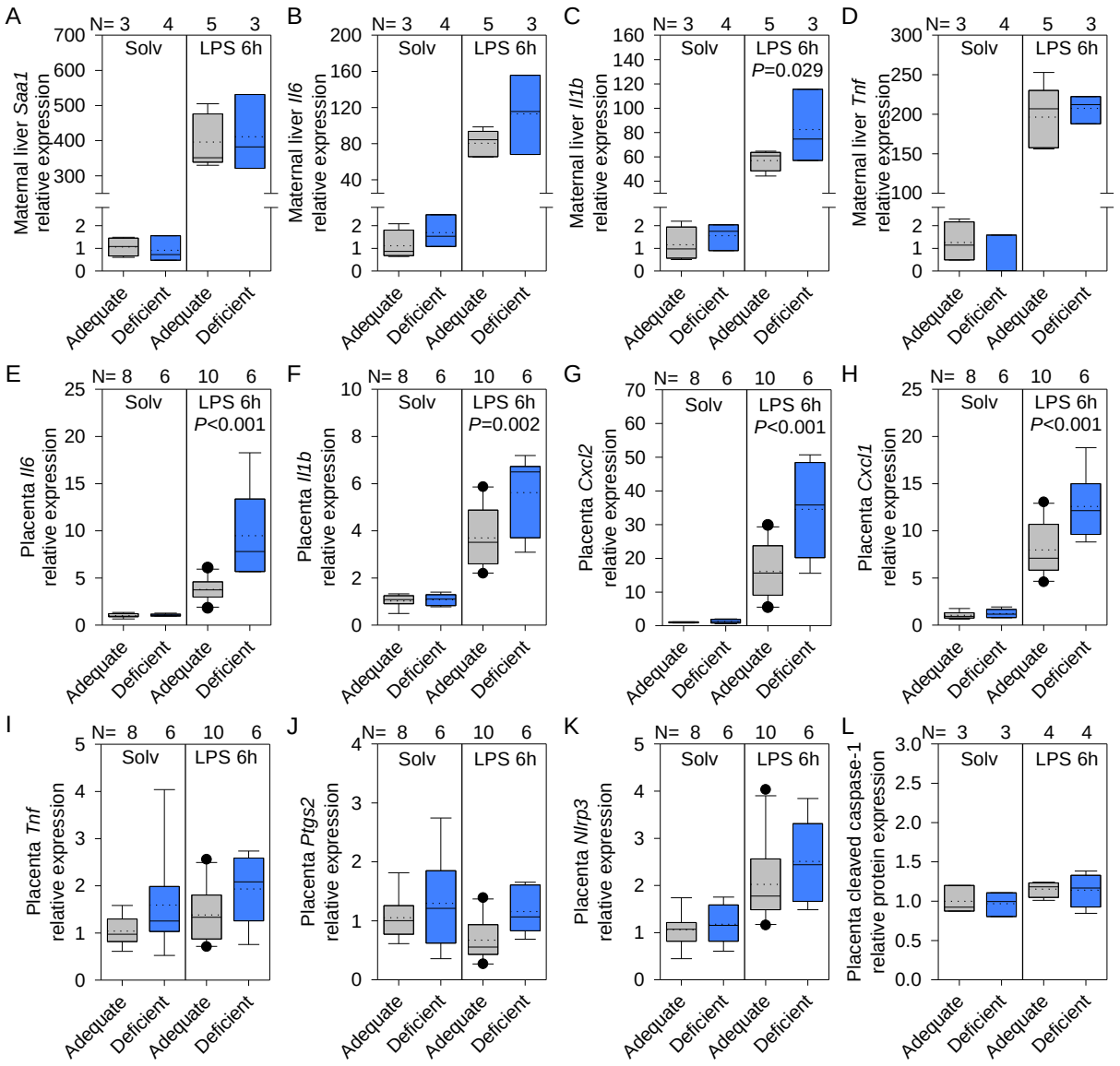

Figure 6-4. Maternal iron deficiency potentiates placental inflammation. Maternal inflammation was induced in the third trimester (E15.5) by a single subcutaneous injection of LPS in iron-adequate (fed standard diet) and iron-deficient (fed iron-poor diet) dams. Maternal and placental inflammation was evaluated 6h later. Maternal liver **(A)** serum amyloid A-1 (*Saa1*), **(B)** *Il*6, **(C)** *Il1b* and **(D)** *Tnf* expression relative to *Hprt*. Placental **(E)** *Il6*, **(F)** *Il1b*, **(G)** *Cxcl2*, **(H)** *Cxcl1*, and **(I)** *Tnf*, **(J)** *Ptgs2*, and **(K)** *Nlrp3* expression relative to *Rpl4*. **(L)** Placenta cleaved caspase-1 protein expression relative to β-Actin. Animal numbers are indicated above the *x*-axis. Statistical differences between groups were determined by two-way ANOVA.

Maternal iron deficiency potentiates placental inflammation and apoptosis of placental and fetal endothelium. We evaluated whether maternal iron deficiency potentiates canonical inflammatory pathways in the dam, placenta, or embryo by measuring mRNA expression of

inflammatory markers in maternal liver, placenta, and embryo liver. In dams, LPS potently induced hepatic expression of serum amyloid A-1 (*Saa1*), interleukin (IL)-6 (*Il6*), and *Tnf* but these inductions were similar between iron adequate and iron deficient dams, whereas induction in *Il1b* was mildly potentiated by iron deficiency (P=0.029) **(Figure 6-4, A-D)**. In placentas, induction of *Il6* (P<0.001), *Il1b* (P=0.002), and chemokines *Cxcl1* and *Cxcl2* (P<0.001) were strongly potentiated in iron-deficient pregnancies, whereas *Tnf* was only mildly potentiated **(Figure 6-4,E-I)**. We did not detect any changes in inflammatory markers in embryo livers (data not shown),

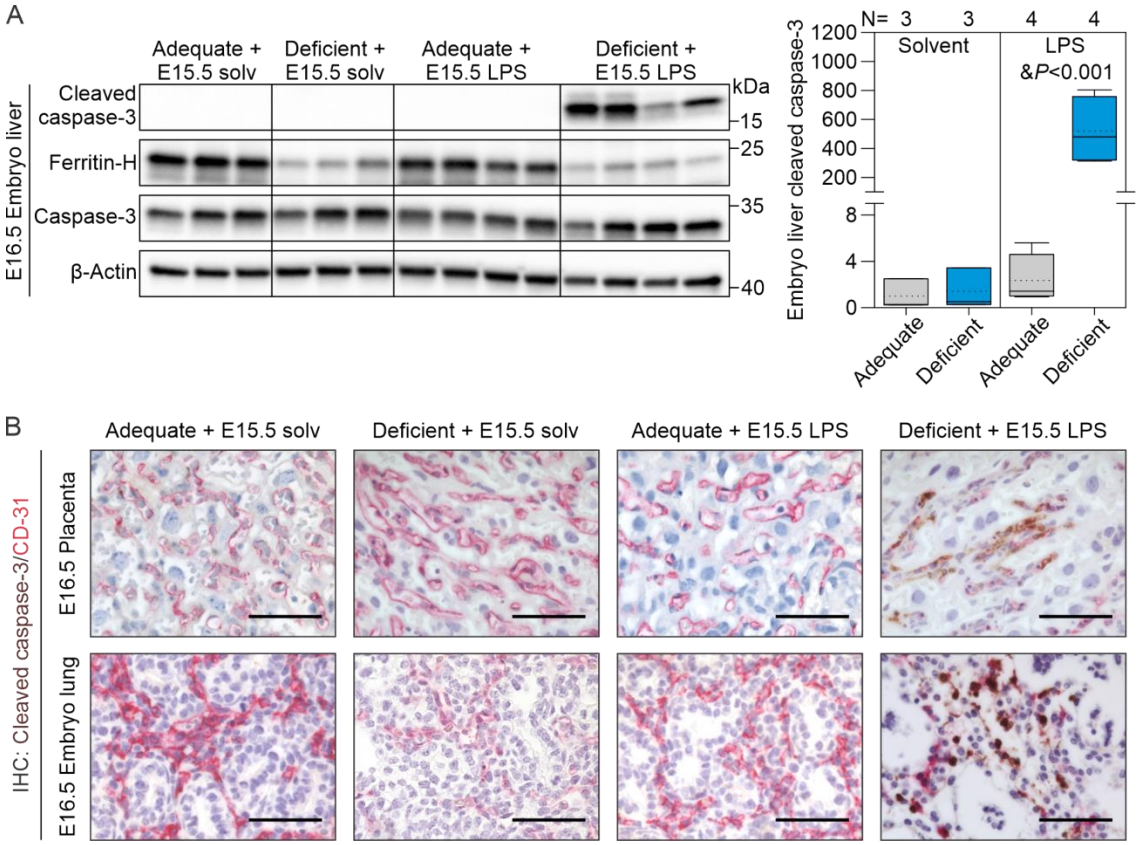

Figure 6-5. Maternal iron deficiency potentiates apoptosis of placental and fetal endothelium. Maternal inflammation was induced in the third trimester by a single subcutaneous injection of LPS on E15.5 in iron-adequate (fed standard diet) and iron-deficient (fed iron-poor diet) dams and embryos were evaluated 24 h later. **(A)** Western blot of whole embryo liver lysate for apoptotic marker cleaved caspase-3. Animal numbers are indicated above the *x*-axis. **(B)** Immunohistochemistry of paraffin-embedded placentas and whole embryos for cleaved caspase-3 (brown) and endothelial marker Cd31 (red). Scale bar= 50µm. Representative image of N=3 sections/group. Statistical differences between groups were determined by two-way ANOVA (indicated by &).

showing that inflammation is restricted to the dam and placenta, and that placental inflammation is exacerbated by maternal iron deficiency. Furthermore, we did not detect any iron-dependent difference in *Ptgs2* **(Figure 6-4J)**, a putative marker of ferroptosis onset [33]. Given that IL-1β is a product of inflammasome activation [34], we measured inflammasome *Nlrp3* mRNA and cleaved caspase-1 protein expression in placentas but did not detect any iron-dependent differences **(Figure 6-4, K-L)** , suggesting that cell death does not occur through pyroptosis or ferroptosis.

We evaluated the mechanism of cell death leading to embryo demise and detected apoptotic marker cleaved caspase-3 in embryo liver only from dams that were both iron deficient and LPS-injected, and did not occur with iron deficiency or LPS alone **(Figure 6-5A)**. Immunohistochemistry localized apoptosis to endothelial cells in the placenta, embryo lung, and other embryonic tissues **(Figure 6-5B)**, indicating that endothelial cells are the primary apoptotic target and are most susceptible to inflammation-driven apoptosis in the setting of iron deficiency.

Iron deficiency increases the susceptibility of cultured endothelial cells to TNFα-mediated apoptosis. To identify the underlying mechanisms of apoptosis in iron-deficient endothelial cells, we developed an in vitro model using primary human umbilical vein endothelial cells (HUVECs). Iron deficiency was induced in HUVECs by treating cells with 100 μM iron chelator deferoxamine (DFO) for 24h. Control and iron-deficient HUVECs were stimulated with LPS (2 ug/ml) and a panel of cytokines (all 50 ng/ml) IL-6, IFNγ, IL-1β, and TNFα to evaluate apoptosis **(Figure 6-6A)**. Neither LPS, IL-6, nor IFNγ induced cleaved caspase-3 expression, and IL-1β mildly potentiated cleaved caspase-3 in iron deficient cells. However, cleaved caspase-3 expression induced by TNFα was strongly potentiated by DFO ($P<0.001$) **(Figure 6-6A)**, suggesting that TNFα in maternal circulation may be causing fetal demi se in our mouse model. This finding was

confirmed in two other endothelial cell types (both $P<0.001$), primary human pulmonary artery endothelial cells (HPAEC) and immortalized human aorta endothelial cells (teloHAEC), the latter being susceptible to DFO-induced apoptosis even without TNFα ($P=0.002$) **(Figure 6-6B)**. This effect was not related to activation of the HIFα pathway by DFO because cotreatment of HUVECs

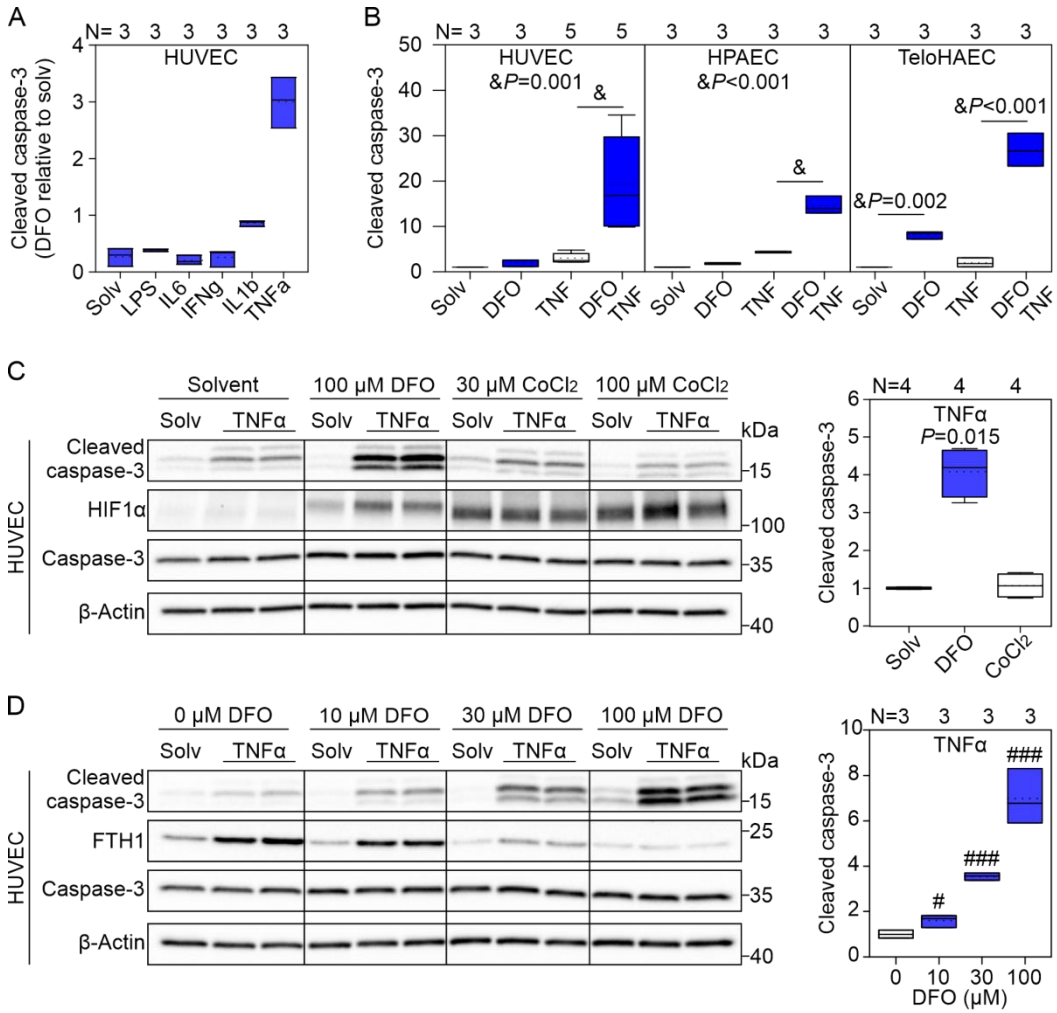

Figure 6-6. Iron deficiency increases the susceptibility of cultured cells to TNFα-mediated apoptosis. (A) Primary HUVECs were rendered iron deficient by pretreatment with 100 µM DFO for 24h prior to stimulation with LPS (2 mg/ml) or 50 ng/ml IL6, IFNγ, IL1β or TNFα for 16h. Western blot quantification of cleaved caspase-3. **(B)** Western blot quantification of cleaved caspase-3 in primary HUVECs, primary HPAECs, and immortalized endothelial cell line teloHAEC after treatment with 100 µM DFO with and without TNFα for 16h. **(C)** Primary HUVECs were treated with 0-100 µM cobalt chloride ($CoCl_2$) or DFO for 24h prior to stimulation with TNFα for 16. Cleaved caspase-3 was analyzed by Western blotting. **(D)** Western blot and quantification of cleaved caspase-3 in HUVECs treated with increasing doses of DFO (0-100 µM) with and without TNFα for 16h. Replicates are indicated above the *x*-axis. β-Actin was used as a loading control. Statistical differences between groups were determined by one-way ANOVA with Dunn's method of multiple comparisons, two-way ANOVA (indicated by &) or *t*-test (indicated by #$P<0.05$, ###$P<0.001$).

with TNFα and $CoCl_2$, an inhibitor of prolyl hydroxylases, did not potentiate apoptosis, suggesting that it is cellular iron deficiency that mediates sensitivity to TNFα toxicity **(Figure 6-6C)**. We further evaluated whether sensitivity to TNFα cytotoxicity is related to the degree of iron deficiency by treating cells with a range of DFO doses (0-100 μM) in the presence of TNFα and found that even mild iron deficiency potentiates apoptosis **(Figure 6-6D)**. However, the contribution of TNFα in adverse outcomes in our mouse model remains to be determined.

Iron deficiency potentiates obesity-induced adverse fetal outcomes. In addition to the LPS mouse model of systemic maternal inflammation that mimics bacterial infection, we expanded our study to a mouse model of obesity, a milder systemic inflammatory condition that is very common in human pregnancy. Female mice were fed a Western diet (iron-adequate, 100 ppm iron) starting at 3 weeks of age for 8 weeks, then half of the females continued on the same diet, and the other half switched to an iron-deficient Western diet (4 ppm iron) for 1 or 3 more weeks. Females were

Table 6-2. E18.5 Maternal hematological parameters in obese mouse pregnancy

	Iron deficient Western diet	**Iron adequate Western diet**	***P*-value**	**Iron deficient Western diet**	**Iron adequate Western diet**	***P*-value**
	Dams E18.5 (N=8)	**Dams** E18.5 (N=7)		**Embryos** E18.5 (N=24)	**Embryos** E18.5 (N=18)	
RBC (10^6/μL)	8.6±0.4	9.2±0.4	***P*=0.009**	1.6±0.3	2.3±0.3	***P*<0.001**
Hb (g/dL)	11.4±0.4	13.2±0.3	***P*<0.001**	4.1±0.9	7.4±1.2	***P*<0.001**
HCT (%)	34.1±1.4	39.6±1.6	***P*<0.001**	13.1±2.9	24.0±5.3	***P*<0.001**
MCV (fL)	39.5±0.8	43.0±0.9	***P*<0.001**	79.5±8.6	110.1±12.2	***P*<0.001**
MCH (pg)	13.2±0.7	14.3±0.6	***P*=0.006**	24.7±3.3	32.9±2.2	***P*<0.001**
MCHC (pg/dL)	33.4±1.5	33.2±1.6	*P*=0.819	31.2±3.4	30.0±2.1	*P*=0.058

Table 6-2. E18.5 maternal and embryo hematological parameters in obese mouse pregnancy. Hematological parameters of E18.5 obese iron-deficient dams (fed low iron Western diet) and iron-adequate wild type dams (fed Western diet with standard iron) and their embryos. Data are presented as mean ± SD. RBC, red blood cell; Hb, hemoglobin; HCT, hematocrit; MCV, mean corpuscular volume; MCH, mean corpuscular hemoglobin; MCHC, mean corpuscular hemoglobin concentration. Statistical differences between groups were determined by *t*-test.

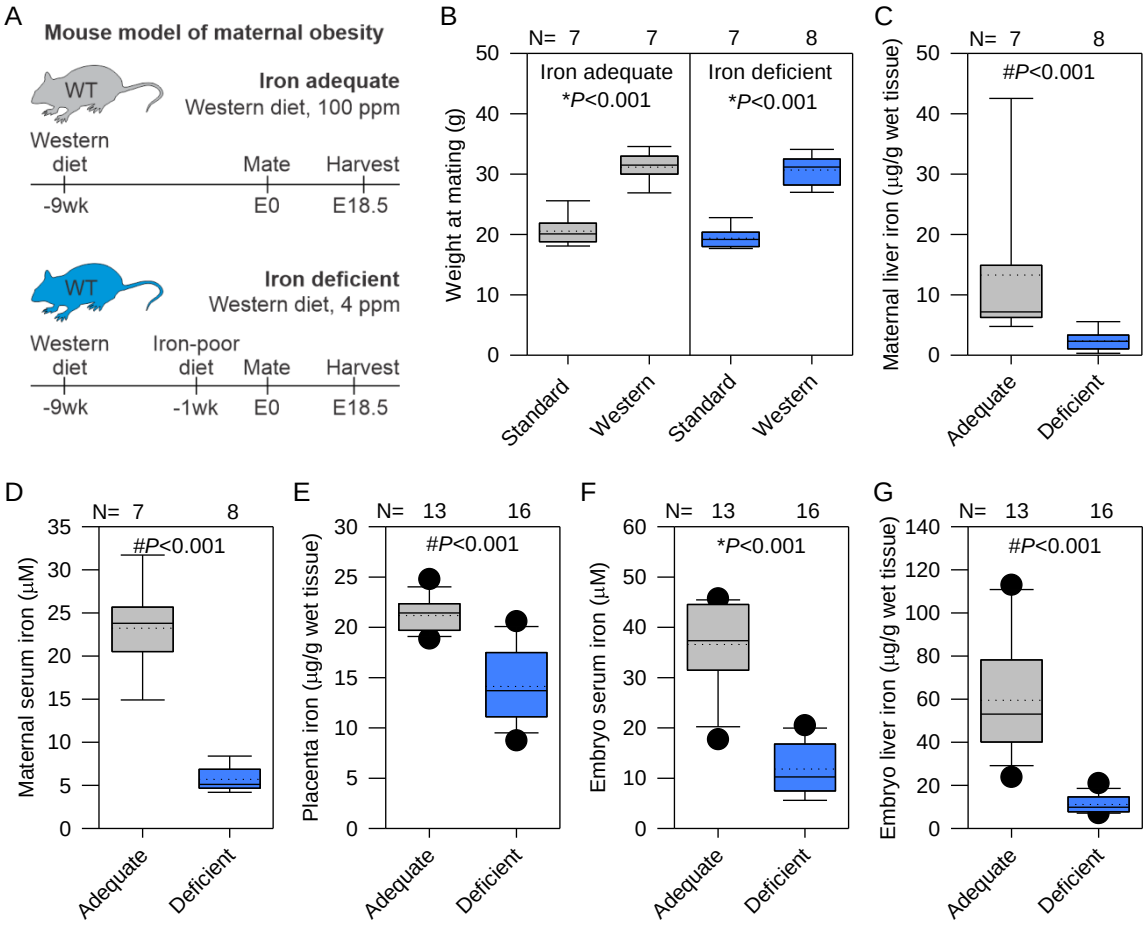

Figure 6-7. Iron parameters in iron replete and iron deficient obese pregnant mice. (A) WT female mice were fed iron-adequate Western diet (100 ppm iron) starting at 3 weeks of age for 8 weeks, then half of the mice continued on the same diet, and the other half switched to an iron-poor Western diet (4 ppm iron) for 1 more week. Females were mated and continued the same diets during pregnancy and were analyzed at E18.5. **(B)** Body weights at mating from iron-adequate and iron-deficient females fed standard or Western diet. Non-heme iron measurements from iron-adequate and iron-deficient mice fed Western diet: **(C)** maternal liver and **(D)** maternal serum, **(E)** placenta, and **(F)** embryo serum and **(G)** embryo liver. Animal numbers are indicated above the *x*-axis. Statistical differences between groups were determined by Student's *t*-test for normally distributed values (indicated by *) or Mann-Whitney *U* for non-normally distributed values (indicated by #).

mated and continued the same types of diets throughout pregnancy and were analyzed at E18.5 **(Figure 6-7A)**. As expected, dams on Western diet weighed 50% more than dams fed standard chow ($P<0.001$) **(Figure 6-7B)**. Dams fed the iron-deficient Western diet had lower liver iron and serum iron concentrations (both $P<0.001$) **(Figure 6-7C, D)**, and lower hematologic parameters (~2 g/dL lower hemoglobin at E18.5, $P<0.001$) **(Table 6-2)**, indicative of iron deficiency and

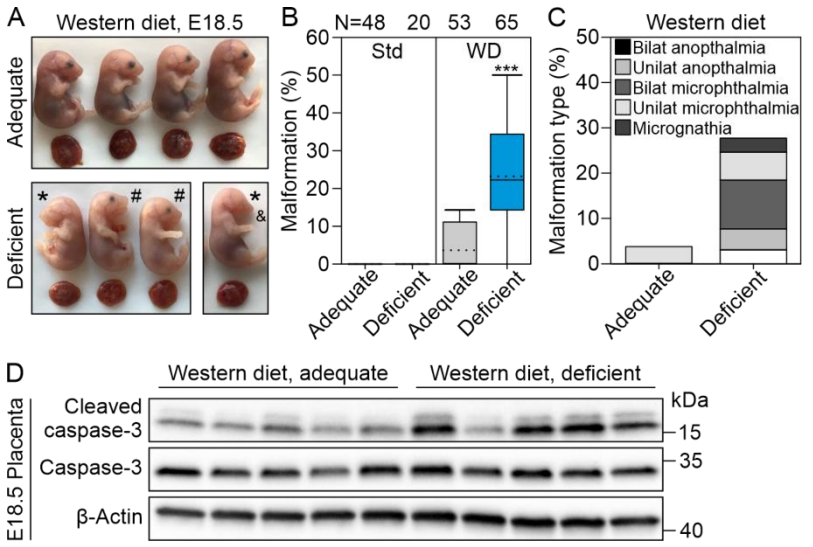

Figure 6-8. Maternal iron deficiency potentiates obesity-induced adverse outcomes. E18.5 embryos from obese iron-adequate (fed 100ppm iron Western diet) and iron-deficient (fed 4ppm iron Western diet) dams. Iron deficiency worsened embryo defects: **(A)** embryo gross morphology (*anophthalmia, #microphthalmia, and &micrognathia), **(B-C)** malformation incidence and type. **(D)** Western blot of whole placenta lysates for apoptotic marker cleaved caspase-3. β-Actin was used as a loading control. Animal numbers are indicated above the *x*-axis. Statistical differences were determined by one-way ANOVA (***P<0.001).

anemia. Placentas from iron deficient obese dams were also mildly iron-deficient (P<0.001) **(Figure 6-7E)**. Embryos from iron deficient obese mothers were severely iron deficient with lower serum iron levels and liver iron concentrations (both P<0.001) **(Figure 6-7F, G)**, and lower hematologic parameters (3 g/dL lower hemoglobin at E18.5, P<0.001) **(Table 6-2)**. Notably, we observed significantly more frequent embryo malformations in the iron-deficient than iron-adequate obese cohort **(Figure 6-8A, B)**. Embryo malformations included eye (bilateral and unilateral anophthalmia and microphthalmia) and jaw abnormalities (micrognathia) **(Figure 6-8C)**. Furthermore, placental apoptosis, as assessed by the cleaved caspase-3 Western blotting, was increased in the iron-deficient group **(Figure 6-8D)**, suggesting similarities in the mechanism by which iron deficiency causes adverse outcomes in the LPS and obese mouse model.

Maternal iron deficiency induces placental TNFα receptor 1 expression. Our data in cultured endothelial cells suggests that iron deficiency modulates TNFα signaling. Indeed, TNFα receptor-1 (TNFR1) was reported to be increased in trophoblasts of iron-deficient rats, although assessed by semi-quantitative immunostaining [35]. We examined placental expression of TNFR1, the

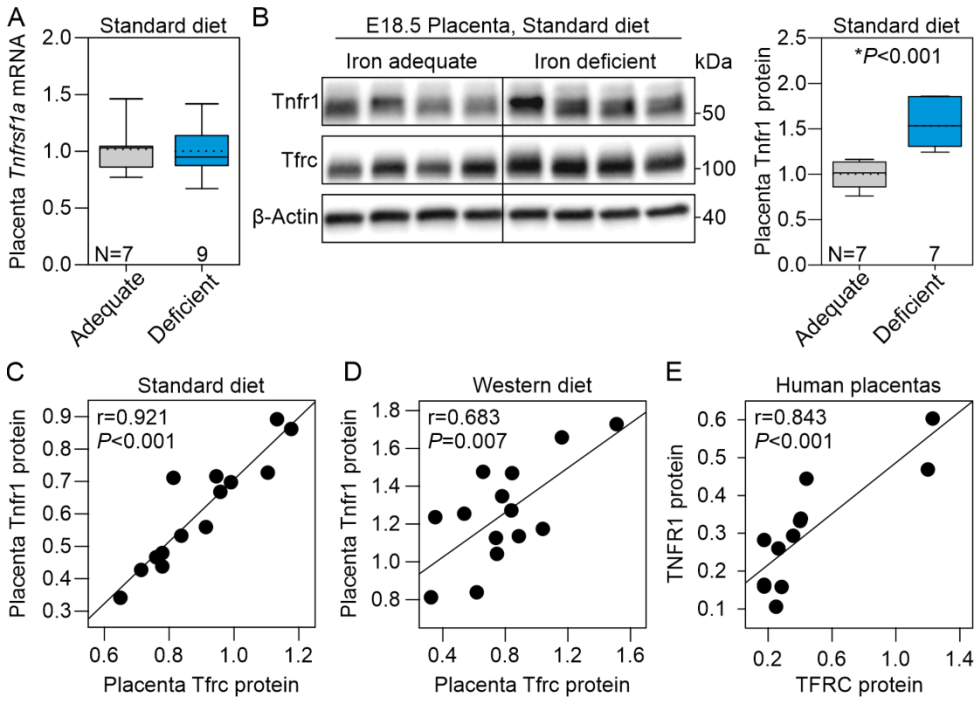

Figure 6-9. Maternal iron deficiency induces placental TNFα receptor 1 expression. E18.5 placental Tnfr1 expression was compared between iron adequate and iron deficient dams fed **(A-C)** standard diet or **(D-E)** Western diet. **(A)** *Tnfrsf1a* mRNA expression. **(B)** Tnfr1 protein expression by Western blot normalized to β-Actin. Animal numbers are indicated above the *x*-axis. Correlation of placental transferrin receptor 1 (Tfrc) and Tnfr1 normalized to β-Actin in dams fed **(C)** standard iron deficient diet or **(D)** iron-deficient Western diet. **(E)** Correlation between TFRC and TNFR1 in human placentas. Statistical differences between groups were determined by Student's *t*-test (indicated by *) or Pearson correlation.

ubiquitously expressed receptor for TNFα, known to mediate its apoptotic effects [36]. *Tnfrsf1a* mRNA was not affected by maternal iron status of our mice **(Figure 6-9A)**. However, placental TNFR1 protein was induced in iron-deficient pregnancies in the absence of inflammation **(Figure 6-9B)**, with a surprisingly strong correlation noted between TNFR1 and iron importer transferrin receptor 1 (TFRC), a marker of cellular iron deficiency (r=0.921, *P*<0.001) **(Figure 6-9C)**, which was also noted in obese iron deficient pregnancies in mice (r=0.683, *P*=0.007) **(Figure 6-9D)**. Importantly, in a set of human placental samples obtained from pregnant women that either had iron deficiency anemia (Hemoglobin <8 g/dL) or were not anemic (Hemoglobin >11 g/dL), we noted a similar increase in placental TNFR1 with iron deficiency anemia, and a strong significant correlation with placental TFRC **(Figure 6-9E)**. Any iron-dependent regulation of TNFR1 has not

been reported before and reveals a possible underlying mechanism for how iron deficiency worsens outcomes in inflamed pregnancies.

Iron deficiency potentiates apoptosis in other models of inflammation. We extended our studies to trophoblast cell line (BeWo) and kidney cell line (Hek293) and similarly found that iron deficiency potentiates TNFα-mediated apoptosis **(Figure 6-10A)**, suggesting a more common effect of iron deficiency in increasing sensitivity to apoptosis. We tested this in mouse models by inducing systemic inflammation in iron-deficient and iron-adequate adult nonpregnant male (N=6) and female mice (N=6). Female and male mice were rendered iron deficient by feeding iron deficient diet (4 ppm iron) for 5 weeks starting at 4 weeks of age **(Figure 6-10B)** and were compared to iron-adequate mice maintained on standard diet (185 ppm iron). Mice on the iron-poor diet had lower hemoglobin than those on iron-adequate diet (*P*=0.041), indicative of iron deficiency, although the decrease in hemoglobin was less pronounced in female mice **(Table 6-3)**. To induce systemic inflammation, iron-adequate and iron-deficient mice were treated with a single

Table 6-3. Hematological parameters in iron adequate and iron deficient 8-week old adult mice

	Iron deficient	**Iron adequate**	***P*-value Males**	**Iron deficient**	**Iron adequate**	***P*-value Females**	***P*-value Combined**
	Males (N=3)	**Males** (N=3)		**Females** (N=3)	**Females** (N=3)		
RBC (10^6/μL)	8.5±1.4	8.8±0.1	*P*=0.700	9.1±0.7	8.9±0.7	*P*=0.729	*P*=0.940
Hb (g/dL)	8.9±1.6	12.6±0.4	***P*=0.020**	11.0±1.8	12.9±0.6	*P*=0.148	***P*=0.041**
HCT (%)	29.9±4.5	39.5±0.5	***P*=0.022**	34.1±4.1	40.2±2.0	*P*=0.084	***P*=0.002**
MCV (fL)	35.3±1.8	45.0±0.3	*P*=0.100	37.3±2.4	45.2±1.3	***P*=0.007**	***P*<0.001**
MCH (pg)	10.5±0.5	14.3±0.4	***P*<0.001**	12.1±1.7	14.5±0.5	*P*=0.075	***P*=0.004**
MCHC (pg/dL)	29.8±0.9	31.8±0.9	***P*=0.043**	32.2±3.0	32.1±0.3	*P*=0.957	*P*=0.359

Table 6-3. Hematological parameters in iron adequate and iron deficient mice. Hematological parameters of 8-week old iron-adequate (fed diet with standard iron) and iron-deficient (fed low iron diet) mice. Data are presented as mean ± SD. RBC, red blood cell; Hb, hemoglobin; HCT, hematocrit; MCV, mean corpuscular volume; MCH, mean corpuscular hemoglobin; MCHC, mean corpuscular hemoglobin concentration. Statistical differences between groups were determined by *t*-test.

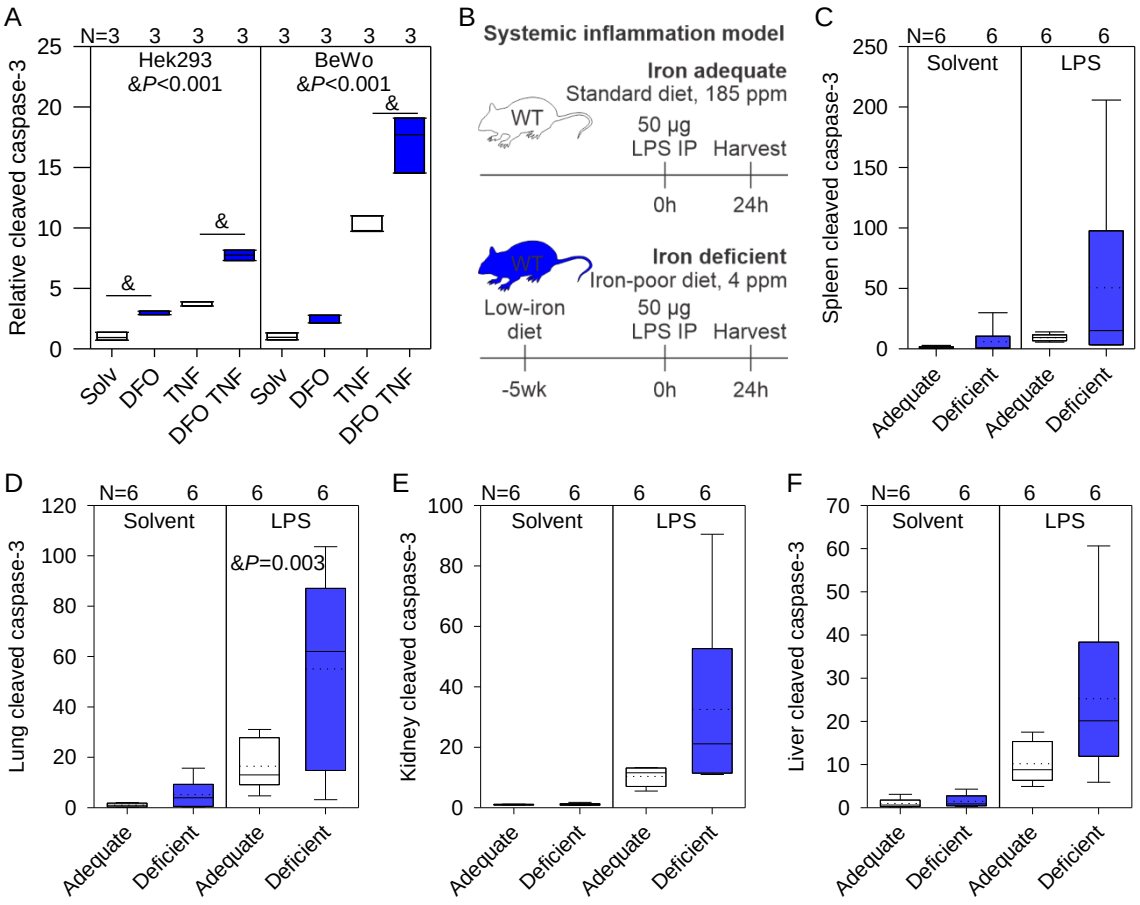

Figure 6-10. Iron deficiency potentiates apoptosis in other models of inflammation. (A) Kidney cell line (Hek293) and trophoblast cell line (BeWo) were treated with 100 µM DFO for 24h prior to 16h of TNFα stimulation. Western blot quantification of cleaved caspase-3 normalized to β-Actin (N=3/group). **(B)** Four-week old WT female and male mice were fed a low iron diet for 5 weeks. Iron-adequate (fed standard diet) and iron-deficient mice received a single intraperitoneal injection of 50 µg LPS for 24h. Western blot quantification of cleaved caspase-3 normalized to β-Actin in **(C)** spleen, **(D)** lung, **(E)** kidney, and **(F)** liver. Animal numbers are indicated above the *x*-axis. Statistical differences between groups were determined by two-way ANOVA (indicated by &).

intraperitoneal injection of 50 µg LPS for 24h **(Figure 6-10B)**, and organs were harvested for cleaved caspase-3 expression analysis by Western blotting. In the heart and brain, we were unable to accurately detect cleaved caspase-3. However, in the spleen, lung, kidney, and liver, we detected cleaved caspase-3 expression following LPS, and the induction was potentiated by iron deficiency (significant in the lung, *P*=0.003) **(Figure 6-10C-F)**, suggesting a broader role of iron deficiency in worsening injury in inflammatory conditions outside of pregnancy.

DISCUSSION AND FUTURE DIRECTIONS

In this Chapter, we made a novel observation of an adverse interaction between maternal iron deficiency and inflammation during pregnancy that causes embryotoxicity, including embryo malformations and demise, which was not observed with either condition alone. Importantly, adverse consequences were seen in two mouse models of inflammation: LPS-induced acute inflammation mimicking bacterial infection, and diet-induced obesity model of chronic inflammation, suggesting that the interaction does not require intense inflammation. Furthermore, we observed that iron deficiency potentiated LPS-induced apoptosis in the lungs, kidney and liver of non-pregnant animals, suggesting that similar mechanisms may also be pathogenic outside of pregnancy.

Notably, we found that in our mouse model of LPS-induced inflammation, maternal iron deficiency potentiated inflammation in the placenta but not in the dam or embryo. We noted increased gene expression of *Il6*, *Il1b*, *Tnf*, *Cxcl1*, and *Cxcl2* in the placentas from iron-deficient dams treated with LPS compared to iron-adequate dams, showing that iron deficiency worsens LPS-induced inflammation. We did not detect any changes in inflammatory markers without LPS treatment, demonstrating that maternal iron deficiency, in the absence of any inflammatory stimulus, does not worsen placental inflammation. Although we did not detect major differences in expression of inflammatory markers in maternal liver, future experiments determining the cytokine profile in maternal serum are needed to solidify changes in maternal inflammation, as well as the use of cytokine neutralizing antibodies to determine the cytokine primarily driving apoptosis. Once identified, injection of pregnant dams with recombinant cytokine would delineate whether the cytokine alone is sufficient to drive adverse outcomes in iron-deficient dams.

Our preliminary data strongly suggest that the endothelial cells are most susceptible to changes in iron status, rendering them sensitive to cytokine-driven apoptosis. In our HUVEC model, we observed that apoptosis was strongly potentiated by TNFα and to a lesser extent IL1β, but not IL6 or IFNγ, suggesting that either TNFα or IL1β could be mediating apoptosis in vivo, either locally from inflammation-driven production by the placenta or in combination with elevated maternal cytokines. In addition to endothelial cultures, we demonstrated that placental cell line BeWo and kidney cell line Hek293 were also more sensitive to apoptosis when iron deficient, suggesting a more common mechanism of iron deficiency in sensitizing cells to apoptosis We further demonstrated that non-pregnant mice of both sexes are more susceptible to apoptotic injury when iron-deficient, primarily the lung, which is composed of 50% endothelial cells, but also the kidney and liver. Whether the apoptosis localizes to endothelium in inflamed iron-deficient non-pregnant mice remains to be determined.

In mouse and human placenta, we demonstrated that maternal iron deficiency induces expression of the receptor for TNFα, providing another possible mechanism of adverse outcomes, whereby increased receptor expression potentiates apoptotic signaling. Preliminary data using cell sorting of placentas from iron-adequate pregnant mice suggest that TNFR1 is primarily expressed in endothelial cells in the placenta **(Figure 6-11)**, but further experiments are required to determine whether the endothelial cells or the non-endothelial fraction induce TNFR1 expression in response to maternal iron deficiency. Furthermore, we can utilize *Tnfr1*-floxed mice [37] to delete *Tnfr1* in either fetal endothelial cells (Vec-Cre) or in trophoblast cells (TpbparAdafAdaP-Cre [38]) and define if the cell-type specific

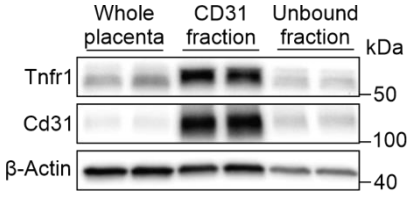

Figure 6-11. TNFR1 in placental endothelial cells. Endothelial cells were isolated from placentas from WT mice on E18.5 by magnetic separation. Western blot for TNFR1 in placenta, CD31 pellet (endothelial cells), and unbound fraction. β-Actin was used as a loading control.

loss of the iron-regulated TNFR1 is sufficient to prevent adverse outcomes.

In summary, we observed in mouse models an adverse interaction between maternal iron deficiency and acute or chronic inflammation during pregnancy that causes adverse fetal outcomes. Based on our preliminary data, our proposed model is that maternal iron deficiency potentiates apoptosis and fetal demise, possibly through iron deficiency-induced increases in placental TNFR1, or potentiated placental inflammation, or a combination of both **(Figure 6-12)**. Our studies raise the possibility that correcting iron deficiency in an inflamed pregnancy could be a modifiable factor to lessen the severity of adverse outcomes. Considering the global prevalence of iron deficiency, and the increasing occurrence of inflammatory conditions such as obesity, our findings have the potential to explain common pregnancy complications and could influence the clinical management of pregnant women worldwide.

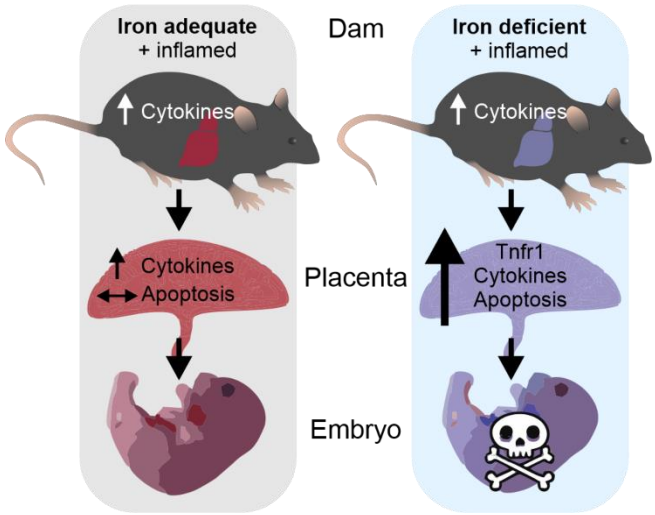

Figure 6-12. Model of adverse interaction between maternal iron deficiency and inflammation during pregnancy. Following inflammation, maternal hepatic expression of cytokines is similarly induced between iron-adequate (left panel) and iron-deficient (right panel) dams. In placenta, maternal iron deficiency increases TNFR1 expression, potentiates placental inflammation, inducing apoptosis and fetal demise. Our preliminary data indicate that the endothelial cells are the primary apoptotic target.

MATERIALS AND METHODS

Animals. All animal experiments were approved by the UCLA Institutional Animal Care and Use Committee and were carried out in accordance with the Guide for Care and Use of Laboratory Animals (National Institutes of Health, Bethesda, MD). Wild type (WT) C57BL/6J mice were obtained from the Jackson Laboratory (Bar Harbor, ME) (stock #000664). Unless where specified, mice were fed a standard diet (PicoLab Rodent Diet 20, 5053 Irradiated, 185 ppm iron) ad libitum. All purified diets were obtained from Envigo-Teklad.

To model maternal iron deficiency, female WT mice were fed a purified low iron diet (TD.80396) for 1-3 weeks prior to mating and during pregnancy. For obesity studies, 3-week old female WT mice were fed a Western diet with 100-ppm ferric citrate (TD.180722). After 8 weeks, half of the mice continued the diet and half were fed a low-iron Western diet (TD.140525) for 1-3 weeks prior to mating and during pregnancy. The Western diet contains 0.2% cholesterol, saturated fat >60% of total fat (42% of calories), and high sucrose (43% of calories), and 15% calories from protein. For non-pregnant studies, 4-week old male and female WT mice were fed standard or low-iron diet for 5 weeks.

Systemic inflammation models. For second trimester inflammation, pregnant mice on E8.5 were weighed and received a single subcutaneous injection of 0.5 μg/g LPS (Escherichia coli serotype O55:B5, Sigma-Aldrich L2880) or equivalent volume of sterile solvent as a control. Mice were weighed daily after injection, and mice that lost pregnancy weight gain were euthanized from E11.5-E18.5 to confirm embryo loss. For third trimester inflammation, pregnant mice on E15.5 received a single subcutaneous injection of LPS for 24h. Preterm birth was recorded as the delivery of at least one embryo within 24h of injection.

For non-pregnant studies, iron-adequate and iron-deficient female and male mice received a single intraperitoneal injection of 50 μg LPS for 24h. At the indicated times, mice were euthanized by isoflurane overdose and tissues collected for analysis.

Complete blood counts. Mouse complete blood counts were performed on EDTA whole blood using a Hemavet 950FS hematology system (Drew Scientific).

Non-heme iron measurements. Serum was obtained from maternal and embryo blood by centrifugation at 2,700 x g for 10 min. Serum iron concentration was measured by colorimetric spectrophotometry using an iron calibrator (Iron-SL, Sekisui Diagnostics 157-30) [39], excluding hemolyzed samples. For maternal liver iron measurements, 75 μL of whole liver homogenate was weighed and incubated in 1125 μL protein precipitation solution (0.53 N HCl 5.3% tricholoracetic acid) at 100°C for 1 h. For embryo tissue iron measurements, half of each placenta and liver were weighed and homogenized in 1200 μL protein precipitation solution prior to boiling. Samples were centrifuged at 17,000 x g for 10 min and supernatant was analyzed by colorimetric spectrophotometry using an iron standard (1,000-ppm iron in 3% HCl, Ricca Chemical Company).

Cell culture. Primary human umbilical vein endothelial cells (HUVECs, PCS-100-013), primary human pulmonary artery endothelial cells (HPAECs, PCS-100-022), and human placenta cell line (BeWos, CCL-98) were obtained from ATCC. HUVECs and HPAECS were cultured in complete endothelial cell growth medium (Cell Applications #211-500) and experiments were performed from passages 3 to 5. Immortalized human aortic endothelial cells (teloHAECs) were a gift from Luisa Iruela-Arispe (Northwestern University) and were cultured in MCDB-131 complete media (VEC Technologies). BeWos were cultured in Ham's F-12K (Kaighn's) media (ThermoFisher) with 10% FCS, and Hek293s were cultured in DMEM (ThermoFisher) with 10% FCS.

For experiments, cells were seeded at 1 x 10^5/well on collagen (HUVEC, HPAEC, teloHAEC, BeWO) or poly-D-Lysine (Hek293) coated plates (Corning BioCoat). The optimal time of culture and treatment was based on preliminary concentration and time-dependence studies.

For iron depleting experiments, cells were plated in in regular media or media supplemented with deferoxamine (Sigma D9533) at the indicated concentrations for 24h.

For inflammation studies, cells were treated with solvent, 2mg/ml LPS, or 50ng/mL recombinant human IL-6 (R&D Systems #206-IL), IFN-γ (PeproTech #300-02), IL-1β (PeproTech #200-01B), or TNFα (Biolegend #570102) for 16h.

Cell sorting. Endothelial cells were isolated from E18.5 pregnant iron-adequate WT mice. Five placentas/dam were pooled, and endothelial cells were isolated by magnetic separation using the MidiMACS system per the manufacturer's instructions (Miltenyi #130-095-927, #130-097-418).

Quantification of gene expression by RT-PCR. Frozen liver and placenta pieces were homogenized in TRIzol (Life Technologies) and total RNA was isolated by chloroform extraction. One μg of RNA was reverse transcribed using the iScript cDNA Synthesis Kit (Bio-RAD). Quantitative real-time PCR was performed on cDNA using Sso Advance SYBER Green Supermix (Bio-RAD) on the CFX Real-Time PCR Detection System (Bio-RAD). Samples were measured in duplicate and target genes were normalized to *Hprt* or *Rpl4*. Data are expressed as $2^{-\Delta\Delta Ct}$.

Primer sequences:

Gene	Sequence
Tnf	Forward: 5'- AAT GGC CTC CCT CTC ATC AG -3' Reverse: 5'- GCT ACG ACG TGG GCT ACA GG -3'
Il6	Forward: 5'- CTC TGC AAG AGA CTT CCA TCC AGT -3' Reverse: 5'- CGT GGT TGT CAC CAG CAT CA -3'
Il1b	Forward: 5'- AAG GAG AAC CAA GCA ACG ACA AAA -3' Reverse: 5'- TGG GGA ACT CTG CAG ACT CAA ACT -3'
Saa1	Forward: 5'- AGT CTG GGC TGC TGA GAA AA -3' Reverse: 5'- ATG TCT GTT GGC TTC CTG GT -3'
Cxcl2	Forward: 5'- GAA GTC ATA GCC ACT CTC AAG G -3' Reverse: 5'- CCT CCT TTC CAG GTC AGT TAG C -3'
Cxcl1	Forward: 5'- AGA CCA TGG CTG GGA TTC AC -3' Reverse: 5'- AGT GTG GCT ATG ACT TCG GT -3'
Hprt	Forward: 5'- CTG GTT AAG CAG TAC AGC CCC AA -3' Reverse: 5'- CAG GAG GTC CTT TTC ACC AGC -3'
Rpl4	Forward: 5'- TGA AAA GCC CAG AAA TCC AA -3' Reverse: 5'- AGT CTT GGC GTA AGG GTT CA -3'
Ptgs2	Forward: 5'- TGA GTA CCG CAA ACG CTT CT -3' Reverse: 5'- CAG CCA TTT CCT TCT CTC CTG T -3'
Nlrp3	Forward: 5'- AAA ATG CCT TGG GAG ACT CA -3' Reverse: 5'- AAG TAA GGC CGG AAT TCA CC -3'

Western blot analysis. Embryo tissues and cells were homogenized in RIPA lysis buffer with freshly added protease inhibitors (Santa Cruz #24948). Lysates were centrifuged at 17,000 x g for 15 min at 4°C and protein concentration was measured by the bicinchoninic acid assay. Proteins were separated by SDS-PAGE, transferred to nitrocellulose membranes, blocked for 1 hr in 5% w/v dried nonfat milk or bovine serum albumin in TBS with 0.1% Tween-20, and incubated with primary antibodies in blocking buffer overnight at 4°C. The secondary reaction was performed using HRP-conjugated IgG. Protein blots were visualized by chemiluminescence using the ChemiDoc XRS+ imaging system and quantified using Image Lab software (Bio-RAD).

Antibodies:

Target protein	Primary antibody
Mouse / human cleaved caspase-3	Rabbit monoclonal antibody 9664, Cell Signaling
Mouse / human total caspase-3	Rabbit monoclonal antibody 9662, Cell Signaling
Mouse / human ferritin heavy chain	Rabbit monoclonal antibody 4393, Cell Signaling
Mouse cleaved caspase-1	Rabbit monoclonal antibody 89332, Cell Signaling
Mouse / human β-actin	Monoclonal antibody-peroxidase A3854, Sigma
Mouse CD31/PECAM-1	Goat polyclonal antibody AF3628, Novus
Mouse / human TFR1	Mouse monoclonal antibody H68.4, ThermoFisher
Mouse TNFR1	Rabbit monoclonal antibody 13377, Cell Signaling
Human TNFR1	Rabbit monoclonal antibody 3736, Cell Signaling
Secondary antibodies:	
Anti-mouse IgG HRP antibody 7076, Cell Signaling	
Anti-rabbit IgG HRP antibody 7074, Cell Signaling	
Anti-goat IgG HRP antibody 2354, Santa Cruz	
ImmPRESS horse anti-rabbit IgG HRP detection kit MP-7401, Vector Laboratories	
ImmPRESS horse anti-goat IgG AP detection kit MP-5405, Vector Laboratories	

Histopathology and immunohistochemistry. Placentas and whole embryos were fixed in 10% neutral buffered formalin for 48 h at room temperature and stored in 70% ethanol until processing. Tissues were paraffin-embedded and sectioned at 4 μm thickness by the UCLA Translational Pathology Core Laboratory. Prior to staining, sections were deparaffinized through serial changes of xylenes and ethanol and rehydrated to distilled water. For immunohistochemistry, antigen retrieval was performed by boiling in Tris-EDTA (10 mM Tris base 1 mM disodium EDTA dihydrate, pH 9.0) for 10 min. Sections were quenched with BLOXALL (Vector Laboratories SP-6000) for 10 min and washed with TBS containing 0.1% Tween-20. Blocking was performed using 2.5% normal horse serum in PBS. Sections were incubated with primary antibodies in blocking buffer at 4°C overnight in a humidified chamber. Negative control sections were incubated with normal IgG from the same species and at the same concentrations as primary antibodies. The

secondary reaction was performed using ImmPRESS IgG (Vector Laboratories) conjugated to horseradish peroxidase (HRP) or alkaline peroxidase (AP). HRP and AP were developed using DAB and vector red per the manufacturer's instructions (Vector Laboratories). Sections were counterstained with Gill's hematoxylin. Images were captured using light microscopy.

Statistical Analysis. Statistical analysis was performed using SigmaPlot version 12.5 (Systat Software). Data are presented as box-and-whisker plots. The box portion represents the upper 75th and lower 25th percentile, whiskers indicate variability outside the upper 90th and lower tenth percentile, and individual points represent outliers. The solid line represents the median and the dotted line the mean. Statistical differences between groups were determined by two-way ANOVA, one-way ANOVA, two-tailed *t*-test, or Mann-Whitney *U* test. Statistical test, number of animals in each group, and *P*-value are indicated in each figure panel. A *P*-value of <0.05 was considered significant.

REFERENCES

1. Bothwell, T.H., *Iron requirements in pregnancy and strategies to meet them.* Am. J. Clin. Nutr, 2000. **72**(1 Suppl): p. 257S-264S.
2. Fisher, A.L. and E. Nemeth, *Iron homeostasis during pregnancy.* The American journal of clinical nutrition, 2017. **106**(Suppl 6): p. 1567S-1574S.
3. *Iron deficiency--United States, 1999-2000.* MMWR Morb Mortal Wkly Rep, 2002. **51**(40): p. 897-9.
4. World Health Organization, *The global prevalence of anaemia in 2011*. 2015: Geneva.
5. Sangkhae, V., et al., *Effects of maternal iron status on placental and fetal iron homeostasis.* The Journal of Clinical Investigation, 2020. **130**(2): p. 625-640.
6. Arija, V., et al., *Association of Iron Status and Intake During Pregnancy with Neuropsychological Outcomes in Children Aged 7 Years: The Prospective Birth Cohort Infancia y Medio Ambiente (INMA) Study.* Nutrients, 2019. **11**(12).
7. Cogswell, M.E., et al., *Iron supplementation during pregnancy, anemia, and birth weight: a randomized controlled trial.* Am J Clin Nutr, 2003. **78**(4): p. 773-781.
8. Corwin, E.J., L.E. Murray-Kolb, and J.L. Beard, *Low hemoglobin level is a risk factor for postpartum depression.* J Nutr, 2003. **133**(12): p. 4139-4142.
9. Georgieff, M.K., *Long-term brain and behavioral consequences of early iron deficiency.* Nutr. Rev, 2011. **69 Suppl 1**: p. S43-S48.
10. McArdle, H.J., L. Gambling, and C. Kennedy, *Iron deficiency during pregnancy: the consequences for placental function and fetal outcome.* Proc. Nutr. Soc, 2014. **73**(1): p. 9-15.
11. Scanlon, K.S., et al., *High and low hemoglobin levels during pregnancy: differential risks*

for preterm birth and small for gestational age. Obstet. Gynecol, 2000. **96**(5 Pt 1): p. 741-748.

12. Scholl, T.O. and T. Reilly, *Anemia, iron and pregnancy outcome.* J Nutr, 2000. **130**(2S Suppl): p. 443S-447S.
13. Stoltzfus, R.J., *Iron deficiency: global prevalence and consequences.* Food Nutr. Bull, 2003. **24**(4 Suppl): p. S99-103.
14. Nemeth, E., et al., *IL-6 mediates hypoferremia of inflammation by inducing the synthesis of the iron regulatory hormone hepcidin.* The Journal of Clinical Investigation, 2004. **113**(9): p. 1271-1276.
15. Nemeth, E., et al., *Hepcidin Regulates Cellular Iron Efflux by Binding to Ferroportin and Inducing Its Internalization.* Science, 2004. **306**(5704): p. 2090-2093.
16. Stefanova, D., et al., *Endogenous hepcidin and its agonist mediate resistance to selected infections by clearing non-transferrin-bound iron.* Blood, 2017. **130**(3): p. 245-257.
17. Stefanova, D., et al., *Hepcidin Protects against Lethal Escherichia coli Sepsis in Mice Inoculated with Isolates from Septic Patients.* Infect Immun, 2018. **86**(7).
18. Nemeth, E. and T. Ganz, *Anemia of inflammation.* Hematology/oncology clinics of North America, 2014. **28**(4): p. 671-vi.
19. Yockey, L.J. and A. Iwasaki, *Interferons and Proinflammatory Cytokines in Pregnancy and Fetal Development.* Immunity, 2018. **49**(3): p. 397-412.
20. Morelli, S.S., et al., *The maternal immune system during pregnancy and its influence on fetal development.* Research and Reports in Biology, 2015: p. 171-189.
21. Elovitz, M.A., et al., *Intrauterine inflammation, insufficient to induce parturition, still evokes fetal and neonatal brain injury.* Int. J. Dev. Neurosci, 2011. **29**(6): p. 663-671.

22. Jones, K.L., et al., *Autism with intellectual disability is associated with increased levels of maternal cytokines and chemokines during gestation.* Mol Psychiatry, 2017. **22**(2): p. 273-279.

23. Le Belle, J.E., et al., *Maternal inflammation contributes to brain overgrowth and autism-associated behaviors through altered redox signaling in stem and progenitor cells.* Stem Cell Reports, 2014. **3**(5): p. 725-34.

24. Kalagiri, R.R., et al., *Inflammation in Complicated Pregnancy and Its Outcome.* Am J Perinatol, 2016. **33**(14): p. 1337-1356.

25. Brown, A.S., et al., *Elevated maternal interleukin-8 levels and risk of schizophrenia in adult offspring.* Am J Psychiatry, 2004. **161**(5): p. 889-95.

26. Choi, G.B., et al., *The maternal interleukin-17a pathway in mice promotes autism-like phenotypes in offspring.* Science, 2016. **351**(6276): p. 933-939.

27. Hsiao, E.Y. and P.H. Patterson, *Activation of the maternal immune system induces endocrine changes in the placenta via IL-6.* Brain Behav Immun, 2011. **25**(4): p. 604-15.

28. Ponzio, N.M., et al., *Cytokine levels during pregnancy influence immunological profiles and neurobehavioral patterns of the offspring.* Ann N Y Acad Sci, 2007. **1107**: p. 118-28.

29. Goldenberg, R.L., et al., *Plasma ferritin and pregnancy outcome.* Am. J. Obstet. Gynecol, 1996. **175**(5): p. 1356-1359.

30. Tamura, T., et al., *Serum ferritin: a predictor of early spontaneous preterm delivery.* Obstet. Gynecol, 1996. **87**(3): p. 360-365.

31. Scholl, T.O., *High third-trimester ferritin concentration: associations with very preterm delivery, infection, and maternal nutritional status.* Obstet. Gynecol, 1998. **92**(2): p. 161-166.

32. Pujol Lopez, Y., et al., *Effects of subcutaneous LPS injection on gestational length and intrauterine and neonatal mortality in mice.* Neuroimmunomodulation, 2015. **22**(4): p. 274-8.

33. Xie, Y., et al., *Ferroptosis: process and function.* Cell death and differentiation, 2016. **23**(3): p. 369-379.

34. Latz, E., T.S. Xiao, and A. Stutz, *Activation and regulation of the inflammasomes.* Nature reviews. Immunology, 2013. **13**(6): p. 397-411.

35. Gambling, L., et al., *Effect of iron deficiency on placental cytokine expression and fetal growth in the pregnant rat.* Biol Reprod, 2002. **66**(2): p. 516-23.

36. Haider, S. and M. Knofler, *Human tumour necrosis factor: physiological and pathological roles in placenta and endometrium.* Placenta, 2009. **30**(2): p. 111-23.

37. Van Hauwermeiren, F., et al., *Safe TNF-based antitumor therapy following p55TNFR reduction in intestinal epithelium.* The Journal of Clinical Investigation, 2013. **123**(6): p. 2590-2603.

38. Zhou, C.C., et al., *Targeted expression of Cre recombinase provokes placental-specific DNA recombination in transgenic mice.* PLoS One, 2012. **7**(2): p. e29236.

39. Fisher, A.L., et al., *Fetal and amniotic fluid iron homeostasis in healthy and complicated murine, macaque, and human pregnancy.* JCI Insight, 2020.

CHAPTER 7: CONCLUDING REMARKS

CONCLUDING REMARKS

In this dissertation, we defined the molecular pathophysiology of iron regulation during pregnancy and elaborated several novel concepts. Using mouse models, we comprehensively evaluated the maternal, placental, and fetal consequences of changes in iron status during pregnancy. We showed that during maternal iron deficiency, maternal iron homeostatic mechanisms that restrict iron availability are further suppressed but this was not enough to maintain plasma iron levels and iron transfer to the developing embryo, resulting in embryo iron deficiency and anemia. Notably, with severe iron deficiency, the placenta altered the expression of iron import and export proteins to preserve its own iron and metabolic function at the expense of the embryo's iron endowment. The placental adaptation to limited iron available likely evolved to protect the embryo from the consequences of placental dysfunction. Furthermore, we showed that maternal hepcidin is the critical determinant of embryo iron endowment and its suppression is essential for a healthy pregnancy, as high hepcidin activity induced by administering a hepcidin mimetic to pregnant mice caused severe iron restriction and anemia in dams and embryos, low birthweight and mortality.

We evaluated the role of embryo-derived hepcidin in healthy and complicated pregnancies. Although embryo hepcidin is low during normal pregnancy and does not affect placental iron transfer, we found that in the presence of inflammation, maternal and embryo hepcidin are increased in mice, causing iron restriction, and limiting iron supply to the fetus. Using rhesus macaque models of intraamniotic inflammation, and humans with intraamniotic inflammation, we evaluated whether inflammation could induce embryo hepcidin independent of maternal inflammation and determined that embryo hepcidin was increased and associated with embryo hypoferremia. The embryo's ability to respond to inflammatory signals in utero represents a

conserved mechanism important in fetal host defense, as limiting iron availability would protect the embryo from certain pathogenic bacteria.

Importantly, we discovered in mouse models an adverse interaction between maternal **iron excess** and inflammation that leads to embryotoxicity, which does not occur with iron excess or inflammation alone. In iron-loaded embryos, we observed severe malformations and demise in a mouse model of acute inflammation induced by bacterial lipopolysaccharide, but also with chronic inflammation from diet-induced obesity. We provided specific evidence that iron loading of placental and fetal endothelial cells induces oxidative stress, thereby increasing susceptibility to inflammation-induced apoptosis. Importantly, we determined that the adverse interaction between maternal iron excess and inflammation was dependent on TNFα-signaling and could be prevented by maternal anti-TNFα or antioxidant therapy. Considering the global prevalence of inflammation during pregnancy, and the common practice of indiscriminate iron supplementation of pregnant women, our findings raise important questions about the safety of this practice.

We further uncovered that **iron deficiency** also interacts with both acute and chronic inflammation, causing placental and fetal endothelial apoptosis, and ultimately fetal malformations and demise. We found that maternal iron deficiency potentiates inflammation in the placenta and increases TNFα-receptor 1 expression in mouse and human placentas, representing possible mechanisms for how iron deficiency worsens outcomes in inflamed pregnancies. Furthermore, the iron-dependent regulation of TNFα-receptor 1 is a novel mechanism that could explain commonly observed adverse pregnancy outcomes in the setting of maternal iron deficiency. Overall, the discovery of the interactions between inflammation and both sides of the iron spectrum - iron deficiency and iron excess - underscores the importance of screening for preexisting iron disorders in pregnant women with underlying inflammation.

In addition to the work in pregnancy mouse models, we demonstrated how non-transferrin bound iron affects cultured endothelial cells. We found that cellular iron loading induces cholesterol biosynthesis, and that both iron and cholesterol excess by themselves potentiate apoptosis by TNFα. We similarly found that iron and cholesterol excess induce proteolytic processing of a novel TNFα-receptor 1 isoform, but determined that during iron excess, the contribution of altered cholesterol homeostasis is the driving pathogenic mediator of apoptosis. Our findings have important implications for iron loading conditions, especially when inflammation is present. Altered cholesterol metabolism by iron excess in endothelial cells may contribute to iron-mediated toxicity in human iron overload disorders.

In summary, the innovative concepts identified in this dissertation have both fundamental and translational impact and may eventually inform the clinical management of pregnant women worldwide. The mechanism by which iron interacts with inflammation may be relevant to inflammatory disorders beyond pregnancy, an important conceptual advance in understanding modifiers of inflammatory conditions.